

University of Southampton Research Repository ePrints Soton

Copyright © and Moral Rights for this thesis are retained by the author and/or other copyright owners. A copy can be downloaded for personal non-commercial research or study, without prior permission or charge. This thesis cannot be reproduced or quoted extensively from without first obtaining permission in writing from the copyright holder/s. The content must not be changed in any way or sold commercially in any format or medium without the formal permission of the copyright holders.

When referring to this work, full bibliographic details including the author, title, awarding institution and date of the thesis must be given e.g.

AUTHOR (year of submission) "Full thesis title", University of Southampton, name of the University School or Department, PhD Thesis, pagination

UNIVERSITY OF SOUTHAMPTON

FACULTY OF SOCIAL AND HUMAN SCIENCES

Geography and Environment

**Evaluating the Potential of Sentinel Optical Sensors
for the Retrieval of Vegetation Biophysical Variables**

by

William James Frampton

Thesis for the degree of Doctor of Philosophy

June 2014

Abstract

In recent years a heightened awareness of the vulnerability of our environment to anthropogenic activity combined with the need for better management of natural resources to sustain a rapidly growing population has drawn attention to the importance satellite remote sensing. Remotely sensed estimations of the biophysical variables of vegetation are applicable at many spatial scales with many uses. Each new generation of satellites provides opportunities to refine the retrieval of such variables and accordingly this thesis will focus on evaluating the potential of the future Sentinel series of satellites for the retrieval of vegetation biophysical variables. Sentinel-3 (S-3), tentatively planned for launch in mid-2015, will provide a continuation of the successful MERIS sensor with enhanced temporal resolution. Alternatively Sentinel-2 (S-2) will acquire high spatial resolution (20 m) reflectance measurements operationally across an unprecedented number of bands on, and around, the red edge and is set for launch in April 2015. Initial research investigated the effect of the soil background on the L2 operational MERIS product the MTCI. MERIS imagery was used to explore the vegetation green up period and subsequently to establish the Soil Discrimination Index, a flag to enhance the robustness of the MTCI at low canopy covers. Following work utilised data from two field campaigns, SicilyS2EVAL and SEN3Exp, to compare LAI and LCC measurements with synthetic S-2 data generated from contemporaneous hyperspectral acquisitions. Two new methods were proposed to estimate the biophysical variables of vegetation using S-2, IRECI which incorporates four bands situated on and either side of the RE and S2REP, a version of Red Edge Position (REP) estimation for S-2 using linear interpolation. Next the application of MTCI using S-2 and S-3 was investigated as well as the feasibility to downscale between the sensors. With regards to S-3 the view angle of the sensor will be tilted 12.58° away from the sun to minimise glint. This will lead to a maximum observed view angle of 55.6° , 15.6° higher than that of MERIS while application of the MTCI using S-2 is more complicated due to the large spectral differences the sensor has with Envisat MERIS. The combined effect means that S2TCI will be between 44.28% and 68.8% higher than the MTCI and an initial formula has been provided to convert between the indices. Findings also indicate that using MSI band 7 will be more favourable than band 6 in the S2TCI formula.

Successfully downscaling between S-3 and S-2 could increase the temporal coverage of S-2 dramatically. A first trial of this was achieved via fusion modelling that synergised MERIS and CHRIS data to represent S-3 and S-2 respectively. Synthetic S-2 imagery was generated from S-3 images at times of the year where high resolution imagery was not available. Results strongly indicate that the time of the year that S-2 and S-3 imagery is linked will be of critical importance and optimal results were achieved when the canopy was at maximum density. Finally a test application of the Sentinel satellites was conducted in the evergreen forests of Edo, a state in Nigeria, to assess degradation using a seven year MERIS dataset within the REDD+ framework. By using the MTCI to estimate forest cover it was found that between 2005 and 2011 99.09 km² of evergreen forest had been completely deforested while 415.71 km² had been significantly degraded. These figures are between 4% and 16.4% of the total area of evergreen forest that had covered the Edo state in 2005. It was shown that it is possible to indicate deforestation by year using MERIS data with a method easily quantifiable using threshold analysis. By using the default Tier 1 guidance values of AGB from the IPCC the MTCI was successfully used to predict the total loss of potential carbon sequestration. It was estimated that the primary forests of the Edo state sequestered 131,095 t less of carbon in 2011 than in 2005.

Table of Contents

ABSTRACT	I
TABLE OF CONTENTS	II
LIST OF FIGURES	V
LIST OF TABLES	IX
DECLARATION OF AUTHORSHIP	X
ACKNOWLEDGMENTS	XI
DEFINITIONS AND ABBREVIATIONS	XII
CHAPTER 1: INTRODUCTION	1
1.1. BACKGROUND	1
1.2. AIMS OF THE RESEARCH	2
1.2.1. <i>Objectives of the Research</i>	3
1.3. CHAPTER OVERVIEW	4
CHAPTER 2: LITERATURE REVIEW	8
2.1. MEASUREMENTS OF VEGETATION BIOPHYSICAL VARIABLES.....	8
2.1.1. <i>Leaf Pigments</i>	8
2.1.2. <i>Leaf Area Index</i>	9
2.2. SPECTRAL PROPERTIES OF VEGETATION	10
2.3. SATELLITE SENSORS	11
2.3.1. <i>Envisat MERIS</i>	11
2.3.2. <i>Copernicus Program</i>	13
2.3.3. <i>Sentinel 2</i>	13
2.3.4. <i>Sentinel 3</i>	14
2.3.5. <i>Non-Operational/Commercial Sensors with RE Capabilities</i>	15
2.4. IMPORTANCE OF THE RED EDGE POSITION	16
2.4.1. <i>The Red Edge</i>	16
2.4.2. <i>The MTCI</i>	17
2.5. RETRIEVAL OF BIOPHYSICAL VARIABLES FROM SATELLITE DATA	18
2.5.1. <i>Modelling</i>	18
2.5.2. <i>Use of Vis</i>	20
2.6. APPLICATIONS OF SATELLITE DERIVED BIOPHYSICAL VARIABLES.....	22
2.6.1. <i>Global Climate Models</i>	22
2.6.2. <i>Monitoring Forest</i>	22
2.6.3. <i>Precision Agriculture</i>	23
2.7. UNCERTAINTY IN VEGETATION INDICES.....	24
2.7.1. <i>Universal Uncertainties</i>	26
2.7.2. <i>Vegetation Specific Uncertainties</i>	30

2.8.	CONCLUSION	31
CHAPTER 3:	THE SOIL DISCRIMINATION INDEX AND ITS APPLICATION TO THE MTCI	34
3.1.	INTRODUCTION	34
3.1.1.	<i>Discussion on Current Soil Discriminators</i>	34
3.2.	DEVELOPMENT OF A SUITABLE MEASURE TO DISTINGUISH SOIL FOR VEGETATION INDICES AND SPECIFICALLY THE MTCI	36
3.2.1.	<i>Study Sites</i>	36
3.2.2.	<i>Data and Methods</i>	38
3.3.	DEVELOPMENT OF THE SOIL DISCRIMINATION INDEX	40
3.4.	DEVISING A THRESHOLD	48
3.5.	VALIDATION OF THE SOIL DISCRIMINATION INDEX	52
3.6.	CONCLUSIONS	55
CHAPTER 4:	EVALUATING THE CAPABILITIES OF SENTINEL-2 FOR QUANTITATIVE ESTIMATION OF BIOPHYSICAL VARIABLES IN VEGETATION	56
4.1.	INTRODUCTION	56
4.2.	DATA AND METHODS	59
4.2.1.	<i>PROSAIL Model Data</i>	61
4.2.2.	<i>Airborne Acquisitions</i>	63
4.2.3.	<i>Band Weighting and Data Processing</i>	63
4.3.	DESIGNING OPTIMAL INDICES FOR BIOPHYSICAL VARIABLE RETRIEVAL FROM SENTINEL-2 DATA	64
4.3.1.	<i>Relationship Between Spectral Reflectance Generated from PROSAIL and Canopy Chlorophyll Content.</i>	64
4.3.2.	<i>Relationship between Spectral Reflectance and Canopy Chlorophyll Content for SicilyS2EVAL.</i>	65
4.3.3.	<i>Relationship between Spectral Reflectance and Canopy Chlorophyll Content for SEN3Exp ..</i>	67
4.3.4.	<i>Comparison between Field Campaign Data and PROSAIL.</i>	67
4.3.5.	<i>Suitability of S-2 Bands for Retrieval of Biophysical Variables.</i>	70
4.3.6.	<i>New Vegetation Indices for S-2</i>	71
4.4.	EVALUATION OF THE SPECTRAL INDICES	72
4.4.1.	<i>Leaf Chlorophyll Concentration</i>	72
4.4.2.	<i>Leaf Area Index.</i>	73
4.4.3.	<i>Canopy Chlorophyll Content</i>	74
4.5.	CONCLUSIONS	75
CHAPTER 5:	INVESTIGATING THE OPPORTUNITIES FOR APPLICATION OF MTCI USING SENTINEL-2 AND SENTINEL-3 AND THE FEASIBILITY TO DOWNSCALE	76
5.1.	INTRODUCTION	76
5.2.	CONTINUATION OF THE MTCI USING S-3	79
5.2.1.	<i>Spectral Changes</i>	79
5.2.2.	<i>View Angle Changes</i>	80

5.3.	ESTIMATION OF THE MTCI USING S-2.....	81
5.3.1.	<i>Spectral Changes</i>	82
5.3.2.	<i>Comparison of NIR S-2 Bands 6 and 7</i>	87
5.3.3.	<i>Impact of Each Band on the S2TCI Output</i>	87
5.3.4.	<i>S2TCI</i>	92
5.4.	FEASIBILITY TO DOWNSCALE TO S-2 FROM S-3 AND MERIS DATA.....	94
5.4.1.	<i>Data and Methods</i>	94
5.4.2.	<i>Results</i>	103
5.5.	CONCLUSIONS.....	106
CHAPTER 6: QUANTIFICATION OF CHANGE IN PHOTOSYNTHETIC CAPABILITIES OF DEFORESTED LOCATIONS AND OPPORTUNITY FOR FUTURE RECOVERY UNDER THE REDD+ FRAMEWORK.....		108
6.1.	INTRODUCTION.....	108
6.1.1.	<i>Study Location</i>	109
6.2.	DATA AND METHODS	110
6.3.	TOTAL DEFORESTATION IN THE EDO STATE	112
6.4.	DERIVING DEFORESTATION BY YEAR	116
6.5.	ESTABLISHING RECOVERY OF THE FOREST.	120
6.6.	PREDICTING THE LOSS OF POTENTIAL CARBON SEQUESTRATION.	123
6.7.	CONCLUSIONS.....	124
CHAPTER 7: CONCLUSIONS AND FUTURE WORK.....		126
7.1.	SUMMARY.....	126
7.2.	KEY OUTCOMES.....	130
7.3.	LIMITATIONS.....	131
7.4.	FUTURE WORK.....	132
7.4.1.	<i>Enhanced Field Campaign Procedure</i>	132
7.4.2.	<i>Downscaling Method with Multiple Pairings</i>	133
7.4.3.	<i>Retrieval of Biophysical Variables</i>	133
7.4.4.	<i>Further Comparison of OTCI and S2TCI</i>	133
7.5.	CONCLUDING REMARKS	134
REFERENCES.....		136

List of Figures

Figure 1.1: Chapter Overview of the thesis highlighting where datasets are utilised.....	4
Figure 2.1: Example of a typical vegetative spectra. Figure shows average spectral reflectance of 50 corn fields during July-August 2005 in central-western Iowa.....	10
Figure 2.2: Schematic representation of PROSAIL: the coupling of the leaf (PROSPECT) and canopy (SAIL) models. First presented in the MTCI-EVAL project (Watmough et al. 2011)	19
Figure 2.3: Flow diagram highlighting the uncertainties affecting the retrieval of the biophysical variables of vegetation.....	25
Figure 2.4: 50 corn (blue) and 50 soybean (red) averaged bimonthly reflectances derived from GLOBCOVER MERIS FR imagery for 2005.....	28
Figure 3.1: Test site location north west of Des Moines, Iowa, North America.....	37
Figure 3.2: Test site location surrounding Dalhart, Texas, North America.....	37
Figure 3.3: MERIS band normalised spectral response functions.	38
Figure 3.4: Synthetic MERIS band spectral reflectances for various soil types derived from the ASTER spectral soil library.....	39
Figure 3.5: High spatial resolution (56 m) crop cover information from the USDA NASS for 2005 (left) and false colour FR (300 m) MERIS data (right) showing site selection and standard field size (1500 m x 1500 m).	40
Figure 3.6: Landsat image courtesy of Google Earth (Landsat) of the study site in Dalhart Texas (left) where SDI distribution analysis was performed with the corresponding MERIS image (right).	40
Figure 3.7: Applying the MTCI to a selection of soils from the ASTER soil library.....	41
Figure 3.8: 50 corn and 50 soybean averaged bimonthly reflectances derived from GLOBCOVER MERIS FR imagery for 2005.....	42
Figure 3.9: 50 corn (blue) and 50 soybean (red) averaged bimonthly reflectances derived from GLOBCOVER MERIS FR imagery for 2005.....	43
Figure 3.10: NDVI and MTCI values for 50 corn and 50 soybean locations in Iowa for 2005.....	44
Figure 3.11: Bimonthly average surface reflectances for 100 corn and soybean sites in Iowa for 2005.	45
Figure 3.12: Percentage difference between initial vegetation growth (bimonth 3) and soil dominated bimonths (1, 2 and 6).	46
Figure 3.13: Example of discrimination between sparse canopy cover using the SDI for three target locations in Iowa. Series one (purple) and three (orange) show bare soil pixels for bimonth 6 in Iowa; series two (blue) shows a sparsely vegetated location in bimonth 3.....	47

Figure 3.14: SDI values for 40 example soil reflectances from the ASTER spectral soil library.....	49
Figure 3.15: Graph to show the percentage of total pixels from the Dalhart MERIS scene that are flagged at a specific SDI threshold and their MTCI value.	50
Figure 3.16: Comparing the use of SDI < 0.9 as a flag to account for soil pixels in the MTCI algorithm on corn locations in Iowa 2005. Spectral reflectances shown are for pixels in corn fields taken from FR MERIS data as previously highlighted.....	51
Figure 3.17: Location of the agricultural test site surrounding Albacete.....	52
Figure 3.18: Location of the forest test site to the south-west of Albacete.	52
Figure 3.19: Average MTCI of the agricultural and forest test sites in Albacete, Spain for 2004. ...	53
Figure 4.1: Location of test site (courtesy of google earth, Landsat 04/10/2013) with flight lines added from the SEN3Exp campaign acquisition report (SEN3Exp 2011).	60
Figure 4.2: SicilyS2EVAL test site with example of the crop canopy.....	61
Figure 4.3: Sampling strategy for LAI measurements from SicilyS2EVAL campaign. 16 readings were taken below the canopy spread throughout the 10 x 10 m sampling area centred on a GPS coordinate. Two above the canopy readings were taken to adjust for changes in solar intensity..	62
Figure 4.4: Comparing the correlation coefficient (R) between spectral reflectance and canopy chlorophyll content with changing wavelength for both PROSAIL datasets.....	65
Figure 4.5: Comparing the correlation coefficient (R) between spectral reflectance and canopy chlorophyll content with changing wavelength for the SicilyS2EVAL and SEN3Exp field campaigns with indications of S-2 band positions and dashed lines to show where p = 0.....	66
Figure 4.6: Comparing the correlation coefficient (R) between canopy chlorophyll content and spectral reflectance for the SEN3Exp field campaign and SEN3Exp PROSAIL with changing wavelength.	68
Figure 4.7: Comparison of PROSAIL SEN3Exp (b and d) and SEN3Exp field data (a and c) at 680nm (a and b) and 730nm (c and d).....	69
Figure 4.8: Coefficient of determination comparisons between MTCI, S2REP and LCC.	72
Figure 4.9: IRECI and NDI45 compared for LAI from SEN3Exp and SicilyS2EVAL field campaigns. ...	73
Figure 4.10: IRECI, NDI45, NDVI and PSSR compared to canopy chlorophyll content for field data from SicilyS2EVAL and SEN3Exp field campaigns.	74
Figure 5.1: Positions of MERIS reflectance bands with width indicators overlaid onto the spectra of sunflower ESU from Sen3EXP measured using the hyperspectral AISA Eagle sensor.....	78
Figure 5.2: Positions of S-2 reflectance bands with width indicators overlaid onto the spectra of sunflower ESU from Sen3EXP measured using the hyperspectral AISA Eagle sensor.....	78
Figure 5.3: Positions of S-3 reflectance bands with width indicators overlaid onto the spectra of sunflower ESU from Sen3EXP measured using the hyperspectral AISA Eagle sensor.....	79

Figure 5.4: Representation of the view angle across a scene using MERIS and OLCI to emphasise the tilt of S-3 and the resulting increased view angle compared to MERIS.	80
Figure 5.5: Average MTCI output of dataset over the 2009 growing season.	80
Figure 5.6: OTCI and MTCI generated from PROSAIL data over an entire growing season for example locations in Barrax, Spain.	81
Figure 5.7: S-2 and MERIS band positions located on a CASI hyper-spectral reflectance curve between 500-800 nm for a potato ESU evaluated during the SEN3Exp field campaign.	82
Figure 5.8: MERIS and S-2 spectral bands located near the RE generated from CASI hyperspectral data of a potato ESU evaluated during the SEN3Exp field campaign. Annotated with absolute reflectance values and bandwidth indicators.	83
Figure 5.9: Comparing percentage change in absolute reflectance from MERIS band 8 to Sentinel-2 band 4 by chlorophyll content for 33 ESUs from the SEN3Exp field campaign.	84
Figure 5.10: Comparing percentage change in absolute reflectance from MERIS band 9 to Sentinel-2 band 5 by chlorophyll content for 33 ESUs from the SEN3Exp field campaign.	85
Figure 5.11: Comparing percentage change in absolute reflectance from MERIS band 10 to MSI band 6 by chlorophyll content for 33 ESUs from the SEN3Exp field campaign.	86
Figure 5.12: Comparing percentage change in absolute reflectance from MERIS band 10 to MSI band 7 by chlorophyll content for 33 ESUs from the SEN3Exp field campaign.	87
Figure 5.13: Correlation of the MTCI with chlorophyll content for the SEN3Exp field campaign.	88
Figure 5.14: Changing relative percentage difference between the TestTCI1 and the MTCI with chlorophyll content taken from the SEN3Exp field campaign.	89
Figure 5.15: Comparing the correlation of the MTCI and the TestTCI1.	89
Figure 5.16: Changing relative percentage difference between the TestTCI2 and the MTCI with chlorophyll content taken from the SEN3Exp field campaign.	90
Figure 5.17: Changing relative percentage difference between the TestTCI3 and the MTCI with chlorophyll content taken from the SEN3Exp field campaign.	91
Figure 5.18: Changing relative percentage difference between the S2TCI and the MTCI with chlorophyll content taken from the SEN3Exp field campaign.	92
Figure 5.19: Comparison between S2TCI and the MTCI derived from CASI hyperspectral reflectance data for the SEN3Exp field campaign.	93
Figure 5.20: Location of Barrax test site in Spain. Landsat image (04/10/2013) courtesy of NOAA, accessed via Google Earth.	96
Figure 5.21: CHRIS true colour image of Barrax test site (16/07/2004).	96
Figure 5.22: All CHRIS acquisitions for the Barrax test site. A geometrically similar red ring has been added to aid visual comparison.	98

Figure 5.23: Crop map from SPARC 2004 taken directly from the final acquisition report (ESA 2004) highlighting the various crops and their locations.	101
Figure 5.24: Predicted CHRIS imagery using STARFM for the July base pair for the NIR.	102
Figure 5.25: Base pair performance at predicting NDVI for alfalfa.	103
Figure 5.26: Base pair performance at predicting NDVI for corn.	104
Figure 6.1: Global Land Cover of the Edo State Nigeria generated using GLC2000 data from Mayaux et al. (2003).	110
Figure 6.2: Monthly cloud cover as a percentage of Nigeria’s total land area for 2005, 2007, 2009 and 2011 using the MOD06 product.	111
Figure 6.3: Comparison of MTCI histograms for evergreen forests in Edo between 2005 (left) and 2011 (right).	112
Figure 6.4: MTCI difference for evergreen forest pixels between 2005 and 2011, Edo state, Nigeria.	113
Figure 6.5: MTCI loss in evergreen forest for the Edo state between 2005-2011. Locations of test sites are provided for further discussion.	115
Figure 6.6: MTCI pixel differences in the Edo state for a) 2005-2006 and b) 2006-2007.	116
Figure 6.7: Deforestation by year for the Edo State, Nigeria.	118
Figure 6.8: Annual deforestation at sites a, b and e.	119
Figure 6.9: MERIS (300 m) imagery highlighting three point deforestation during 2005-2011 for site A.	119
Figure 6.10: 2005-2006 deforestation test site locations.	121
Figure 6.11: Average MTCI of forest calibration test site.	122
Figure 6.12: Monitoring the MTCI of test sites after a deforestation event.	122
Figure 6.13: Average MTCI of evergreen forest for the Edo state between 2005 and 2011 based on land category from GLC2000 data.	124

List of Tables

Table 2.1: Details of the spectral characteristics of MERIS bands in operational mode.	12
Table 2.2: Spectral bands of S-2 MSI.....	14
Table 2.3: Spectral bands of S-3 OLCI.	15
Table 2.4: Example of input variables for PROSAIL.....	19
Table 2.5: Summary of Key Vegetation Indices.	21
Table 3.1: Table to indicate key crop production times for Iowa in 1996 and 2009.	42
Table 3.2: Table to summarise performance of the SDI for the agricultural test site.	53
Table 3.3: Table to summarise performance of the SDI for the forest test site.	54
Table 4.1: Spectral bands of Sentinel-2 MSI.	58
Table 4.2: A list of Vegetation Indices that have been analysed for use with Sentinel-2 using field data.	59
Table 4.3: Biophysical parameters chosen for PROSAIL data set.	61
Table 4.4: Summary of field campaign data used in analysis.	63
Table 4.5: Outcomes of correlation signal investigation.	67
Table 4.6: Coefficient of determination results of each Vegetation Index for varying field data sets and biophysical variables, light green highlights where $0.7 < R^2 < 0.8$ and dark green highlights where $0.8 < R^2$. Results denoted with * have p values of <0.001	72
Table 5.1: Summary of Spectral band of MERIS, Sentinel-2 and Sentinel 3.	77
Table 5.2: Most suitable CHRIS bands as surrogate data of Sentinel 2.	95
Table 5.3: Summary of CHRIS and MERIS images used and the gap between possible base pairs.	97
Table 5.4: Linking of nearest spectral bands between sensors.	100
Table 5.5: Average Difference in NDVI values for each pairing.	104
Table 5.6: Average difference in MTCI values for each pairing except November.....	105
Table 6.1: Details of MERIS Acquisitions used in analysis.....	112
Table 6.2: Deforestation in the Edo State between 2005-2011 *based from 2000 GLC estimates of evergreen forest	114
Table 6.3 Differences in average MTCI between 2005 and 2011.	117
Table 6.4: Size of primary forest deforestation test sites in the Edo state.	121
Table 6.5: Total loss of AGB and potential sequestration for the Edo region between 2005 and 2011 due to deforestation of primary forests.	123

Declaration of Authorship

I, William James Frampton, declare that the thesis entitled ‘Evaluating the Potential of Sentinel Optical Sensors for the Retrieval of Vegetation Biophysical Variables’ and the work presented in the thesis are both my own and have been generated as the result of my own original research. I confirm that:

- This work was done wholly while in candidature for a research degree at this University.
- Where any part of this thesis has previously been submitted for a degree or any other qualification at this University or any other institution, this has been clearly stated.
- Where I have consulted the published work of others accreditation has always been given.
- Where I have quoted from the work of others, the source is always given. With the exception of such quotations, this thesis is entirely my own work.
- I have acknowledged all main sources of help.
- Where the thesis is based on work done by myself jointly with others, I have made clear exactly what was done by others and what I have contributed myself.
- Parts of this work have been published as:

Journal Paper

FRAMPTON, W. J., DASH, J., WATMOUGH, G. R., and MILTON, E. J., 2013, Evaluating the capabilities of Sentinel-2 for quantitative estimation of biophysical variables in vegetation. *Journal of Photogrammetry and Remote Sensing*, **82**, 83-92.

Conference Proceedings

FRAMPTON, W. J., VUOLO, F., DASH, J. D., MILTON, E. J., 2010, Quantifying the effect of soil on retrieval of chlorophyll content from remotely sensed data. In: *Proceedings of the 2010 RSPSoc and Irish Earth Observation Symposium ‘Visualising the World: From the Sea-bed to the Cloud-tops’*, 1st-3rd of September, Cork, Ireland.

FRAMPTON, W. J., DASH, J., WATMOUGH, G. R., and MILTON, E. J., 2011, Estimating vegetation chlorophyll content from ESA’s Sentinel-2 Multi-Spectral Instrument. In, *Annual Conference of the Remote Sensing and Photogrammetry Society: Earth Observation in a Changing World (RSPSoc 2011)*, 13th-15th of September, Bournemouth, GB.

Signed:

Date:.....

Acknowledgments

I would like to thank my supervisors Dr. Jadu Dash and Prof. Ted Milton for their vital guidance and encouragement during every stage of this thesis. Without their extensive knowledge and open nature none of this would have been possible.

I'm indebted to the School of Geography at the University of Southampton not only as an establishment where I have happily spent the last seven years but for the joint financial support of this work along with the European Space Agency (ESA).

I'd quickly like to highlight the establishments that provided the data that has enabled this research: ESA for MERIS, CHRIS and related field campaign data, the National Aeronautical and Space Administration (NASA) for MODIS and soil records and finally NERC Airborne Research and Survey Facility for airborne acquisitions.

I especially want to thank Dr. Francesco Vuolo for his role as a surrogate supervisor during his time at Southampton and as a true friend, especially so during field trips. I also want to thank Dr. Gary Watmough for his joint work in related projects.

Finally I want to thank my family for their love, understanding and support throughout my academic studies. I'm particularly grateful to my father, a true role model and anchor of the family as well as my mother who has always put things into perspective, motivated and given so much for me. Thank you Tatyana for all that you do, the future is brighter knowing you are with me.

Definitions and Abbreviations

ARSF: Airborne Research & Survey Facility

ARVI: The Atmospherically Resistant Vegetation Index

ASTER: Advanced Spaceborne Thermal Emission and Reflection Radiometer

ATSR: Along-Track Scanning Radiometer

AVHRR: Advanced Very High Resolution Radiometer

BIOME-BGC: BioGeochemical Cycles model

BOA: Bottom of Atmosphere

ECVs: Essential Climate Variables

Envisat: Environmental Satellite

EO: Earth Observation

EOLI: The Earth Observation Link

ESUs: Elemental Sampling Units

EVI: Enhanced Vegetation Index

FAO : Food and Agriculture Organisation

FAPAR: Fraction of Absorbed Photosynthetically Active Radiation

FOV: Field of View

GCMs: Global Climate Models

GCOS: Global Climate Observing System

GD: Green Difference

GLC: Global Land Cover

GMES: Global Monitoring for Environment and Security

GPP: Gross Primary Productivity

IRECI: Inverted Red Edge Chlorophyll Index

JRC: Joint Research Centre

LAD: Leaf Angle Distribution

LCC: Leaf Chlorophyll Concentration

MCARI: Modified Chlorophyll Absorption Reflectance Index

MERIS: The Medium Resolution Imaging Spectrometer

MODIS: MODerate-resolution Imaging Spectroradiometer

MRV: Monitoring Reporting and Verification

MSAVI: Modified Soil Adjusted Vegetation Index

MSI: Multi-Spectral Instrument

NASS: National Agricultural Statistics Service

NERC: Natural Environment Research Council

NIR: Near-Infrared

OLCI: Ocean and Land Colour Imager

OTCI: Ocean and Land Colour Imager Terrestrial Chlorophyll Index

PAR: Percentage of Absorbed Radiation

PSSRa: Pigment Specific Simple Ratio

RE: Red Edge

REDD+: Reducing Emissions from Deforestation and Degradation

RSPSoc: Remote Sensing and Photogrammetry Society

S-2: Sentinel-2

S2REP: Sentinel 2 Red Edge Position

S-3: Sentinel 3

SAVI: Soil Adjusted Vegetation Index

SDI: Soil Discrimination Index

SWIR Short-Wave Infrared

SPARC: SPectra bARrax Campaign

SPOT: Satellite Pour l'Observation de la Terre

TOC: Top of the Canopy

TRAC: Tracing Radiation and Architecture of Canopies

UNEP: United Nations Environment Programme

UNFCCC: United Framework Convention on Climate Change

USDA: United States Department of Agriculture

VI: Vegetation Index

VIs: Vegetation Indices

WDVI: Weighted Difference Vegetation Index

Chapter 1: Introduction

1.1. Background

In recent years a heightened awareness of the vulnerability of our environment to anthropogenic activity combined with the need for better management of natural resources to sustain a rapidly growing population has drawn attention to the importance satellite remote sensing. Remotely sensed estimates of the biophysical variables of vegetation have many uses at many spatial scales. They provide key inputs into global climate models, regional monitoring of desertification and deforestation and at a field scale as a commercial tool in precision agriculture. Chlorophyll, a green pigment in vegetation, is a critical component of photosynthesis; consequently a measure of chlorophyll can be indicative of vegetation health and the photosynthetic capacity of a given area. Remote sensing of vegetation depends on the biophysical composition of vegetation giving it unique spectral properties. Chlorophyll strongly absorbs energy in the blue and red parts of the spectrum while leaf internal structure determines reflectance in the near-infrared (NIR). This resulting contrast in reflectance over the 680-750 nm range is referred to as the red edge (RE). The position of the RE, defined as the point of greatest change in reflectance, is related to total chlorophyll content (Collins 1978; Horler et al. 1983). A measure of red edge position (REP) can be retrieved remotely at a global scale through spaceborne sensors that contain narrow bands in the 680-750 nm range. The Medium Resolution Imaging Spectrometer (MERIS) is such a sensor aboard the Environmental Satellite (Envisat) which was launched on the 1st of March 2002 and operated until the 8th of April 2012. The MERIS sensor measured the Earth's surface spectral reflectance features every 3 days in 15 spectral bands between 412.5-900 nm. These bands can in turn be used by the MERIS Terrestrial Chlorophyll Index (MTCI), a vegetation index (VI), to estimate REP and consequently provide a surrogate measure of chlorophyll content. The MTCI has been implemented operationally as a full L2 MERIS product.

Each new generation of satellites provides opportunities to refine the retrieval of biophysical variables at enhanced scales. The next generation of satellites will be part of Europe's Copernicus programme which was previously known as Global Monitoring for Environment and Security (GMES). Of the total five Sentinel missions planned for with Copernicus, the Sentinel-2 (S-2) and Sentinel-3 (S-3) missions have a key focus on global vegetation monitoring and are capable of making measurements in the RE. The S-3 Ocean and Land Cover Imager (OLCI), tentatively planned for launch in mid-2015, will ensure continuation of the 10 year long MERIS dataset into the future with the discontinuation of Envisat. Such long running datasets are paramount in providing perspective for investigations into surface and climate change and the impacts they

William James Frampton

bring for ecological viability and phenological transitions in vegetation (Zhu et al. 2013). The S-2 Multi-Spectral Instrument (MSI) is set for launch in April 2015 and will enable measurements in the RE portion of the electromagnetic spectrum at a greatly enhanced spatial resolution of 20m. There is much uncertainty in the characterisation of heterogeneous landscapes using MERIS data at full resolution of 300 m due to pixels of mixed vegetation type. The issue is particularly relevant in Europe due to irregular and small field sizes in agriculture compared to agriculture in other parts of the world. The enhanced spatial resolution of S-2 should mitigate this issue, reducing mixed class anomalies and incorrectly classified pixels.

1.2. Aims of the Research

This study aims to investigate the use of remote sensing to monitor vegetation condition and distribution through time while evaluating the scope for improvement using the upcoming Sentinel series over current methods and sensors. One of the key objectives of the analysis will be to advance the MERIS Terrestrial Chlorophyll Index (MTCI) which was adopted operationally as a full MERIS product. It is unknown specifically how the MTCI will perform at the increased spatial (20 m) and spectral resolutions available via S-2 with multiple bands situated on and around the RE; a region sensitive to chlorophyll concentration. Furthermore there is scope for investigation into creating a synergy product that combines the attractive properties of S-2 with the greater spatial coverage and temporal resolution of S-3. This research is important as there are many scientific and commercial applications that rely on local, regional and global estimations of the biophysical variables of vegetation. Consequently there is room for detailed analysis into the opportunities the future Sentinel sensors bring when combined with robust algorithms for the practice of vegetative remote sensing. Research therefore shall be divided into three parts. Firstly, the study aims to investigate the opportunities and implications that the future sensors S-2 and S-3 have for the MTCI and also their compatibility. Secondly, the study aims to investigate the possibility for retrieval of biophysical parameters for S-2 and S-3 and the key scientific opportunities of these future sensors. Finally the work aims to apply research findings and develop methodology within the Reducing Emissions from Deforestation and Degradation (REDD+) framework.

This thesis builds upon research conducted at the University of Southampton during the ESA funded MTCI-EVAL project which was focused on validation of the MTCI using the MERIS platform with additional preliminary investigations into application of the MTCI to S-2 and S-3. Each chapter is a novel piece of work conducted separate to the MTCI-EVAL project and where data or figures are incorporated they are clearly referenced.

1.2.1. Objectives of the Research

- 1 Review existing literature on the retrieval of vegetation biophysical variables with an emphasis on operational applicability at a global scale.
- 2 Investigate the uncertainties in retrieval of biophysical variables using remotely sensed data and assess if any of these uncertainties can be mitigated through algorithm changes or the development of flags with specific investigation for the MTCI. Reduction in associated uncertainty and accounting for unknown uncertainty in the retrieval of biophysical variables is paramount in the development of methods which are as robust as possible.
- 3 Evaluate S-2 and the Multispectral Instrument (MSI) for the opportunities they bring for the EO of vegetation and specifically the retrieval of biophysical parameters. Current algorithms will need to be assessed using an extensive and suitable dataset which will need to match the high spatial and spectral characteristics of the sensor. Improved methods for retrieval of biophysical parameters using S-2 should be proposed if justified enhancements are observed.
- 4 Investigate the opportunities for application of MTCI on S-3 and the feasibility to downscale to S-2 creating a synergy product. If possible creation of a synergy product of S-2 and S-3 could allow the high spatial scale of S-2 with the rapid temporal scale of S-3.
- 5 Apply scientific findings of previous objectives to develop methodology to measure change in the photosynthetic capability of forested areas to demonstrate the operational use of Earth Observation data within the REDD+ framework.

1.3. Chapter Overview

<p>CHAPTER 1: Introduction</p>	<p>DATASETS:</p> <ul style="list-style-type: none"> • ASTER Soil Library • Iowa Globcover • MERIS: Dalhart Texas • MERIS: Albacete <ul style="list-style-type: none"> • SEN3Exp • SicilyS2EVAL <ul style="list-style-type: none"> • SEN3Exp • SPARC 2004 <ul style="list-style-type: none"> • MODIS: MOD06 • MERIS: Edo, Nigeria
<p>CHAPTER 2: Literature Review</p>	
<p>CHAPTER 3: The Soil Discrimination Index and its Application to the MTCI</p>	
<p>CHAPTER 4: Evaluating the Capabilities of Sentinel-2 for Quantitative Estimation of Biophysical Variables in Vegetation</p>	
<p>CHAPTER 5: Investigating the Opportunities for Application of MTCI using Sentinel-2 and Sentinel-3 and the Feasibility to Downscale</p>	
<p>CHAPTER 6: Quantification of Change in Photosynthetic Capabilities of Deforested Locations and Opportunity for Future Recovery under the REDD+ Framework</p>	
<p>CHAPTER 7: Conclusions and Future work</p>	

Figure 1.1: Chapter Overview of the thesis highlighting where datasets are utilised.

William James Frampton

Chapter 2 – Literature Review.

An initial literature review was performed on material relevant to the research objectives in the first few months of the project timeframe. Since then this has been adjusted and updated as required resulting in the current format. A particular focus was put on fully reviewing the Sentinel satellites, their prospects and possible applications. Furthermore an investigation into uncertainties associated with the retrieval of vegetative biophysical variables was performed that included the following topics: hardware deterioration, view geometry, atmospheric variance, background condition, canopy structure, spatial resolution and phenology.

Chapter 3 – The Soil Discrimination Index and its Application to the MTCI.

As a result of the literature review and preliminary investigations it was found that the background variation can have a significant effect on the output of VIs and especially the MTCI. It was decided that a flag should be developed for the MTCI product to account for uncertainty due to soil without changing its formulation. Consequently a dataset of background reflectances was acquired and compared to a long running dataset of agricultural land in Iowa. The output was a new Soil Discrimination Index (SDI) which should enhance the robustness of the MTCI at low canopy covers and subsequently an initial validation was performed in Texas and the Iberian Peninsula. Results of the analysis were presented in September 2010 at the Remote Sensing and Photogrammetry Society (RSPSoc) 2010 Conference and an extended abstract, 'Quantifying the Effect of Soil on Retrieval of Chlorophyll Content from Remotely Sensed Data', was accepted for inclusion into the proceedings (Frampton et al. 2010).

Chapter 4 – Evaluating the Capabilities of Sentinel-2 for Quantitative Estimation of Biophysical Variables in Vegetation.

During a review of current of field campaigns that involved ground chlorophyll content measurements the majority were found to be insufficient to achieve one of the key objectives of this research; evaluating the opportunities of S-2 for the retrieval of biophysical parameters, due to the spatial and spectral characteristics of S-2. Consequently a data collection field campaign, SicilyS2EVAL, was planned and conducted in May 2010. It involved 2025 Minolta SPAD-502™ measurements of 225 plants across 25 elemental sampling units (ESUs) of ground measurements of leaf chlorophyll concentration (LCC) as well as 450 leaf area index (LAI) measurements using a Li-Cor LAI-2000. Contemporaneous hyperspectral airborne data acquired by the Natural Environment Research Council (NERC) Airborne Research & Survey Facility (ARSF) from which synthetic S-2 data could be generated. In addition to this, another dataset, SEN3Exp which took place in June 2009 in Barrax, Spain was acquired from the European Space Agency (ESA). Current

William James Frampton

methods and algorithms were considered for retrieval of LAI, LCC and canopy chlorophyll content and two novel algorithms presented; Sentinel-2 Red Edge Position (S2REP) and the Inverted Red Edge Chlorophyll Index (IRECI). The findings were presented as a talk at RSPSoc 2011 and accepted as an extended abstract for inclusion in the conference proceedings (Frampton et al. 2011). A further version of the chapter was published as FRAMPTON, W. J., DASH, J., WATMOUGH, G. R., and MILTON, E. J., 2013, Evaluating the capabilities of Sentinel-2 for quantitative estimation of biophysical variables in vegetation. *Journal of Photogrammetry and Remote Sensing*, **82**, 83-92.

Chapter 5 – Investigating the Opportunities for Application of MTCI using S-2 and S-3 and the Feasibility to Downscale

This chapter investigated the application of MTCI using S-2 and S-3 as well as the feasibility to downscale between the sensors. With regards to S-3 the view angle of the sensor will be tilted 12.58° away from the sun to minimise glint. This will lead to a maximum observed view angle of 55.6° , 15.6° higher than that of MERIS while application of the MTCI using S-2 is more complicated due to the large spectral differences the sensor has with Envisat MERIS. The combined effect means that S2TCI will be between 44.28% and 68.8% higher than the MTCI and an initial formula has been provided to convert between the indices. Findings also indicate that using MSI band 7 will be more favourable than band 6 in the S2TCI formula. Successfully downscaling between S-3 and S-2 could increase the temporal coverage of S-2 dramatically. A first trial of this was achieved via fusion modelling that synergised MERIS and CHRIS data to represent S-3 and S-2 respectively. Synthetic S-2 imagery was successfully generated from S-3 images at times of the year where it was not available achieving a relative accuracy of 20-50%. Results strongly indicate that the time of the year that S-2 and S-3 imagery is linked will be of critical importance and the best results were achieved when the canopy was at maximum density.

Chapter 6 – Quantification of Change in Photosynthetic Capabilities of Deforested Locations and Opportunity for Future Recovery under the REDD+ Framework

Chapter 6 tested an application of the Sentinel satellites in the evergreen forests of Edo state, Nigeria. Research assessed forest degradation using a seven year MERIS dataset within the REDD+ framework. By using the MTCI to estimate forest cover it was found that between 2005 and 2011 99.09 km^2 of evergreen forest had been completely deforested while 415.71 km^2 had been significantly degraded. These figures are between 4% and 16.4% of the total area of evergreen forest that had covered the Edo state in 2005. It was shown that it is possible to indicate deforestation by year using MERIS data with a method easily quantifiable using threshold analysis. By using the default Tier 1 guidance values of above-ground biomass (AGB) from the IPCC the

William James Frampton

MTCI was successfully used to predict the total loss of potential carbon sequestration. It was estimated that the primary forests of the Edo state sequestered 131,095 t less of carbon in 2011 than in 2005.

Chapter 7 – Conclusions and Future Work

Chapter 7 provides a summary of the achievements of this research, highlights key findings and proposes several new lines of investigation for future work.

Chapter 2: Literature Review

2.1. Measurements of Vegetation Biophysical Variables

Biophysics is the concept of combining physics and chemistry by using mathematical analysis and modelling to fundamentally understand biological systems. With respect to vegetation the structure of the canopy and leaf chemistry are key biophysical variables in interpreting the dynamics of these biological systems.

2.1.1. Leaf Pigments

Leaves are mainly constituted by chlorophyll, water filled vacuoles, nitrogen and cell walls made up from cellulose and pectin (Campbell and Reece 2005). Chlorophyll, a vital molecule for photosynthesis, is embedded in the membrane of chloroplasts in all green vegetation. The pigment serves two purposes; firstly it absorbs light energy and secondly uses this to perform a redox reaction converting water and carbon dioxide into carbohydrate and oxygen. It should be noted that plants also use carotenes (oxygen free carotenoids) and xanthophylls (carotenoids containing oxygen) to absorb light energy (Campbell et al. 2006), however as Gates et al. (1965) noted chlorophyll accounts for 60-75% of the energy absorption by the plant in the visible part of the spectrum while Verdebout et al. (1994) highlighted that chlorophyll is ten times more concentrated than carotenoids. There are two types of chlorophyll, chlorophyll-a and chlorophyll-b. Chlorophyll-a is the primary pigment responsible for the biochemical action of photosynthesis while chlorophyll-b is an accessory that collects additional energy to supply chlorophyll-a with (Lichtenthaler 1987). As well as collecting additional energy chlorophyll-b has been shown to regulate the antenna array which links the reaction centre to the chlorophyll absorbing energy (Hankamer et al. 1997; Green and Durnford 1996; Tanaka and Tanaka 2000).

Chlorophyll can be assessed destructively or *in vivo*, i.e. within the living. Destructive leaf sampling involves removal of the chlorophyll from the leaf using a solvent. Moran and Porath (1980; Moran 1982) found Dimethylformamide to be the most suitable solvent for chlorophyll extraction superior to acetone as it enabled extraction from intact tissues. To achieve consistent results the same area of leaf should be removed from each sample, easily achieved using a circular hole punch, and added to a fixed quantity of solvent. It should also be noted that the location on the leaf that the cutting is taken from is important as chlorophyll density varies. After chlorophyll has been extracted from chloroplasts by the solvent the solution is placed into a spectrophotometer which measures absorption at very high spectral resolution to derive the wavelengths of maximum absorption of the solution. Deriving absorption maxima *in vivo* at a canopy scale

William James Frampton

involves taking chlorophyll measurements in a fixed area and directly comparing them with remotely sensed reflectance data using regression analysis to find the most strongly related wavelength. Chlorophyll content estimations can also be derived using handheld devices such as the Minolta SPAD-502™ which measures absorption at 440 nm and 670 nm and subsequently correlates the results with destructive measurements.

2.1.2. Leaf Area Index

Leaf area index (LAI) is a key biophysical variable that determines, with leaf chlorophyll concentration (LCC), the total canopy chlorophyll content per metre of ground area. LAI is effectively canopy density and has important implications for the energy balance of the land due to the reflective nature of vegetation in the NIR (Bonan 1995). Consequently LAI is key in determining photosynthetic activity and gross primary productivity (GPP). LAI is widely measured as the total area of leaves per square metre of ground (m^2/m^2) (Wilhelm et al. 2000). In the case of non-flat leaves such as pine needles LAI can be defined as half the total surface area of the needle per ground unit area (Chen and Black 1992).

LAI can be sampled directly or indirectly. Direct measurement involves destructive leaf sampling where leaves are physically removed from the canopy and area is measured. Indirect methodologies involve the use of models and optical instruments (Chen et al. 1997). Direct sampling can be time and resource intensive depending on the scale of the investigation. Morisette et al. (2006) noted indirect LAI measurements are most commonly made using an Li-Cor LAI-2000™ (Campbell and Norman 1990) or a Tracing Radiation and Architecture of Canopies (TRAC) (Chen 1996; Leblanc 2002). The LAI-2000 uses 5 concentric rings from 0-75° (approximately 0-13°, 16-28°, 32-43°, 47-58°, 61-74°) (Li-COR INC. 1992) to measure the transmitted light in the blue part (400-490 nm) of the spectrum through the canopy (Chen et al. 1997). In turn it uses these measurements over five zenith angles to calculate gap fraction (Miller 1967). TRAC measures the percentage of absorbed radiation (PAR) over a larger range of 400-700 nm than the LAI-2000 (Leblanc 2002). Through the use of a data logger TRAC records canopy gap fraction and size over planned transects and calculates LAI. Ground measurements of LAI are in turn correlated to remotely sensed data to in turn validate algorithms to retrieve LAI and provide an estimate of vegetation density at the required scale. While LAI determines the density of the canopy the leaf angle distribution (LAD) is an important factor in determining the amount of light intercepted by the canopy (Clevers et al. 1994). Due to this LAD has an impact of crop growth and measurements made by optical sensors.

2.2. Spectral Properties of Vegetation

Incoming solar radiation intercepted by vegetation is partly reflected, absorbed and transmitted. Biophysical variables of vegetation affect these light interactions and consequently give the vegetation unique spectral properties. The absorption features that can be seen in vegetation under spectral analysis are due to electron transitions and vibrational stretching of molecular bonds (Curran et al. 1992). Chlorophyll strongly absorbs energy in the blue (450-475 nm) and red (620-740 nm) parts of light while conversely the cell walls, primarily composed of cellulose, and gaps between them reflect and transmit energy in the visible and NIR (Curran 1989; Glenn et al. 2008) preventing damage that would occur due to overheating through excess energy absorption. As chlorophyll absorbs red and blue light the lack of absorption in the green (495-570 nm) part of the spectrum gives vegetation its colour. The green colour of vegetation is dependent on the absence of species specific high concentrations of carotenoids, anthocyanins and betalains which are non-green pigments. The described absorption and reflectance features of chlorophyll and cellulose are presented in Figure 2.1.

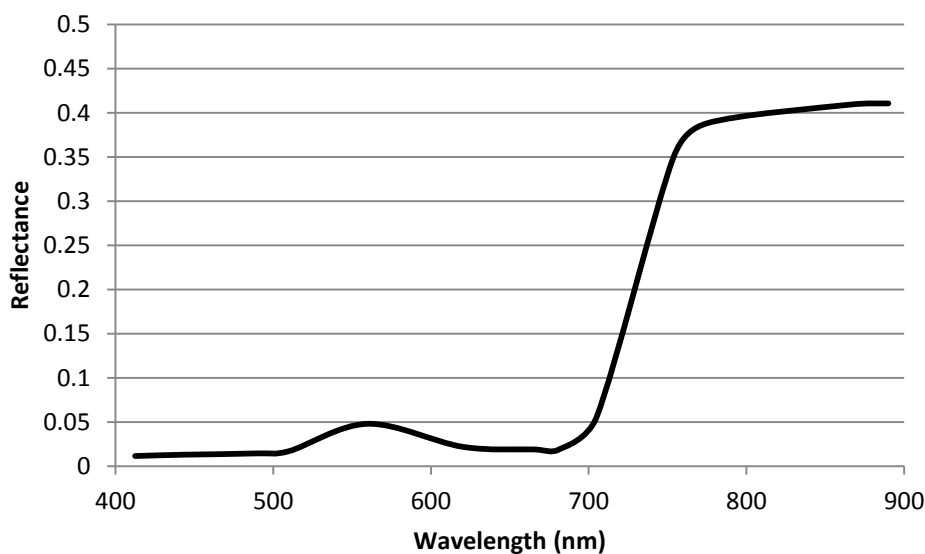


Figure 2.1: Example of a typical vegetative spectra. Figure shows average spectral reflectance of 50 corn fields during July-August 2005 in central-western Iowa.

Early work by Jordan (1969) and Federer and Tanner (1966) highlighted the combined maximum absorption to be at 675nm while Tucker (1979) presented it to be at 690nm *in vivo* at a canopy scale. Destructive work by Vernon (1960) and Moran (1982) separated chlorophyll a and b and noted the maximum absorptions to be at wavelengths of 664 nm and 647 nm respectively while Curran (1989) reported them to be at 0.66 μm (660 nm) and 0.64 μm (660 nm). Gross (1991) highlighted essentially the same result at a finer spectral resolution of 662 nm and 642 nm while

William James Frampton

Wellburn (1994) found the maxima to be at 665 nm and 647 nm. It can be seen that there are differences between the maxima for *in vivo* and destructive results. Lichtenthaler (1987) reported spectral shifts of 10 nm between the methods which agree with results from literature. The differences can be linked to the influence of the solvent and that chlorophyll, *in vivo*, are combined with proteins and other pigments (Verdebout et al. 1994). Wellburn (1994) showed the variation in central wavelength maxima retrieved depending on the solvent used. He compared chloroform, dimethylformamide and dimethylsulphoxide and found 2 nm variance in both chlorophyll-a and b. Variation of leaf water content has been found to not affect the optical and NIR parts of the spectrum up to 800 nm (Ceccato et al. 2001). Nevertheless there have been many studies which use the Short-Wave Infrared (SWIR) region (located between 800 – 1700 nm), which is sensitive to change in water content, to establish leaf water content (Tucker 1980a; Eidenshink et al. 1990; Paltridge and Mitchell 1990; Chuvieco et al. 1999).

The Beer-Lambert law relates the attenuation of light to the properties of the material through which the light is travelling (Daintih 2009). Consequently an increase in chlorophyll content causes both a broadening and deepening of the absorption feature. However in very dense canopies with high leaf chlorophyll concentrations saturation can occur resulting in an asymptotic relationship (Tucker 1977). This saturation point will be reached first at the absorption maxima. As the off-centre wavelength feature broadens with increased chlorophyll it is less affected by saturation. Therefore off-centre wavelengths can sometimes be more accurate estimators of chlorophyll content than the absorption maxima itself.

2.3. Satellite Sensors

2.3.1. Envisat MERIS

The first EO satellite launched by the European Space Agency (ESA) was the European Remote-Sensing Satellite-1 (ERS-1) in 1991 (ESA 2012b). ERS-1 carried the Along-Track Scanning Radiometer (ATSR) which was capable of making measurements in the infrared and microwave parts of the spectrum. Its successor ERS-2 came into service in 1995 with an improved ATSR-2 which included channels in the green (550 nm), red (670 nm) and NIR (870 nm) and consequently was the first European satellite able to quantify the Normalized Difference Vegetation Index (NDVI) and a range of other VIs.

Envisat was launched on the 1st of March 2002 and reached a sun synchronous polar orbit at an altitude of 790 km (ESA 2012a). Envisat orbits the Earth every 101 minutes and has a repeat cycle of 35 days. MERIS, a spectrophotometer aboard Envisat, has 15 programmable spectral bands

William James Frampton

within the range of 390-1040 nm (Rast et al. 1999). Table 2.1 shows the bands MERIS retrieves surface reflectance for in operational mode.

Table 2.1: Details of the spectral characteristics of MERIS bands in operational mode.

Band Number	Central Wavelength (nm)	Band Width (nm)
1	412.5	10
2	442.5	10
3	490	10
4	510	10
5	560	10
6	620	10
7	665	10
8	681.25	7.5
9	708.75	10
10	753.75	7.5
11	760	3.75
12	775	15
13	865	20
14	890	10
15	900	10

In full resolution mode (FR) MERIS has a spatial resolution of 300 m and 1200 m in reduced resolution mode (RR) (Kealy and Dewart 1999). Selecting a spatial resolution to meet study specific requirements is important as FR data is 12 times larger than RR and can add significant computation unnecessarily. MERIS has a large swath of 1150 km at a field of view of 68.5° which results in a global temporal resolution of 7 days at the equator improving to nearly 2 days at 70° latitude (Rast et al. 1999). Although MERIS was optimised for oceanic applications Verstraete et al. (1999) noted that with its fine spectral and moderate spatial resolution MERIS was a great opportunity for EO of the terrestrial environment. With respect to vegetation EO the key benefit of MERIS to other spaceborne sensors are the several high spectral resolution bands in the RE region. MERIS band 9 was the first spaceborne sensor to obtain reflectance information operationally in the RE.

When launched Envisat had a 5-year nominal lifetime. A limited supply of hydrazine fuel was carefully managed through orbital manoeuvre adjustment to allow extension of the lifetime a further three and a half years up until 2010. The expected lifecycle of Envisat was further extended in October 2010 until 2014 through moving to a lower orbit and disabling inclination controls meaning that Envisat no longer has orbit maintenance performed. The disabling of these controls has possible inclination drift consequences which could reduce accuracy of the ground tracking (ESA 2010b). However on the 8th of April 2012 communication with Envisat was lost.

William James Frampton

Although a series of attempts were made to reconnect with Envisat there was no response and now the chances of recovering the satellite are extremely low. Consequently there is increased urgency to produce the next series of European satellites with capabilities in the Red Edge; the Sentinels.

2.3.2. Copernicus Program

Copernicus is the programme for establishment of a European capacity for EO (GMES 2012). Copernicus aims to provide accurate and reliable data that can aid decision makers in developing the most appropriate environmental and security policies. With the EO devices rapid monitoring capacity Copernicus will support prompt response to natural disasters, industrial accidents or humanitarian crises to provide worldwide aid relief. Copernicus is coordinated by the European Commission, ESA and the European Environment Agency. Five spaceborne sensors, named the Sentinel series, are currently being developed by ESA that will provide EO data for the Copernicus program (ESA 2012c). Of the five, two are specifically relevant to the EO of vegetation.

2.3.3. Sentinel 2

Sentinel 2 (S-2) will provide systematic global acquisitions of high resolution multispectral imagery for Copernicus. The Multi-Spectral Instrument (MSI) aboard S-2 is the solitary sensor and has been designed to enable the continuity of Satellite Pour l'Observation de la Terre (SPOT) and Landsat type data into the future. S-2 however it will provide an enhanced spectral resolution, with 13 bands used to follow on from the MODerate-resolution Imaging Spectroradiometer (MODIS) and MERIS. The S-2 mission envisions of a pair of satellites simultaneously circulating the Earth in a sun-synchronous 180° phase orbit with a 290km swath (ESA 2010). The first satellite, S-2A, is planned for launch in April 2015 which is to be followed by S-2B tentatively planned for launch two years after S-2A (ESA 2011a). Tandem operation of S-2A and B will deliver a revisit period of up to five days under cloud free conditions at a band dependant 10-60 m spatial resolution with key vegetation bands having a spatial resolution of 10 and 20 m highlighted in Table 2.2.

Table 2.2: Spectral bands of S-2 MSI.

S-2 Band	Central Wavelength (nm)	Bandwidth (nm)	Spatial Resolution (m²)
1	443	20	60
2	490	65	10
3	560	35	10
4	665	30	10
5	705	15	20
6	740	15	20
7	783	20	20
8	842	115	10
8a	865	20	20
9	945	20	60
10	1375	30	60
11	1610	90	20
12	2190	180	20

There is much uncertainty in the characterisation of heterogeneous landscapes using MERIS operating at full resolution of 250-300 m due to pixels of mixed vegetation type. The issue is particularly relevant in Europe due to irregular and small field sizes in agriculture compared to agriculture in other parts of the world. The enhanced spatial resolution of S-2 should mitigate this issue reducing mixed class anomalies and incorrectly classified pixels.

2.3.4. Sentinel 3

Sentinel 3 (S-3) is designed to support Copernicus services related to the marine environment while also providing contributions to terrestrial EO and security. Like S-2, S-3 will function as a series of satellites to allow enhanced temporal resolution. Three satellites are planned to operate in a sun-synchronous orbit at an altitude of 814 km with a swath of 1270 km. A pair alone in operation will enable the entire terrestrial environment to be monitored every two days at the equator improving with increasing latitude (ESA 2011b). S-3 will have an extensive payload of seven sensors with the Ocean and Land Colour Instrument (OLCI) providing measurements in the visible and NIR parts of the spectrum. Like MERIS OLCI will operate at two resolutions, 300 m at FR and 1200 m at RR. OLCI includes 21 bands (Table 2.3) that take heritage from MERIS and SPOT and will have improved radiometric stability compared to MERIS (ESA 2011b). S-3A is planned for launch in mid-2015 followed by S-3B 18 months later while S-3C is tentatively planned for launch before 2020 (ESA 2011a).

Table 2.3: Spectral bands of S-3 OLCI.

S-3 Band	Central Wavelength (nm)	Bandwidth (nm)
1	400	15
2	412.5	10
3	442.5	10
4	490	10
5	510	10
6	560	10
7	620	10
8	665	10
9	673.75	7.5
10	681.25	7.5
11	708.75	10
12	753.75	7.5
13	761.25	2.5
14	764.375	3.75
15	767.5	2.5
16	778.75	15
17	865	20
18	885	10
19	900	10
20	940	20
21	1020	40

S-3 will ensure continuation of the 10 year long MERIS dataset into the future as Envisat reaches the end of its intended lifetime. Such long running datasets are paramount in providing perspective for investigations into surface and climate change and the impacts they bring for ecological viability and phenological transitions in vegetation (Zhu et al. 2013).

2.3.5. Non-Operational/Commercial Sensors with RE Capabilities

The Compact High Resolution Imaging Spectrometer (CHRIS) is the main sensor of Proba-1, ESA’s smallest satellite. Proba-1 is a technology demonstrator, albeit a highly successful one that resulted in continuation of the series with Proba-2 launched in November 2009 and Proba-V (Proba Vegetation) in May 2013 (ESA 2014b). CHRIS is an opportunistic sensor which targets planned sites at specified times. Typically only one or two sites are observed each day with irregular revisit times to accommodate accepted research proposals. In operational mode 1 CHRIS acquires reflectance in 63 separate spectral bands for a ground area of 13 km² at a spatial resolution of 34 m.

William James Frampton

The Hyperspectral Imager (Hyperion) is one of the sensors aboard NASA's Earth Observing-1 Mission (EO-1) satellite which measures reflectance for 220 wavelengths at 30 m spatial resolution for a 7.7 km by 42 km area (NASA 2014). Originally the sensor was designed for a 12 month lifecycle when launched on the 21st of November 2000 however it is still in operation today. Like CHRIS observations are opportunistic and subject to a successful data acquisition request application.

RapidEye is a constellation of five satellites that was launched on the 29th of August 2008 capable of collecting reflectance values in spectral five bands covering up to 5,000,000 km² at 5 m spatial resolution each day (Blackbridge 2014). Bands are positioned at 475 nm, 555 nm, 657.5 nm, 710 nm and 805 nm covering the blue, green, red, RE and NIR respectively.

2.4. Importance of the Red Edge Position

2.4.1. The Red Edge

The RE is denoted as the region of great change in vegetation reflectance due to the opposing features of plant pigment absorption in the red and cellulose reflectance in the NIR (Gates et al. 1965; Horler et al. 1983; Curran 1989; Glenn et al. 2008). The RE has been shown to be indicative of biophysical variables (Collins 1978; Horler et al. 1983). Increases in chlorophyll content causes both a broadening and deepening of the absorption feature centred around 665-680 nm (Banninger 1991; Dawson and Curran 1998). This causes a shift in the RE slope towards longer wavelengths (Clevers et al. 2002; Horler et al. 1983). The point of maximum change of the RE has been dubbed the REP and this inflexion point has been shown to be related to total chlorophyll content (Horler et al. 1983; Clevers and B ker 1991; Dawson and Curran 1998; Dash and Curran 2006). The REP can be calculated at various spatial scales and accuracies depending on availability of reflectance band measurements and spectral scales in the RE. MERIS meets such requirements with band 9 (Table 2.1) consequently becoming the first spaceborne sensor to obtain global reflectance information operationally in the RE. Estimation of REP on discontinuous data was undertaken for MERIS by Dawson and Curran (1998) where they proposed a technique based on the three-point Lagrangian interpolation (Jeffery 1985). Clevers et al. (2002) noted that use of the Lagrangian technique resulted in a jumping feature in a nonlinear REP/chlorophyll content relationship (Dash and Curran 2004). Consequently the method would require manual confirmation of the first derivative reflectance maxima and therefore could not be used operationally. A second method of REP estimation as proposed by Guyot et al. (1988) involves linear interpolation using the red and NIR reflectance. Clevers et al. (2002) applied the method for MERIS bands and can be seen below (Eq. (2.1)).

$$REP (MERIS) = 708.75 + 45 * \frac{\left(\frac{rNIR+rR}{2}\right)-rRE1}{rRE2-rRE1} \quad \text{Eq. (2.1)}$$

Where rNIR is the reflectance at 775 nm, rR at 665 nm, rRE1 at 708.75 nm (originally 705 nm) and rRE2 at 753.75 nm.

While the method has the advantage of being computationally simple Clevers et al. (2002) reported the relationship was a robust method of estimating REP. However, there are some issues with this method when applied using MERIS bands as accurate measurement requires both the RE inputs to be directly on the linear slope of the RE. While this is the case with RE1, RE2 is located beyond this linear part as the gradient flattens towards the NIR plateau. It should be highlighted that, while discussed in more detail further into the chapter, the band positions of S-2 in theory should allow enhanced estimation of the REP using this method over MERIS or S-3.

2.4.2. The MTCI

The MTCI (Eq. (2.2)) is a surrogate REP index which became an official MERIS level-2 product of ESA in March 2004 (Dash and Curran 2004).

$$MTCI = \frac{rNIR-rRE}{rRE-rRed} = \frac{r753.75nm-r708.75nm}{r708.75nm-r681.25nm} \quad \text{Eq. (2.2)}$$

Dash and Curran (2004) reported the MTCI to be more sensitive than using a measure of REP for high chlorophyll content values. Follow up work showed MTCI to be strongly positively related to chlorophyll indirectly through comparison to concentrations of herbicide used in Vietnam (Dash and Curran 2006). Dash et al. (2010a) compared the MTCI to ground chlorophyll measurements in southern England and found, with the exclusion of an outlier, an R^2 of 0.8 with an accuracy estimation (in relation to the mean) of 71%. The MTCI has also been used in studies not directly measuring chlorophyll but processes where it could be used as a proxy. Harris and Dash (2010) reported that the across site relationship of MTCI compared to GPP performed with a stronger relationship than the MODIS GPP or Enhanced Vegetation Index (EVI). Wu et al. (2008) also used the MTCI in a GPP analysis of wheat and showed it to outperform other chlorophyll-related VIs. The MTCI has also been used by Jegathan et al. (2010) and Dash et al. (2010b) to assess phenological transitions in India at a regional scale. Boyd et al. (2011) further used the MTCI as a surrogate for chlorophyll content while monitoring the phenology of woodland and grass/heath land in Southern England. Findings supported the use of MTCI for constructing phenological profiles due to its sensitivity with canopy chlorophyll content. Boyd et al. (2012) also incorporated the MTCI into three GPP models which were correlated with flux tower GPP measurements across 30 sites in USA, Canada and Brazil. Results indicated that the MTCI, as a surrogate measure of chlorophyll content, was able to give favourable approximations of GPP.

William James Frampton

The MTCI dataset reached over a decade of global coverage with the 10th anniversary of the Envisat launch in March 2012. Continuation of this long running dataset was originally thought to be likely without significant disruption as, at the time, S-3 was scheduled for launch in 2013 and orbital adjustments to Envisat were thought to have ensured the operation of MERIS until 2014. However on the 8th of April 2012 contact was lost with Envisat and chances of recovery are extremely low meaning until the launch of S-3 the MTCI is limited to past acquisitions. Long running datasets such as the MERIS dataset are specifically useful to phenological studies with regards to climate variability and change.

2.5. Retrieval of Biophysical Variables from Satellite Data

2.5.1. Modelling

Modelling of vegetation is based on radiative transfer theory; the fundamental idea that changes to radiation intensity are related to local absorption along the ray path. Consequently models link the spectral variation of the canopy, governed by the pigment concentrations, with the directional variation which is influenced by the canopy structure. PROSAIL (Baret et al. 1992, Jacquemoud et al. 2009) is the combination of the PROSPECT leaf optical properties model (Jacquemoud and Baret 1990) and the Scattering by Arbitrary Inclined Leaves (SAIL) canopy bidirectional reflectance model (Verhoef 1984; 1985). The model can be used to simulate canopy reflectance for a range of leaf biochemistry and canopy parameters which the user can select. Consequently the user can easily produce a dataset for validation purposes for a range of biophysical variables in the optical region at a 1 nm spectral resolution. Nevertheless a dataset that is derived from a model will be limited to how well it represents reality almost certainly missing out on natural dynamic response of vegetation.

SAIL was developed by Verhoef (1984) to simulate reflectance at the canopy level and was later extended by Kuusk (1991) to account for the hot spot effect. The SAIL model simulates canopy bi-directional reflectance as a function of three structural parameters: LAI, average leaf angle (ALA) and the hot spot parameter (HOT). HOT can be considered an empirical parameter that is strongly related to the sharpness of the hot spot peak; which, as a guideline, one can use the ratio of leaf width to canopy height as an estimate of its magnitude (Verhoef and Bach 2003). SAIL also incorporates the soil spectral reflectance, fraction of diffuse irradiance and the view and illumination geometry. PROSPECT simulates leaf reflectance and transmittance as a function of four structural and biochemical leaf parameters: LCC, dry matter content, leaf water thickness and a leaf mesophyll structural parameter (N). The combination of these two models, PROSAIL, has been reported to produce realistic results of bi-directional reflectance spectra for many

different crops in various investigations. Andrieu et al. (1997) found a good agreement for SAIL using the structure of sugar beet canopies outside of the hot-spot direction. Jacquemoud et al. (1995) also investigated the performance of the model using sugar beet data, however, with less success attributing the performance to especially bright soils. Major et al. (1992) found the model adequate at predicting the LAI of maize throughout the entire growing season. Examples of PROSAIL model inputs are presented in Table 2.4 and an overview of the model is exhibited in Figure 1.1 Figure 2.2 which was used in the MTCI-EVAL project (Watmough et al. 2011)

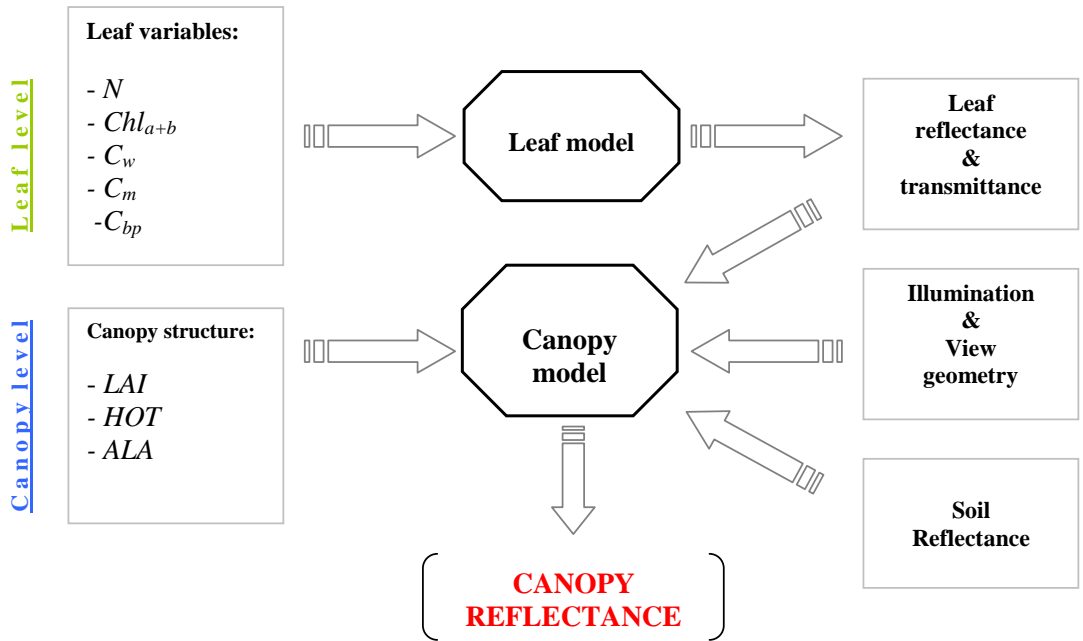


Figure 2.2: Schematic representation of PROSAIL: the coupling of the leaf (PROSPECT) and canopy (SAIL) models. First presented in the MTCI-EVAL project (Watmough et al. 2011).

Table 2.4: Example of input variables for PROSAIL.

Model Variables		Units	Range
PROSPECT			
<i>N</i>	Leaf structure index	Unitless	1.5
<i>C_{ab}</i>	Leaf chlorophyll content	[$\mu\text{g cm}^{-2}$]	5-70
<i>C_m</i>	Leaf dry matter content	[g cm^{-2}]	0.009
SAIL			
LAI	Leaf area index	[$\text{m}^2 \text{m}^{-2}$]	0-8
ALA	Average leaf angle	[$^\circ$]	35
HotS	Hot spot parameter	[m m^{-1}]	0.01
<i>S</i>	Sun zenith angle	[$^\circ$]	30
<i>V</i>	View zenith angle	[$^\circ$]	10

2.5.2. Use of VIs

Since the early 1970s early Earth observation (EO) spaceborne platforms such as Landsat 1 and the National Oceanic and Atmospheric Administration (NOAA; NOAA 2011) series, which were equipped with the Advanced Very High Resolution Radiometer (AVHRR) sensor, have provided the capability of measuring reflectance within the red and near-infrared (NIR) regions to researchers. These bands were quickly exploited through the use of Vegetation Indices (VIs) to simply and quickly identify areas of vegetation and draw further conclusions about their 'state'. The basis of the algorithms is that the biophysical composition of vegetation gives it unique spectral properties, as discussed in section 2.2. and **Error! Reference source not found.**, compared to on-vegetated surfaces such as soil. VIs are combinations of multiple reflectance measurements where multispectral imagery is available (Chuvieco and Huete 2010) and enhance the vegetative signal in remotely sensed data consequently enabling the extraction of useful information about the vegetation (Asrar et al. 1992; Gutman 1991). The Normalized Difference Vegetation Index (NDVI; Eq. (2.3)) was the earliest large scale use of a VI which was first formally reported by Rouse et al. (1973) (see Kreigler et al. 1969; Tucker 1979) and remains today as the most widely used method of monitoring vegetation at a global scale.

$$NDVI = \frac{r_{NIR} - r_{Red}}{r_{NIR} + r_{Red}} \quad \text{Eq. (2.3)}$$

VIs aim to measure the amount of photosynthetically active vegetation by manipulating bands within a spectral signature gained remotely at varying scales (Curran et al. 1997). The majority of VIs, like the NDVI, build upon the difference between the reflectance in the NIR and the red which was theorised before the NDVI in two ways by Jordan (1969) in the form of the Simple Ratio (SR; Eq. (2.4)) and the Difference Vegetation Index (DVI; Eq. (2.5)).

$$SR = \frac{r_{NIR}}{r_{Red}} \quad \text{Eq. (2.4)}$$

$$DVI = r_{NIR} - r_{R} \quad \text{Eq. (2.5)}$$

While studies have shown the DVI to be superior at low canopy covers (Roujean and Breon 1995) due to being less affected by the spectral signature of the background the NDVI is more robust in full canopies mitigating solar and atmospheric variation. The NDVI is effectively an optical measure of canopy 'greenness', which is a composite between LCC and LAI while taking into account the effect of variation in the structure of the canopy. LCC is typically measured in g chl m^{-2} (grams of chlorophyll per square metre of leaf) while LAI is widely measured as the total area of leaves per square metre of ground (Wilhelm et al. 2000). More recent VIs use reflectance measurements in the RE to estimate REP. The MERIS Terrestrial Chlorophyll Index (MTCI; Eq. 2.2)

(Dash and Curran 2004) enabled estimation of the REP at a global scale operationally in 2002 with the launch of the Environmental Satellite (Envisat) and the Medium Resolution Imaging Spectrometer (MERIS) on board.

Various field studies and theoretical analysis using modelling have shown that the results of VIs are near-linearly related to photosynthetically active radiation absorbed by the vegetative canopy (Jordan 1969; Tucker 1979; Huete 1988). Being computationally simplistic was a key strength of VIs in early EO. A VI such as the NDVI can be applied at varying scales to any multi- or hyper-spectral data with a red and NIR band. With few requirements and data from spaceborne sensors the resulting temporal resolution of a global acquisition a given VI can achieve is high. As an example MERIS operating in reduced operation mode (1000-1200 m) has a revisit time of 3 days, although local weather conditions can effectively reduce this figure if a specific area of study is required. Due to these strengths VIs hold great opportunity for many practical uses. VIs have become essential tools for; large scale land management within the farming industry, assessing forest health, desertification (United Nations Conference of Desertification 1977), rate of deforestation (Hecht and Cockburn 1989), and predicting the local and regional impact of drought to name but a few examples (Pettorelli et al. 2005, Kerr et al. 2003). With respect to climate change VIs quantify plant density and vigour at a global scale which can in turn be used to estimate carbon sequestration through photosynthesis (Paruelo et al. 2004).

Table 2.5: Summary of Key Vegetation Indices.

Vegetation Index	Formulation	Original Author
SR	NIR/R	Jordan 1969
DVI	$NIR-R$	Jordan 1969
NDVI	$(NIR-R)/(NIR+R)$	Rouse et al. 1973
REP	$700+40*(((NIR+R)/2)-RE1)/(RE2-RE1)$	Guyot and Baret 1988
SAVI	$((NIR-R)/(NIR+R+L))*(1+L)$	Huete 1988
MSAVI	SAVI where $L = 1-2y*NDVI*(NIR-yR)$	Qi et al. 1994
RDVI	$(NIR-R)/\sqrt{NIR+R}$	Roujean and Breon 1995
GNDVI	$(NIR-G)/(NIR+G)$	Gitelson et al. 1996
OSAVI	$(NIR-R)/(NIR+R+0.16)$	Rondeaux et al. 1996
MCARI	$[(RE-R)-0.2(RE-G)]*(RE-R)$	Daughtry et al. 2000
TVI	$0.5(120(NIR-G)-200(R-G))$	Broge and Leblanc 2000
GESAVI	$(NIR-BR-A)/(R+Z)$	Gilabert et al. 2002
MTCI	$(NIR-RE)/(RE-R)$	Dash and Curran 2004
MTVI	$1.2(1.2(NIR-R)-2.5(R-G))$	Haboudane et al 2004

2.6. Applications of Satellite Derived Biophysical Variables

2.6.1. Global Climate Models

Global Climate Models (GCMs) are used for weather forecasting, understanding our current climate and predicting how it might change in the future. The carbon cycle is the transfer of carbon between the atmosphere, hydrosphere and the terrestrial environment and it has a large input in the Earth's current and future climate. Carbon dioxide (CO₂) is a greenhouse gas which is an insulator in the atmosphere and has been significantly increasing in concentration due to anthropogenic activity since 1750 (Fung 2002). Before 1750 CO₂ concentrations had been stable below 280 parts per million (ppm) for 400,000 years however since have increased to 380 ppm in 2005 (Keeling et al. 1996; IPCC 2007). Increasing concentrations of CO₂ have been linked to increasing global temperatures which would likely lead to rising sea levels and land surface change putting pressures on an increasing population. Consequently in the last decade there has been increased interest in CO₂ sequestration by the oceans and terrestrial vegetation through photosynthesis. Satellite derived measurements of LAI and LCC can be used to estimate global and regional photosynthetic capacities and in turn the amount of carbon that can be sequestered. There are many global scale carbon models which incorporate an estimation of vegetation to derive an estimation of photosynthesis such as the BioGeochemical Cycles model (BIOME-BGC) (Running and Coughlan 1988) or the Lund-Potsdam-Jena Dynamic Global Model (LPJ) (Sitch et al. 2003). Estimates of the photosynthetic capability of an area depend on the performance of the algorithm that is used to calculate chlorophyll content. Consequently VIs, a commonly utilised method in GCMs, depend on the spectral capabilities of the sensor combined with adequate temporal and spatial characteristics. As S-2 will provide multiple spectral reflectance measurements directly on the RE at 20 m spatial resolution with global coverage every five days it holds much opportunity for enhancing inputs into GCMs. However using 20 m spatial resolution data will increase the size of data greatly and it could be argued whether it would provide much more accuracy than a medium or low spatial resolution. Multiple S-3 satellites will enable global calculation of the MTCI every two days at 300 m providing unparalleled temporal coverage and excellent scope as a surrogate measurement of chlorophyll content into GCMs.

2.6.2. Monitoring Forest

Forests are important areas for biodiversity and a source of livelihood for many and cover 30% of the total land surface (FRA 2010). Monitoring the rate of deforestation is important as forests account for 90% of the annual interchange of carbon between the atmosphere and the land surface. The Global Forest Resources Assessment 2010 (FRA 2010) highlights that there is more

William James Frampton

carbon in the world's forest than in the atmosphere or remaining oil stocks. An estimated net loss of 13.5 million hectares of forest has occurred in the last 20 years although there was 37% less net deforestation in 2000-2010 than in 1990-2000 which suggests the rate is slowing. The Reduced Emissions from Deforestation and Degradation (REDD+) policy was launched at the United Framework Convention on Climate Change (UNFCCC) summit 2008 with the key aim to provide the framework for financial compensation to countries who are able to reduce emissions from deforestation (REDD 2012). The key sections of the REDD+ proposal involve defining which activities are eligible, how emission reductions are calculated and over what time period, who finances the reduction and where the compensation goes. Conditions allowing satellite derived measurements of a forest's photosynthetic capabilities can be directly used within the REDD+ framework to quantify deforestation over a set period. It is important to highlight the difference between total clearance of the forest and degradation. Thresholds of VIs can be used to indicate land cover change, such as total forest loss, which are combined with class based sequestration values to calculate change in sequestration rates. Alternatively if the relationship that a VI has with photosynthetic capability has been established sequestration rates can be monitored as a function of change in the VI output. This method is especially useful for monitoring degradation of the forest. As previously discussed as the future Sentinel satellites provide enhanced spatial and temporal resolution therefore there is great opportunity for refined estimations of forest degradation. IPCC guidelines suggest, if possible, high spatial resolution satellite data is incorporated into the REDD+ framework. With regards to calculation of the MTCI S-2 will be the first sensor to allow operational calculation at the suggested high spatial resolution.

2.6.3. Precision Agriculture

With impressive spatial, temporal and spectral characteristics in the visible and RE S-2 will provide new opportunities for precision agriculture. Precision agriculture is a farming management concept that provides satellite and geospatial information to optimise farming practices to crop and field specific needs. Precision agriculture can aid the proficient use of fertilizers through understanding the spatial distribution of plant health by using remotely sensed biophysical variables which in turn can lead to financial savings and protection of the environment through reduced nitrate leaching and greenhouse gas emissions (Kim and Dale 2008). The Farmstar programme by EADS Infoterra is a good example of a precision agriculture scheme that provides information (Farmstar 2011).

2.7. Uncertainty in Vegetation Indices

Due to their attractive properties for vegetation monitoring, ease of implementation and seemingly robust use as a proxy for many phenomena, VIs receive much cross-disciplinary use by users often unfamiliar with the more complex intricacies of remote sensing. Without background knowledge within the area the user is at risk of not accounting for uncertainty, which in turn will affect the overall interpretation. Myneni et al. (1995) described uncertainty within vegetation monitoring as a series of caveats which to the unknowing can significantly degrade the value of remotely sensed data. Accounting for uncertainty and specifically working with the resulting limitations is a significant finesse within remote sensing.

Problems of uncertainty are often simplified when criteria only require assessment of a single date or short period. Generally investigations over longer temporal periods have larger the ranges of uncertainties to account for. Nevertheless it is more often the case in the application of VIs that monitoring a change over multiple acquisitions is required. Consequently the temporal context significantly exacerbates problems of uncertainty as there are many unwanted variables which change with time such as: atmospheric conditions, view geometry, soil moisture content, the physical canopy structure and the transition of the phenology of the plant (Myneni et al. 1995; Foody and Atkinson 2002). Each of these variables can influence the results of the investigation if unaccounted for and in turn imply mistaken or inaccurate vegetative change. There are also uncertainties governed by hardware such as satellite sensor drift (Hay 2000). This work suggests uncertainty to be divided into two groups; the first containing uncertainty independent of the vegetation and ground conditions and the second governed by scene specifics. The reason for the divide is to establish and account for universal uncertainties within remote sensing while recognising those which require further information and understanding about the ground level vegetation.

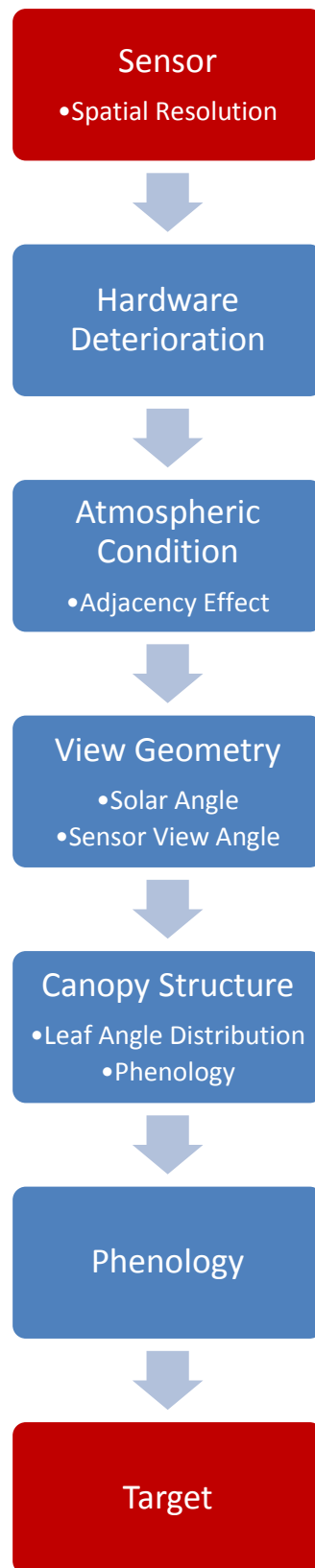


Figure 2.3: Flow diagram highlighting the uncertainties affecting the retrieval of the biophysical variables of vegetation.

2.7.1. Universal Uncertainties

2.7.1.1. Hardware Deterioration

Satellite sensor drift is the change in performance of satellite sensors as their components age (Gorman and McGregor 1994). Kaufman and Holben (1993) reported deterioration for NOAA-9 of $10 \pm 3\%$ in the visible band and $16 \pm 2\%$ in the NIR band shortly after launch and $22 \pm 2\%$ in both bands three years later. This can be attributed to vibration during launch, out-gassing in the vacuum of space, temperature changes and electronic degradation. These changes consequently resulted in variation of calculated NDVI by 0.0-0.09 effectively the difference between bare soil and a sparsely vegetated canopy at a low range of NDVI. If bands were to deteriorate at different rates this would also affect estimations of the REP when using popular methods such as the MTCI or linear interpolation methods (Guyot and Baret 1988, Clevers et al. 2000). Recently Wang et al. (2012) found that NDVI calculated using MODIS was decreasing at a rate of 0.001-0.004 per year. Hardware deterioration is in most cases accounted for through post launch calibration, often through methods like vicarious calibration (Thome 2004), which use large, homogenous, topographical and change stable surfaces with high reflectance such as dry lake beds (Thome et al. 1998) to assess temporal variance which can then be accounted for.

2.7.1.2. Atmospheric Conditions

The process of atmospheric correction (AC) is well documented by the Network for Calibration and Validation of Earth Observation Data (NCAVEO 2005). The group states that although performing AC is of benefit in the majority of examples within remote sensing it holds extra value to VIs as the influence of the atmosphere is not uniform along the spectrum. This means that there will be varying degrees of uncertainty in the separate bands that are used in VIs adding further complexity to the problem. The net influence of the atmosphere is the difference between the top-of-the-atmosphere (TOA) and the top-of-the-canopy (TOC) values. This net atmospheric effect decreases almost linearly with increasing surface reflectance (Kaufman 1989). Thus the relationship allows methods such as the Empirical Line Method (Ferrier 1995, Smith and Milton 1999) to account for, and ultimately mitigate, atmospheric conditions over a discrete or continuous temporal scale. Atmospheric influences have a positive effect on radiance in the shorter wavelengths, namely the blue and green bands (Milton et al. 1994), and a slightly negative effect at longer wavelengths, such as the NIR, due to the domination of absorption by aerosols (Myneni et al. 1995). With regards to the influence of the atmosphere on REP studies by Guyot et al. (1988) concluded that it was unaffected (Clevers et al. 2000).

The Atmospherically Resistant Vegetation Index (ARVI; Eq. (2.6)) (Kaufman and Tanré 1992) has been designed to improve the vegetation signal through de-coupling of the atmospheric

William James Frampton

influences. Kaufman and Tanré (1992) showed ARVI to be on average four times less sensitive to atmospheric effects than the NDVI and that the improvements are even greater for vegetated surfaces than soils.

$$ARVI = \frac{rNIR - rRed - y(rBlue - rRed)}{rNIR + rRed - y(rBlue - rRed)} \quad \text{Eq. (2.6)}$$

Where y can have either, as suggested by Kaufman and Tanré (1992), a fixed value of 1 or be varied based on the atmospheric and background conditions.

Included within the uncertainty due to the atmosphere is the adjacency effect; the issue that the radiance field measured by the remote sensor may also contain contributions of reflectance from outside the field of view (FOV) that has been scattered by the atmosphere (Myneni et al. 1995). As well as possibly including reflectance from outside the target study area; the resulting loss of contrast due to the adjacent effect can impair visual interpretation of the image (NCAVEO 2005).

2.7.1.3. Background: Soil Condition

Light which reaches the ground through the canopy interacts with the surface; spatial variations in the albedo will in turn have a varying effect on the TOC radiation measurements. Accounting for variation in background reflectance is important for vegetation monitoring as 70% of the Earth's terrestrial surface consists of open canopies (Graetz 1990). Kauth and Thomas (1976) highlighted the difference between dark and light bare soil and importantly that although initially different with respect to absolute red and NIR reflectances they converge to similar reflectance values as canopy cover reaches a maximum. Previous work by Condit (1970) analysed 160 soil spectral reflectances in North America between 320-1000 nm and found that soils could be classified into three general types. Type 1 curves have low reflectance with a shallow increment in gradient giving a concave form while type 2 curves have decreasing gradient till 600 nm which results in a convex shape. The gradient of type 3 curves decay less than that of type 2 soils however at 760 nm the gradient reduces sharply and even becomes negative because of an absorption feature present due to the high iron content. Stoner and Baumgardner (1981) analysed 485 soils from 520-2320 nm and presented five distinct soil spectral reflectance types from the 30 suborders of the 10 orders of soil taxonomy. Their five types included the three Condit proposed while adding two further subclasses to type 3 soils using the 800-1300 nm region. Type 4 and 5 related to high iron contents with varying organic concentrations which consequently cause type 4 soil to exhibit lower reflectance in the optical region and higher NIR reflectance than type 5 soils. Work in turn coined the term the soil line which refers to the near constant gradient that a soil spectra exhibits over the visible and NIR wavelengths (Figure 2.4).

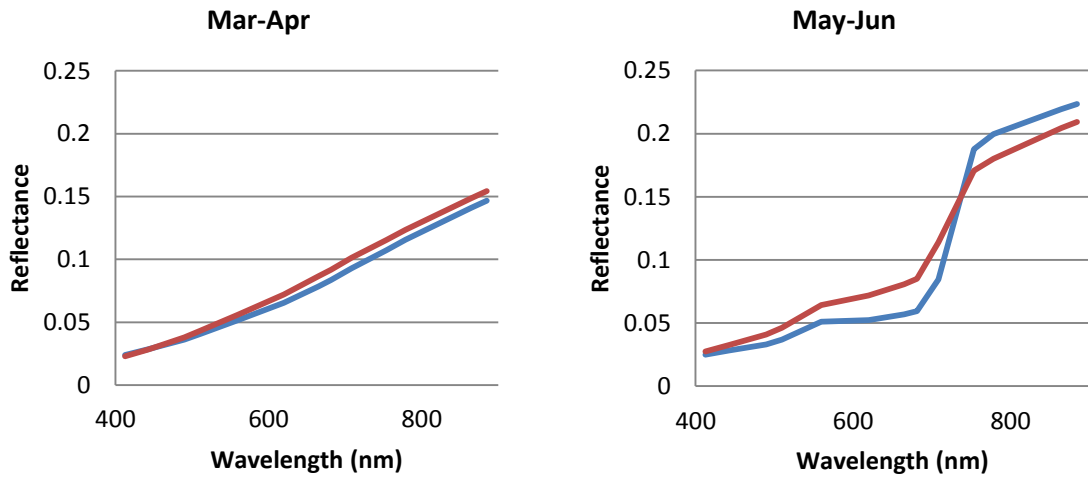


Figure 2.4: 50 corn (blue) and 50 soybean (red) averaged bimonthly reflectances derived from GLOBCOVER MERIS FR imagery for 2005.

A typical soil line can be witnessed in Mar-Apr while by May-Jun crops have grown and exhibit clear vegetation spectra. These lines are important to consider as VIs differentiate between this background reflectance with the presence of vegetation as the red reflectance decreases because of chlorophyll absorption while overall infrared reflectance increases with the presence of leaf mesophyll structure and cellulose. Thus, deviations of spectral data from the bare soil line may be attributed to the presence of green biomass (Widlowski et al. 2004). The uncertainty due to the soil is exacerbated by weather as local water content will have a varying effect on the reflectance. While it is well documented that wet soils will overall reflect less than drier brighter soils (Baret et al. 1993) as most vegetation indices use ratios of reflectance bands the impact of this is negligible and soil type is the main factor in variation of the soil line (Baret et al. 1993). The background has the largest impact when vegetative cover is in the region of 40-60% as the combined effect of background reflectance with the transmissive properties of the open canopy increase the possible noise in the VI output (Huete et al. 2002).

Like the ARVI for accounting for atmospheric influences the Soil-Adjusted Vegetation Index (SAVI; Eq. (2.7)) (Huete 1988) was developed with the aim to mitigate the variation due to background reflectance.

$$SAVI = \frac{rNIR - rRed}{rNIR + rRed + L} (1 + L) \quad \text{Eq. (2.7)}$$

SAVI introduces a soil-brightness dependent correction factor, L , into the NDVI equation which Huete (1988) argued was very sensitive to background radiation. Prior to the work of Huete et al. (1984) it was common place to assume a universal 'global' soil line encompassing a wide range of

William James Frampton

soil types in remote sensing practice (Miller et al. 1984). It could be argued that a better representation actually consists of numerous nonparallel soil lines that represent soil-moisture variations within scene specific types, however correcting for this would be a significant undertaking (Asrar 1989).

2.7.1.4. View Geometry

To obtain repeated global coverage at a high temporal and spatial scale it is unfeasible for space-borne sensors to use consistent solar and small view angle range to collect data. Changing solar and view zenith angles in turn cause variation in the consistency of measured reflectance from the target area. Research by Kollenkark et al. (1982) showed that, apart from an initial decrease up to a solar zenith angle of 10 degrees, the reflectance of areas with near total vegetation cover does not significantly change as solar zenith increases in both the red and NIR bands. However diurnal variations had significant implications for canopies of 64% cover with red reflectance decreasing by half between 0 and 30 degree solar zenith. Importantly NIR reflectance did not change significantly for this percentage cover. Consequently the results support the argument that as the solar zenith increases canopy shadowing becomes a significant factor influencing spectral reflectance of an area of vegetation that does not completely cover the background.

Uncertainty does not only come from varying solar angle but also changing the sensor view geometry. This is due to the way a vegetative canopy creates a gradient of scattered solar flux with a maximum at the top of the canopy and a minimum at the bottom. In turn, as the nadir view angle increases the sensors FOV includes a larger proportion of upper canopy, which is scattering the most solar flux, and the proportion of the lower canopy in the FOV decreases (Kimes 1983). This effect depends on leaf inclination, density and the scattering coefficient of the leaves to their transmittance properties as these factors influence the gradient of scattering through the canopy.

If the canopy cover is low and therefore shadowing is occurring (especially relevant at higher solar zenith angles) an increasing sensor zenith will contain a higher proportion of vegetative material and less effect from shadows and soils in the FOV thus theoretically increasing measured vegetation. It must be considered however that the described variations due to solar and sensor zenith angle can conflict with each other and their influence on the output reflectance. Jordan (1969) highlighted the robustness of VIs that incorporate ratios, such as the SR, to varying solar intensity. Although the intensity of light received by the canopy dropped by half the NIR and the red wavelengths reflectance of light decreased equally and therefore the output of the VI showed insignificant variation.

2.7.1.5. Spatial Resolution

Studies can be limited by the spatial resolution of the available sensor (Boyd and Foody 2010). With regards to vegetation this often leads to a mixed pixel problem where two separate vegetation classes are contained within a single physical pixel as the targets physical size is smaller than the resolution of the sensor. This issue is more relevant in some locations than others. For example MERIS in full resolution (300 m) will have many more mixed pixels observing heterogeneous European cropland than the larger homogenous fields of North America. Ideally the desire is to have imagery with a spatial resolution finer than the size of the features of interest (Woodcock and Strahler 1987). Single trees or a row of crops could be considered the smallest features for a vegetative study, however to differentiate between these and the soil background sub metre resolution data would be required (Boyd and Foody 2010). Most sensors that acquire data at this level are either not operational or retrieving reflectance measurements on the RE. As S-2 will operationally acquire spectral measurements on the RE at 20 m spatial resolution calculation of the REP and MTCI will be possible with far fewer mixed pixels than was previously possible with MERIS and the uncertainty due to this reduced.

2.7.2. Vegetation Specific Uncertainties

2.7.2.1. Canopy Structure

The significance of an open or closed canopy and the consequential effect depending on the view angle has been discussed previously in the view geometry section as have the implications canopy cover has with regards to the influence of the background reflectance.

The output of VIs are structured to reduce if red reflectance gets higher, theoretically due to lack of chlorophyll, and greater if the NIR increases, suggesting a more dense canopy. Relationships of VIs frequently hold strong for low values of LAI, with saturation occurring at higher LAI values due to lack of reflection in the red part of the spectrum. NDVI has been shown to lack sensitivity above an LAI of around 2-2.5 and become non-linear with an increase in biophysical parameters (Lillesaeter 1982, Asrar et al. 1984, Baret and Guyot 1991, Gitelson 2004). The relationship of VIs with LAI has been tested in a number of studies (Curran 1980; Badhwar et al. 1986) for varying cover types. Generally results over arable land were non-linear with LAI but near linear relationships were found over forested areas. While LAI determines the density of the canopy the leaf angle distribution (LAD) is an important factor in determining the amount of light intercepted by the canopy (Clevers et al. 1994). Sellers (1985) found that canopies with heterogeneous LAD display more variance in output of reflectance. Nevertheless it should be considered that the impact of canopy structure variation is often mitigated by the large scales that VIs operate at compared to average plant canopy size.

2.7.2.2. Phenology

Senescence is the biological aging of an organism. Deciduous plants are genetically programmed to respond to seasonal weather through structural and metabolic changes (Boyer et al. 1988). During leaf senescence chlorophylls degrade faster than carotenoids (Sanger 1971), consequently over the course of senescence leaves will change colour to shades of yellow or orange/red. Sanger (1971) reported that oak leaves that had dropped from the tree in the autumn still had measureable quantities of the carotenoids lutein (xanthophyll) and β -carotene (carotene) in the spring while aspen and hazel leaves were devoid of all pigments. Resulting changes in pigment content due to senescence have impacts on the spectral reflectance of the canopy specifically in the visible region while structural changes affect canopy reflectance in the NIR (Boyer et al. 1988). Such changes can add uncertainty to the output of VIs in the autumn season both in deciduous forests and also for crops. During review it was found that there is a distinct lack of research into the effect of phenological transitions on the RE and specifically REP.

2.8. Conclusion

Spectral VIs aim to provide near-linear estimates of a given areas photosynthetic capacities and canopy variables. They provide measurements at otherwise unfeasible temporal and spatial scales for a variety of scientific uses. This literature review has explored the current methods for deriving biophysical variables using spaceborne sensors and assessed the future opportunities of S-2 and S-3. The uncertainties within the use VIs have been presented as a series of caveats.

Understanding uncertainty processes are an inconvenient reality as the concept and application of VIs can appear simple; this combined with their attractiveness to fields outside vegetative observation as a proxy can produce misguided results to the unknowing. Although the problems are numerous there is no other feasible way to requisition the biophysical parameters of vegetation at such a high scale both spatially and temporally with our current technology. In turn the field must accentuate accounting for uncertainty and ensure that good practice is universally applied to reduce the limitations that are faced. Importantly this will bring heightened dependability to draw conclusions and accordingly allow faster development and testing of ideas within the remote sensing community, as well as increased assuredness that current paths of thought are a worthwhile investment.

There is great worth in the RE to retrieve the biophysical parameters of vegetation without saturation at high vegetation densities due to avoiding algorithm dependence on reflectance in the red region. This has been shown by the MTCI at MERIS FR (300 m). Sentinel-2 provides enhanced spectral resolution in the RE compared MERIS with two bands directly over the RE.

William James Frampton

These two bands should allow improved operational retrieval of biophysical parameters at a fine spatial resolution of 20 m. Consequently S-2 holds great appeal for precision agriculture especially in Europe where heterogeneous field sizes often cause large error due to mixed pixels.

Alternatively with the recent end of MERIS operation Sentinel-3 will have the important role of continuing the 10 year dataset. It is currently not known how the operational MERIS product the MTCI will perform for S-2 and S-3 and this leaves scope for investigation in this research.

Chapter 3: The Soil Discrimination Index and its application to the MTCI

3.1. Introduction

The MTCI-EVAL project was conducted to evaluate and validate the MTCI algorithm. Several key factors were established that influenced its performance; the soil background, view geometry and aerosol optical thickness. It was found that as the MTCI puts large weight on the reflectance of the RE band in relation to the position of the red and NIR the effect of the soil background reflectance at low canopy covers can cause significant uncertainty. Preliminary investigations into equating this uncertainty using guidelines suggested by the Quality Assurance Framework for Earth Observation (QA4EO) suggested below an MTCI of 2 for sparse canopy covers the variation in the background condition could affect the output of the algorithm by up to 20% (Watmough 2011). Consequently a study has been devised to account for this uncertainty.

Variation of the reflective properties of soil combined with the structural, optical and geometric attributes of vegetation cover within a scene dictates the overall influence that the background will have on top of the canopy (TOC) radiation measurements (Miller et al. 1984). Accounting for variation in the background reflectance is important in vegetation monitoring as 70% of the Earth's terrestrial surface consists of open canopies where this can add significant uncertainty to the output of Vegetation Indices (VIs) (Graetz 1990). With reference to discussion in section 2.7.1.3. this chapter aims to investigate the variance in the common soil types of North America and the influence that they have on the MTCI product. In turn work aims to provide additional functionality for the algorithm to account for or mitigate this uncertainty. North America has been chosen for the focus of the study due to the large homogenous fields which are well documented with regards to phenology and crop type as well as having a freely available soil library.

3.1.1. Discussion on Current Soil Discriminators

Prior to work of Huete's (1988) Soil Adjusted Vegetation Index (SAVI; Eq. (2.7)) it was common place to assume a universal global soil line encompassing a wide range of soil types (Miller et al. 1984). However, SAVI works through applying an adjustment (L) to the NDVI based upon LAI or fraction of green cover. Huete (1988) suggested that using a constant value for L of 0.5 would improve remotely sensed vegetation interpretations by minimizing soil noise; however Huete (1988) also noted that the use of a constant L results in a loss of response in the dynamic range of vegetation. This loss of dynamic response can be attributed to the L constant of 0.5 usually being

William James Frampton

much larger than a pixels red reflectance (MERIS band 8, see Figure 3.4 for examples) therefore buffering variation that could occur.

$$SAVI = \frac{rNIR - rRed}{rNIR + rRed + L} (1 + L) \quad \text{Eq. (2.7)}$$

Rondeaux et al. (1996) further added to development of SAVI through publishing data that suggested that there was no benefit to using an L value of above 0.1-0.2 and instead proposed Optimized SAVI (OSAVI; Eq. (3.1)) using an L value of 0.16.

$$OSAVI = \frac{rNIR - rRed}{rNIR + rRed + 0.16} \quad \text{Eq. (3.1)}$$

Qi et al. (1994) proposed the Modified Soil Adjusted Vegetation Index (MSAVI) which self-adjusted the L factor to account for these shortcomings. The L factor (Eq. (3.3)) in MSAVI is adjusted based upon the NDVI and the Weighted Difference Vegetation Index (WDVI; Eq. (3.2)) (Clevers 1988);

$$NDVI = \frac{rNIR - rRed}{rNIR + rRed} \quad \text{Eq. (2.3)}$$

$$WDVI = rNIR - \gamma rRed \quad \text{Eq. (3.2)}$$

$$L = 1 - 2\gamma NDVI * WDVI \quad \text{Eq. (3.3)}$$

Where γ is the soil line parameter.

It is questionable that L is partly based upon the NDVI which Huete (1988) presented SAVI as trying to improve through trying to account for the soil effect. Furthermore there are issues with the practicality for global application of MSAVI as the WDVI which is used to self-adjust L depends on varying the soil line based on variation of the background conditions of the target location which would require extensive information to implement operationally.

Gilabert et al. (2002) proposed the Generalized SAVI (GESAVI) which was reported to have better performance than the other SAVI derivatives as the algorithms isolines in the NIR-R plane are neither parallel to the soil line nor convergent at the origin. The formula uses two soil line parameters as well as a soil adjustment factor and is presented as Eq. (3.4).

William James Frampton

$$GESAVI = \frac{rNIR - BrRed - A}{rRed + Z} \quad \text{Eq. (3.4)}$$

Where A and B are soil line parameters and Z is the cross point between the soil line and vegetation isolines.

The key underlying issue with SAVI and the subsequent modifications is that to effectively adjust the L value, and account for soil, ground knowledge of LAI is required (Rondeaux et al. 1996; Gilabert et al. 2002) a parameter which is not commonly known and the NDVI is often used to estimate. Also it should be considered that every study reviewed made L adjustments based upon LAI irrespective of variation in chlorophyll concentration. As previously mentioned in section 2.7.1.3. while it could be argued that the idea solution consists of numerous nonparallel soil lines that represent soil-moisture variations within scene specific types, applying a correction for this would be a significant undertaking and beyond the objectives and possibilities of this research.

During the validation of the MTCI investigations found that the MTCI as well as other indices based around the RE were less robust in areas of low canopy cover than other vegetation indices such as the NDVI. In the process of researching what was the best way to enhance the robustness of the MTCI it was found that many of the methods accounted for the influence and effects of soil through requirement of extra field data which is not feasible at an operational level. Consequently there is scope to develop a new method to account for soil while, if possible, not changing the MTCI algorithm.

3.2. Development of a Suitable Measure to Distinguish Soil for Vegetation Indices and Specifically the MTCI

With the limitations considered of the current most prolific soil based index work has proceeded to develop a suitable measure to distinguish soil from vegetation. With doing so the method will allow as clear as possible differentiation between soil and vegetation to assess areas of contamination. The method should be able to be implemented operationally without requirement of extra site information not available using MERIS.

3.2.1. Study Sites

3.2.1.1. Iowa

Iowa was chosen as a study area due to its large homogenous fields of well documented crops; soybean and corn. In addition as the field sizes are exceptionally large at 1500 m x 1500 m (Figure 3.5) with frequently only one crop grown per field uncertainties such as the adjacency affect and

William James Frampton

problems with heterogeneous canopies are mitigated. The vast coverage of agriculture across the majority of the state also provided great scope for selection of optimal study areas over an extensive time period after a cloud mask had been applied. An area 180 km² north west of Des Moines was chosen and is highlighted in Figure 3.1.

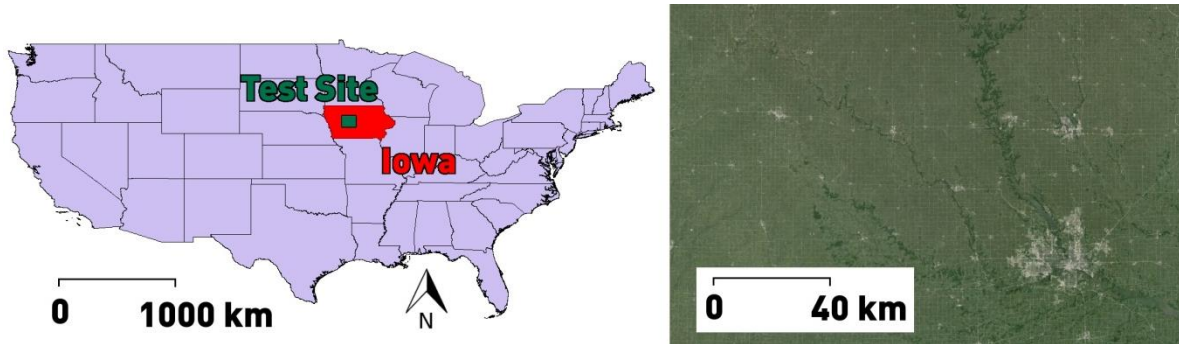


Figure 3.1: Test site location north west of Des Moines, Iowa, North America.

3.2.1.2. Dalhart Texas

Dalhart's economy is focused around agribusiness with warm wet summers that are ideal for crop production (NOAA 2012). Dalhart was chosen as a study site to test methods developed from the Iowa data set. Dalhart would be suitable for this because of the contrast between large fields of crops with dense homogenous canopy cover and the large amount of land dedicated to ranching with sparser to open canopies that the methodology could account for. The test site is highlighted in Figure 3.2.

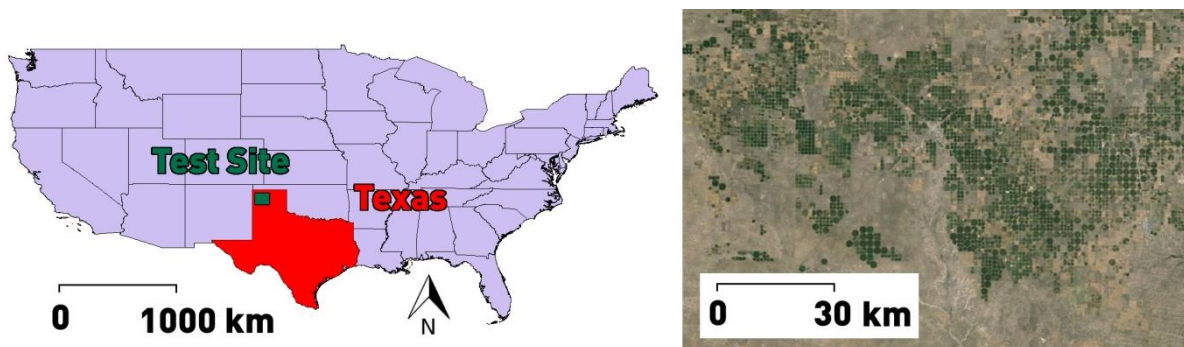


Figure 3.2: Test site location surrounding Dalhart, Texas, North America.

3.2.2. Data and Methods

3.2.2.1. Advanced Spaceborne Thermal Emission and Reflection Radiometer Spectral Library Hyperspectral Reflectance Records

The Advanced Spaceborne Thermal Emission and Reflection Radiometer (ASTER) Spectral Library (v2.0) is a collection of hyperspectral reflectance records from the Jet Propulsion Laboratory, Johns Hopkins University and the United States Geological Survey which were generated with field reflectance measurements using hand held radiometers such as the Analytical Spectral Devices FieldSpec (see Baldrige et al. 2009) as part of activities to validate the ASTER sensor. To understand how variations in the soil background affect the MTCI 42 separate soil spectra were acquired from the ASTER library and converted into MERIS bands according to spectral response documents (Figure 3.3; see Weinreb et al. 1981).

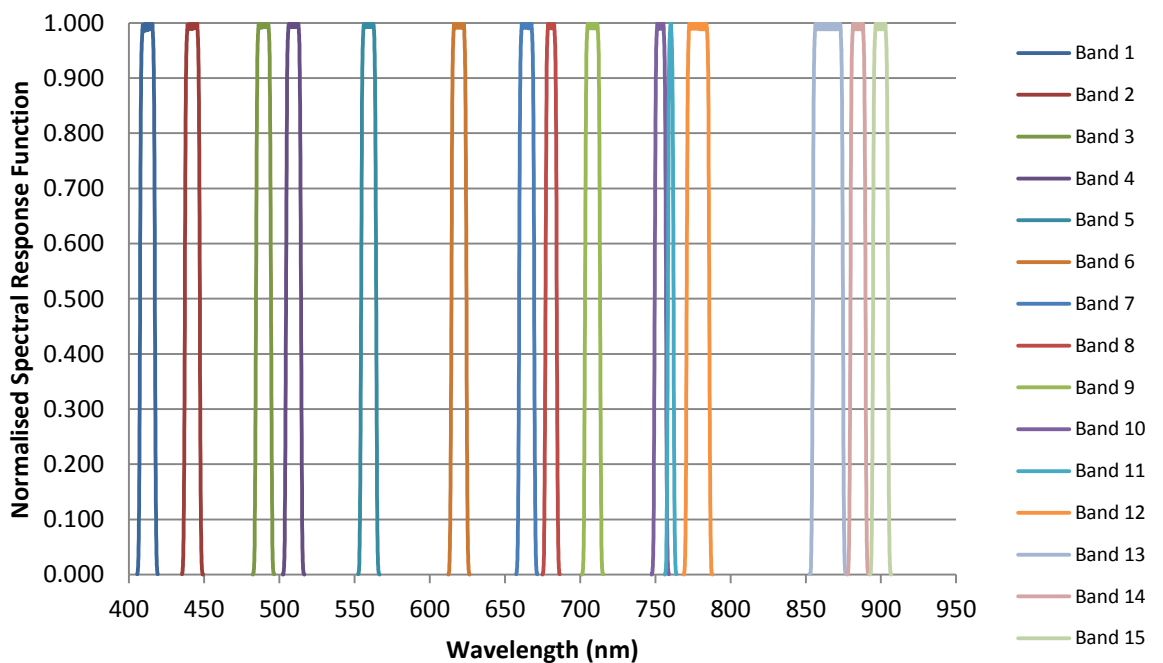


Figure 3.3: MERIS band normalised spectral response functions.

A selection of the spectral response of the various soil types are presented in Figure 3.4.

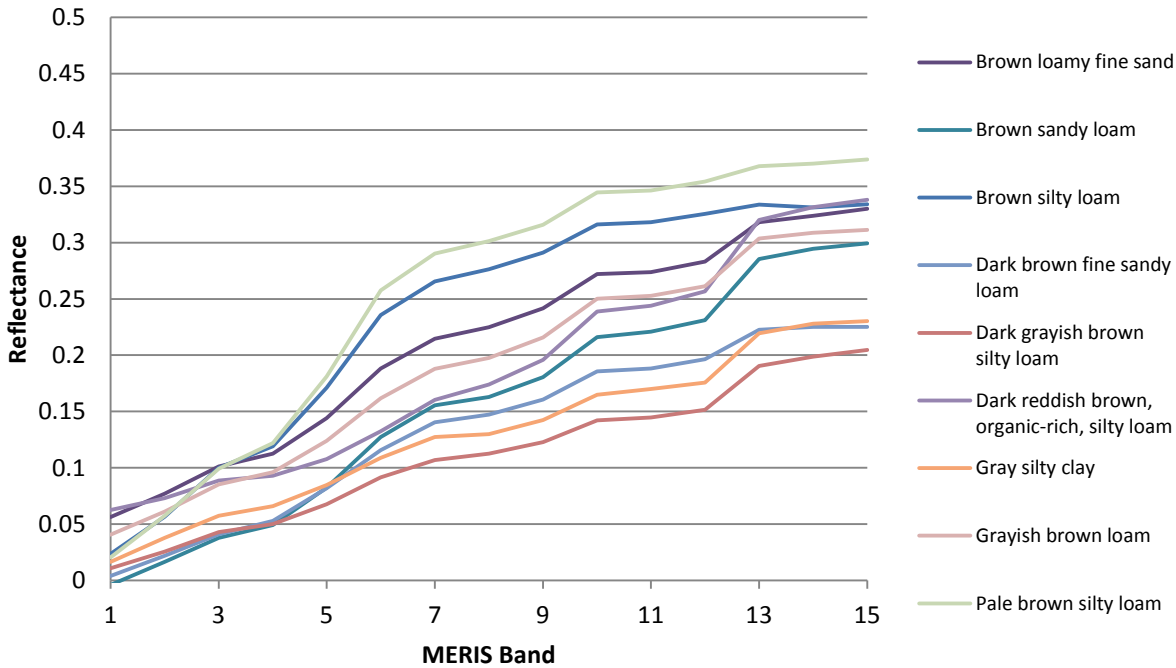


Figure 3.4: Synthetic MERIS band spectral reflectances for various soil types derived from the ASTER spectral soil library.

3.2.2.2. MERIS Data: Iowa and Dalhart Texas

To investigate the spectral signatures at satellite sensor level land cover information was taken from the GlobCover Bimonthly MERIS FR mosaics at a spatial resolution of 300 m; six resulting composite images cover the year of 2005 (Figure 3.5). The GLOBCOVER project is conducted by ESA and several other large organisations such as: the United Nations Environment Programme (UNEP), the Food and Agriculture Organisation (FAO), the European Commission’s Joint Research Centre (JRC). The result is a well processed data set for the year 2005-2006. GLOBCOVER MERIS acquisitions had already been geometrically corrected as well as screened for cloud with Rayleigh scattering, aerosol and smile corrections applied (POSTEL 2012). Consequently the data is immediately useable without much further processing.

Contemporaneous high resolution (56 m) crop cover information was obtained from the United States Department of Agriculture (USDA) National Agricultural Statistics Service (NASS) (Figure 3.5). The 2009 USDA NASS report for Iowa estimated 97.85% and 96.95% accuracy for corn and soybean respectively.

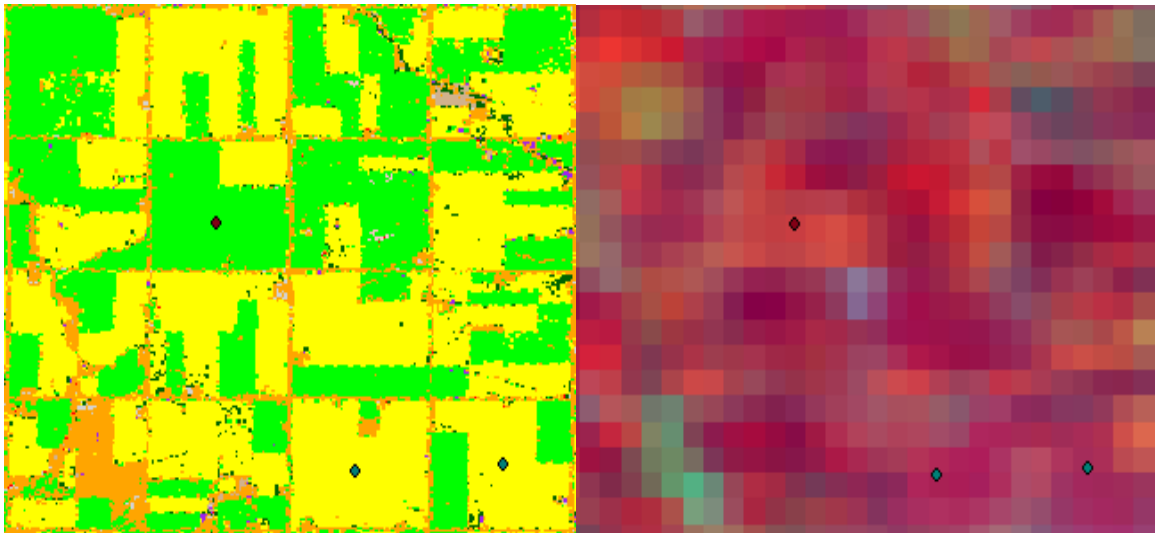


Figure 3.5: High spatial resolution (56 m) crop cover information from the USDA NASS for 2005 (left) and false colour FR (300 m) MERIS data (right) showing site selection and standard field size (1500 m x 1500 m).

A single MERIS FR acquisition was chosen from Dalhart Texas acquired on 23-06-2005 that could be seen to have established vegetative canopies and clear soil backgrounds. This would in turn provide scope for training sites and the contrast would aid initial VI analysis (Figure 3.6).

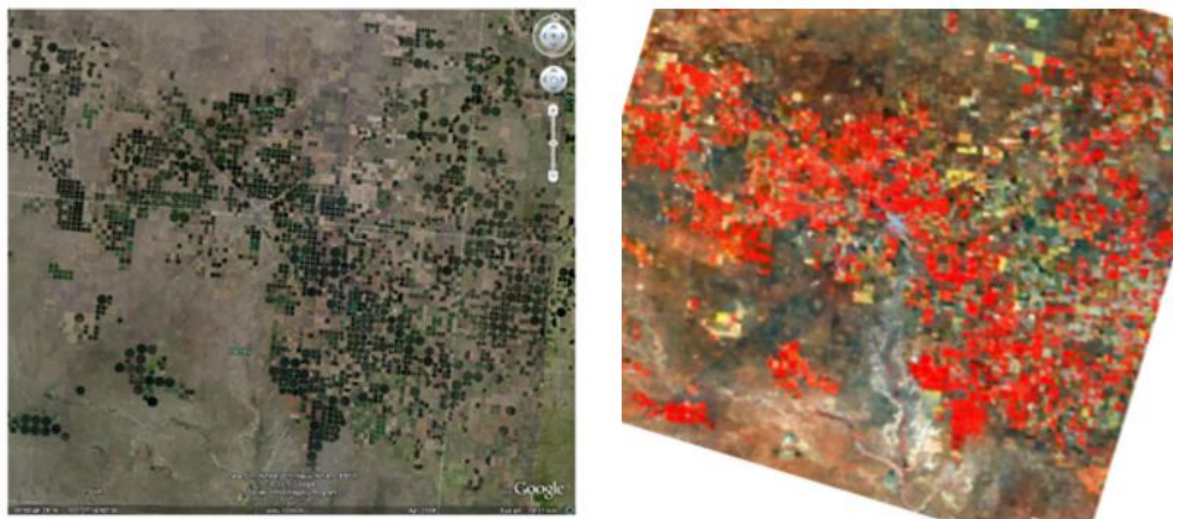


Figure 3.6: Landsat image courtesy of Google Earth (Landsat) of the study site in Dalhart Texas (left) where SDI distribution analysis was performed with the corresponding MERIS image (right).

3.3. Development of the Soil Discrimination Index

During MTCI-EVAL it was found that the MTCI ranged between 1.5 and 5 for sparse to densely vegetated pixels (Watmough et al. 2011). With the hyperspectral records of the ASTER soil library

synthesised into MERIS bands the MTCI could be calculated for the comprehensive list of soil backgrounds. Average MTCI of the dataset was 1.9 with a variance of 0.07, standard deviation of 0.31 and a max of 2.52 (Figure 3.7). Applying the NDVI using MERIS bands 10 and 8 as the NIR and red produced an average of 0.10 with a standard deviation of 0.04 and a max of 0.16. These results highlight the key problem with uncertainty due to soil on RE focused VIs such as the MTCI; a low output of the VI could be either due to sparse vegetation or a pure soil background with a spectral reflectance which produces higher than anticipated VI results.

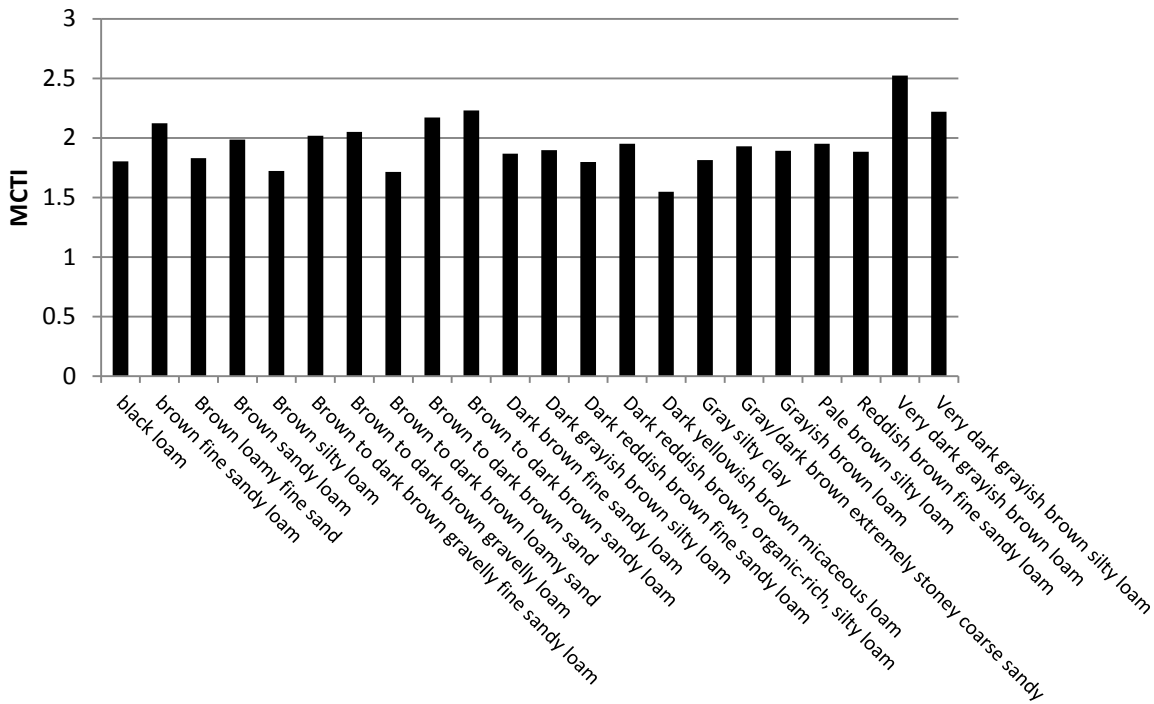


Figure 3.7: Applying the MTCI to a selection of soils from the ASTER soil library.

A sequential investigation was developed to assess pixel values of an agricultural location over an entire growing season. Monitoring the entire phenological cycle of a given pixel would effectively require spectral measurements from bare to fully vegetated to senescent and bare once again.

50 fields each for corn and soybean were selected from homogeneous areas of each crop in central-western Iowa using the USDA NASS crop data for 2005. The average field size in the study area is 1500 m² resulting in 25 MERIS FR pixel per field. Single pixels were chosen in fields dominated by one crop (Figure 3.5); consequently the spectral reflectance of the target pixels should be unmixed and uncertainty from the adjacency effect significantly reduced. To understand how the vegetated pixels should have varied over the course of a year details of planting and harvest for Iowa were obtained from the USDA NASS (1997; 2010) and are presented in Table 3.1.

Table 3.1: Table to indicate key crop production times for Iowa in 1996 and 2009.

Year	Crop	Planting			Harvest		
		Begin	Most Active	End	Begin	Most Active	End
1996	Corn	22 nd Apr	2 nd May to 16 th May	3 rd Jun	17 th Sep	7 th Oct to 31 st Oct	17 th Nov
1996	Soybean	4 th May	14 th May to 2 nd Jun	17 th Jun	21 st Sep	1 st Oct to 15 th Oct	27 th Oct
2009	Corn	19 th Apr	19 th Apr to 18 th May	26 th May	21 st Sep	5 th Oct to 9 th Nov	21 st Nov
2009	Soybean	2 nd May	8 th May to 2 nd Jun	16 th Jun	21 st Sep	28 th Sep to 20 th Oct	31 st Oct

Although the records in Table 3.1 are not for 2005 which is the year the GLOBCOVER acquisitions occurred they still correlate with sources found in further review (Lefebure 2005, ICPB 2008). Agricultural records from 2005 suggest that it was a good year for crop production in Iowa; corn was planted in late April for and soybean in the first week of May. Harvest began in September with the vast majority of fields reaped by October. With qualitative estimates of the key crop production dates assessment could in turn be made to investigate if field reflectances agreed.

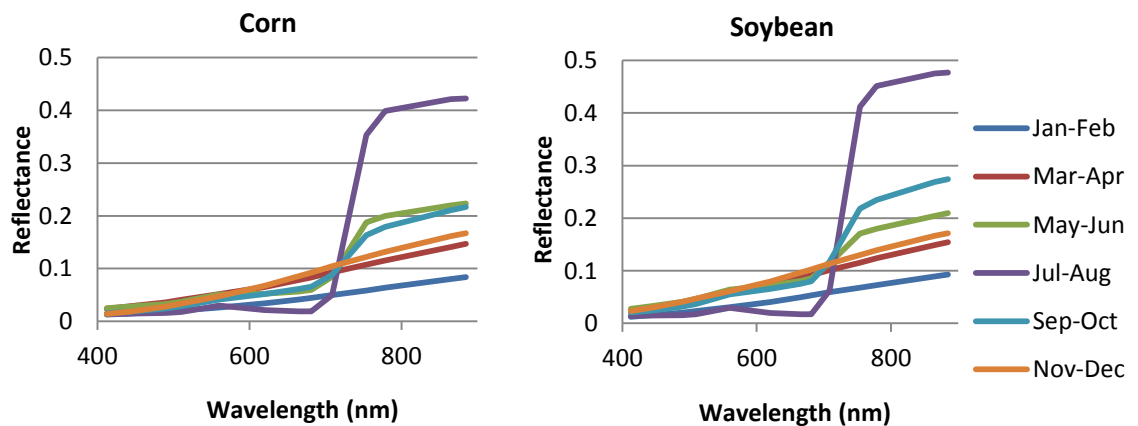


Figure 3.8: 50 corn and 50 soybean averaged bimonthly reflectances derived from GLOBCOVER MERIS FR imagery for 2005.

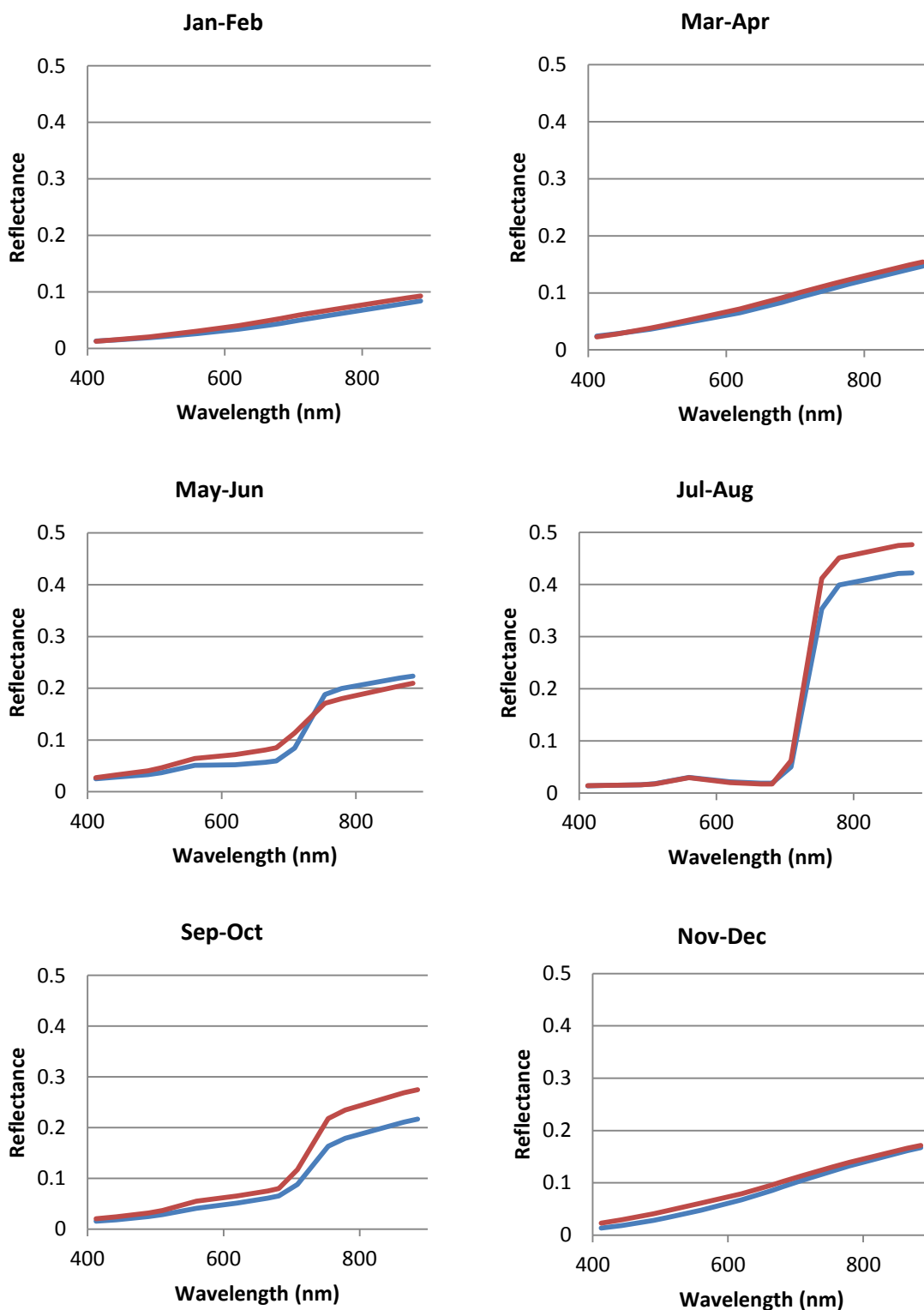


Figure 3.9: 50 corn (blue) and 50 soybean (red) averaged bimonthly reflectances derived from GLOBCOVER MERIS FR imagery for 2005.

Initial investigations were conducted into the differences between corn and soybean development. Both can be seen to have similar spectral responses representing soil lines in Jan-Feb and Mar-Apr. During May-Jun initial growth can be seen where corn appears to develop

faster with greater absorption in the red and increased reflectance in the NIR compared to soybean. These results are supported by work by Gitelson et al. (2005) where it was found that soybean reached peak canopy chlorophyll content half a month after corn did. The difference can also be attributed to (with reference to Table 3.1) that for the years 1996 and 2009 soybean was planted two weeks after corn which would suggest this also occurred in 2005. In the sequential bimonth during the peak of the growing season soybean has increased reflectance in the NIR compared to corn which could suggest a denser canopy structure or the influence of a different LAD. However the result could be also be attributed to the sharper degradation of chlorophyll in corn after the canopy structure has peaked (Gitelson et al. 2005). The increased NIR can be seen to extend into Sep-Oct however it should be noted that the bare soil line reflectances are higher for soybean than corn which this difference could be attributed to.

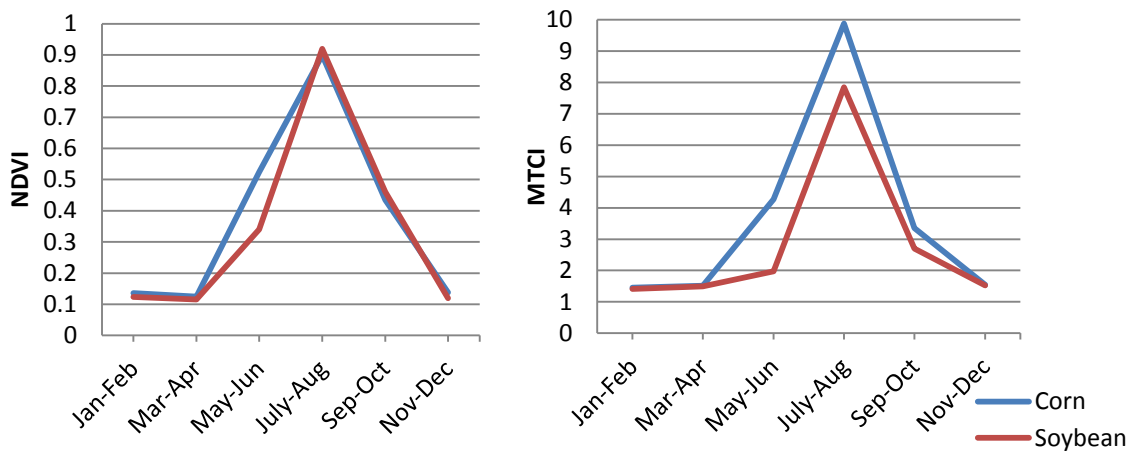


Figure 3.10: NDVI and MTCI values for 50 corn and 50 soybean locations in Iowa for 2005.

Figure 3.8 shows the MTCI and NDVI for corn and soybean over the entire growing season. In Jul-Aug the MTCI is higher for corn than soybean whereas the NDVI can be seen to saturate; saturation is well covered in literature due to the high influence of the red band in the NDVI algorithm (Asrar et al. 1984; Baret and Guyot 1991; Gitelson 2004; Lillesaeter 1982).

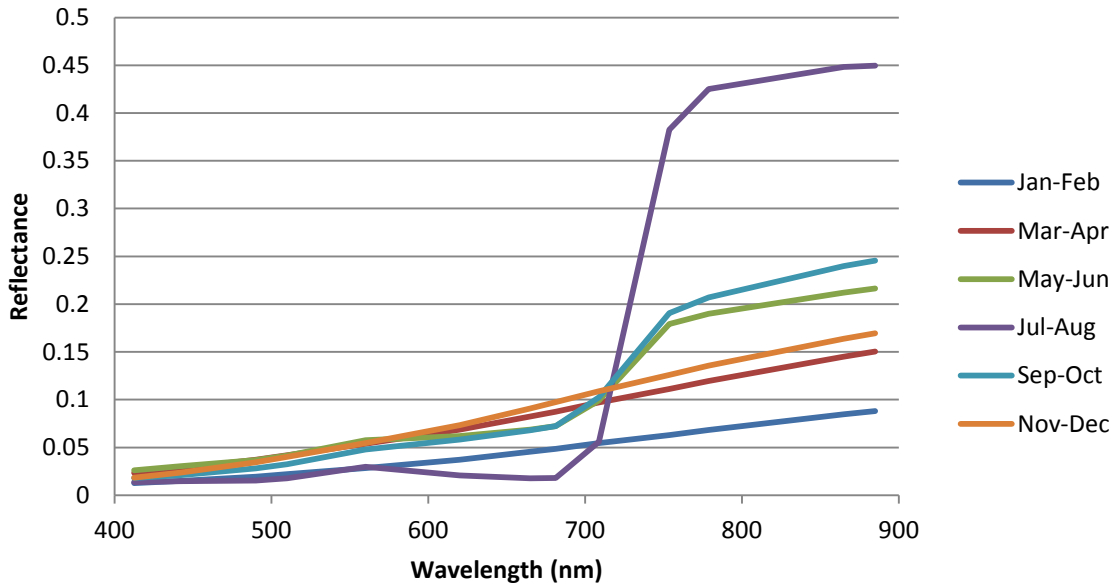


Figure 3.11: Bimonthly average surface reflectances for 100 corn and soybean sites in Iowa for 2005.

When amalgamating the dataset it can be seen that pixel spectral reflectances (Figure 3.11) display typical soil lines for bimonths 1 (Jan-Feb), 2 (Mar-Apr) and 6 (Nov-Dec) across all sites; while 3 (May-Jun), 4 (Jul-Aug) and 5 (Sep-Oct) showed evidence of vegetative cover with a distinct RE. These results coincide with the crop production pattern for the area previously described (Lefebure 2005; IowaCorn 2008). Therefore, a threshold needs to discriminate between the described months which represent soil and vegetated pixel spectra. To assess what possible band combinations to utilise to best discriminate between vegetation and soil based on this dataset the percentage difference between the average pixel reflectance for all site locations during the May-Jun composite and the combined soil dominated months was calculated (Figure 3.12).

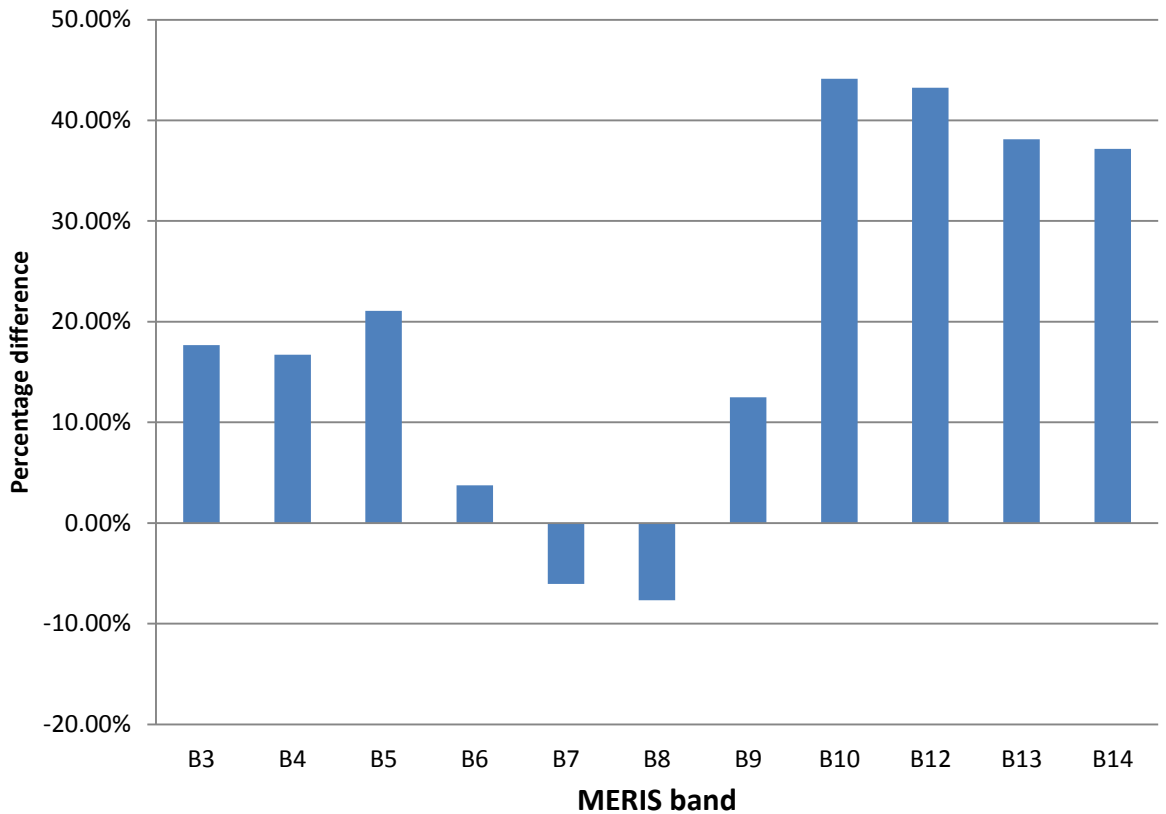


Figure 3.12: Percentage difference between initial vegetation growth (bimonth 3) and soil dominated bimonths (1, 2 and 6).

For the 100 corn and soybean ESUs in Iowa the largest difference in reflectance between sparsely vegetated and barren pixels can be seen in the NIR (band 10) part of the spectrum. A negative difference can be observed in the red part of the spectrum (band 8) while the green band (band 5) also has significant value. In turn the red can be contrasted with the green and NIR to discriminate between soil and vegetation.

$$Green\ Difference = \frac{r_{Red}}{r_{Green}} \quad Eq. (3.5)$$

As discussed in detail in section 2.2. the green part of the spectrum, represented by MERIS band 5, has increased reflectance for a vegetated pixels compared to the red and blue wavelengths due to the chlorophyll absorption minima. On the other hand the chlorophyll absorption maximum is found in the red part of the visible spectrum. Using these two relationships together can be described as the Green Difference (GD; Eq. (3.5)) which is negatively related to increasing chlorophyll content. According to Carter et al. (1996), Gitelson et al. (1997) and Metternicht (2003) the use of the green and red can highlight the differences between healthy and stressed vegetation. The GD expression can tend from 0 to infinity, however in reality it has a range of 0.5 for green vegetation to 3 for bright red soils.

$$\text{Simple Ratio} = \frac{r^{NIR}}{r^{Red}} \quad \text{Eq. (2.4)}$$

The Simple Ratio (Jordan 1969) combines the absorption in the red part of the spectrum with the sharp increase of scattering around 700 nm (RE). Consequently this expression is strongly linked to vegetation density and the output ranges in reality between 1 for soil to 5 or higher for a densely vegetated surface. These two ratios can be combined into a new formulation which utilises the negative relationship with chlorophyll of the GD with the positive of the SR.

$$\text{Soil Discrimination Index} = \frac{r^{NIR}/r^{Red}}{r^{Red}/r^{Green}} \quad \text{Eq. (3.6)}$$

Effectively three key reflectance features of vegetation are combined into the Soil Discrimination Index (SDI; Eq. (3.6)) which aims to be as sensitive as possible to low density vegetation canopies. The use of reflectance directly on the slope of the RE has been omitted from this index as although it has been shown by the MTCI to be strongly related to increasing chlorophyll at high contents, without as much saturation that the NDVI, it is less robust in areas of sparse vegetation which is the most important density for the SDI.

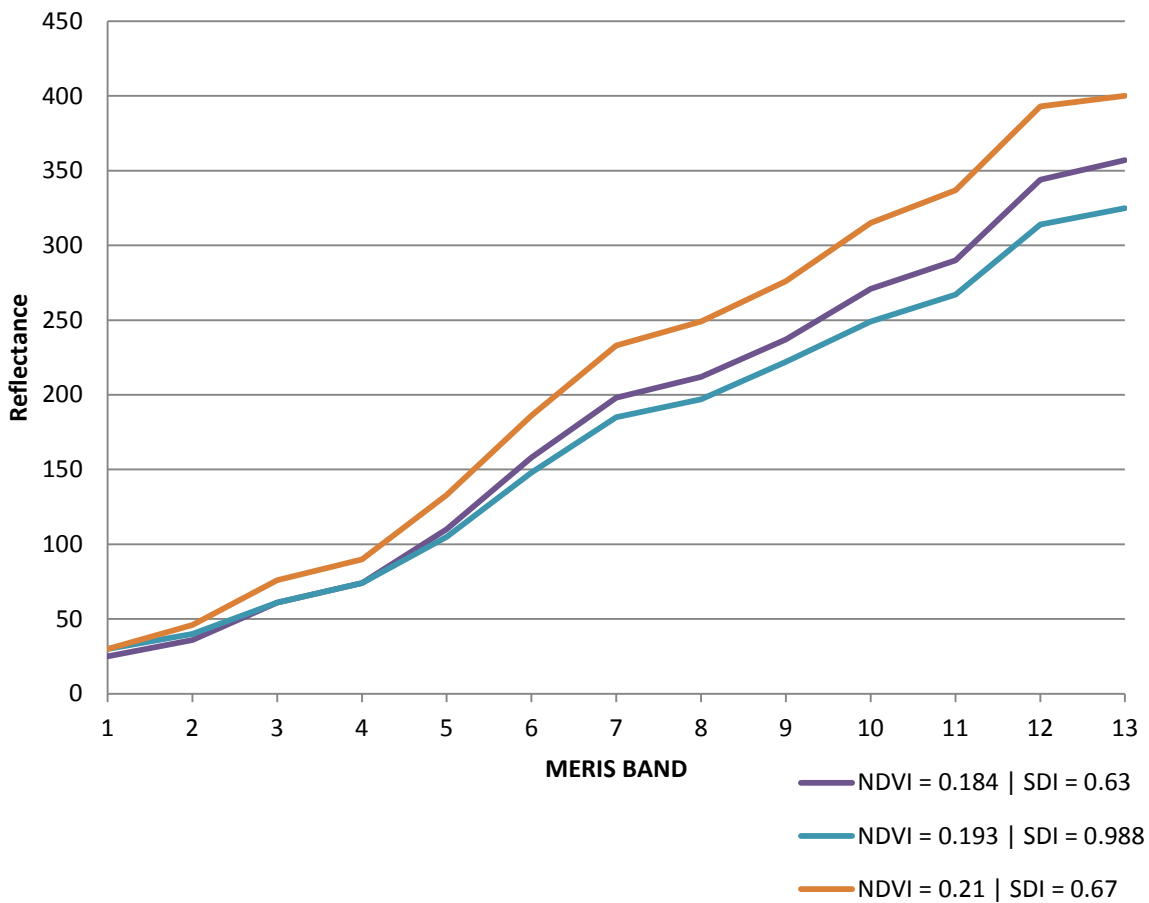


Figure 3.13: Example of discrimination between sparse canopy cover using the SDI for three target locations in Iowa. Series one (purple) and three (orange) show bare soil pixels for bimonth 6 in Iowa; series two (blue) shows a sparsely vegetated location in bimonth 3.

William James Frampton

Figure 3.13 shows an example of the benefits of utilising the GD in conjunction with the SR compared to dependence on the NIR and red alone. Series one (purple) and three (orange) show bare soil pixels for bimonth 6 in Iowa; series two (blue) shows a sparsely vegetated location in bimonth 3. Close examination of the RE between bands 8 to 10 highlight this. NDVI values can be seen to be similar for all locations and it should be highlighted that series two (sparse vegetation) is lower than series three (background reflectance). As a ratio of differences, rather than a ratio of ratios, NDVI alone has been unable to discriminate between the slight, yet important, differences in green, red and NIR reflectance with respect to the overall gradient of the soil line. Conversely the SDI has distinguished between the locations with a high relative difference; this in turn makes it easier to apply a threshold to differentiate between vegetation and bare soil.

3.4. Devising a Threshold

When accounting for the effect of soil on the MTCI it is important to establish clear aims. Changing the formulation should clearly be avoided unless overriding issues are discovered. Work using the ASTER soil library also showed that there is little chance an MTCI result of above 2.3 can be due to soil alone. In turn developing a flag to discriminate between values due to soil and values due to sparse vegetation will return robustness to the MTCI for low canopy cover. With this considered a flag of a specific threshold SDI value could highlight pixels for the user which exhibit the spectral reflectances likely due to soil.

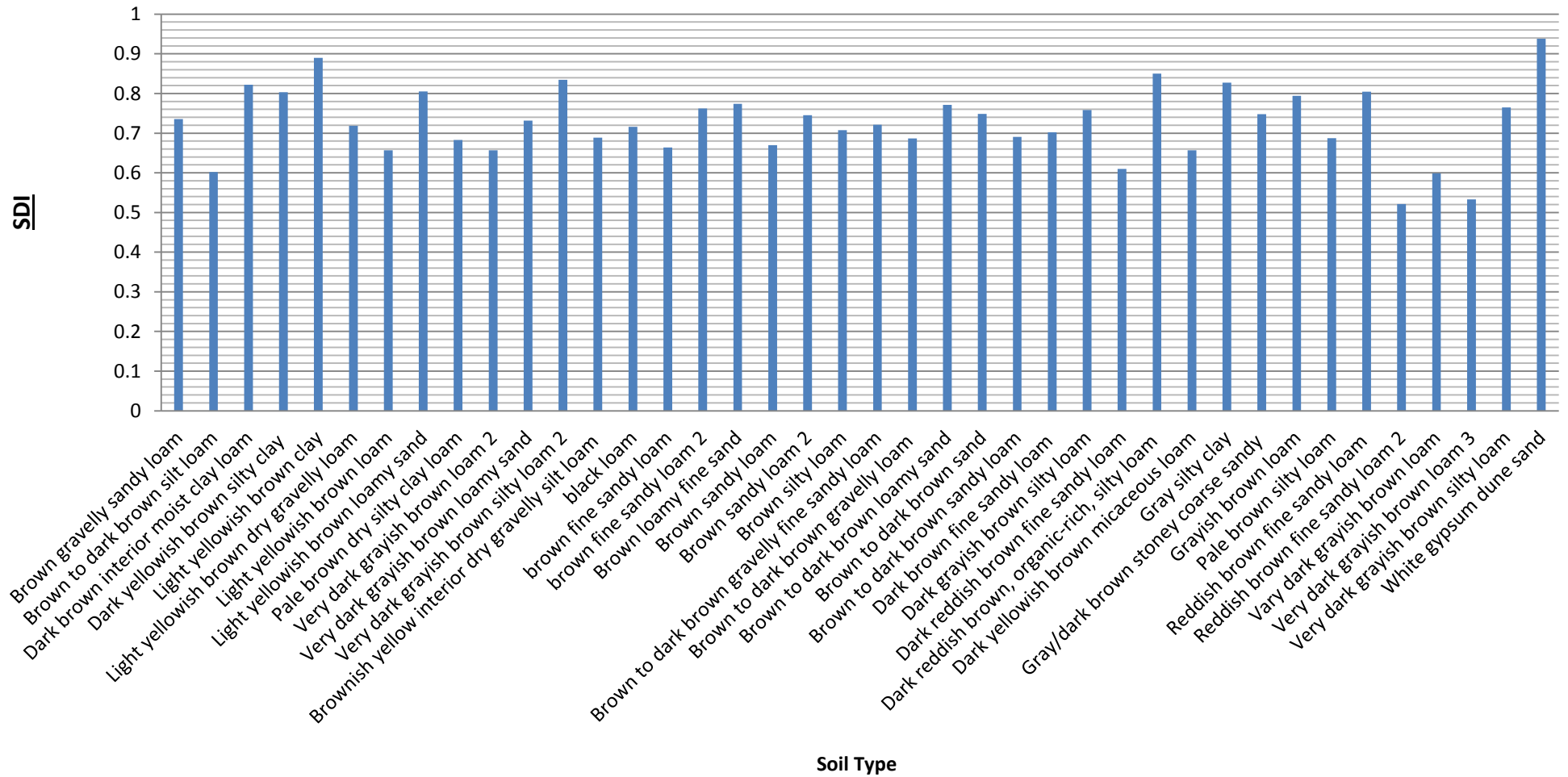


Figure 3.14: SDI values for 40 example soil reflectances from the ASTER spectral soil library.

William James Frampton

To use the SDI as a soil flag for the MTCI an analysis was carried out to test its performance for bare soil locations in North America. The SDI was applied to a range of 40 soil locations from the ASTER spectral soil library (Figure 3.14). It can be seen that the SDI has a maximum of 0.94 for white gypsum sand. This is due to the very high reflectance characteristics it exhibits which can be attributed to its high quartz content (Chuvienco and Huete 2010). The next highest result was for light yellowish brown clay with 0.88 and the lowest was reddish brown fine sandy loam with 0.52. It should be noted that due to the high saline nature of white gypsum it cannot support dense vegetation and will not be populated by more than sporadic bushes resulting in a an extreme heterogeneous canopy. Nevertheless these extreme surface VI results are important to consider when vegetation density is estimated at a regional or global scale as an input into a carbon sequestration model as a surface with a naturally high VI result could add error to the analysis exaggerating an areas capability for photosynthesis.

Subsequently the SDI was applied to Dalhart Texas for varying thresholds to assess what MTCI value pixels are flagged for a specific SDI value.

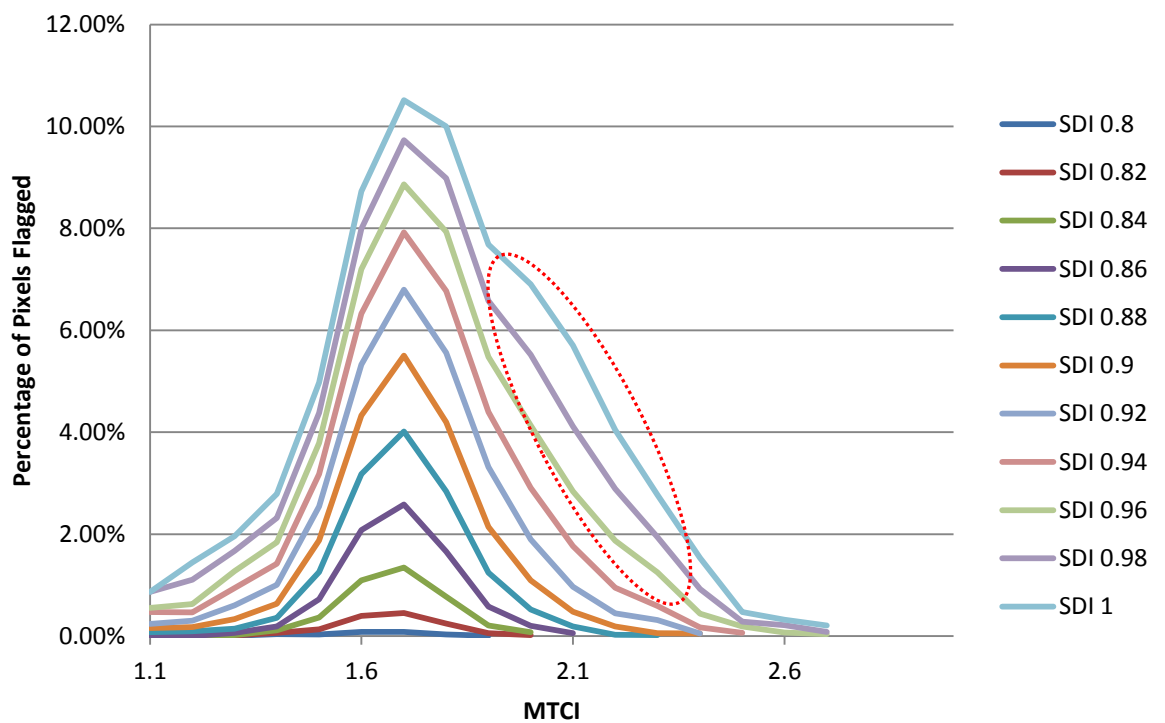


Figure 3.15: Graph to show the percentage of total pixels from the Dalhart MERIS scene that are flagged at a specific SDI threshold and their MTCI value.

Depending on the SDI threshold applied up to 7% of the total pixels in the full resolution MERIS scene (2005-06-23) are flagged. Figure 3.15 shows that the flag can be seen to operate most effectively to pixels within the target MTCI range of soil. However for the higher thresholds of SDI (0.9+) the distribution shows a resurgence of flagged pixels with MTCI values of 2 to 2.3

(highlighted in Figure 3.15). These pixels are likely sparsely vegetated or mixed vegetation locations which are undesirable for the SDI to flag. As the transition from bare soil with naturally high VI results to sparse is gradual the threshold applied needs to flag the most possible soil pixels while not adversely flagging a large proportion of sparse vegetation. Taking into account the lowa dataset and the distribution analysis results from Texas an SDI value of 0.9 is recommended as a threshold for the flag. Using this threshold on the 600,000 pixels from the Texas dataset only 18 out of 50,000 pixels with an MTCI greater than 2.1 were flagged.

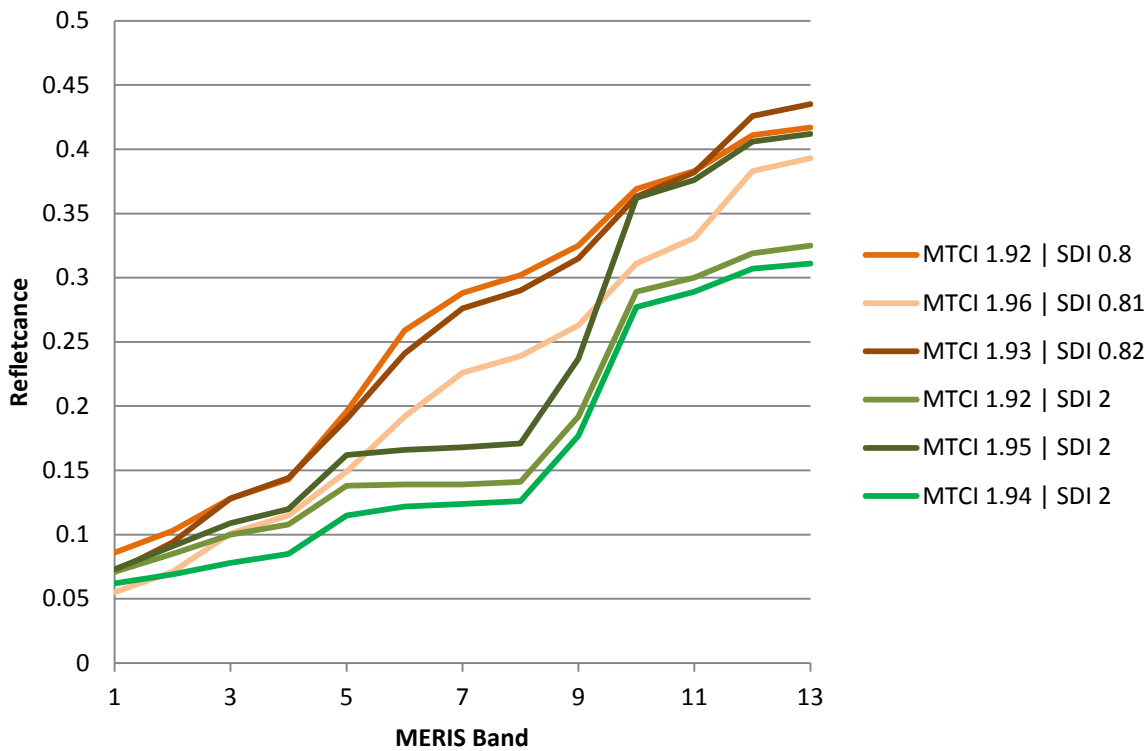


Figure 3.16: Comparing the use of SDI < 0.9 as a flag to account for soil pixels in the MTCI algorithm on corn locations in Iowa 2005. Spectral reflectances shown are for pixels in corn fields taken from FR MERIS data as previously highlighted.

Figure 3.16 visualises the benefits of the SDI < 0.9 flag. Spectral reflectances for pixels in corn fields taken from FR MERIS data as previously highlighted are shown. All 6 examples produce similar MTCI values of 1.9 to 1.95. However examination of the RE shows that the first three series are soil lines while series 4, 5 and 6 are vegetated pixels. It is not possible to discriminate between the soil and vegetated pixels using the MTCI in this example however the proposed threshold of 0.9 SDI clearly flags the first three series of pixels as soil.

3.5. Validation of the Soil Discrimination Index

To validate the performance of the SDI in a different part of the world to North America a study site was selected around Albacete in Spain. Albacete is a market centre for agricultural produce which dominates the land use of the surrounding area and is the most populated city in the autonomous community Castilla-La Mancha. To assess the performance of the SDI in a forested environment an additional site was chosen to the south-west of Albacete and the north-east province of Jaén. The test site covers several national parks including Parque Natural Sierras de Cazorla which is Spain's largest protected natural area. Both test sites are presented in Figure 3.17 and Figure 3.18.

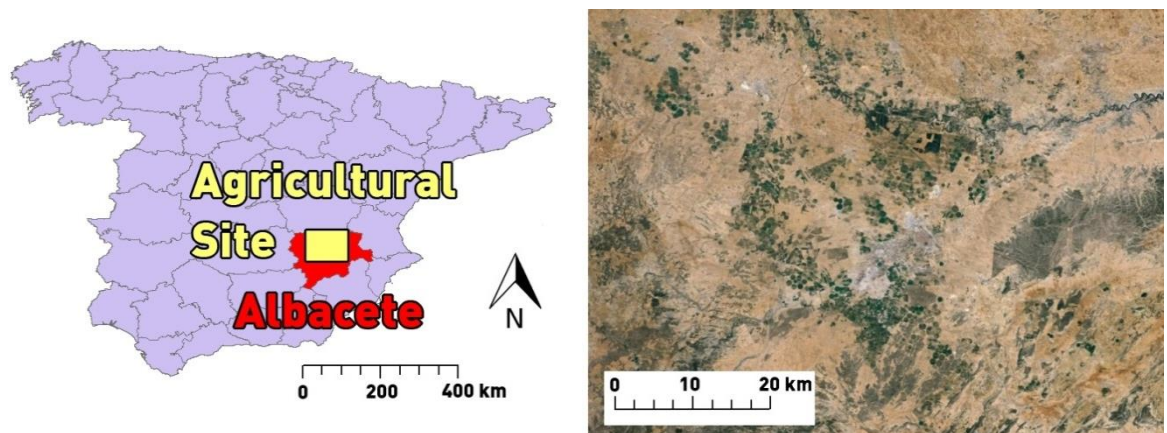


Figure 3.17: Location of the agricultural test site surrounding Albacete.

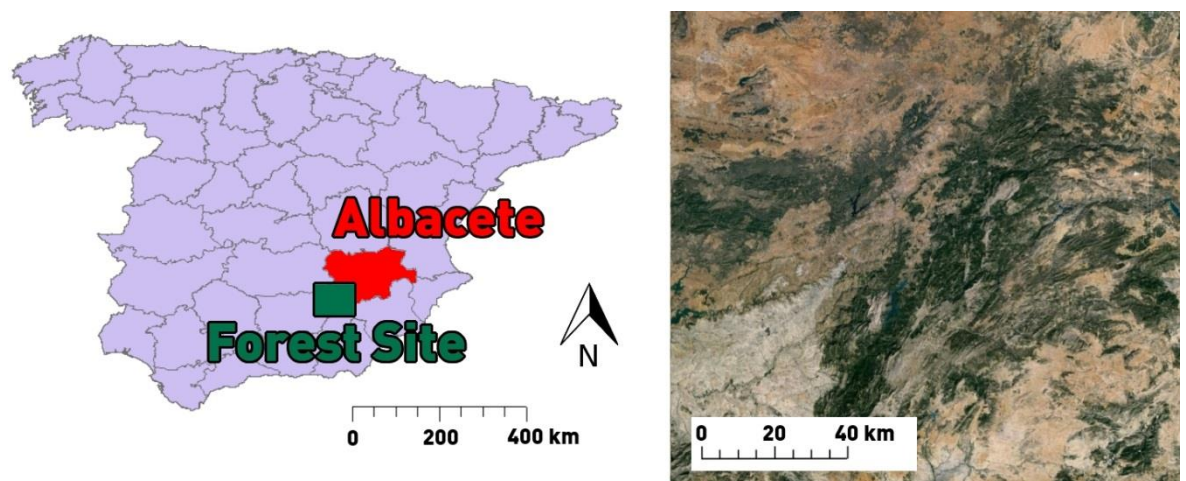


Figure 3.18: Location of the forest test site to the south-west of Albacete.

Total area of the agricultural test site is 5760 km² while the forest test site is slightly smaller at 4860 km². Test sites were selected to cover a range of canopy covers as well as pure soil pixels. The forest test site covers a wide range of trees including evergreen pine forests and deciduous oak climax communities which will affect the MTCI outputs accordingly (UNESCO 2007). MERIS 52

images were acquired monthly for an entire growing season in 2004 from March to December which covered both test sites from the EOLI-SA (Earth Observation Link – Stand Alone) portal. Images from April and May were unusable due to high cloud cover. BOA (Bottom of Atmosphere) MTCI and reflectance data were reprojected and the SDI flag applied with the previously devised threshold of 0.9. Figure 3.19 shows the changing average MTCI of both test sites throughout 2004.

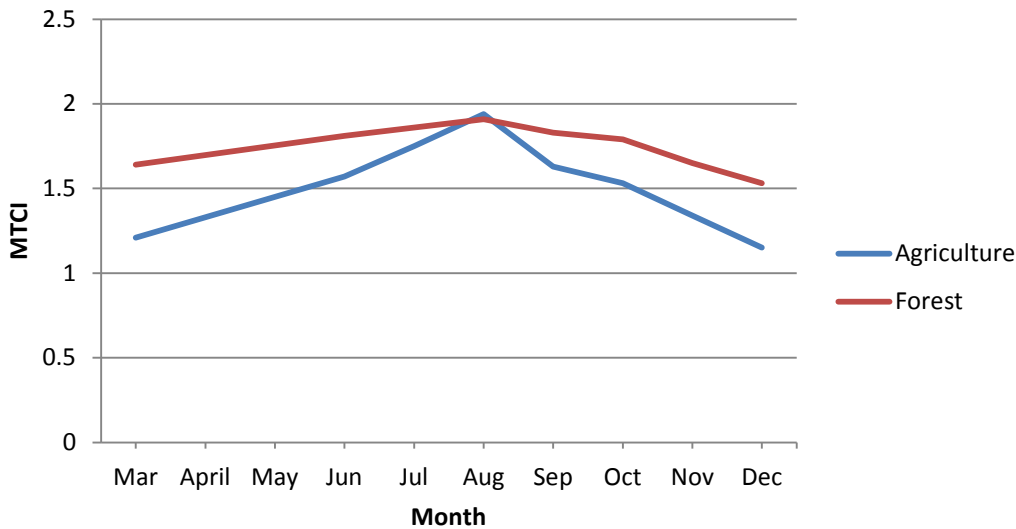


Figure 3.19: Average MTCI of the agricultural and forest test sites in Albacete, Spain for 2004.

As would be expected MTCI steadily increases to a peak in August with an average MTCI of 1.94 and standard deviation of 0.08 for the agricultural site and an average of 1.91 with a standard deviation of 0.09 for the forest site which decreases as the areas senesce in the autumn. During the autumn and spring months the MTCI of the forest test site is higher than the agricultural test site due to the stable evergreen forest for which MTCI does not significantly change unlike the agricultural land for which crop canopy maxima are in the summer months. Nevertheless the MTCI of the forest site still decreases due to the part cover of deciduous forest.

Table 3.2: Table to summarise performance of the SDI for the agricultural test site.

Agricultural Site	Mar	Jun	Jul	Aug	Sep	Oct	Nov	Dec
Total Pixels	63495	64562	63495	64737	64035	63494	63494	63493
Pixels Where MTCI > 2	2016	6909	11911	19338	7603	4127	1529	818
Pixels Where MTCI > 2 SDI < 0.9	33	42	548	992	114	70	9	0
Pixels Where MTCI > 2 SDI < 0.9 as a Percentage of Total	0.05%	0.06%	0.86%	1.53%	0.17%	0.11%	0.01%	0.00%
Pixels Where MTCI > 2 SDI < 0.9 as a Percentage of MTCI > 2	0.19%	0.61%	4.60%	5.13%	1.50%	1.70%	0.59%	0.00%

To assess the performance of the SDI flagged pixels that had an MTCI value of higher than two are presented in Table 3.2. MTCI values of two are generally indicative of medium density vegetation and ideally should not be flagged by the SDI. It can be seen that the highest percentage of flagged pixels, as a percentage of total test site pixels, with an MTCI value of higher than two was 1.53% during August. When these values are calculated as a percentage of total pixels with an MTCI value of higher than two the figure increases to 5.13%. Interestingly while there are a significant number of pixels (6909) with an MTCI of higher than two in June, a time by which many crops will have already reached a canopy maximum, the SDI flags a much smaller percentage, 0.61%, than in July, August, September or October. The reason for this is likely to be crop senescence where changes in pigment content impact the spectral reflectance of the canopy (Boyer et al. 1988) as highlighted in section 2.7.2.2.. Consequently it is possible that the inclusion of green band reflectance into the SDI formula, which helps it to distinguish between vegetation and soil during initial growth, makes it less robust at differentiating as crops yellow in the autumn.

Table 3.3: Table to summarise performance of the SDI for the forest test site.

Forest Site	Mar	Jun	Jul	Aug	Sep	Oct	Nov	Dec
Total Pixels	51712	51705	51713	52633	51235	51713	51713	51712
Pixels Where MTCI > 2	12594	14334	17009	20505	16737	15657	14054	13260
Pixels Where MTCI > 2 SDI < 0.9	0	35	248	386	281	147	9	0
Pixels Where MTCI > 2 SDI < 0.9 as a Percentage of Total	0.00%	0.07%	0.48%	0.73%	0.55%	0.28%	0.02%	0.00%
Pixels Where MTCI > 2 SDI < 0.9 as a Percentage of MTCI > 2	0.00%	0.24%	1.46%	1.88%	1.68%	0.75%	0.06%	0.00%

It can be seen that for the forest test site the highest percentage of flagged pixels, as a percentage of total test site pixels, with an MTCI value of higher than two was 0.73% during August which is 1.88% of total pixels with an MTCI value of higher than two in that month. This value is significantly lower than the agricultural test site result of 5.13% for August. Moreover the forest site had less vegetated pixels flagged relative to the total pixels with an MTCI value of two or more in all months except September. This suggests the flag performs better outside of an agricultural environment. In March only 3.18% of the agricultural test sites land cover had an MTCI of greater than two compared to the forest site of which 24.35% was greater than two. Of these 12,594 pixels not one was flagged by the SDI with similar result witnessed in December. Results for the forest test site are similar to that of the agricultural one with regards to the difference in performance between June and post July results further suggest that senescence

William James Frampton

causes the SDI to be less robust at differentiating as vegetation yellows in the autumn. Nevertheless with on average 0.35% and 0.27% and at most 1.53% and 0.73% of pixels incorrectly flagged by the SDI for the agricultural and forest test sites respectively overall the flag has performed well for the study location.

3.6. Conclusions

As the MTCI puts large weight on the reflectance of the RE band in relation to the position of the red and NIR the effect of the soil background reflectance at low canopy covers can cause uncertainty. It was considered to make adjustments to the MTCI algorithm specifically at low values to account for this however such a method would affect the use of the index as a linear surrogate measure of chlorophyll content. By creating the SDI as an independently functional flag the original MTCI formulation is retained which will not affect compatibility with previous investigations. It was found that 0.9 was a suitable threshold to use for the SDI in Dalhart Texas and it flagged all 40 types of soil that were retrieved from the ASTER soil library. Subsequently the SDI was applied to two study sites in Spain as an initial validation of the flag. While it performed well analysis highlighted two issues that are worth investigating in future study. Firstly, that inclusion of green reflectance into the formula results in less robust flagging of senescent vegetation and secondly, that the flag performs better in a forest environment than an agricultural setting. Nevertheless applying the SDI with a threshold of 0.9 as a soil flag will warn the user that the MTCI result is likely due to a soil background with a naturally high VI output consequently increasing the robustness of the MTCI at values below two. The flag will be most useful when using the MTCI across large scenes with many varying canopy covers and soil background types and conditions and should increase accuracy of the MTCI when used to estimate photosynthetic capabilities of an area.

Chapter 4: Evaluating the Capabilities of Sentinel-2 for Quantitative Estimation of Biophysical variables in Vegetation

4.1. Introduction

Europe's Copernicus programme (ESA 2011a) includes two Sentinel-2 (S-2) satellites designed to provide systematic global acquisitions of high resolution multispectral imagery. The Multi-Spectral Instrument (MSI) aboard S-2 has been designed to enable the continuity of Satellite Pour l'Observation de la Terre (SPOT) and Landsat type data into the future. MSI also builds upon the heritage of the MERIS and NASA MODerate-resolution Imaging Spectroradiometer (MODIS) instruments in providing more spectral bands than Landsat or SPOT. Bands known to be important in sensing vegetation will have a spatial resolution of 10 m or 20 m, others will have 60 m resolution. S-2 will have a radiometric accuracy of <5% and operate at 12 bit radiometric resolution (ESA 2010) which is suitable for vegetation (Tucker 1980b). The mission envisions a pair of satellites simultaneously circulating the Earth in a sun-synchronous 180° phase orbit with a 290 km swath (ESA 2010). The first satellite, S-2A, is planned for launch in April 2015 followed by S-2B which is tentatively planned for launch two years after (ESA 2011a). Tandem operation of S-2A and B will deliver a revisit period of up to five days under cloud-free conditions.

Knowledge of canopy chlorophyll content and LCC can indicate plant health and potential gross primary productivity (Gitelson et al. 2006; Boyd et al. 2012), while LAI can provide an insight into the function and structure of the canopy (Wilhelm et al. 2000). Land cover (including vegetation type), LAI and the fraction of absorbed photosynthetically active radiation (FAPAR) are all Global Climate Observing System (GCOS) Essential Climate Variables (ECVs) required by the United Nations Framework Convention on Climate Change (UNFCCC) and the Intergovernmental Panel on Climate Change (IPCC) (GCOS 2010). Satellite derived estimations of LAI and canopy chlorophyll content are key inputs into climate models as they provide estimates of carbon sequestration (Ciais et al. 1997). Consequently they have been used in services such as the Farmstar programme by EADS Infoterra to provide information supporting precision agriculture through timely and efficient use of fertilisers (Farmstar 2011). A number of techniques have evolved in the past to derive the biophysical variables of vegetation using remote sensing data; these can be grouped into three broad categories: the inversion of radiative transfer models (Shultis and Myneni 1988), machine learning (neural networks) (Carpenter et al. 1999) and the use of Vegetation Indices (VIs). Methods based on VIs have the benefit of being computationally simple while they are generally less site specific and more universally applicable than the other methods. Consequently

VIs are a widely used method to provide quantitative ground measurements of the biophysical parameters of vegetation by contrasting specific spectral reflectance characteristics of vegetation and are frequently implemented operationally using remotely sensed data. Satellite derived VIs provide one of the best possible ways to obtain the biophysical parameters of vegetation over large areas (regional or global) while retaining the high temporal coverage required for many applications and consequently their development and validation is of great importance.

The first VIs contrasted the strong reflectance in the near-infrared (NIR) by plant matter with strong absorption by chlorophyll in the red part of the electromagnetic spectrum to quantify vegetation greenness parameters. Jordan (1969) made references to the retrieval of canopy chlorophyll content and LAI using the ratio of NIR/R which became known as the Simple Ratio (SR). The SR is the basis of the Normalized Difference Vegetation Index (NDVI) (Rouse et al. 1973) which is currently the most widely used VI as a measure for many variables. Much work has been done investigating the optimal reflectance wavelengths for use in the SR and the NDVI algorithms (for example, the Pigment Specific Simple Ratio (PSSR_a), Blackburn 1998). Although VIs such as the NDVI were primarily developed for the purpose of LAI retrieval they have also been argued to be capable of accurate canopy chlorophyll content estimations (Myneni et al. 1995, Huete et al. 2002). Refinements of the NDVI and SR such as the Perpendicular Vegetation Index (PVI) (Richardson and Wiegand 1977) and the Soil Adjusted Vegetation Index (SAVI) (Huete 1988) aimed to account for uncertainty due to variation in background condition. The PVI achieved this through implementing NIR and red reflectance measurements of soil pixels into the equation while SAVI incorporated the correction factor L into the NDVI formula. L accounts for soil variation by varying the factor between 1, for low vegetation, and 0, for dense vegetation. This effectively retains original NDVI output at higher values of vegetation density. Qi et al. (1994) subsequently presented a modified version of the SAVI (MSAVI) which utilised a self-adjusting L factor as the product of NDVI and the Weighted Difference Vegetation Index (WDVI) (Clevers 1988) which incorporates the slope of the soil line. It should be noted that the self-adjusting L means MSAVI adjusts SAVI, an index based around the NDVI, by NDVI and WDVI and in the process results in a loss in the vegetation dynamic response (Qi et al. 1994). Other VIs have also been developed to account for aerosol variation such as the atmospherically resistant vegetation index (ARVI) which makes use of aerosol resistance coefficients to reduce atmospheric influences (Kaufman and Tanré 1992). Sequentially a combination of SAVI and ARVI was presented by Huete et al. (2002) as the enhanced vegetation index (EVI). Although NDVI refinements have aimed to account for, or mitigate, many of the uncertainties in VIs through doing so they often require additional scene specific information. Acquiring and applying such scene specific information can adversely affect the universal application of VIs as well as their dynamic response.

William James Frampton

A wealth of VIs have been developed to estimate canopy chlorophyll content with varying strengths and levels of robustness (e.g., Daughtry et al. 2000, Broge and Mortensen 2002, Dash and Curran 2004, Gitelson et al. 2005). Many such VIs presented band variations of the NDVI formula such as the Green Normalized Difference Vegetation Index (GNDVI) (Gitelson et al. 1996) which challenged the approach of using red reflectance and instead used the green reflectance in its place. It was argued to be at least five times more sensitive to chlorophyll-a concentration than the NDVI and specifically useful for differentiation in stressed and senescent vegetation. Daughtry et al. (2000) presented a modified chlorophyll absorption in reflectance index (MCARI) which was developed for minimising the effects of non-photosynthetic materials. Work reported strong response to LCC variation while noting that the index encounters issues at low LAI due to higher influence of background variation.

After the success of the NDVI and its specialised refinements subsequent work made use of developments in spectral capabilities to provide better characterisation of the RE which is the prominent spectral feature of vegetation located between the red absorption maximum and high reflectance in the NIR. Quantification of the RE is often achieved through calculation of the REP which is recognised as the point of maximum slope along the RE and has been argued to provide enhanced estimates of LCC and canopy chlorophyll content (Horler et al. 1983, Curran et al. 1990). Evaluation of the REP at a global scale with high temporal resolution was first achieved using data from the MERIS sensor. MERIS had a spectral band located directly on the RE (band 9 708.75 ± 5 nm) which led to the development of the MERIS Terrestrial Chlorophyll Index (MTCI) (Dash and Curran 2004) a surrogate REP index which has been implemented operationally as a standard level 2 global product from the Envisat MERIS sensor. The MTCI has demonstrated that it is possible to use the REP parameter to estimate chlorophyll content over very extensive spatial areas at a high temporal resolution (Dash and Curran 2006).

Table 4.1: Spectral bands of Sentinel-2 MSI.

S-2 Band	1	2	3	4	5	6	7	8	8a	9	10	11	12
Central Wavelength (nm)	443	490	560	665	705	740	783	842	865	945	1375	1610	2190
Bandwidth (nm)	20	65	35	30	15	15	20	115	20	20	30	90	180
Spatial Resolution (m)	60	10	10	10	20	20	20	10	20	60	60	20	20

As S-2 will enable multiple operational reflectance measurements on and around the RE at a greatly enhanced spatial resolution of 20 m with a short revisit time it holds much appeal for vegetation monitoring. The combination of S-2 bands 5 and 6 (Table 4.1) provide the opportunity for improved characterisation of the RE than was previously possible operationally at a global scale. Consequently there is much scope for the development of algorithms to retrieve the biophysical parameters of vegetation using S-2. Some algorithms have already been presented in work by Delegido et al. (2011b) which specifically investigated the optimal bands to use in the NDVI formula with synthesised S-2 data. Research found that bands 4 and 5 were the optimal combination and the formula will be further investigated in this analysis and referred to as the NDI45. There are many different VIs each designed for a separate purpose and validated at varying levels using different datasets. Consequently each has its own strengths and weaknesses in application and some are more optimal at retrieving certain parameters of vegetation than others. With the caveat of saturation considered, this chapter will investigate the strength of VIs presented in Table 4.2 for the SicilyS2EVAL and SEN3Exp field campaigns. VIs have been selected that do not self-normalise or linearise which forfeits sensitivity to vegetation variance. Also VIs that require the use of scene specific information that consequently affects their universal applicability and operational use with S-2 have also been excluded from analysis.

Table 4.2: A list of Vegetation Indices that have been analysed for use with Sentinel-2 using field data.

Vegetation Index	Formulation	S-2 Bands Used	Original Author
NDVI	$(\text{NIR}-R)/(\text{NIR}+R)$	$(B7-B4)/(B7+B4)$	Rouse et al. 1973
NDI45	$(\text{NIR}-R)/(\text{NIR}+R)$	$(B5-B4)/(B5+B4)$	Delegido et al. 2011b
MTCI	$(\text{NIR}-RE)/(RE-R)$	$(B6-B5)/(B5-B4)$	Dash and Curran 2004
MCARI	$[(RE-R)-0.2(RE-G)]*(RE-R)$	$[(B5-B4)-0.2(B5-B3)]*(B5-B4)$	Daughtry et al. 2000
GNDVI	$(\text{NIR}-G)/(\text{NIR}+G)$	$(B7-B3)/(B7+B3)$	Gitelson et al. 1996
PSSR _a	NIR/R	B7/B4	Blackburn 1998

4.2. Data and Methods

The approach adopted in this chapter compared simulated S-2 data with field measurements and the output of an established vegetation canopy model (PROSAIL) (Baret et al. 1992, Jacquemoud et al. 2009). The simulated data were derived from two airborne hyperspectral sensors, an Itres

William James Frampton

Instruments Compact Airborne Spectrographic Imager (CASI-1500) and a Specim AISA Eagle instrument collected during two field campaigns: SEN3Exp (SEN3Exp 2011), and SicilyS2EVAL. SEN3Exp was conducted in June and July 2009 to prepare for the Sentinel-3 mission and to aid the development of scientific algorithms; however, ground data is highly suitable for S-2 investigations.



Figure 4.1: Location of test site (courtesy of google earth, Landsat 04/10/2013) with flight lines added from the SEN3Exp campaign acquisition report (SEN3Exp 2011).

SicilyS2EVAL was a campaign conducted in Sicily 2010 which was funded by ESA specifically to support validation of vegetation products for S-2. The combination of these two field campaign datasets provided 60 elementary sampling units (ESUs), from which ground canopy chlorophyll content measurements were obtained from sample areas of 10 x 10 m and 20 x 20 m to represent the spatial resolution of S-2.



Figure 4.2: SicilyS2EVAL test site with example of the crop canopy.

4.2.1. PROSAIL Model Data

PROSAIL is the combination of the PROSPECT-5 leaf optical properties model (Jacquemoud and Baret 1990) and the 4SAIL canopy bidirectional reflectance model (Verhoef 1984, 1985). The model was used to simulate canopy reflectance for a range of leaf biochemistry and canopy parameters (Table 4.3). During the model simulation both LAI and LCC were varied to provide a good range (LAI was varied from 0-8, whereas LCC was varied from 5-70 $\mu\text{g cm}^{-2}$). Other parameters were taken as an average value from the literature; this was to ensure that the changes in the modelled spectral reflectance are only due to changes in LAI and leaf chlorophyll content. Two datasets were generated; All PROSAIL Data and SEN3Exp PROSAIL. The 'All PROSAIL Data' was the correlation between reflectance and canopy chlorophyll content for a wide range of biophysical variables between the wavelengths of 500-800 nm. Alternatively, the SEN3Exp PROSAIL dataset represented reflectances generated from the PROSAIL model while using the same ESU biophysical variables of the SEN3Exp campaign. SicilyS2EVAL was not considered due to the low range of LAI and LCC compared to SEN3Exp.

Table 4.3: Biophysical parameters chosen for PROSAIL data set.

Model Variables		Units	Range
PROSPECT			
N	Leaf structure index	Unitless	1.5
C_{ab}	Leaf chlorophyll content	$[\mu\text{g cm}^{-2}]$	5-70
C_m	Leaf dry matter content	$[\text{g cm}^{-2}]$	0.009
SAIL			
LAI	Leaf area index	$[\text{m}^2 \text{m}^{-2}]$	0-8
ALA	Average leaf angle	$[\text{°}]$	35
HotS	Hot spot parameter	$[\text{m m}^{-1}]$	0.01
S	Sun zenith angle	$[\text{°}]$	30
V	View zenith angle	$[\text{°}]$	10

4.2.1.1. In Situ Data Collection: SicilyS2EVAL

SicilyS2EVAL targeted a single crop type, *grillo* (grapevine) during May 2010. Each of the 25 ESUs was a composition of multiple LAI and LCC measurements representing a 10 x 10 m sample area. LAI was systematically sampled 18 times at different locations within each ESU using the Li-Cor LAI-2000 near dusk and dawn under diffuse radiation conditions.

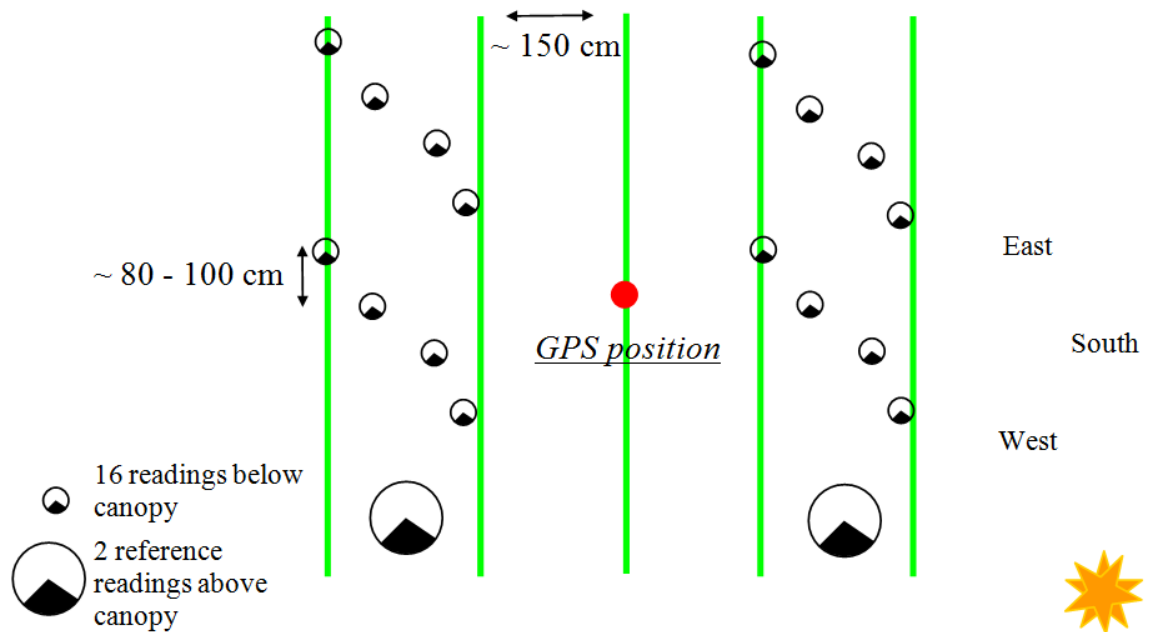


Figure 4.3: Sampling strategy for LAI measurements from SicilyS2EVAL campaign. 16 readings were taken below the canopy spread throughout the 10 x 10 m sampling area centred on a GPS coordinate. Two above the canopy readings were taken to adjust for changes in solar intensity.

A total of 81 Relative LCC measurements were taken using a Minolta SPAD-502™ (Delegido et al. 2011a), these measurements were spread evenly across the canopy of 9 separate plants at each ESU. In addition to the SPAD measurements leaf cuttings (5 mm diameter) were removed from 30 separate plants selected using a systematic sampling strategy. The leaf cuttings were taken at a consistent position of each leaf and stored in dimethylformamide for later analysis. Absorption in 647 nm and 664 nm were measured using a Rayleigh UV-1800™ spectrophotometer and used to estimate chlorophyll a and chlorophyll b of the sample using Eq. (4.1) and Eq. (4.2) (Moran and Porath 1980, Moran 1982). Total chlorophyll concentration estimated from this analysis was correlated with the SPAD measurements to provide an absolute LCC value using Eq. (4.3).

$$\text{Chlorophyll a} = 11.65 * A_{664} - 2.69 * A_{647} \quad \text{Eq. (4.1)}$$

Where A_{647} and A_{664} are sample absorptions at wavelengths of 647 nm and 664 nm.

$$\text{Chlorophyll b} = 20.81 * A_{647} - 4.53 * A_{664} \quad \text{Eq. (4.2)}$$

William James Frampton

Where A_{647} and A_{664} are sample absorptions at wavelengths of 647 nm and 664 nm.

$$\text{Total Chlorophyll} = 3.79 * S + 79.79 \quad \text{Eq. (4.3)}$$

Where S is the representative SPAD value.

4.2.1.2. In Situ Data Collection: SEN3Exp

Data from the SEN3Exp campaign, which took place in June and July 2009, included 35 canopy chlorophyll content measurements from agricultural sites in the Barrax region of Spain (SEN3Exp 2011). The crop dataset composition consisted of: corn, garlic, oat, onion, potato, sunflower, alfalfa and grapevine. Within each of the 20 x 20 m ESUs, 24 LAI field measurements were taken using a Li-Cor LAI-2000™ (SEN3Exp 2011) and relative LCC measurements were made using a SPAD. Relative LCC measurements were converted to absolute LCC using destructive leaf sampling of a subset of five samples per ESU in a Varian spectrophotometer after extraction of chlorophyll with dimethylformamide (SEN3Exp 2011). Table 4.4 provides a summary of the field campaign data used in this analysis.

Table 4.4: Summary of field campaign data used in analysis.

Campaign	Location	Number of ESUs	ESU Size	Date
SicilyS2EVAL	Castelvetrano - Sicily	25	10 x 10 m	May 2010
SEN3Exp	Barrax – Spain	35	20 x 20 m	June/July 2009

4.2.2. Airborne Acquisitions

SEN3Exp hyperspectral data was collected using a CASI-1500 sensor operating at 2.4 nm spectral and 1.5 m spatial resolution. Five flight lines were acquired with an overlap of 50% at an altitude of 2743 m. Atmospheric conditions were good with some reported high cloud appearing during the survey (SEN3Exp 2011). For the SicilyS2EVAL campaign hyperspectral airborne data was collected and processed to level 1B by the natural environment research council (NERC) airborne research and survey facility (ARSF) using a Specim EAGLE sensor. The sensor operated at a spectral resolution of 2.2 nm between the range of 400-1000 nm with a spatial resolution of less than 1.5 m flying at an altitude of 5000 m under clear sky conditions with a solar zenith angle of 70°. All ESUs were contained within two flight lines with an overlap of 50%.

4.2.3. Band Weighting and Data Processing

Prior to simulating S-2 bands, the Eagle data from SicilyS2EVAL were geometrically corrected using a parametric method, AZGCORR (Azimuth Systems 2005) based on in-flight altitude and

William James Frampton

heading data. Geometrically corrected images were atmospherically corrected using ATCOR-4 (ReSe Applications 2011) which is based around an atmospheric look-up table (Richter 2008) that contains the results of radiative transfer calculations from the MODTRAN-4 model. After atmospheric correction the available S-2 bands were synthesised from CASI and Eagle data using a weighting function based on the S-2 spectral response files.

4.3. Designing Optimal Indices for Biophysical Variable Retrieval from Sentinel-2 Data

Direct assessments have been made between canopy chlorophyll content measurements and spectral reflectances for available wavelengths. Canopy chlorophyll content (g m^{-2}), the product of LCC and LAI, is the total amount of chlorophyll in a given area. The following results show how reflectance is affected for a range of canopy chlorophyll contents over a large part of the visible and NIR spectrum. The method aimed to highlight the strongest vegetative absorption and reflectance signatures and subsequent analysis explored how well they could be harnessed using the available S-2 bands with the goal of formulating the optimal vegetation index for deriving each of the key biophysical variables previously outlined in section 2.1.. An optimal index, for all intents and purposes, is the most accurate combination of reflectance measurements to provide a surrogate measure, over the entire natural range, of the biophysical variable in question.

4.3.1. Relationship Between Spectral Reflectance Generated from PROSAIL and Canopy Chlorophyll Content.

Analysis of the PROSAIL results provided insight into; (i) how reflectance related to the biophysical variables of interest, and; (ii) how these correlations compared to ground data from the field campaigns presented in this chapter. This method of investigation highlighted the most highly correlated vegetative features with respect to wavelength for the two PROSAIL datasets and is presented in Figure 4.4.

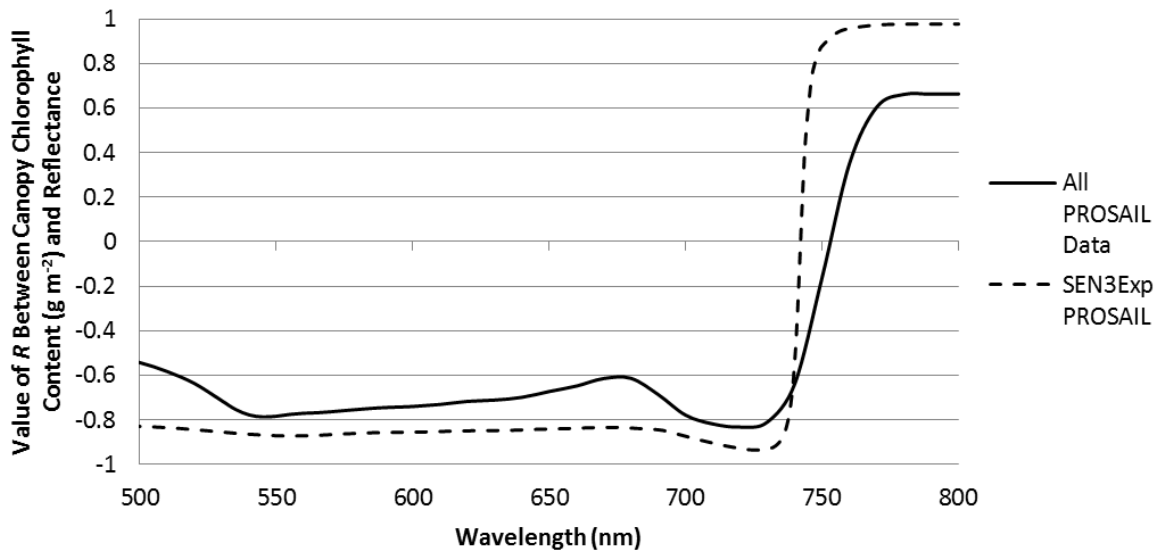


Figure 4.4: Comparing the correlation coefficient (R) between spectral reflectance and canopy chlorophyll content with changing wavelength for both PROSAIL datasets.

LAI and LCC were varied between 0-8 using increments of 0.2 and 5-70 $\mu\text{g cm}^{-2}$ using increments of 5 $\mu\text{g cm}^{-2}$ respectively for the All PROSAIL Data while SEN3Exp PROSAIL represented reflectances generated from the PROSAIL model by inputting biophysical variables attributes as the SEN3Exp campaign. There were issues with using the all PROSAIL dataset in this correlation analysis as the difference between the lower and higher step values of LCC cause the RE to be more drawn out, as can be seen in Figure 4.4, in comparison to the smaller SEN3Exp PROSAIL dataset. PROSAIL was found to highlight the correlation between reflectance and canopy chlorophyll content in the red to peak between 705-735 nm and after a very steep and narrow RE it can be seen that spectral reflectance is positively correlated to canopy chlorophyll content above 750 nm.

4.3.2. Relationship between Spectral Reflectance and Canopy Chlorophyll Content for SicilyS2EVAL.

Figure 4.5 illustrates the relationship between canopy chlorophyll content and spectral reflectance for 25 ESU locations in SicilyS2EVAL. Firstly, assessing the NIR correlation showed that the relationship was consistently positive above 745 nm. Increased reflectance in the NIR due to vegetation is a well-documented feature of vegetation density due to internal leaf scattering (Gausman 1974, Knipling 1970). The correlation coefficient (R value) of the relationship between the canopy chlorophyll content and wavelength in the NIR was low partly due to the vegetative sample having a relatively low LAI range (0.16-1.05) but also due to the influence of soil background reflectance at low LAI. Although the resulting correlation strength was low (Figure

4.5) and the p value of > 0.05 indicated that the result was not significant, the change in correlation with respect to the transition of the RE is noteworthy when compared to results from SEN3Exp highlighted in section 3.3. During atmospheric correction several bands in the red (680-690 nm) had to be removed due to sensor saturation issues. Noting this caveat, the red part of the spectrum was found to have a strong and statistically significant ($p < 0.05$) negative relationship between spectral reflectance and canopy chlorophyll content with maximum correlation at 678 nm. This was primarily due to absorption by canopy chlorophyll content. The strength of the red correlation decayed either side of this narrow peak, especially above 690 nm. Correlation between visible light reflectance and canopy chlorophyll content can be seen to decay to a minimum strength in the green (543 nm +/- 15 nm) where chlorophyll absorption reached a minimum. The green relationship had a negative correlation with canopy chlorophyll content due to the sparse ESU locations of bright soil having higher reflectance than the vegetated pixels. Nevertheless, the trend specifically showed the strongest green signal according to this dataset (528-558 nm).

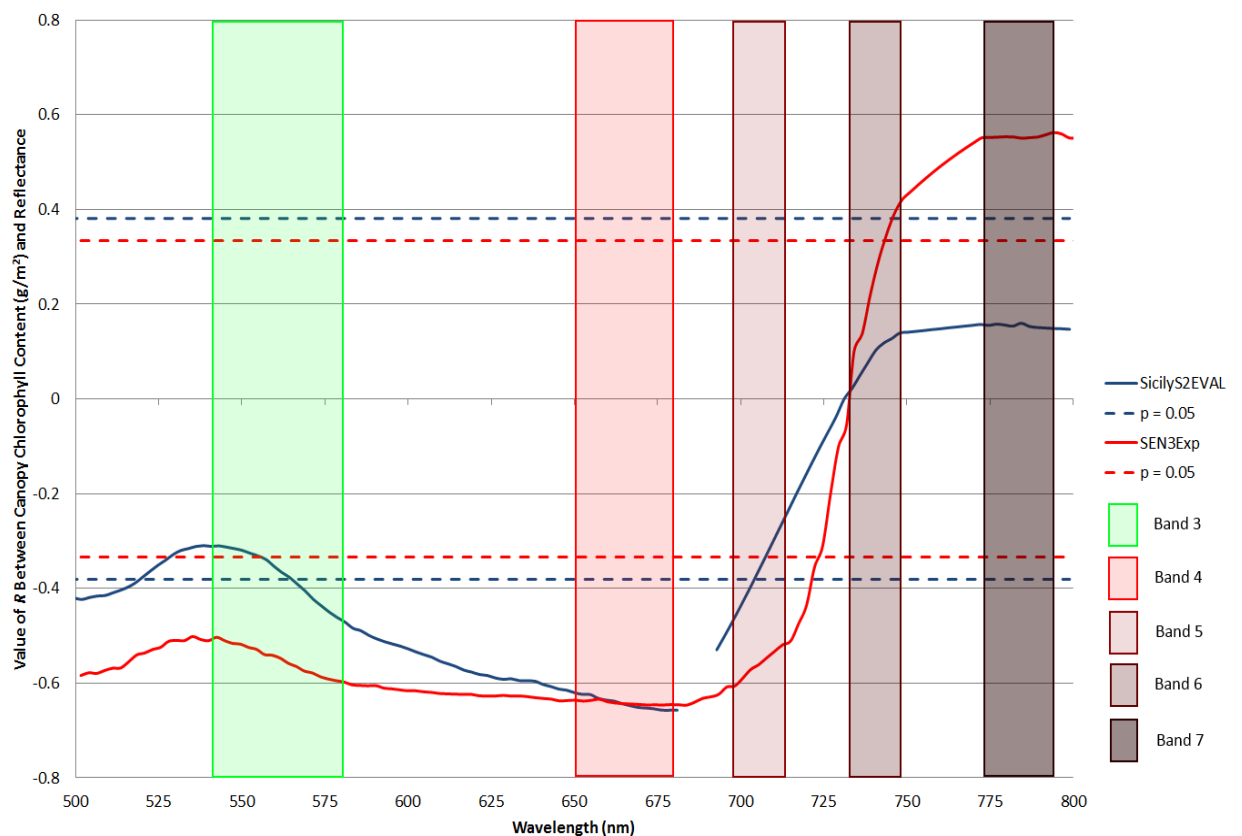


Figure 4.5: Comparing the correlation coefficient (R) between spectral reflectance and canopy chlorophyll content with changing wavelength for the SicilyS2EVAL and SEN3Exp field campaigns with indications of S-2 band positions and dashed lines to show where $p = 0$.

4.3.3. Relationship between Spectral Reflectance and Canopy Chlorophyll Content for SEN3Exp

Figure 4.5 displays the correlation between the spectral reflectance and canopy chlorophyll content at specific wavelengths for the 35 ESU SEN3Exp dataset. The NIR correlation can be seen to be stronger and statistically significant ($p < 0.05$) compared to the SicilyS2EVAL data above 750 nm reaching maximum strength above 770 nm. The correlation between red reflectance and canopy chlorophyll content reached a maximum at 680 nm and, as with the SicilyS2EVAL dataset, quickly decayed above 690 nm. Similar to the SicilyS2EVAL results the SEN3Exp results show visible absorption correlation decayed to a minimum in the green at 540 nm (+/- 15 nm).

4.3.4. Comparison between Field Campaign Data and PROSAIL.

Table 4.5 summarises the outcomes of the correlation coefficient analysis for both SEN3Exp, SicilyS2EVAL and the PROSAIL SEN3Exp data. The ‘central wavelength’ is the point at which the correlation reaches a maximum strength of R in the NIR, red and green. However, in the case of ‘RE 0’ it was where the correlation in the RE = 0. It should be noted that ‘RE 0’ was not a REP measurement but used as a statistical measure to compare between datasets. In Table 4.5 the ‘range of correlation’ is the extent of the strongest correlation with regards to wavelength for each dataset that can be used to characterise the three key spectral reflectance features in the green, red and NIR.

Table 4.5: Outcomes of correlation signal investigation.

Part of Spectrum	Central Wavelength			Range of Correlation		
	SicilyS2EVAL	SEN3Exp	PROSAIL SEN3Exp	SicilyS2EVAL	SEN3Exp	PROSAIL SEN3Exp
NIR	750 nm	770 nm	770 nm	750 nm+	750 nm+	760 nm+
RE 0	730 nm	730 nm	742 nm	n/a	n/a	n/a
Red	678 nm	677 nm	725 nm	660-685 nm	600-690 nm	705-735 nm
Green	543 nm	540 nm	555 nm	528-558 nm	525-555 nm	545-565 nm

Table 4.5 highlights close similarities between the two field campaigns in most parts of the visible and NIR spectrum with the only noticeable differences being; (i) the width of the red correlation feature which is narrower in SicilyS2EVAL towards the green than SEN3Exp, and; (ii) the strength, but not position, of the NIR reflectance feature. However there are significant differences

between the field and PROSAIL datasets.

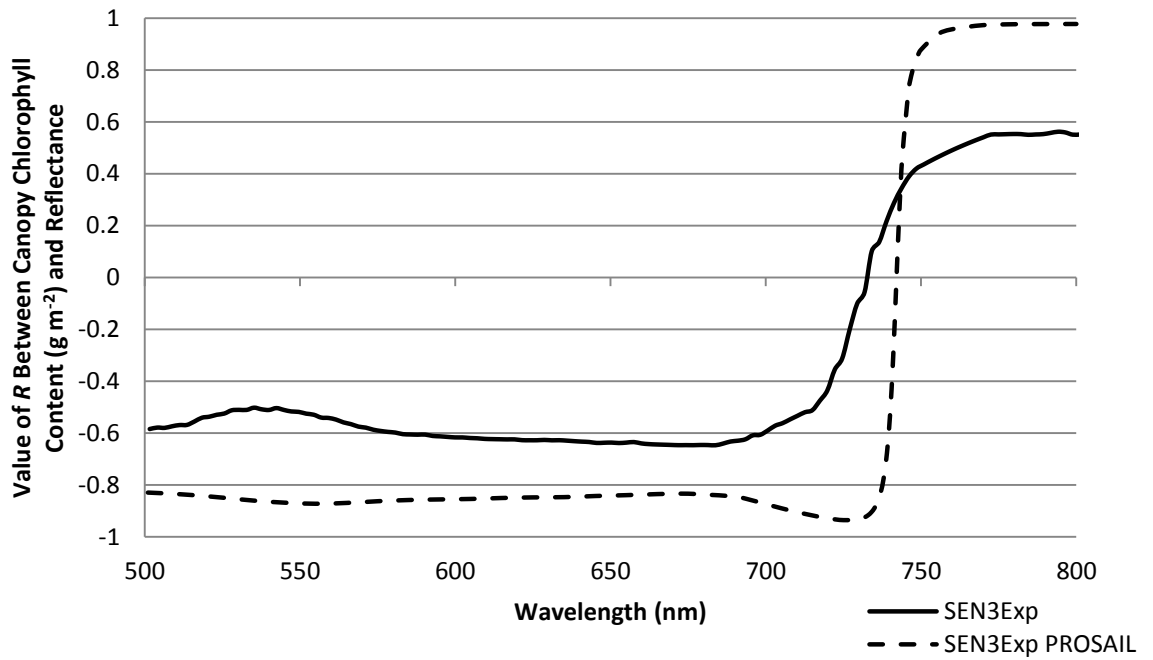


Figure 4.6: Comparing the correlation coefficient (R) between canopy chlorophyll content and spectral reflectance for the SEN3Exp field campaign and SEN3Exp PROSAIL with changing wavelength.

The PROSAIL model data was compared with SEN3Exp data in which is displayed in Figure 4.6. It is interesting to note that the PROSAIL data had a strong negative correlation with canopy chlorophyll content until 735 nm. This was not the same for the SEN3Exp and SicilyS2EVAL field data where the correlation between spectral reflectance and canopy chlorophyll content in the red part of the spectrum rapidly decreased above 690nm (see Figure 4.5) and is positive above 730 nm.

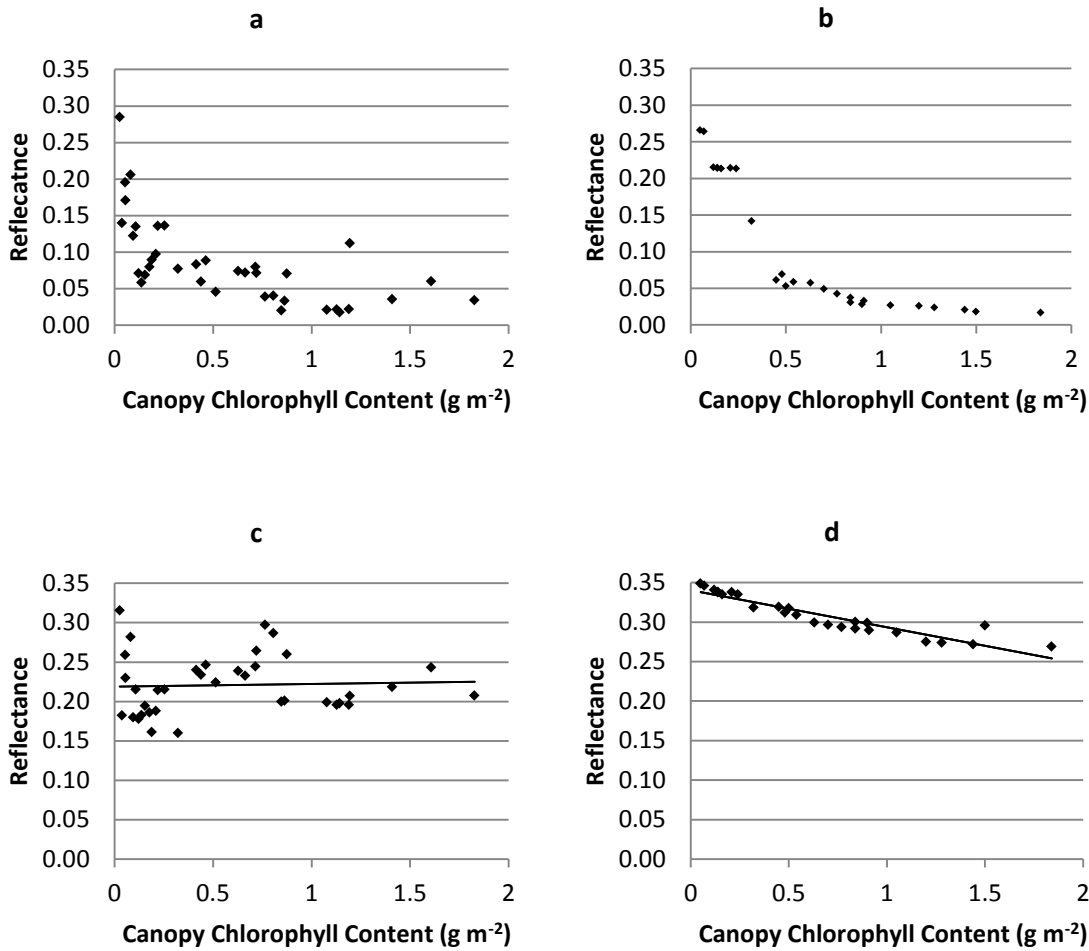


Figure 4.7: Comparison of PROSAIL SEN3Exp (b and d) and SEN3Exp field data (a and c) at 680nm (a and b) and 730nm (c and d).

In light of the differences in correlation between the field and PROSAIL data in the RE reflectance was compared at 680 nm and 730 nm (Figure 4.7). It can be seen that at 680 nm the field data (Figure 4.7(a)) and the PROSAIL data (Figure 4.7(b)) show a decline in reflectance with an increase in chlorophyll content. However, at 730 nm no relationship was present for the field data (Figure 4.7(c)) while the RTM (Figure 4.7(d)) remained negative with an R^2 of 0.87 where $p < 0.001$. Although the slope between reflectance and canopy chlorophyll content at this wavelength was 0.05 for the RTM this still results in a 23% reduction in absolute reflectance over the range of 0.05-1.84 g m⁻² canopy chlorophyll content. In the NIR part of the spectrum, RTM results are similar to the field campaign data becoming strongly positive at 750 nm and reaching maximum strength at 770 nm (Figure 4.7). There was also a difference between the datasets in the green. The field data showed a weakening of the negative relationship while the PROSAIL data showed the negative relationship becoming slightly stronger. Upon further investigation the cause of this difference with the PROSAIL data was an issue of saturation of canopy chlorophyll content with change in green reflectance. When ESUs with high canopy chlorophyll content values were

William James Frampton

removed the R^2 between canopy chlorophyll content and spectral reflectance in the green was weaker than in blue and red for the SEN3Exp PROSAIL dataset correlating with the SEN3Exp field data trend.

4.3.5. Suitability of S-2 Bands for Retrieval of Biophysical Variables.

SicilyS2EVAL and SEN3Exp field campaigns correlation results at specific wavelengths are combined in Figure 4.5 which also highlights the available bands for S-2 near the RE (Table 4.2). Firstly, according to the two field campaign datasets, S-2 band 3 (542.5-577.2 nm, green band) does not cover the optimal wavelengths where, due to increased canopy chlorophyll content, the green reflectance is less strongly correlated to canopy chlorophyll content than in the red and blue parts of the visible spectrum. Using a band width of 525 to 555 nm would be theoretically optimal for the datasets presented. Secondly S-2 band 4 (red band) captures absorption due to chlorophyll as its bandwidth extends until just before the RE where spectral reflectance begins to shift from a negative to positive relationship with canopy chlorophyll content. Furthermore, the bandwidth of S-2 band 4 is not adversely wide whereas, according to the two datasets and especially SicilyS2EVAL, if the lower band limit extended below 650 nm the bands strength of characterising the chlorophyll absorption feature would be weakened. The MERIS continuation RE band (S-2 band 5: 705 nm +/-7.5 nm) has increased spectral bandwidth compared to MERIS band 9 (708.75 nm +/-5 nm). However, with the central band position only slightly changed this should not make significant impact for RE characterisation considering it is situated over a linear part of the RE. S-2 band 6 is a new RE/NIR band with respect to previous satellite sensors such as RapidEye and MERIS. Considering vegetative monitoring and capturing the NIR feature S-2 band 6 will, as a replacement for MERIS band 10 (753.75 nm +/- 3.75 nm), receive increased mixed signal from the RE as it is situated at the peak of the RE rather than slightly beyond it. However the position of the band and its combination with S-2 band 5 will, consequently, provide the opportunity for enhanced estimation of the REP compared to MERIS or RapidEye. Finally S-2 band 7, which is similar to MERIS band 12 (775 nm +/- 7.5 nm), is the optimal band in the NIR for capturing the vegetative signal in the NIR based on SicilyS2EVAL and SEN3Exp data sets.

It should be highlighted that, with reference to Table 4.5, the correlation in vegetation spectral reflectance and canopy chlorophyll content shown between these two separate field campaigns is consistent considering their differences with respect to airborne sensor, location, operating team, time of year and field campaign procedures. Taking this into account gives confidence in using this presented dataset to compare methods for canopy chlorophyll content, LAI and LCC retrieval from S-2 data.

4.3.6. New Vegetation Indices for S-2

Based on the relationship between spectral reflectance in individual S-2 MSI bands and canopy chlorophyll content, LAI and LCC, this chapter proposes two new methods to estimate biophysical variables for use with S-2 MSI data. First, the Inverted Red Edge Chlorophyll Index (IRECI, Eq. (4.4)) which incorporates the reflectance in four S-2 bands to estimate canopy chlorophyll content, and second, the Sentinel-2 Red Edge Position (S2REP, Eq. (4.5)); a version of REP estimation for S-2 using linear interpolation (Guyot and Baret 1988, Clevers et al. 2000).

$$IRECI = \frac{r_{NIR} - r_R}{r_{RE2}/r_{RE1}} = \frac{r_{783} - r_{665}}{r_{705}/r_{740}} \quad \text{Eq. (4.4)}$$

IRECI makes use of both RE bands, that S-2 will provide, to characterise the RE slope by using the reflectance at 740nm and 705nm (Table 4.1) while also making use of the maximum and minimum vegetation reflectances found in the NIR and red at 783 nm and 665 nm respectively. By using the LCC indicative RE reflectance IRECI does not put heavy emphasis on the red, which will help to avoid saturation, while still utilising the strong contrast of the SR sensitive to LAI. Based on field dataset from SEN3Exp and SicilyS2EVAL campaigns, IRECI is a near direct calculation of field measured canopy chlorophyll content (g m^{-2}) with a slope of 0.9004 and intercept of 0.1795 with a coefficient of determination of 0.87 (see section 4.3., Table 4.6). However, further validation will be required with other datasets and specifically a larger range of canopy chlorophyll content.

$$S2REP = 705 + 35 * \frac{\left(\frac{r_{NIR} + r_R}{2}\right) - r_{RE1}}{r_{RE2} - r_{RE1}} = 705 + 35 * \frac{\left(\frac{r_{783} + r_{665}}{2}\right) - r_{705}}{r_{740} - r_{705}} \quad \text{Eq. (4.5)}$$

S2REP (Eq. (4.5)) is based on linear interpolation as presented by Guyot and Baret (1988) where the reflectance at the inflexion point is estimated and in turn the REP is retrieved through interpolation of S-2 band 5 and 6 which are positioned on the RE slope. This linear interpolation method has been previously applied to MERIS data by Clevers et al. (2000) and was found to be more robust than the Lagrangian method (Dawson and Curran 1998) with the benefit of requiring a limited number of spectral bands making it suitable for spaceborne sensors (Clevers et al. 2002). S-2 has a key benefit compared to MERIS for the application of the linear interpolation method. S-2 band 6 (740 nm) measures the reflectance situated at the top of the linear part of the RE slope whereas MERIS band 10 (753.75 nm) measures reflectance slightly above the linear part of the RE where the gradient is decreasing as it reaches the NIR plateau. In theory this means that S2REP should provide better characterisation of the RE slope compared to application of the method using the MERIS or the future Sentinel-3 sensors.

4.4. Evaluation of the Spectral Indices

Each VI output was derived from the synthesised S-2 data for the field campaigns presented in Table 4.4. The correlation with LAI, LCC and canopy chlorophyll content for each assessed VI is presented in Table 4.6.

Table 4.6: Coefficient of determination results of each Vegetation Index for varying field data sets and biophysical variables, light green highlights where $0.7 < R^2 < 0.8$ and dark green highlights where $0.8 < R^2$. Results denoted with * have p values of < 0.001 .

Variable	Data Set	NDVI	NDI45	MTCI	MCARI	GNDVI	PSSR	S2REP	IRECI
Canopy Chlorophyll Content	Combined	0.70*	0.78*	0.51*	0.42*	0.66*	0.72*	0.47*	0.87*
	SicityS2EVAL	0.83*	0.78*	0.65*	0.66*	0.45*	0.84*	0.35	0.64*
	SEN3Exp	0.62*	0.70*	0.24	0.75*	0.58*	0.59*	0.23	0.84*
LAI	Combined	0.63*	0.76*	0.39	0.55*	0.58*	0.61*	0.36	0.88*
	SicityS2EVAL	0.86*	0.84*	0.55*	0.72*	0.42*	0.83*	0.19	0.74*
	SEN3Exp	0.57*	0.68*	0.15	0.88*	0.49*	0.51*	0.12	0.84*
LCC	Combined	0.56*	0.30*	0.77*	0	0.58*	0.36	0.91*	0.24
	SicityS2EVAL	0.62*	0.63*	0.39	0.35	0.54*	0.62*	0.24	0.35
	SEN3Exp	0	0	0.25	0	0.02	0.03	0.51*	0

4.4.1. Leaf Chlorophyll Concentration

Although majority of VIs had poor correlation with LCC (Table 4.6) the MTCI and S2REP achieved strong correlation with LCC with R^2 of 0.77 and 0.91 respectively Figure 4.8.

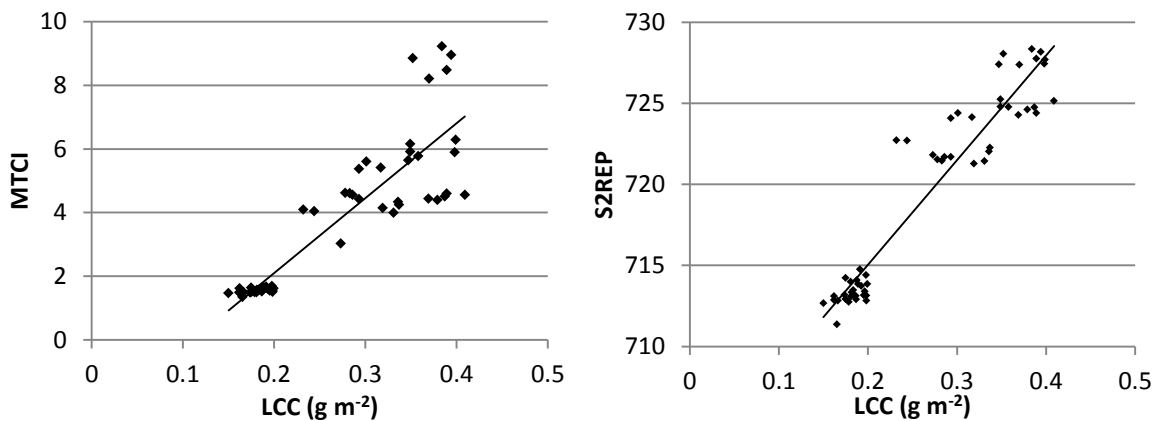


Figure 4.8: Coefficient of determination comparisons between MTCI, S2REP and LCC.

The MTCI and S2REP are the only two VIs in the analysis that solely characterise the RE which has been shown to be sensitive to variation in LCC (Horler et al. 1983, Curran et al. 1990, Dash and Curran 2004). Increases in LCC result in a broadening of the major red absorption feature which causes a shift in the REP towards longer wavelengths (Boochs et al. 1990). Previous experimental

studies have shown low LCC to be associated with REP values near 700 nm and high LCC to attain REP results closer to 725 nm (Boochs et al. 1990, Horler et al. 1980, Lamb et al. 2002). S2REP performed with similar results for the combined SicilyS2EVAL and SEN3Exp datasets producing REP results of 711-728 nm for LCC values of 0.16-0.41 g/m². The high MTCL outliers are discussed later in the thesis.

4.4.2. Leaf Area Index.

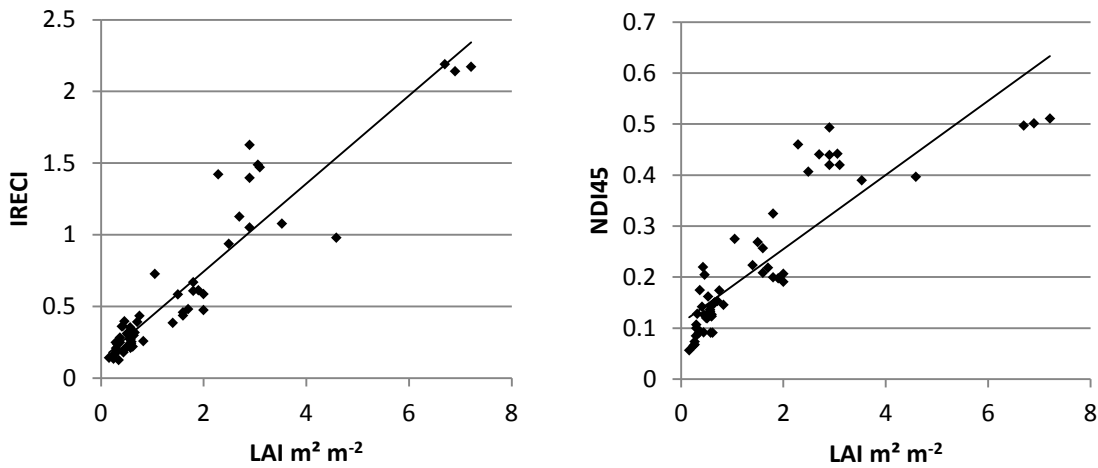


Figure 4.9: IRECI and NDI45 compared for LAI from SEN3Exp and SicilyS2EVAL field campaigns.

The IRECI and the NDI45 were the best performing VIs with respect to LAI with R^2 values of 0.88 and 0.76 respectively. Although developed for correlation with canopy chlorophyll content IRECI is shown in Figure 4.9 to be linear with LAI. When compared for lower values of LAI below 2 the IRECI and the NDI45 have an R^2 of 0.77 and 0.62 ($p < 0.001$) respectively.

4.4.3. Canopy Chlorophyll Content.

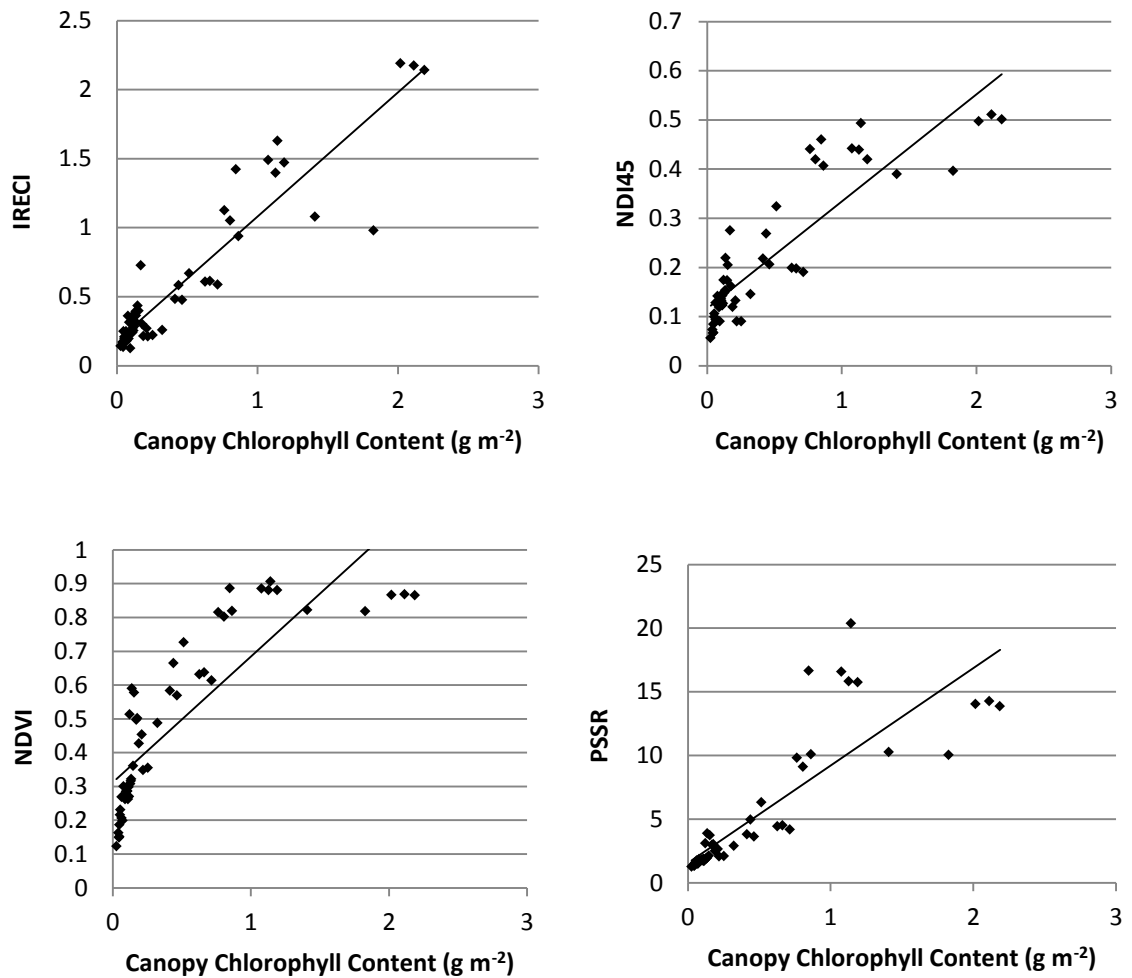


Figure 4.10: IRECI, NDI45, NDVI and PSSR compared to canopy chlorophyll content for field data from SicilyS2EVAL and SEN3Exp field campaigns.

The four best performing VIs (NDVI, PSSR, NDI45 and IRECI) (Table 4.6) in terms of correlation coefficient with respect to canopy chlorophyll content are compared in Figure 4.10. Saturation is noticeably present above a canopy chlorophyll content value of 1 g/m² for the NDVI ($R^2 = 0.70$) due to saturation of red reflectance (Kanemasu 1974, Tucker 1979, Horler et al. 1983, Buschmann and Nagel 1993.) The PSSR ($R^2 = 0.72$) functions linearly with canopy chlorophyll content although its spread increases significantly at higher values. When comparing the NDVI and the NDI45 this dataset suggests the change from using reflectance measurements in the NIR (band 7) to RE1 (band 5) has increased spread at lower canopy chlorophyll content values but made NDI45 more linear with less saturation at higher values than the NDVI. The IRECI was the best performing measure of canopy chlorophyll content using synthesised S-2 field data for the two presented campaigns. The index can be seen to have a strong linear relationship with canopy chlorophyll content without saturation at higher values. As highlighted earlier in section 5, the IRECI also has

William James Frampton

the useful trait of being a near direct calculation of canopy chlorophyll content in g/m^2 for this dataset. The inclusion of RE bands improved correlation over the entire data set while mitigating the saturation effect at higher canopy chlorophyll content. However, the inclusion of these bands also increased the spread of the IRECI at very low canopy chlorophyll content ($<0.13 \text{ g/m}^2$) compared to the NDVI and PSSR_a .

4.5. Conclusions

S-2 provides a great opportunity for global vegetation monitoring due to its enhanced spatial, spectral and temporal characteristics compared with Landsat and SPOT. Simulated S-2 data has been compared to a combined field dataset of 60+ ESUs across two field campaigns covering eight separate crops. Although the field campaigns varied with respect to year, location, airborne sensors and field teams, similar relationships between spectral reflectance and canopy chlorophyll content were obtained. All bands around the RE have been shown to be useful in assessing vegetation condition, specifically canopy chlorophyll content. However, there is a need for further investigation of the green reflectance region 525-555 nm and its potential role in estimating canopy chlorophyll content. The results suggest that the wavelengths covered by the S-2 green band may not be optimal to capture the changes in reflectance due to canopy chlorophyll content.

It has been highlighted that many VIs attempt to correct for uncertainties or inaccuracies through incorporation of scene specific parameters or normalisation functions. Application of such methods affects the universal applicability and ease of operational use. S2REP has been presented and shown as the most suitable method for quantifying LCC using these datasets; nevertheless the MTCI also had noteworthy results. A novel index the IRECI has been shown to be linearly related to canopy chlorophyll content at a near 1:1 ratio in g m^{-2} while still performing well for LAI up to and beyond the common saturation point. It achieves this as it utilises the opportunities S-2 bands 5 and 6 present for RE characterisation while still incorporating the robustness of the SR. Further validation is required with other field campaigns and synthetic S-2 data to reinforce findings.

Chapter 5: Investigating the Opportunities for Application of MTCI using Sentinel-2 and Sentinel-3 and the Feasibility to Downscale

5.1. Introduction

The MTCI is an already well-established algorithm for the retrieval of biophysical parameters in vegetation, specifically as a surrogate measure of chlorophyll content. During the 10 years MERIS was active the MTCI was produced as an operational product. With the loss of Envisat on the 8th of April 2012 the future of the MTCI will therefore be dependent on the S-2 and S-3 missions. S-2 is currently planned for launch in April 2015 while S-3 is tentatively set for Mid-2015 (ESA 2011a). Although due to this there will be a gap in MTCI coverage long running datasets can be integral to certain vegetative studies. Furthermore while S-3 will continue global acquisitions of the MTCI at 300 m spatial resolution S-2 will allow operational calculation of the MTCI at 20 m spatial resolution. Consequently there is need for research to investigate the opportunities of application of the MTCI with S-2 and S-3 and the possible differences that must be accounted for. The availability of reflectance bands of S-3 and S2 compared to MERIS is summarised in Table 5.1 and bands of specific interest between 500 and 800 nm are overlaid onto a typical vegetative reflectance spectra in Figure 5.1, Figure 5.2 and Figure 5.3 for MERIS, S-2 and S-3 respectively.

Table 5.1: Summary of Spectral band of MERIS, Sentinel-2 and Sentinel 3.

MERIS			Sentinel-3			Sentinel-2		
Band	Central Wavelength (nm)	Bandwidth (nm)	Band	Central Wavelength (nm)	Bandwidth (nm)	Band	Central Wavelength (nm)	Bandwidth (nm)
			1	400	15			
1	412.5	10	2	412.5	10			
2	442.5	10	3	442.5	10	1	443	20
3	490	10	4	490	10	2	490	65
4	510	10	5	510	10			
5	560	10	6	560	10	3	560	35
6	620	10	7	620	10			
7	665	10	8	665	10	4	665	30
			9	673.75	7.5			
8	681.25	7.5	10	681.25	7.5			
9	708.75	10	11	708.75	10	5	705	15
10	753.75	7.5	12	753.75	7.5	6	740	15
11	760	3.75	13	761.25	2.5			
			14	764.375	3.75			
			15	767.5	2.5			
12	775	15	16	778.75	15	7	783	20
13	865	20	17	865	20	8	842	115
14	890	10	18	885	10			
15	900	10	19	900	10			
			20	940	20	8a	865	20
			21	1020	40	9	945	20
						10	1375	30
						11	1610	90
						12	2190	180

William James Frampton

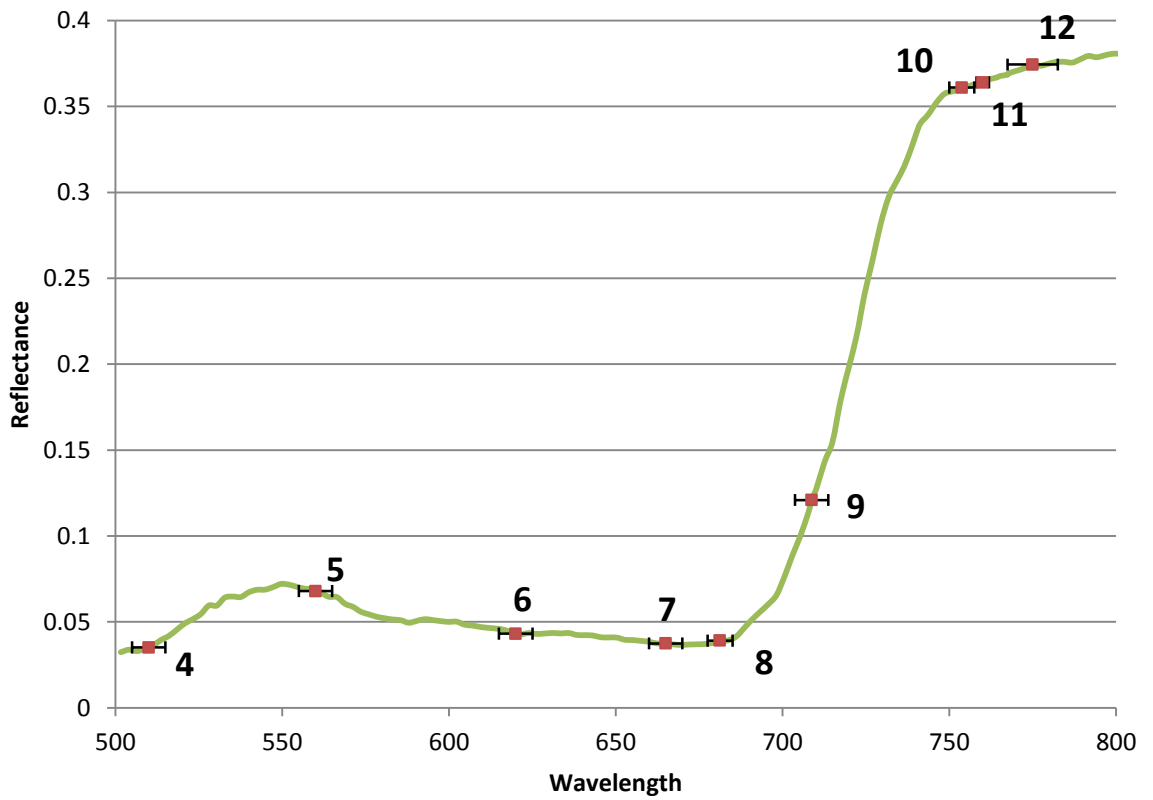


Figure 5.1: Positions of MERIS reflectance bands with width indicators overlaid onto the spectra of sunflower ESU from Sen3EXP measured using the hyperspectral AISA Eagle sensor.

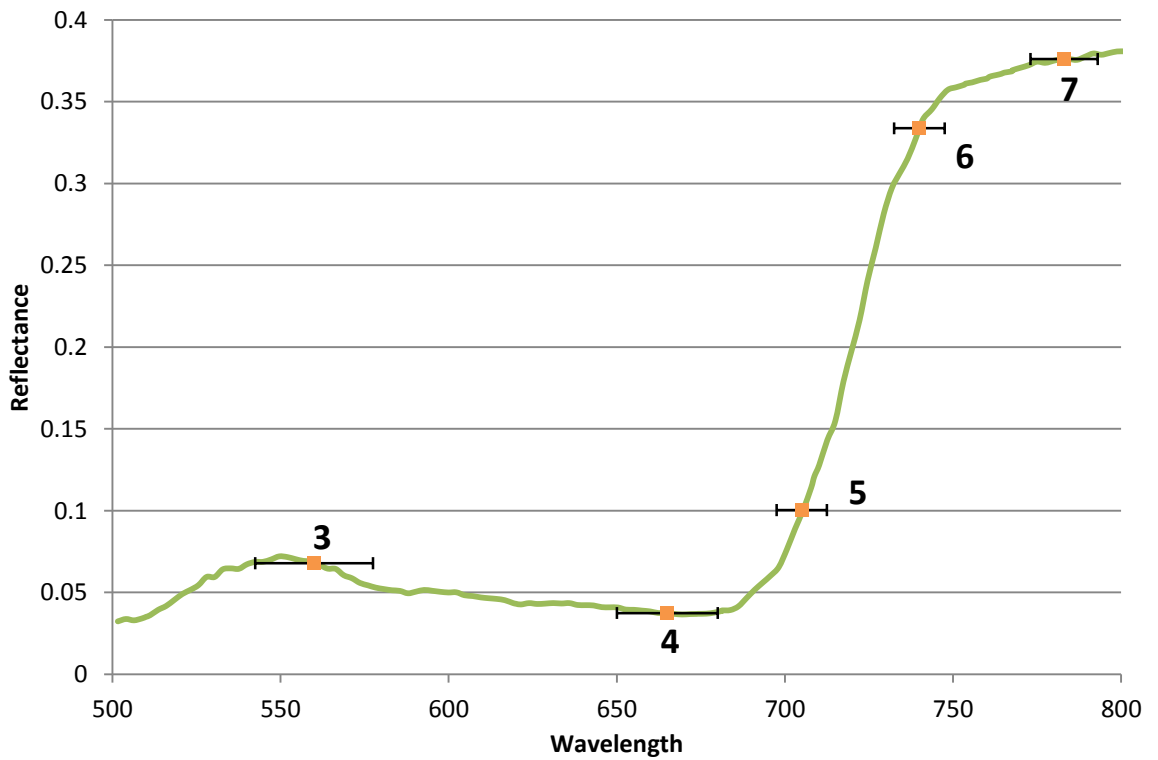


Figure 5.2: Positions of S-2 reflectance bands with width indicators overlaid onto the spectra of sunflower ESU from Sen3EXP measured using the hyperspectral AISA Eagle sensor.

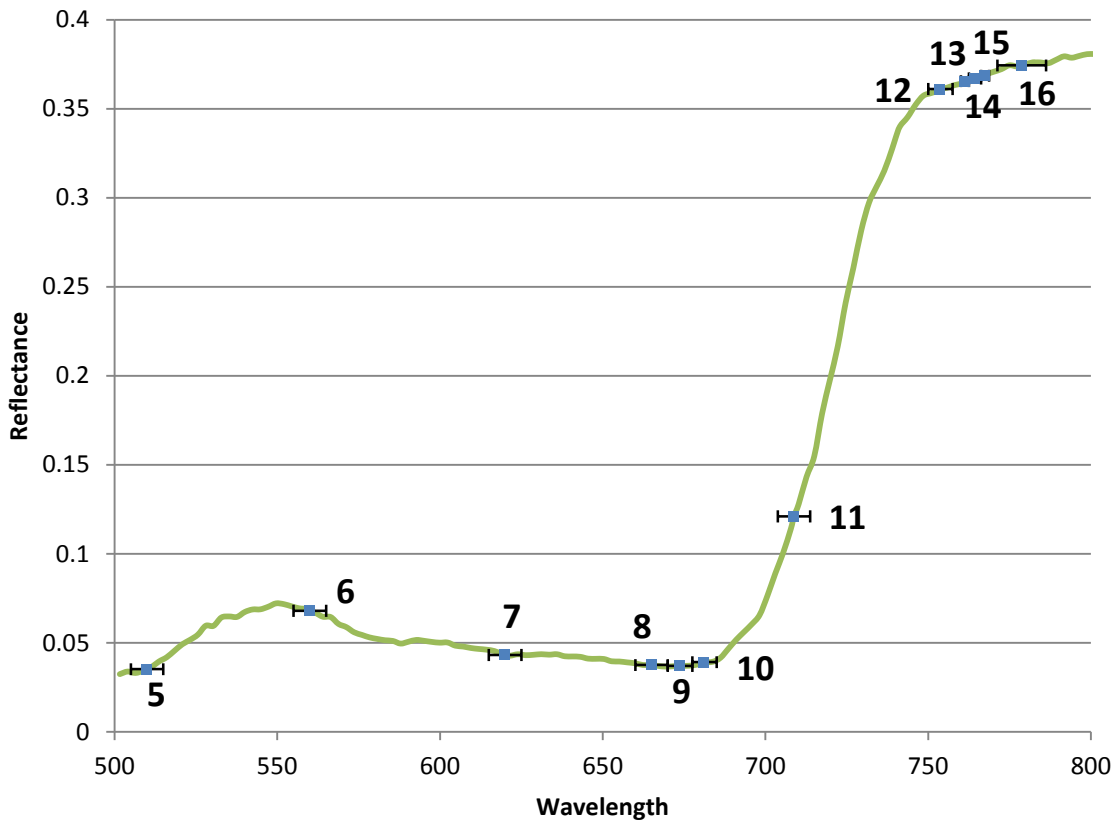


Figure 5.3: Positions of S-3 reflectance bands with width indicators overlaid onto the spectra of sunflower ESU from Sen3EXP measured using the hyperspectral AISA Eagle sensor.

5.2. Continuation of the MTCI using S-3

Continuation of the MERIS dataset is one of the mission objectives of S-3. Fortunately for the MTCI, all bands that were used in its formulation are available using the Ocean and Land Colour Imager (OLCI) on-board S-3. Application of the MTCI using S-3 will hereby be referred to as OTCI (Eq. (5.1); Ocean and Land Colour Imager Terrestrial Chlorophyll Index).

$$OTCI = \frac{r_{NIR} - r_{RE}}{r_{RE} - r_{Red}} = \frac{r_{753.75\text{ nm}} - r_{708.75\text{ nm}}}{r_{708.75\text{ nm}} - r_{681.25\text{ nm}}} = \frac{OLCI\ b12 - OLCI\ b11}{OLCI\ b11 - OLCI\ b10} \quad \text{Eq. (5.1)}$$

5.2.1. Spectral Changes

S-3 bands used in the OTCI share central wavelengths and bandwidths with the heritage MERIS bands used in the MTCI formula. Furthermore the spectral response function of the shared bands is identical meaning the two sensors are directly comparable.

5.2.2. View Angle Changes

One of the unique aspects of OLCI is that unlike MERIS the sensor will be tilted by 12.58° away from the sun to minimise the glint impact. Consequently the view angle will not be symmetrical with the centre of the swath in the image as visualised in Figure 5.4.

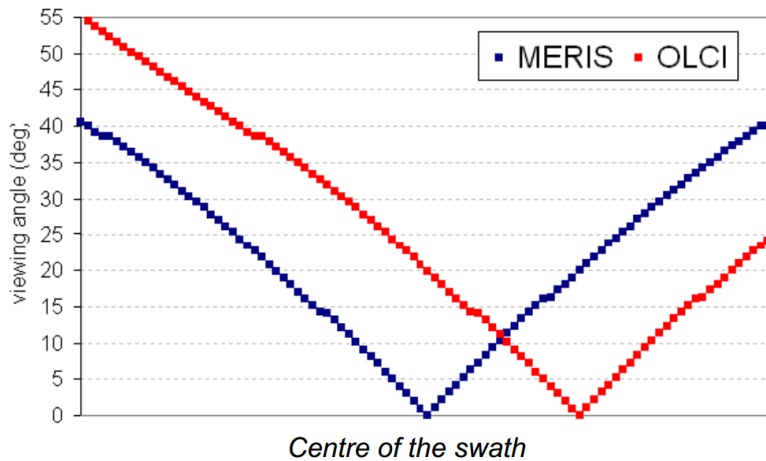


Figure 5.4: Representation of the view angle across a scene using MERIS and OLCI to emphasise the tilt of S-3 and the resulting increased view angle compared to MERIS.

The tilt of the OLCI will mean that the maximum view angle observed will be 55.6° at the far side of the image, 15.6° higher than the maximum in a MERIS scene.

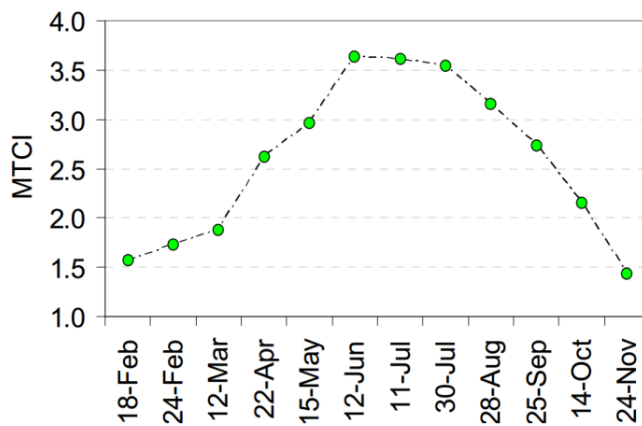


Figure 5.5: Average MTCI output of dataset over the 2009 growing season.

To perform preliminary investigations for the effect this difference in view angle will have MTCI/OTCI was tracked over the growing season for 12 MERIS acquisitions from 2009 (Figure 5.5) for locations in Barrax Spain. Spectral reflectances were extracted from randomly selected pixels that exhibited maximum canopy extent during the summer (based upon MTCI) and subsequently canopy variables were estimated through inversion of the PROSAIL model (Baret et al. 1992; Jacquemoud et al. 2009). In turn, canopy variables retrieved by the inverted model were used to

simulate reflectance using the PROSAIL model in forward mode with the change in view angle accounted for from MERIS to OLCI. Subsequently MTCI and OTCI were calculated for given locations according to the new MERIS view angle and the corresponding OLCI view angle as can be seen in Figure 5.6 where values for two example cases are presented with the relative percentage difference between OTCI and MTCI.

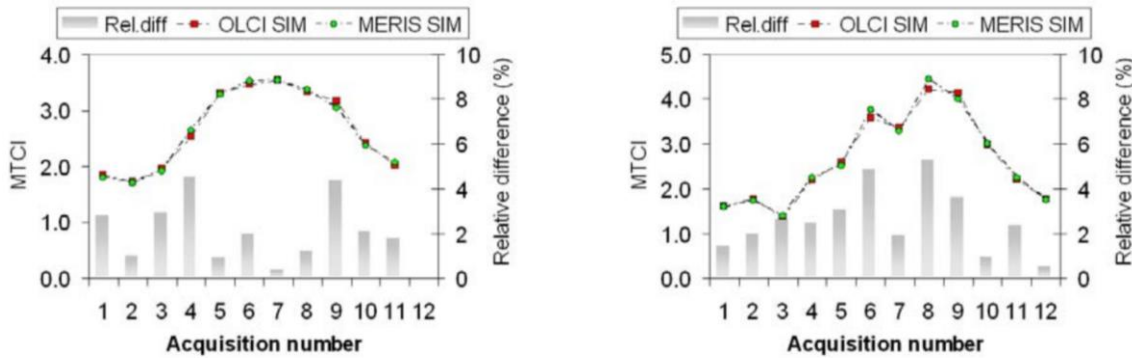


Figure 5.6: OTCI and MTCI generated from PROSAIL data over an entire growing season for example locations in Barrax, Spain.

It can be seen that due to the view angle disparity between MERIS and OLCI that the differences between MTCI and OTCI ranged between 0.35% and 5.3% with a mean relative difference of 2.3%. A key goal of S-3 is the continuation of MERIS. This analysis gives a preliminary idea of what the possible difference between MTCI and OTCI should be based on the changed view angle. It should be noted that when S-3 is operational there will be much scope for investigation into this difference using image based studies rather than the model approach used here. However it is unfortunate that there will be no overlap in operation of MERIS and OLCI as it would have given excellent opportunity for investigations of this nature. Consequently there is much scope for analysis in the difference in performance of the sensors and methods will have to be devised to test this without contemporaneous operation. Nevertheless the MTCI will be continued by OLCI as an operational product and with so few changes between the sensors after initial comparisons are made validation of the MTCI that was performed using MERIS should be carried over and continued using OLCI.

5.3. Estimation of the MTCI Using S-2

Due to the high spatial resolution of the MSI sensor aboard S-2, extensive swath and global coverage the data volume will be substantial. As an example the Level-2A product, which will provide bottom-of-atmosphere reflectances in cartographic geometry, will be 600 MB for each

100x100 km² (ESA 2014). Consequently, unlike MERIS which provided biophysical operational products for each downloaded scene, S-2 will only provide band reflectances to minimise data volume. While initial application of the MTCI using synthetic S-2 data has been shown in previously in Chapter 4 analysis in this chapter aims to more thoroughly highlight the important differences in spectral band positions and the consequences they will have on the output of the MTCI. It can be seen in Table 5.1 that unlike S-3 bands that were used to calculate the MTCI using MERIS will not be available using S-2. Therefore application of the MTCI using S-2 will require new spectral bandwidths and will be labelled as S2TCI (Eq. (5.2)).

$$S2TCI = \frac{rNIR - rRE}{rRE - rRed} = \frac{(r783 \text{ or } 740 \text{ nm}) - r705 \text{ nm}}{r705 \text{ nm} - r665 \text{ nm}} \quad \text{Eq. (5.2)}$$

5.3.1. Spectral Changes

There are three key changes for the S2TCI: a choice of NIR bands to use, the RE band is now positioned at 705 nm rather than 708.75 nm and the red band is situated further from the RE at 665 nm. To investigate the impact of these changes hyperspectral data are required to accurately generate synthetic S-2 data using spectral weighting estimations of sensor performance. The SEN3Exp field campaign that was used during the analysis in Chapter 4 was reprocessed to generate additional MERIS bands according to spectral weighting files from the CASI hyperspectral data. The three key changes are highlighted in Figure 5.7 and Figure 5.8.

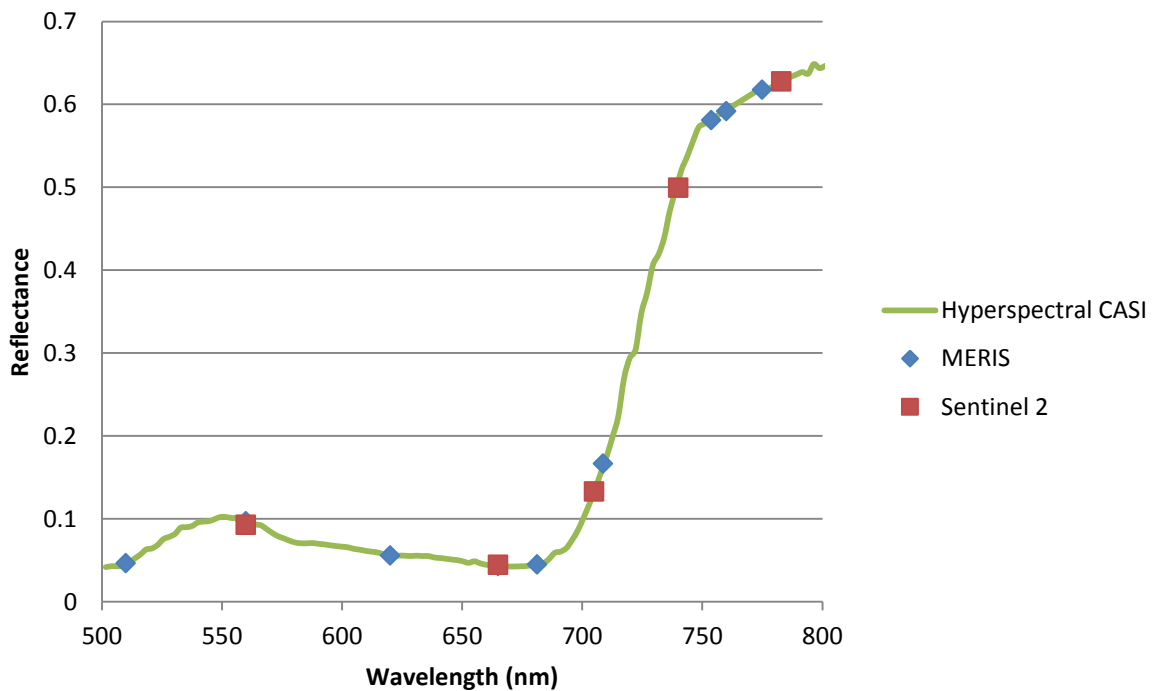


Figure 5.7: S-2 and MERIS band positions located on a CASI hyper-spectral reflectance curve between 500-800 nm for a potato ESU evaluated during the SEN3Exp field campaign.

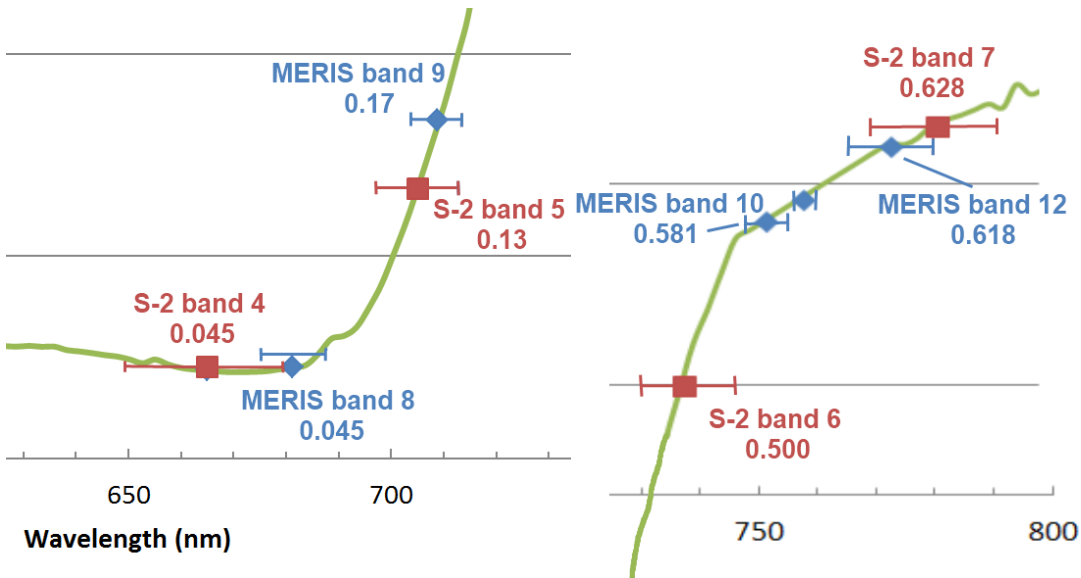


Figure 5.8: MERIS and S-2 spectral bands located near the RE generated from CASI hyperspectral data of a potato ESU evaluated during the SEN3Exp field campaign. Annotated with absolute reflectance values and bandwidth indicators.

5.3.1.1. Spectral Changes in the Red

Compared to MERIS, S-2 only has one available band in the red part of the spectrum at 665 nm. MERIS band 7 has the same band central wavelength at 665 nm however S-2 band 4 has an increased bandwidth of 30 nm compared to MERIS band 7 which is a narrower 10 nm. Nevertheless the MTCI does not use MERIS band 7 but MERIS band 8 which has a central wavelength of 681.25 nm. As this spectral bandwidth is not available with S-2 the impact of using a band focused at 665 nm must be considered. The percentage difference between MERIS band 8 and S-2 band 4 was calculated with each ESU from the SEN3Exp field campaign. The average difference between the bands was -1.5% in relative reflectance for the 33 ESU dataset. Upon further investigation the percentage change was found to be not random; when the ESU locations were compared based on their chlorophyll content there was a statistically significant ($p < 0.05$) relationship between the two red bands shown in Figure 5.9. It should be noted that the difference between the bands will be described in a standard format in this discussion where the percentage denotes how S-2 changes compared to MERIS; i.e. 5% would mean reflectance in S-2 would be 5% greater than the comparable MERIS band while -6% indicates 6% less relative reflectance.

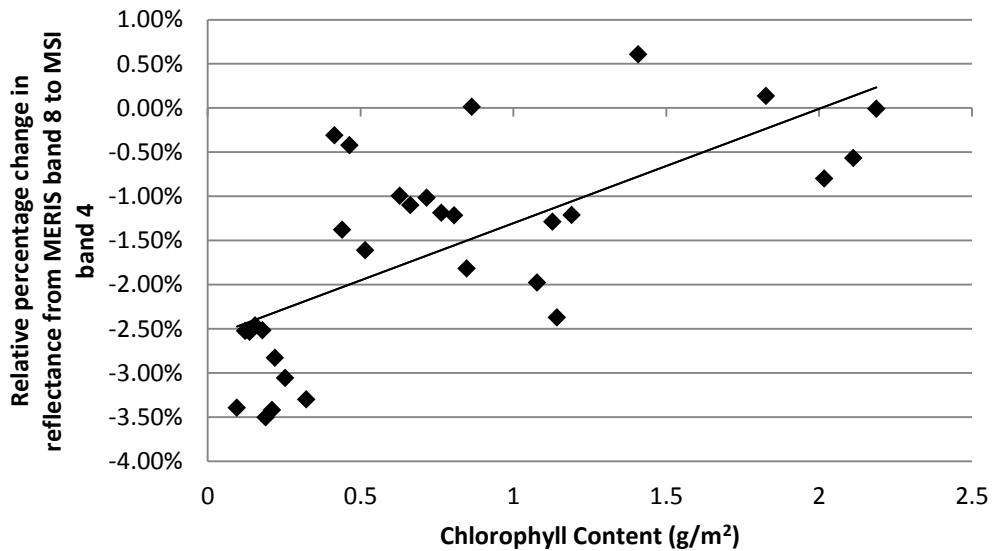


Figure 5.9: Comparing percentage change in absolute reflectance from MERIS band 8 to Sentinel-2 band 4 by chlorophyll content for 33 ESUs from the SEN3Exp field campaign.

It can be seen that at very low chlorophyll values the change in S-2 band 4 relative reflectance is up to -3.5% less than reflectance for the same ESU location using the synthesised MERIS band 8 whereas at higher chlorophyll contents there is minimal change in reflectance between the two bands. The relationship exhibits a statistically significant ($p < 0.05$) moderate correlation where the coefficient of determination (R^2) is 0.47. There is a clear reason why this relationship would occur: lower chlorophyll contents indicate sparse canopy cover which would suggest spectra dominated by a soil line, consequently, in at such locations, the reflectance at 681.25 nm will be higher than 665 nm. On the other hand the spectra of dense canopies with high chlorophyll contents would exhibit a prominent, and saturating, absorption feature in the red. The width of this feature would consequently mean there was little difference in reflectance between 681.25 and 665 nm. With this relationship in mind and consideration given to the formulation of the MTCI algorithm a lower absolute reflectance in the red, which is incorporated negatively into the denominator of the equation, in turn means a lower overall value of MTCI. As this is the case only at lower chlorophyll content values there is likely to be a slight improvement in signal for the S2TCI compared to the MTCI as the index value of sparsely vegetated pixels are reduced while closed canopy locations are retained.

5.3.1.2. Spectral Changes on the Red Edge

The situation for RE band availability using S-2 is similar to that of the red band. The MTCI used MERIS band 9 centrally located at 708.75 nm whereas the first band available directly on the RE using S-2 is centred at 705 nm. Although the difference between the spectral bands (3.75 nm) is smaller than that of the red bands the change in reflectance for vegetation is much greater in this

part of the spectrum as the bands are located directly on the RE. Consequently we find that the average relative change in reflectance for the SEN3Exp dataset is -12.12% between MERIS band 9 and S-2 band 5, much higher than the difference observed between the red bands. Like the red band dissimilarity there is a clear correlation when the relative difference in reflectance is plotted against chlorophyll content for the two RE bands as shown in Figure 5.10.

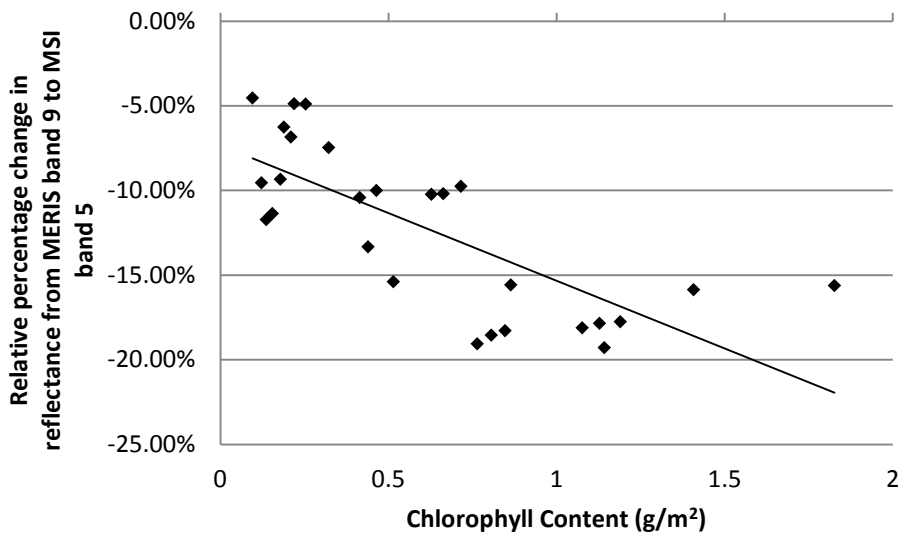


Figure 5.10: Comparing percentage change in absolute reflectance from MERIS band 9 to Sentinel-2 band 5 by chlorophyll content for 33 ESUs from the SEN3Exp field campaign.

It can be seen that the relative change in reflectance increases with chlorophyll content. The correlation of the relationship was found to be statistically significant ($p < 0.05$) with a moderate strength R^2 of 0.56. The reason for this is that higher chlorophyll contents should have a steeper RE with a greater rate of change in reflectance compared to a less densely vegetated soil line. Consequently even the small difference in central spectral band position of 3.75 nm can result in a change in measured reflectance of up to -19.29%. This is very significant for S2TCI as the central RE band is incorporated twice into the formula. The decreased measured reflectance using S-2 band 5 will mean an increased numerator and decreased denominator in the $M/S2TCI$ formula, accordingly the output of the algorithm will be significantly increased especially at higher chlorophyll contents which in theory increases the ability of S2TCI to retrieve biophysical parameters of vegetation compared to the MTCI.

5.3.1.3. Spectral Changes in the NIR

Investigating the differences in the capabilities between S-2 and MERIS in the NIR is a different case to the red and central RE as there are two optional bands. MERIS band 10 is located at 753.75 nm while S-2 has bands located at 740 nm and 783 nm. The average relative difference in reflectance between MERIS band 10 and S-2 band 6 is -11.54% for the SEN3Exp dataset. The

William James Frampton

reason for difference is the same as for the bands at the centre of the RE. MERIS band 10 is located just above the RE at the start NIR plateau while S-2 band 6 at 740 nm is located on the RE meaning the band has lower measured reflectance. When the relative difference is compared with the chlorophyll content of each ESU as can be seen in Figure 5.11 the relationship is clearly negative with a statistically significant ($p < 0.05$) R^2 of 0.73. High chlorophyll contents have up to -19.15% less reflectance using the 740 nm S-2 band rather than the 753.75 nm MERIS band while the difference at very low chlorophyll contents is much less.

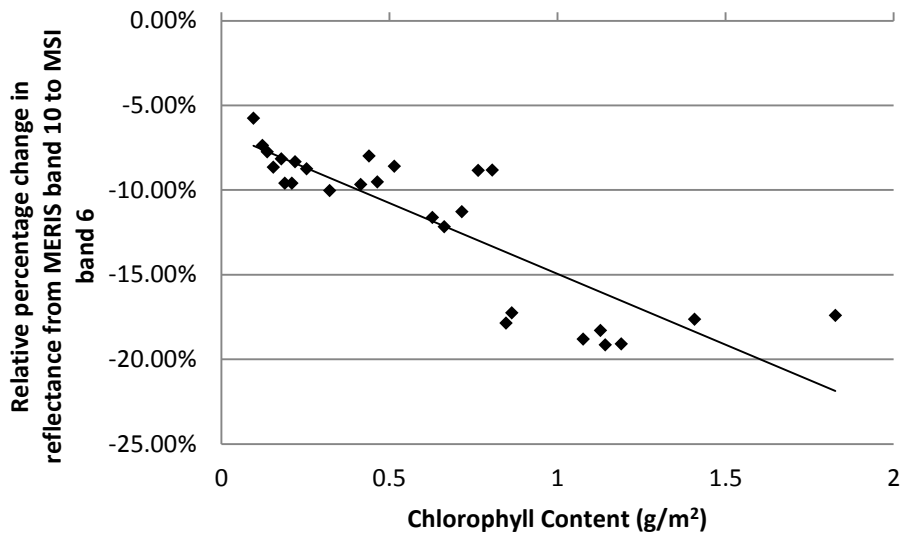


Figure 5.11: Comparing percentage change in absolute reflectance from MERIS band 10 to MSI band 6 by chlorophyll content for 33 ESUs from the SEN3Exp field campaign.

If band 6 is incorporated into the S2TCI formula the large change in measured reflectance will have significant impact on the output of the algorithm. The decreased reflectance of S-2 band 6 included in the numerator of the S2TCI formula would reduce the output of the algorithm, more so at higher chlorophyll content values than lower values. Consequently in theory this would decrease the ability of S2TCI to retrieve biophysical parameters of vegetation compared to the MTCI.

While S-2 band 6 should be recognised as a second band directly on the RE, S-2 band 7 is a definitive NIR band situated at 783 nm on the plateau. Consequently compared to MERIS band 10, which has a central bandwidth of 681.75 nm, S-2 band 7 has increased reflectance which, for the SEN3Exp dataset, was on average 7.48% higher. Comparing the change in relative reflectance with chlorophyll content as shown in Figure 5.12 yields a statistically significant ($p < 0.05$) positive relationship with an R^2 of 0.69. This relationship can be attributed to the higher relative increase in reflectance from leaf structure at high chlorophyll contents compared to the lower NIR observed in sparse canopies typically demonstrating a soil line. With consideration given to the

M/S2TCI formula the increased reflectance measured in the NIR would mean the output of S2TCI would be higher than the MTCI, especially at higher chlorophyll contents. In theory this would slightly increase the ability of S2TCI to retrieve biophysical parameters of vegetation compared to the MTCI.

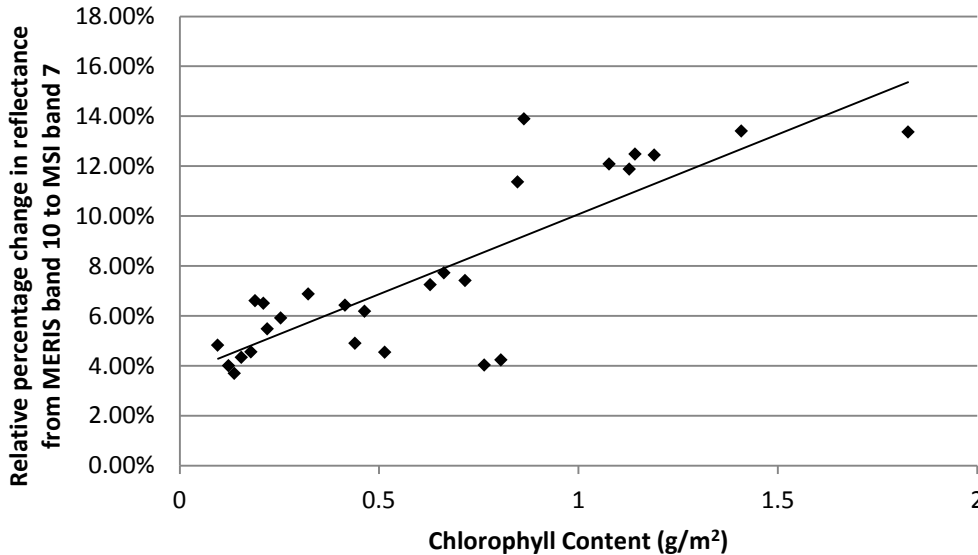


Figure 5.12: Comparing percentage change in absolute reflectance from MERIS band 10 to MSI band 7 by chlorophyll content for 33 ESUs from the SEN3Exp field campaign.

5.3.2. Comparison of NIR S-2 Bands 6 and 7

NIR reflectance is incorporated into the M/S2TCI formula in positive way so that increased reflectance increases the output of the algorithm which indicates increased chlorophyll content. Consequently it is undesirable for reflectance to decrease with increased chlorophyll content as the output of the algorithm will be lower for higher chlorophyll contents; such is the case if S-2 band 6 is used in the S2TCI formula as a replacement for MERIS band 10. Conversely if S-2 band 7 is used the relative reflectance between the two bands increases at higher chlorophyll contents which subsequently should improve the ability of the algorithm to retrieve chlorophyll content. Therefore analysis suggests that when applying the MTCI to S-2 band 7 is used as the NIR band.

5.3.3. Impact of Each Band on the S2TCI Output

To investigate the effect each individual band change has on the output of the MTCI MERIS band reflectances was calculated from the CASI hyperspectral imagery from the SEN3Exp dataset. One by one the red, RE and NIR bands were replaced in the formula with synthetic S-2 bands to investigate the quantitative change attributed to each band in the algorithm. It is important to

establish the difference between the MTCI and the S2TCI to investigate the possible comparability of the algorithms across sensor.

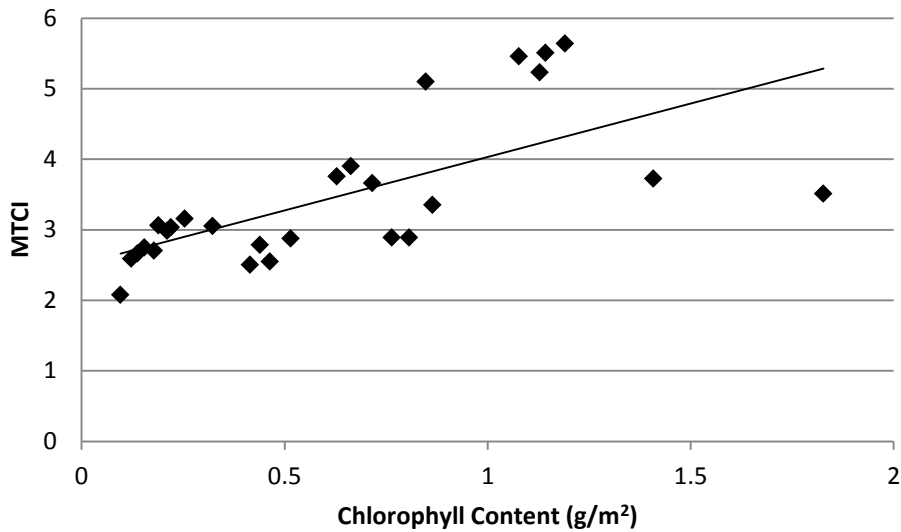


Figure 5.13: Correlation of the MTCI with chlorophyll content for the SEN3Exp field campaign.

Figure 5.13 highlights the relationship of the MTCI with chlorophyll content from the SEN3Exp field campaign. The correlation has a moderate strength with an R^2 of 0.45 and is statistically significant ($p < 0.05$). Having established the correlation of the MTCI with chlorophyll content subsequent sections will investigate the change in correlation using S-2 bands.

5.3.3.1. S-2 Red Band 4

Section 5.3.1.1. highlighted that using S-2 band 4 will reduce the measured reflectance at low chlorophyll contents more than in dense canopies compared to MERIS band 8. Consequently a lower absolute reflectance in the red in turn means a lower output value of S2TCI compared to the MTCI at lower chlorophyll contents. To quantify the change in TCI output for the SEN3Exp dataset the MTCI formula was modified to use S-2 band 4 instead of MERIS band 8 as the input of red reflectance while using still using MERIS band 10 and 9 and will be described as TestTCI1 (Eq. (5.3)).

$$TestTCI1 = \frac{r_{NIR} - r_{RE}}{r_{RE} - r_{Red}} = \frac{MERIS\ b10 - MERIS\ b9}{MERIS\ b9 - S2\ b4} = \frac{r_{753.75\ nm} - r_{708.75\ nm}}{r_{708.75\ nm} - r_{665\ nm}} \text{ Eq. (5.3)}$$

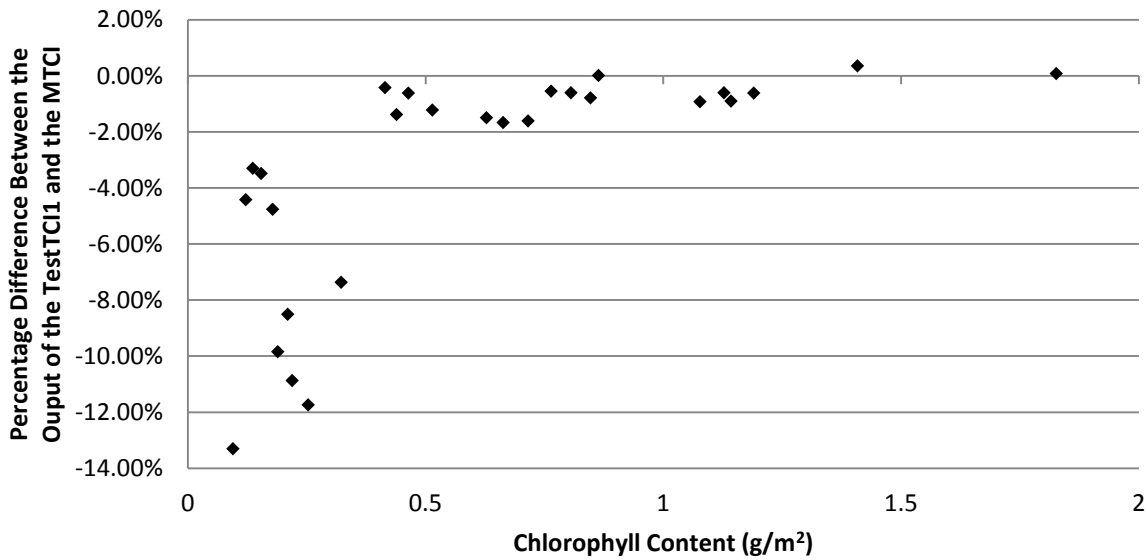


Figure 5.14: Changing relative percentage difference between the TestTCI1 and the MTCI with chlorophyll content taken from the SEN3Exp field campaign.

It can be seen in Figure 5.14 that incorporation of S-2 band 4 causes significant reduction to the MTCI at low chlorophyll content values of up to -13.3%. Conversely, the wide, prominent red absorption feature and resulting stable reflectance in the red region produced at higher chlorophyll content values mitigates the change of using reflectance at 665 nm rather than 681.25 nm which results in negligible change above a chlorophyll content of 0.5 g/m².

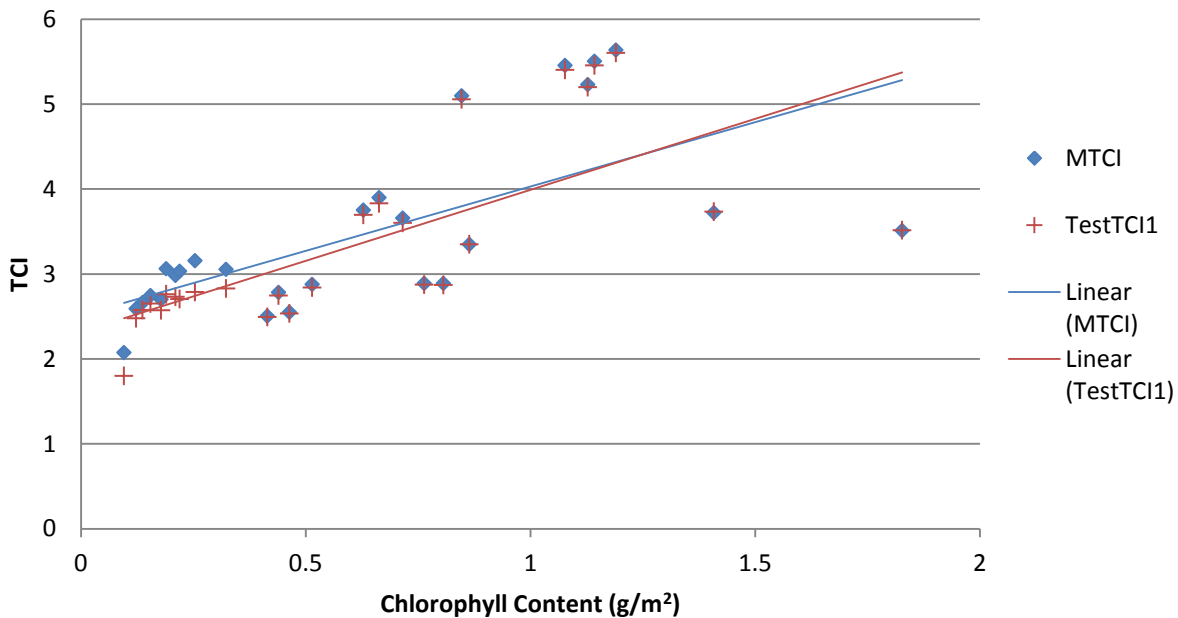


Figure 5.15: Comparing the correlation of the MTCI and the TestTCI1.

Figure 5.15 compares the relationships between the MTCI, the TestTCI1 and chlorophyll content. As the reduction in reflectance, which results in a lower TCI output, only occurs only at low

chlorophyll content values there is a slight improvement in correlation for the TestTCI1 compared to the MTCI with an R^2 of 0.50 and 0.45 respectively where $p < 0.05$.

5.3.3.2. S-2 Red Edge Band 5

Section 5.3.1.2. highlighted that using band 5 will reduce the measured reflectance at high chlorophyll contents more than in sparse canopies using the S2TCI compared to the MTCI. Consequently a lower absolute reflectance in the RE in turn means a significantly higher output of the S2TCI compared to the MTCI. To quantify the exact change for the SEN3Exp dataset the MTCI formula was modified to use S-2 band 5 instead of MERIS band 9 as the input of RE reflectance while using still using MERIS band 10 and 8 and will be described as TestTCI2 (Eq. (5.4)).

$$TestTCI2 = \frac{r_{NIR} - r_{RE}}{r_{RE} - r_{Red}} = \frac{MERIS\ b10 - S2\ b5}{S2\ b5 - MERIS\ b\ 8} = \frac{r_{753.75\ nm} - r_{705\ nm}}{r_{705\ nm} - r_{681.25\ nm}} \quad Eq. (5.4)$$

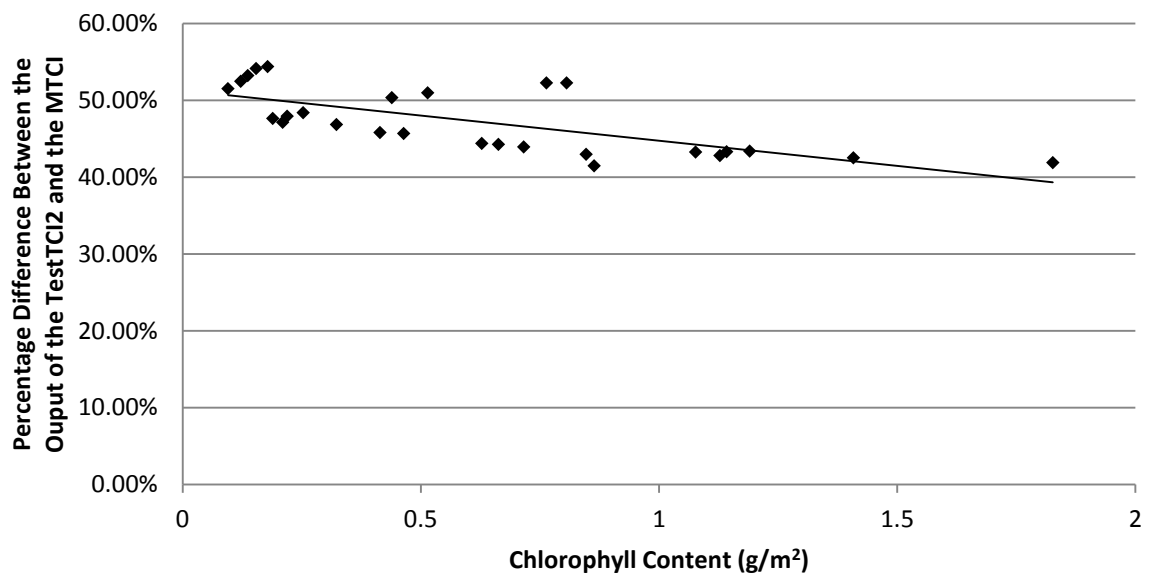


Figure 5.16: Changing relative percentage difference between the TestTCI2 and the MTCI with chlorophyll content taken from the SEN3Exp field campaign.

It can be seen that the output of TestTCI2 is significantly higher than the MTCI by between 54.14% and 41.89% over a range of chlorophyll contents. The lower increase in output at higher chlorophyll contents can be attributed to the rate of change in reflectance of the RE between 708.25 nm and 705 nm. As the RE is typically only linear between 740 nm and 715 nm the gradient of the RE decreases between 708.25 nm (MERIS band 9) and 705 nm (S-2 band 5). Conversely for soil line reflectance and very sparse canopy cover there is very little to no decrease in gradient. This means that the difference in rate of change between high and low chlorophyll contents becomes less between 708.25 nm and 705 nm. The resulting undesirable decrease in

TestTCI2 output at higher chlorophyll contents means it has a slightly lower correlation with chlorophyll content with an R^2 of 0.41 compared with the MTCI of 0.45 (Figure 5.13).

5.3.3.3. S-2 NIR Band 7

Section 5.3.1.3. highlighted that using S-2 band 7 will increase the measured reflectance at high chlorophyll contents more than in sparse canopies with the S2TCI compared to using MERIS band 10 with the MTCI. Consequently a higher absolute reflectance in the NIR also means a higher output of the S2TCI. To quantify the exact change for the SEN3Exp dataset the MTCI formula was modified to use S-2 band 7 instead of MERIS band 10 as the input of NIR reflectance while using still using MERIS band 9 and 8 and will be described as TestTCI3 (Eq. (5.5)).

$$TestTCI3 = \frac{r_{NIR} - r_{RE}}{r_{RE} - r_{Red}} = \frac{S2\ b7 - MERIS\ b9}{MERIS\ b9 - MERIS\ b\ 8} = \frac{r_{783\ nm} - r_{708.75\ nm}}{r_{708.75\ nm} - r_{681.25\ nm}} \quad Eq. (5.5)$$

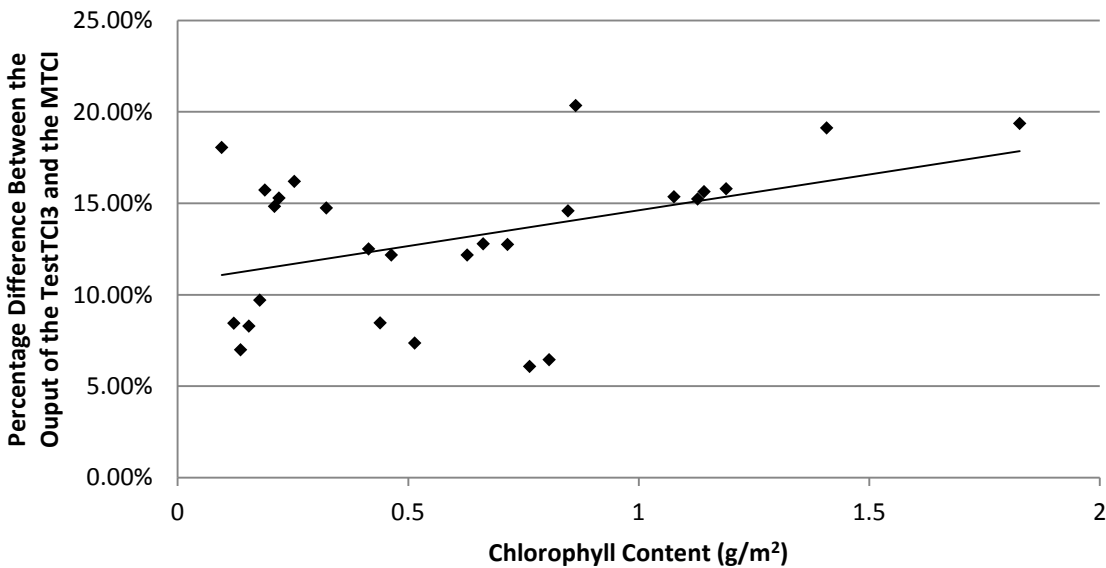


Figure 5.17: Changing relative percentage difference between the TestTCI3 and the MTCI with chlorophyll content taken from the SEN3Exp field campaign.

TestTCI3 is between 6.08% and 20.34% higher than the MTCI over a range of chlorophyll contents. Compared to the replacement of the red and RE bands changing the NIR exhibits a weaker correlation between change in TCI output and chlorophyll with an R^2 of 0.18 but is still statistically significant ($p < 0.05$). The reason for this is likely due to variation in soil reflectance exhibited by sparse canopy locations with low LAI. A smaller relative change in reflectance of a very bright soil will increase TCI output more than a darker soil location. If the SEN3Exp dataset is filtered to only include ESUs with an LAI above 1 the relationship instead exhibits a statistically significant ($p < 0.05$) moderate strength correlation where the R^2 is 0.46. Although the relationship is weak the

William James Frampton

increased output of TestTCI3 at higher chlorophyll contents compared to the MTCI means the index has a slightly stronger R^2 of 0.47 compared to the MTCI where $R^2 = 0.45$ (Figure 5.13).

5.3.4. S2TCI

Section 5.3.1. began by highlighting the three key changes that must be considered when applying the MTCI using S-2. Having analysed each affect individually amalgamating these spectral impacts can be seen to result in a significantly higher TCI output.

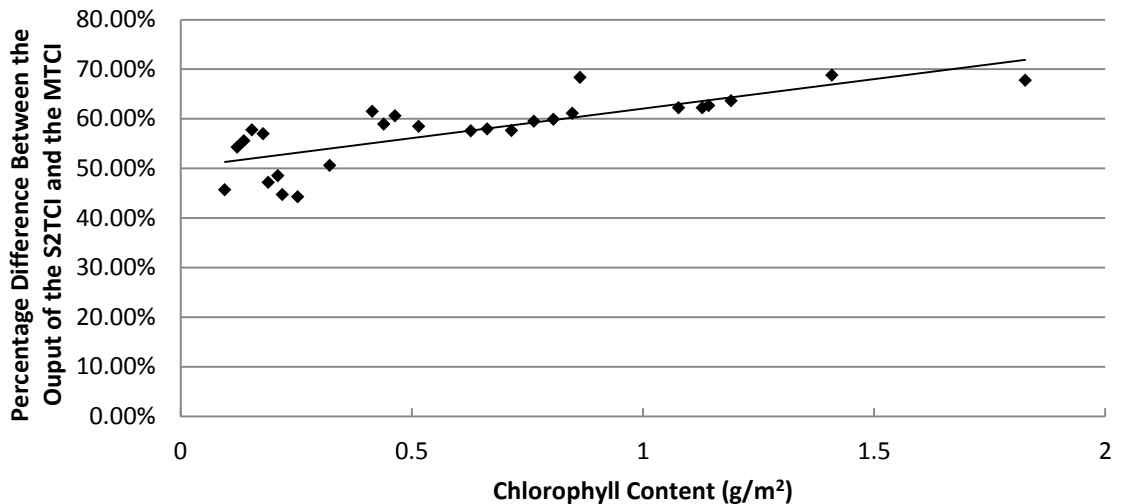


Figure 5.18: Changing relative percentage difference between the S2TCI and the MTCI with chlorophyll content taken from the SEN3Exp field campaign.

The output of the S2TCI is between 44.28% and 68.8% higher than MTCI. The change is linear with increasing chlorophyll content with an R^2 of 0.61. When compared to chlorophyll content for the SEN3Exp dataset S2TCI has an R^2 of 0.52 which is higher than the MTCI R^2 of 0.45. The improvement in correlation can be attributed to the better performance of the red and NIR bands which more than compensate for the slight loss in signal from the RE.

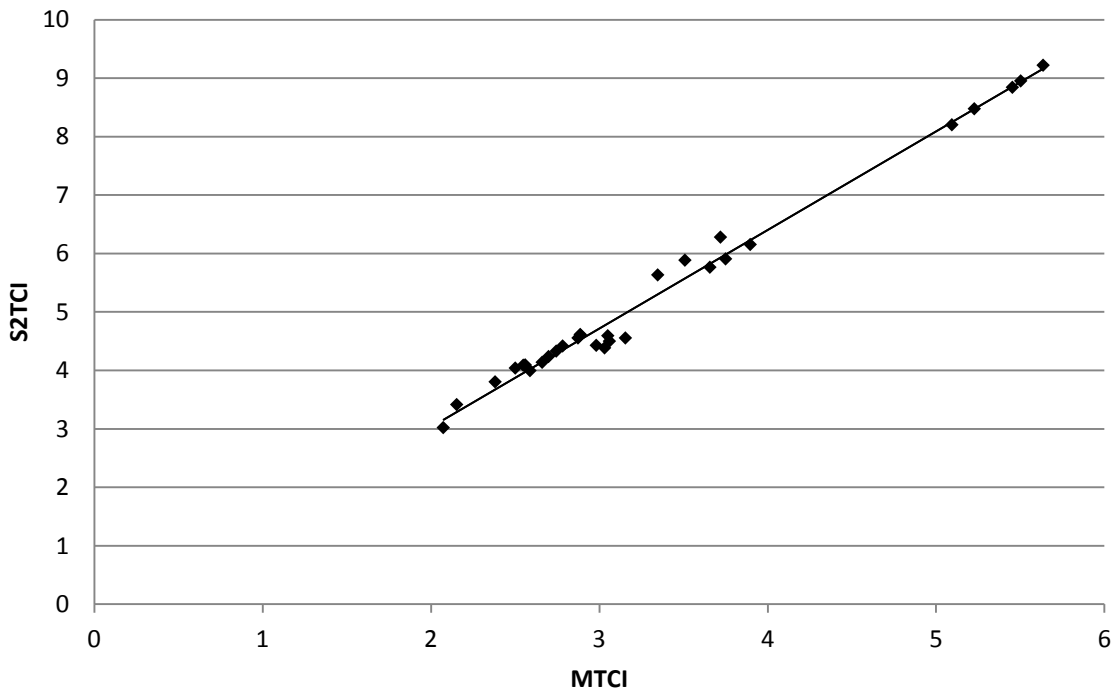


Figure 5.19: Comparison between S2TCI and the MTCI derived from CASI hyperspectral reflectance data for the SEN3Exp field campaign.

Comparing the MTCI and S2TCI for the SEN3Exp dataset results in a relationship with an R^2 of 0.99 for the following equation.

$$S2TCI = 1.6866 * MTCI - 0.3406 \quad \text{Eq. (5.6)}$$

This equation is a starting point for direct comparison between the MTCI or OTCI and S2TCI with the caveat that it is highly likely to be scene specific. Any change in a range of variables such as the sensor type used to generate the synthetic data, vegetation type, view geometry and background condition would almost certainly result in a different comparison equation. Although this analysis has given an initial insight into how the MTCI will change with application using S-2 much further validation with other datasets at different locations would be required to enable a method to be developed to allow direct comparison between data of the two sensors. It should be noted that there is great worth in such a development as the ten year MERIS MTCI dataset could be compared with the high spatial resolution opportunities available using S-2 to monitor change in phenology where mixed pixels are a problem. Although such preliminary equations can be developed using hyperspectral data to generate synthetic bands a true comparison equation will only likely be available when both satellites are in operation where they will provide great opportunity for cross-validation through contemporaneous acquisitions in large, homogenous fields where mixed pixels will not be a problem.

5.4. Feasibility to Downscale to S-2 from S-3 and MERIS Data

Downscaling is the practice of combining high temporal, low spatial resolution imagery with low temporal, high spatial acquisitions. The method aims to create a synergy product that enables a high temporal, spatial and spectral resolution dataset. Consequently development of such a technique between S-2 and S-3 has high appeal for studies in areas where heterogeneous vegetation cover mean that the even in 300 m full resolution mode S-3 spatial resolution would be insufficient and lead to significant uncertainty due to the mixed pixels. There are multiple methods that have created fusion products such as work by Gao et al. (2006) creating the Spatial and Temporal Adaptive Reflectance Fusion Model (STARFM) with Landsat and MODIS data (see Walker et al. 2012) or Zurita-Milla et al. (2009) using MERIS. Recently Amorós-López et al. (2013) tested a fusion approach to monitor small and medium sized crops using the spatial characteristics of Landsat while retaining the fine spectral and temporal resolution of MERIS. Earlier work by Núñez et al. (1999) merged SPOT and Landsat data which was very interesting as it used panchromatic SPOT data, which had a spatial resolution of 10 m, to enhance multispectral Landsat data (30 m).

5.4.1. Data and Methods

5.4.1.1. Data and Study Site

To investigate the opportunities of downscaling using S-2 and S-3 either synthetic or surrogate multi-temporal contemporaneous data was needed with ground based knowledge of vegetative condition. To generate synthetic data for S-2 hyperspectral, high spatial resolution data is needed which is rare at the multi-temporal level required for analysis. Consequently a review was conducted into the suitability of sensors with capabilities of reflectance measurements in the RE region to use as a surrogate for S-2. The most suitable is Proba-1 ESA's smallest satellite. The main sensor of Proba-1 is the Compact High Resolution Imaging Spectrometer (CHRIS). CHRIS is an opportunistic sensor which targets planned sites at specified times. Typically only one or two sites are observed each day with irregular revisit times to accommodate accepted research proposals. In operational mode 1 CHRIS acquires reflectance in 63 separate spectral bands for a ground area of 13 km² at a spatial resolution of 34 m. Band positions are similar to S-2 and are presented in Table 5.2.

Table 5.2: Most suitable CHRIS bands as surrogate data of Sentinel 2.

CHRIS (Mode 1)			Sentinel-2		
Band	Central Wavelength (nm)	Bandwidth (nm)	Band	Central Wavelength (nm)	Bandwidth (nm)
2	442	9	1	443	20
7	490	9	2	490	65
14	561	10	3	560	35
24	661	11	4	665	30
30	703	6	5	705	15
36	742	7	6	740	15
42	785	8	7	783	20
47	841	9	8	842	115
50	868	9	8a	865	20
57	940	20	9	945	20

Section 5.2. highlighted the considerable variance in measured reflectance and algorithm output with spectral changes between S-3 and S-2. However the differences between CHRIS and S-2 are significantly smaller than those analysed previously and should not have a significant impact in assessing the feasibility of a synergy product between S-2 and S-3. Fortunately, FR MERIS imagery is a much simpler surrogate for S-3 and is widely available globally.

To investigate the feasibility of downscaling from S-3 to S-2 vegetation with both homogenous and heterogeneous fields, with respect to FR-MERIS pixels, would be required. The availability of CHRIS data was the key limiting factor in site selection due to the irregular revisit time of the sensor and that few test sites were adequately documented with ground data, specifically crop information. Ideally monthly CHRIS acquisitions were required with availability of contemporaneous FR-MERIS imagery. In the summer of 2004 the ESA and the University of Valencia organised SPectra bARrax Campaign (SPARC) (ESA 2004) which occurred in tandem with CHRIS acquisitions. Vegetative ground measurements and specific crop information were documented. It should be noted that this is the same test location as the SEN3Exp 2009 field campaign previously used in this chapter as well as in Chapter 4 and is highlighted in Figure 5.20 and Figure 5.21.



Figure 5.20: Location of Barrax test site in Spain. Landsat image (04/10/2013) courtesy of NOAA, accessed via Google Earth.

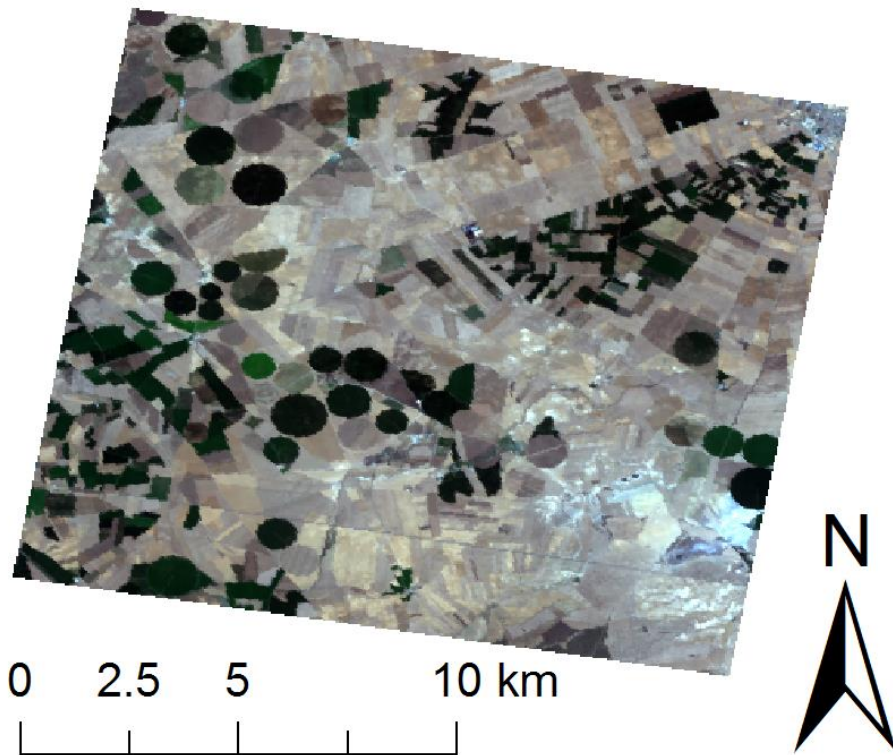


Figure 5.21: CHRIS true colour image of Barrax test site (16/07/2004).

CHRIS availability was analysed using the Earth Observation Link (EOLI) portal via ESA. Six CHRIS acquisitions were found for Barrax in 2004 with a large portion of the 13 km² scene shared between them. In turn the availability of FR-MERIS data was analysed using EOLI with the intention of matching each CHRIS scene with a clear sky MERIS image as close as possible to the date of each CHRIS acquisition.

Table 5.3: Summary of CHRIS and MERIS images used and the gap between possible base pairs.

CHRIS		MERIS		Difference in Days
Image Name	Date	Image Name	Date	
CHRIS_BR_040323_3F20_41	23/03/2004	MER_FR__2PNEPA20040321	21/03/2004	-2
CHRIS_BR_040527_416E_41	27/05/2004	MER_FR__2PNEPA20040520	20/05/2004	-7
CHRIS_BR_040630_42C7_41	30/06/2004	MER_FR__2PNEPA20040628	28/06/2004	-2
CHRIS_BR_040716_436C_41	16/07/2004	MER_FR__2PNEPA20040720	20/07/2004	+4
N/A	N/A	MER_FR__2PNUPA20040824	24/08/2004	N/A
N/A	N/A	MER_FR__2PNUPA20040922	22/09/2004	N/A
N/A	N/A	MER_FR__2PNUPA20041023	23/10/2004	N/A
CHRIS_BR_041116_49CF_41	16/11/2004	MER_FR__2PNEPA20041118	18/11/2004	+2
CHRIS_BR_041228_4BAF_41	28/12/2004	MER_FR__2PNEPA20041223	23/12/2004	-5

It can be seen that there is at most seven days between the paired images and for half the dates there is only two days difference. It is desirable to minimise the difference in time between acquisitions to mitigate the uncertainty from change in vegetative state in the base pairs. Unfortunately the CHRIS images are not equally distributed throughout the year with a significant four month gap between acquisitions in July to November. In agricultural terms for summer crops this means the period of senescence and harvesting will be missed at high spatial resolution. MERIS imagery was available for the period and obtained to generate synthetic high resolution imagery for the period using the other base pairs. All CHRIS images are provided in Figure 5.22.

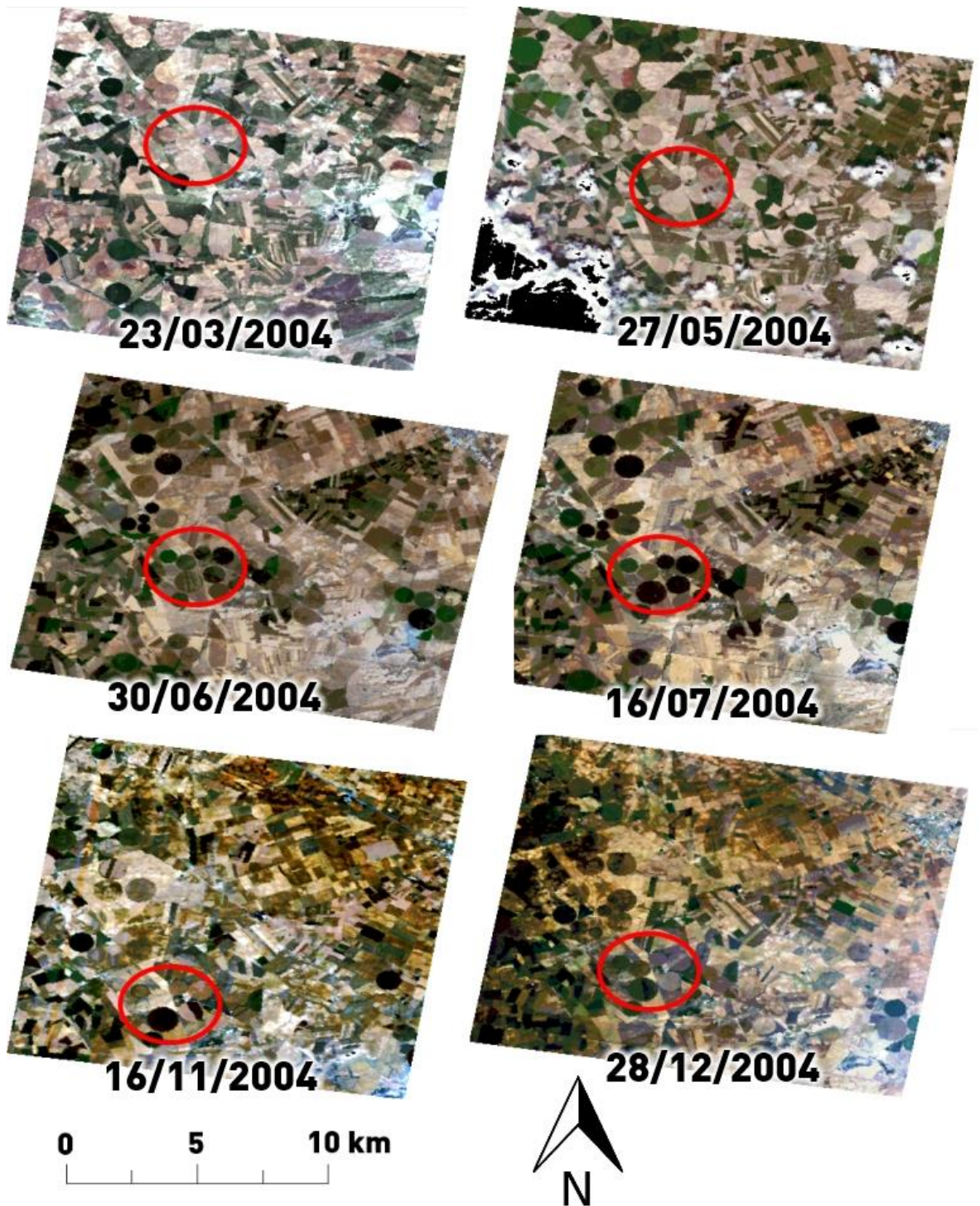


Figure 5.22: All CHRIS acquisitions for the Barrax test site. A geometrically similar red ring has been added to aid visual comparison.

Level 2 FR-MERIS data is delivered as top of the canopy reflectance data. Consequently the only processing required was to investigate pixel positional error between the MERIS dates. User supervised geometric correction was consequently applied to the images to ensure pixels can be directly compared throughout the time series. Processing of the CHRIS data however was computationally more strenuous and performed using Basic ERS & Envisat (A)ATSR and MERIS

William James Frampton

(BEAM) software and the CHRIS Toolbox plugin available. Noise reduction was performed first which helps to remove vertical striping caused by the slit effect and superposition of high-frequency noise. The algorithm can be reviewed in more depth in a paper by Gómez-Chova et al. (2008). Subsequently atmospheric correction was applied to convert top of the atmosphere radiance to top of the canopy reflectance measurements. The process uses MODTRAN4 (Berk et al, 2003) to update the spectral characterisation of the CHRIS data and uses the aerosol optical thickness at 550 nm and columnar water vapour at 940 nm to retrieve surface reflectance. Finally the process performs spectral polishing on the data. The processes can be reviewed in more depth in papers by Guanter et al. (2005a, 2005b). Finally after atmospheric correction the data was geometrically corrected using CHRIS telemetry files which are available for all CHRIS acquisitions. It was found that the correction performed by the CHRIS Toolbox required some further user supervised geometric correction using ground control points from georeferenced SPOT imagery.

5.4.1.2. Methods

STARFM is a widely used blending algorithm (Gao et al. 2006; Hilker et al. 2009; Walker et al. 2012; Emelyanova et al. 2013) that combines low spatial, high temporal resolution MODIS data with high spatial, low temporal resolution Landsat data to create a high spatial product with enhanced temporal coverage. This chapter will continue by outlining the theoretical basis of STARFM and investigate if it will be suitable for use with S-2 and S-3. The process relies on creating a base pair, from an as near as possible contemporaneous acquisition by both sensors that are to be fused. The selection of this pair is paramount as the strength of final synthetic product is dependent on conditions being as similar as possible for the acquisitions (Walker et al. 2012). The theoretical foundation of STARFM is that the difference in pixel reflectance between the base pair images will remain constant for both preceding and succeeding acquisitions (Gao et al. 2006). Therefore if the difference can be calculated it can be used to adjust the high temporal, low spatial resolution data to generate synthetic high spatial resolution data as will be explained in the following steps.

$$S2(x,y,t_0) = S3(x,y,t_0) + d$$

Where S2 and S3 represent Sentinel-2 and Sentinel-3 reflectances at pixel locations (x, y) at the acquisition window t_0 where the difference in reflectance between the sensors is d.

Therefore through rearranging the previous equation d can be established in terms of S-2 and S-3 pixel reflectance.

$$d = S2(x,y,t_0) - S3(x,y,t_0)$$

William James Frampton

If constant and known then the difference (d) between the base pair can be applied to other acquisitions of the high temporal imagery (S-3) where high resolution acquisitions (S-2) are not available to create synthetic high resolution data.

$$S2(x,y,t_n) = S3(x,y,t_n) + S2(x,y,t_0) - S3(x,y,t_0)$$

Therefore S-2 reflectance for the acquisition date t_n is the S-3 pixel reflectance for that date plus the difference in reflectance between the S-2 and S-3 base pair. Consequently using this method high resolution synthetic S-2 data can be generated where S-3 data is available if a base pair of suitable compatibility exists (see Gao et al 2006 for more examples).

CHRIS and MERIS reflectance bands will be linked according to Table 5.4 below.

Table 5.4: Linking of nearest spectral bands between sensors.

CHRIS (Mode 1)		Sentinel-2		Sentinel -3 / MERIS	
Band	Central Wavelength (nm)	Band	Central Wavelength (nm)	Band	Central Wavelength (nm)
2	442	1	443	2	442.5
7	490	2	490	3	490
14	561	3	560	5	560
24	661	4	665	7	665
30	703	5	705	9	708.75
36	742	6	740	10	753.75
42	785	7	783	12	775
50	868	8a	865	13	865

Of specific interest is the best time to select base pairs for the model. Walker et al. (2012) suggested that when the dates of the base pair are close to the time of maximum vegetation growth it is probable that the synthetic images will demonstrate less disparity with regards to vegetation dynamics than they would do if the base pair was observed during the more volatile growth of spring. Use of such base pairs consequently results in a greater level of accuracy of spectral correspondence between the images. To investigate the best time to establish base pair selection multiple base pairs were selected to assess which would provide the most accurate predictions of synthetic data. Consequently base pairs were established for all available CHRIS data except December due to similarities with November to assess any disparity in their performance. It should be noted that the lack of CHRIS data between August and October means that a large part of the senescent period will be missed from base pair analysis.

William James Frampton

Test sites were established for the following crops: alfalfa, corn, sunflower, potato, sugar beet and garlic which was possible through using maps from the SPARC 2004 field campaign data acquisition report (ESA 2004) which can be seen in Figure 5.23.

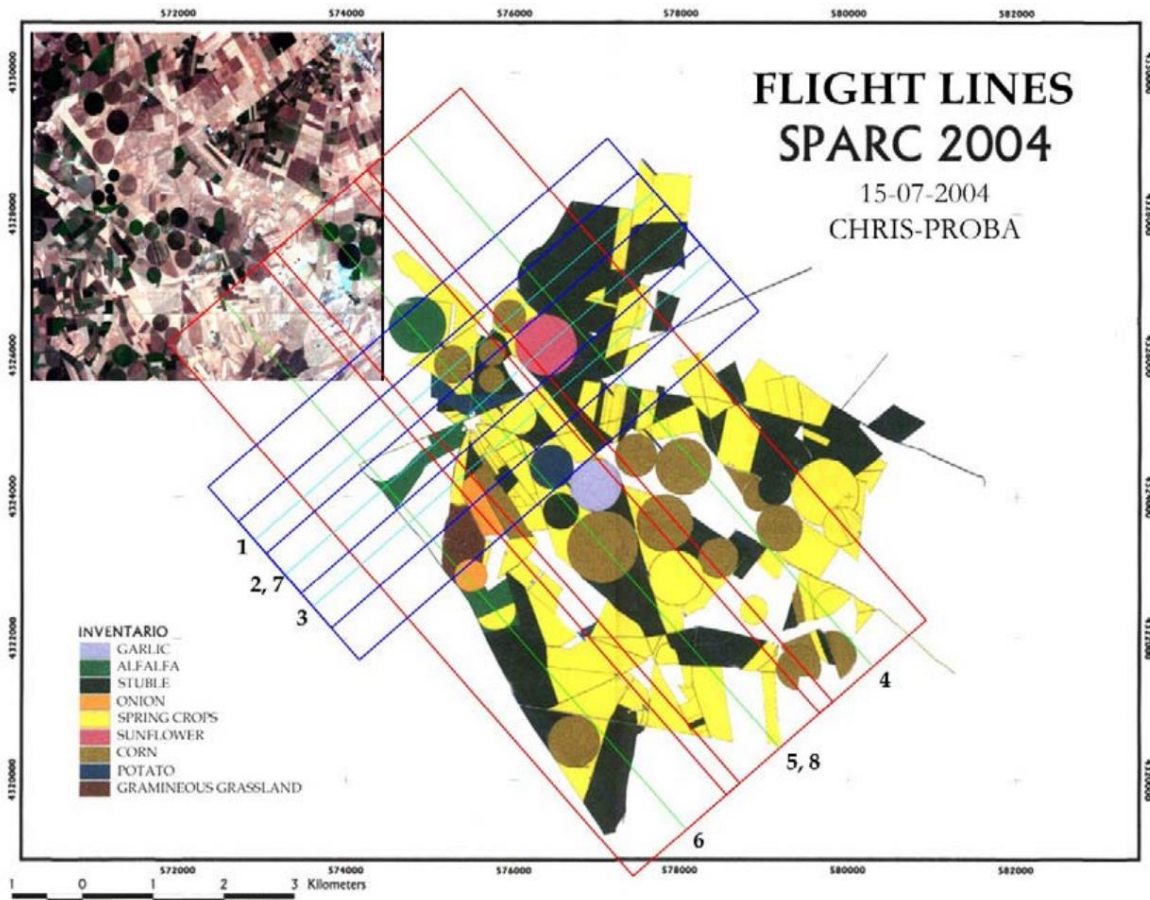


Figure 5.23: Crop map from SPARC 2004 taken directly from the final acquisition report (ESA 2004) highlighting the various crops and their locations.

Spectra of the CHRIS data were assessed for all the months available for all the crop types to establish phenological state in each image. It was found that for some fields of alfalfa there were two distinct production cycles in the space of a year while summer crops exhibited growth in May with a canopy maximum established in June or July. The average MTCI of each crop was calculated using the available CHRIS acquisitions and each base pair was used to predict high spatial imagery for all the months where MERIS data was available (Table 5.3). Initial assessment indicated that the CHRIS data had some issues for November and December that only affected the reflectance measurements directly on the RE. CHRIS reflectance measurements adjacent to band 30 were affected too meaning that a replacement could not be used. Consequently NDVI was calculated in addition to the MTCI to enable assessment of the fusion model during the senescent period in November.

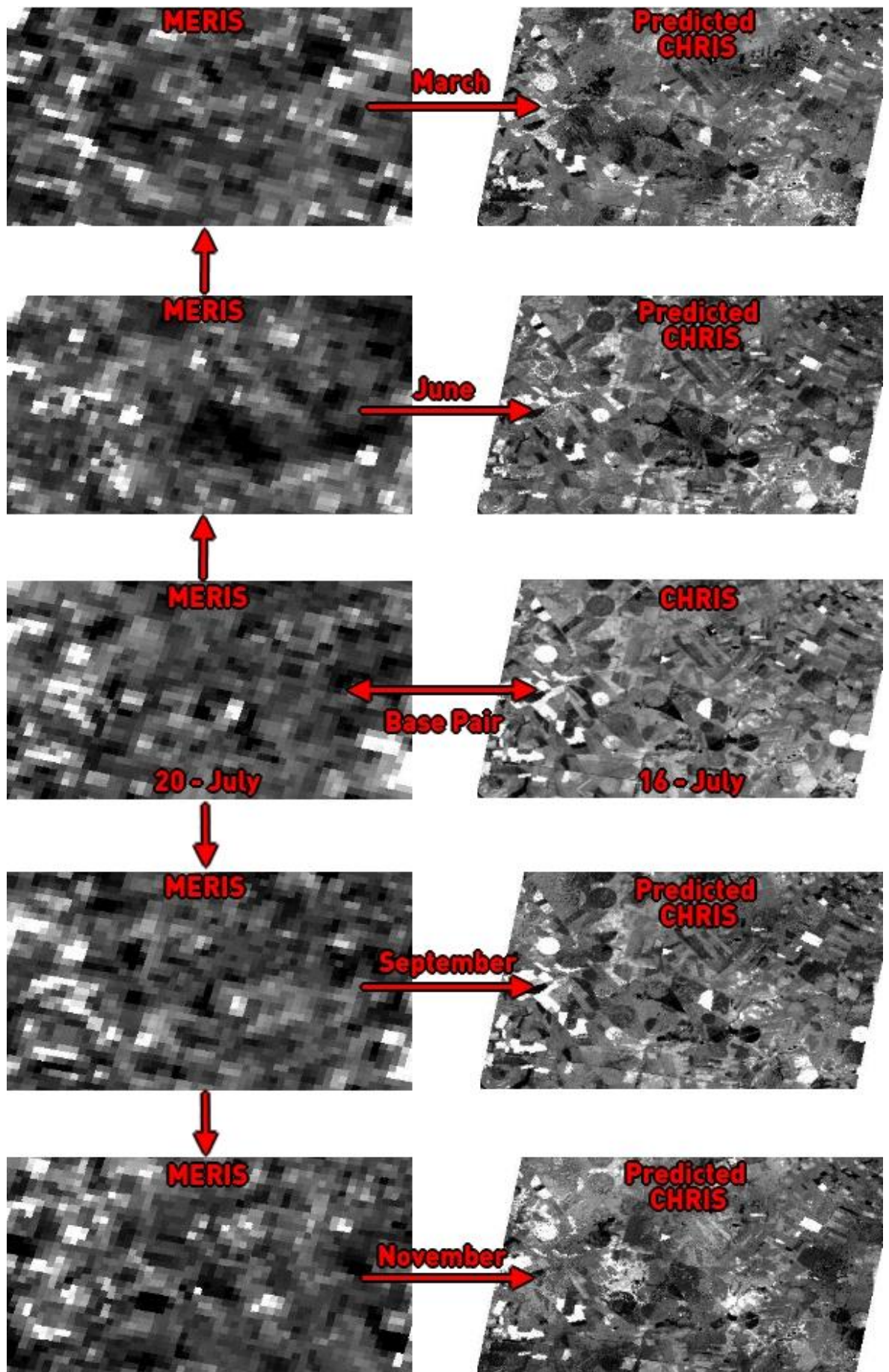


Figure 5.24: Predicted CHRIS imagery using STARFM for the July base pair for the NIR.

5.4.2. Results

Synthetic CHRIS data was produced for all available MERIS dates using the four base pairs. In total 40 predicted images were produced generating high spatial resolution data for any date that the medium spatial resolution MERIS was available.

Figure 5.24 provides an example output of the fusion model for the July base pair. While eight predicted images were produced for all MERIS dates that are outlined in Table 5.3 the figure presents the NIR reflectance for half of these: March, June, September and November. The fusion model can be seen to utilise the difference in MERIS reflectance in conjunction with the base pairing to predict reflectance at a high spatial resolution. Visually the data matches well and differences between the base pair and other MERIS dates are reproduced in the high spatial predicted data. For example the central dark patch of low NIR reflectance that is present in June, but not July, is modelled well in the June predicted CHRIS image. Also changes of the two adjacent fields with very high NIR reflectance located at the eastern limit of the July image are reproduced well by the fusion model. To investigate this in more detail the MTCI and NDVI of six different crops was calculated for each base pair and compared to the measurements from actual CHRIS acquisitions.

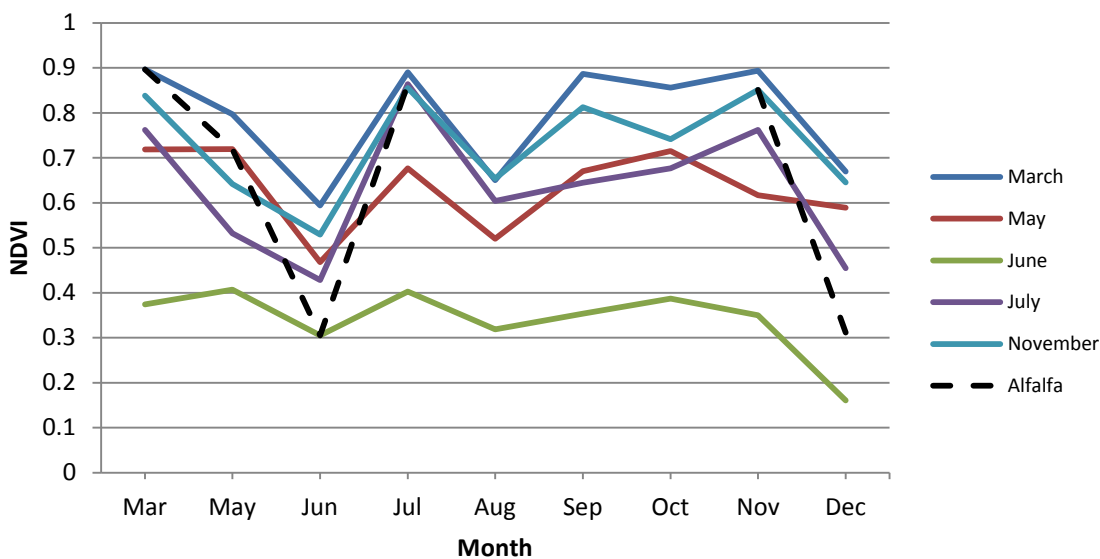


Figure 5.25: Base pair performance at predicting NDVI for alfalfa.

The dashed line in Figure 5.25 represents the NDVI calculated from actual CHRIS acquisition dates, hence why data is unavailable between August and October. The other series denote the estimated NDVI for each base pair which can be used to assess performance compared to the actual field measurements. It can be seen that the Alfalfa canopy was certainly harvested in June and predicted data suggests also a smaller partial loss of the canopy in August. Although each

William James Frampton

base pair has predicted the NDVI with varying success June has significantly underestimated NDVI. This is likely due to the fact that the base pairing was made when the field NDVI was at its minimum which as previously mentioned has been found to be suboptimal in previous studies (Walker et al. 2012). Pairings that were made during canopy maxima, such as: March, July and November, do respond to measured reductions as can be seen clearly in Jun and December. However the results of these canopy maxima pairings do not predict low enough NDVI values for the minima found in June and December.

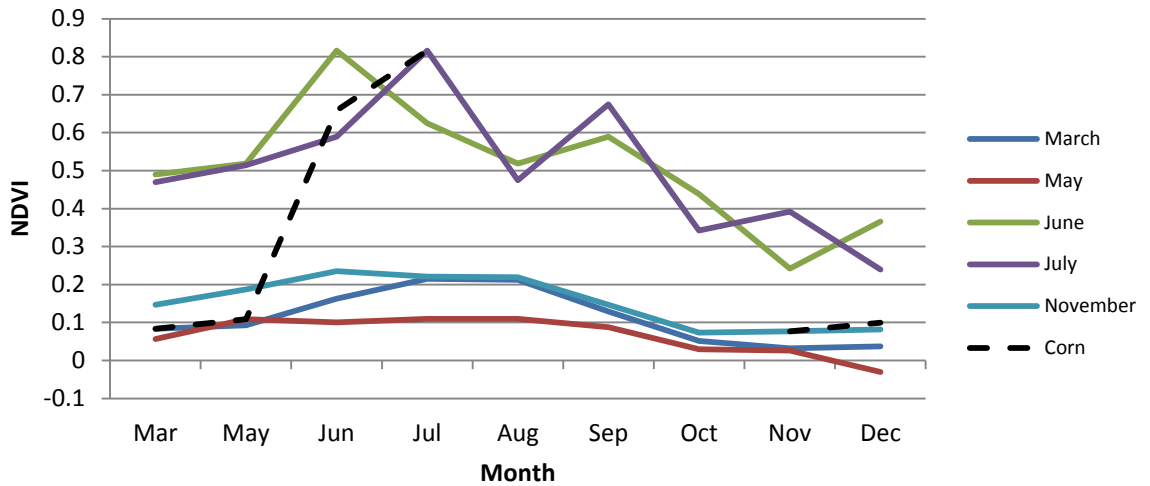


Figure 5.26: Base pair performance at predicting NDVI for corn.

In Figure 5.26 corn can be seen to develop a dense canopy between May and July which is not tracked well by the March and May pairings which were before growth began. Nevertheless as was previously highlighted with alfalfa pairings that were made during the vegetative maximum predict exaggerated NDVI values in months where canopy cover is low. Differences were calculated between the measured and predicted NDVI values for all the crop types for each month of the year where MERIS data was available and the percentage differences are summarised in Table 5.5 for NDVI and Table 5.6 for MTCl.

Table 5.5: Average Difference in NDVI values for each pairing.

	Alfalfa	Corn	Sunflower	Potato	Sugar Beet	Garlic	Average
March	19.94%	151.28%	37.74%	207.33%	281.93%	85.50%	130.62%
May	28.73%	311.87%	167.49%	72.35%	139.52%	41.72%	126.95%
June	94.71%	58.84%	62.62%	46.94%	47.63%	41.85%	58.76%
July	20.80%	51.94%	42.51%	48.18%	49.15%	40.90%	42.25%
November	19.04%	92.54%	45.08%	74.88%	53.23%	171.05%	75.97%

Table 5.6: Average difference in MTCI values for each pairing except November.

	Alfalfa	Corn	Sunflower	Potato	Sugar Beet	Garlic	Average
Mar	31.44%	112.65%	106.06%	66.26%	115.31%	36.38%	78.02%
May	34.95%	156.89%	325.53%	36.97%	44.97%	23.97%	103.88%
Jun	53.72%	58.20%	64.90%	32.86%	48.70%	29.41%	47.96%
Jul	49.25%	48.27%	84.95%	19.77%	13.09%	26.78%	40.35%

It can be seen in Table 5.5 that different pairings were able to predict some crops better than others. Assessment of this indicated again that the best performing pairings were those made at maximum canopy extent. As an example the pairing with the highest average variance, March, performed well for alfalfa and sunflower, the only two crops where there were already canopies in March. As the universal applicability of this downscaling method is important the differences were averaged to see what individual pairing would produce the best results for any crop. July provided the best results with an average NDVI prediction difference of 42.25% while March and May resulted in very poor averages at 130.62% and 126.95% respectively. Results for the MTCI show similar to findings with the July and June base pairs having the best overall average prediction difference of 40.35% and 47.96% respectively. Results strongly suggest that the best time of the year to make a pairing using STARFM is when the canopy is the fullest and for the Barrax region that is in July for the majority of crops.

Although efforts to mitigate uncertainty have been made there are several areas that should be highlighted. Firstly, while extensively geometrically corrected linking 300 m MERIS and 32 m CHRIS data is challenging. Secondly, as noted in Table 5.3 the difference in time between the CHRIS and MERIS base pair acquisitions was up to seven days within which both canopy, solar and background conditions could have changed. Thirdly, there is no way to establish what crops were growing outside of the observations made in July during SPARC 2004. This means that what is presented as corn is only certain to be so during July. Nevertheless as this method is tracking changes in MTCI and NDVI, which are not crop specific, even if a field was harvested and a different crop was sown the downscaling method should account for this. Finally, the fusion of data from different sensors is problematic with differences in view geometry as well as spectral bands especially considering Proba-1 is a technology demonstrator, albeit a highly successful one that resulted in continuation of the series with Proba-2 launched in November 2009 and Proba-V (Proba Vegetation) in May 2013 (ESA 2014b).

5.5. Conclusions

This chapter has investigated application of the MTCI using the future Sentinel optical sensors. With regards to S-3 findings indicate that only the effect of increased view angle between MERIS and OLCI will vary the MTCI by up to 5.3%. For S-2 there are many more considerations. Firstly as the MSI will have only one band in the red part of the electromagnetic spectrum the MTCI will effectively have to use MERIS band 7 rather than 8. Results indicate that as the red absorption feature is wide and relatively stable in vegetated areas the transition will reduce the MTCI by up to 13% more in sparse, than developed, canopies. A much greater difference is caused by the use of a RE band at 705 nm rather than 708.75 nm where results imply that measured reflectance on the RE will decrease by on average 12.12% meaning the MTCI increases by 42-54%. Furthermore findings suggest that using MSI band 7 will be more favourable than band 6 in the S2TCI formula. When all the differences are amalgamated results indicate band changes will mean S2TCI is between 44.28% and 68.8% higher than the MTCI and consequently an initial formula has been provided to convert between S2TCI and MTCI. Nevertheless it should be considered that results were derived from a single field campaign and future work using other data would increase confidence in the preliminary findings that have been presented.

It has been shown that it is possible to downscale from S-3 to S-2 using methods previously developed by Gao (et al. 2006) for the MODIS and Landsat sensors. Results produced reflectance values at the 32 m CHRIS resolution from 300 m MERIS data. Data indicates that better predictions can be made when base pairs are linked during closed canopy conditions supporting previous findings by Walker (et al. 2012). Future work strongly suggests refining the model by possibly adding in multiple pairs of data that document the canopy maximum and minimum. This will effectively give the correct range of values between which the predictions can operate and use the S-3 data to track changes during the phenological transitions of the target vegetation.

Chapter 6: Quantification of Change in Photosynthetic Capabilities of Deforested Locations and Opportunity for Future Recovery under the REDD+ Framework

6.1. Introduction

Forests are important areas for biodiversity and are a source of livelihood for many as they cover 30% of the total land surface (FRA 2010). Monitoring the rate of deforestation is important as forests account for 90% of the annual interchange of carbon between the atmosphere and the land surface. The Global Forest Resources Assessment 2010 (FRA 2010) highlights that there is more carbon in the world's forest than in the atmosphere or remaining oil stocks. An estimated net loss of 13.5 million hectares of forest has occurred in the last 20 years although there was 37% less net deforestation in 2000-2010 than in 1990-2000 which suggests the rate is slowing. The Reduced Emissions from Deforestation and Degradation (REDD) policy was launched at the United Framework Convention on Climate Change (UNFCCC) summit 2008 with the key aim to provide the framework for financial compensation to countries who are able to reduce emissions from deforestation (REDD 2009). REDD+ adds to this by recognising that it is possible to not only prevent deforestation and degradation but also enhance the carbon stock (increasing sequestration) in forests. REDD+ is effectively a mitigation mechanism that non-Annex I Parties (developing countries) are encouraged to utilise to gain compensation for the results of policies that have sequestered carbon.

There are several key sections of the REDD+ proposal; defining which activities are eligible, how emission reductions are calculated over a defined time period, what entity finances the reduction and where the compensation goes. Satellite acquisitions can be used to derive measurements of the photosynthetic capabilities of forests over large areas while also monitoring changes that may occur through regular temporal coverage. Consequently these characteristics make Earth Observation sensors of paramount importance to REDD+ as they can economically quantify the amount of carbon sequestered over a defined period. Therefore there is a need for robust methods for measuring the mitigation performance of a country to enhance the confidence of both the benefactor and the beneficiary. The UNFCCC has called for development of monitoring, reporting and verification (MRV) techniques (UNFCCC 2011). Depending on the study or source different MRV approaches are recommended. A tier based performance approach was recommended by the Intergovernmental Panel on Climate Change (IPCC). The highest confidence levels are achieved at Tier 3 which utilises data spatially specific to a REDD+ policy. When Tier 3 is unachievable Tier 2 country specific data could be used and failing that the most universal and

William James Frampton

easily applicable Tier 1 incorporates globally available data. Herold and Skutsch (2011) called for MRV strategies to be aligned into three groups: conservation, reduced deforestation and positive impacts on the forest stocks. Furthermore they emphasised focus of Tier 3 MRV activities in areas where key drivers are the most active and therefore the threats, and possible economic compensation, are the highest.

Satellite data, with suitable spatial and temporal resolutions, can be used to validate REDD+ activities. Sentinel-3 which is planned for launch in mid-2015 (ESA 2011a) will continue the 10 year MERIS dataset with enhanced temporal resolution. With multiple spectral measurements taken in the RE region MERIS is highly suitable for retrieving chlorophyll content. This analysis will use MERIS data to establish and investigate a methodology to derive the change in photosynthetic capabilities of an area due to deforestation. However it should be considered that the use of optical remote sensing might not be optimal for rainforest locations and the use synthetic-aperture radar (SAR) would allow coverage irrelevant of weather conditions which is a significant concern within these areas. While SAR data is not available operationally, ESA plan to launch Biomass (ESA 2012d), such a device, in 2020 which has been supported by campaigns such as BioSAR 2010 (Gustavsson et al 2011). Nevertheless the performance of Biomass, planned to operate at 200 m spatial resolution (ESA 2014c), is yet to be seen and furthermore there will be a significant period between the launch of the Sentinels and Biomass where optical remote sensing will be the only possibility for global monitoring at a high temporal resolution.

6.1.1. Study Location

In 2005 Nigeria was found to have the highest rate of deforestation in the world according to the Food and Agriculture Organisation of the United Nations (FAO 2010). Deforestation continued between 2005 and 2010 at 410,100 hectares per year according to Batta et al. (2013). The high level of deforestation is driven by rapid population growth stimulating agricultural development and the need for fuel for cooking (Famuyide et al. 2011). Rising energy prices make cooking gas and kerosene unaffordable for many who consequently rely more heavily on wood. The majority of Nigeria's primary forests are tropical and located in the southern part of the country. Benin City, one of the major cities in this region and the capital of the Edo State, is the centre of Nigeria's rubber and palm oil industries. 17,802 km² in size the Edo State is dominated by large areas of primary and secondary forest accounting for 76.5% of the total land area (Formecu 1999). Preliminary analysis utilising a readily available Global Forest Change product derived from Landsat data (Hansen et al. 2013) showed Edo to have some of the most concentrated deforestation in Nigeria between 2000 and 2012. Consequently Edo was set as the focus of the analysis.

6.2. Data and Methods

Global Land Cover (GLC) data from 2000 (Mayaux et al. 2003) for Africa was acquired to distinguish areas of forest from woodland and shrub land (Figure 6.1). According to this the north east of Edo is primarily deciduous wood and mixed shrub land. Benin City, at the centre of south west Edo, is also surrounded by shrub land. Further away from the city there are large areas of mosaicked forest and croplands that constitute 39% of Edo's total land cover. The majority of evergreen forests are near the borders of Edo and make up 15% of the total land cover. GLC 2000 data was used to focus test sites at areas of forest and to help distinguish primary deforestation.

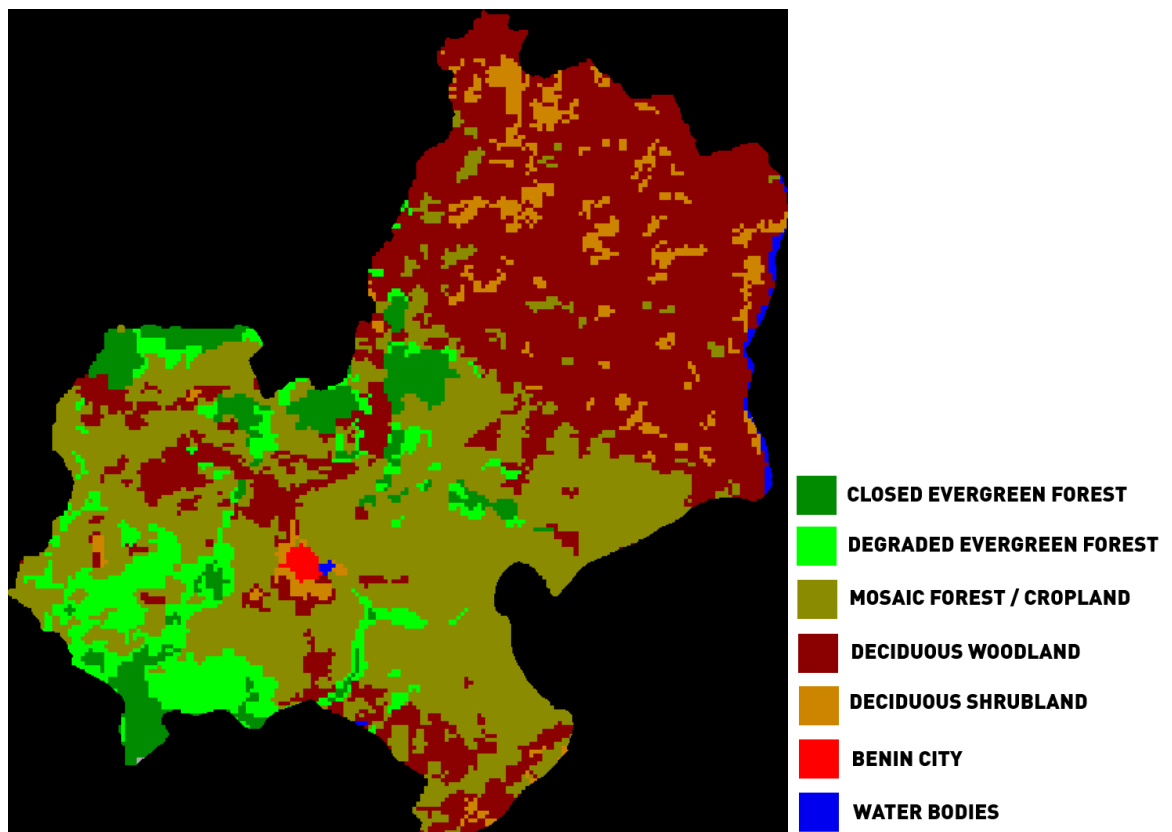


Figure 6.1: Global Land Cover of the Edo State Nigeria generated using GLC2000 data from Mayaux et al. (2003).

MERIS data was accessed using the EOLI-SA portal for the lifecycle of the sensor. It was quickly established that the cloud cover for the region was extensive throughout the majority of the year. To understand the pattern of the typical cloud characteristics of Nigeria four years of the MOD06 (MODIS Cloud Product) were acquired from the NASA Earth Observations portal biannually between 2005 and 2011 at a monthly resolution. The data was then extracted within the boundaries of Nigeria, provided by Global Administrative Areas (GADM 2014), and converted to total cloud cover.

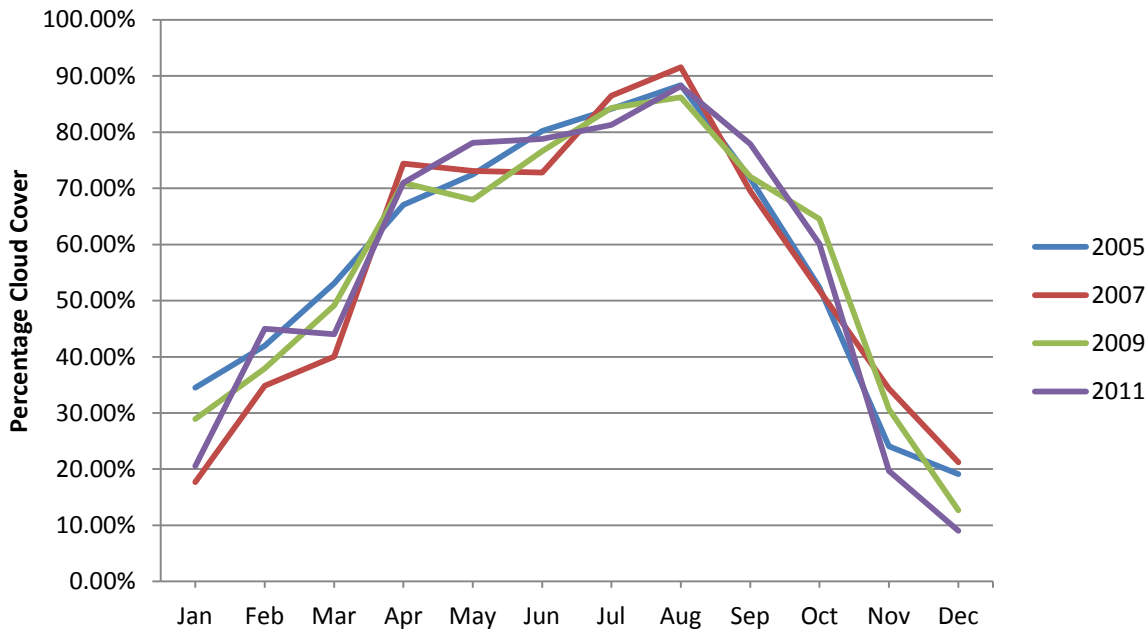


Figure 6.2: Monthly cloud cover as a percentage of Nigeria’s total land area for 2005, 2007, 2009 and 2011 using the MOD06 product.

Figure 6.2 indicates that the total cloud cover of Nigeria, based on the years 2005, 2007, 2009 and 2011, follows a consistent monthly pattern. The maximum cloud extend for the country occurs in August for each year ranging between 88.2-91.5% whereas the minimum cover happened in December for 2005, 2009 and 2011 and January for 2007. December had the lowest average cloud cover of 15.5% with January and November following with 25.4 and 27.2% respectively. All the other months had more than 40% on average with half the year above 70%. This makes the occurrence of clear sky MERIS imagery very unlikely outside of the November-January minimum. Moreover cloud cover was found to not be distributed evenly across Nigeria. The majority occurred over the rainforests located in the south near Edo which meant that clear sky parts of the MERIS scenes more often than not occurred in areas irrelevant to the focus of the study. To further investigate this issue MERIS data, which has a repeat acquisition period of three days of average as this latitude, was assessed. Occurrence of a cloud free acquisition outside of the three month window was nearly non-existent and consequently analysis would have to work within these constraints. Accordingly cloud free MERIS images were acquired annually for 2005-2011, as clear sky acquisitions were not available for 2004 and 2012, which are shown in Table 6.1.

Table 6.1: Details of MERIS Acquisitions used in analysis.

Year	Date	
2005	2004-11-30	MER_FR__2PNUPA20041130_093109_000000982032_00308_14390_3647
2006	2005-12-29	MER_FR__2PNUPA20051229_094800_000000982043_00437_20030_3628
2007	2006-12-11	MER_FR__2PNUPA20061211_094226_000000982053_00394_24997_3630
2008	2007-12-25	MER_FR__2PNUPA20071225_093057_000000982064_00308_30422_3634
2009	2008-12-28	MER_FR__2PNUPA20081228_093346_000000982075_00079_35704_3636
2010	2010-01-23	MER_FR__2PNUPA20100123_094501_000000982086_00165_41301_3639
2011	2011-01-19	MER_FR__2PNUPA20110119_094515_000000983098_00338_46473_3646

It can be seen that each acquisition occurred during the cloud free window during January or the two months prior, e.g. 2009 was acquired between 01-11-2008 and 31-1-2009 under clear sky conditions with little to no haze. All the data has been processed to level 2 which has the MERIS Bottom of Atmosphere Vegetation Index (BOAVI) available; a version of the MTCI which is already atmospherically corrected.

6.3. Total Deforestation in the Edo State

The extent and degree of deforestation that occurred in Edo between 2005 and 2011 can be indicated by the change in MTCI over that time period. To investigate this the BOAVI (MTCI) data was cleaned, subset and masked using the closed and degraded evergreen forest GLC 2000 data to ensure the exclusion of cropland and secondary forest.

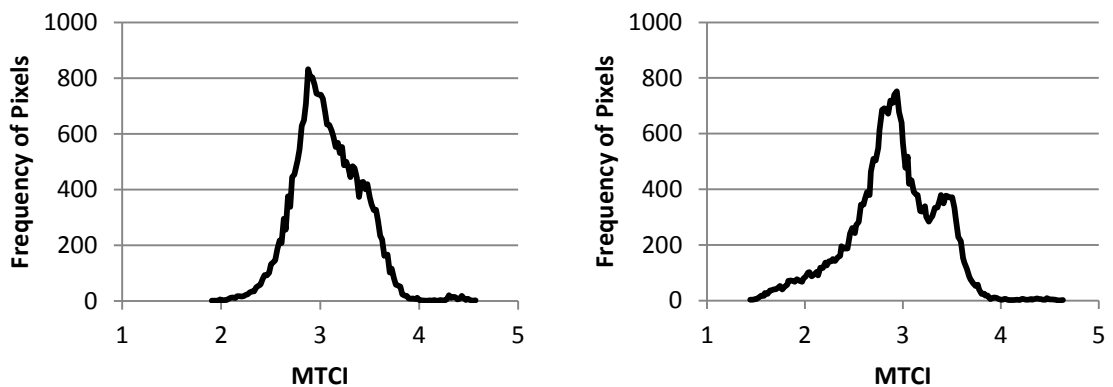


Figure 6.3: Comparison of MTCI histograms for evergreen forests in Edo between 2005 (left) and 2011 (right).

Figure 6.3 shows that in 2005 99.5% of the evergreen forest had an MTCI of >2.25 which falls to 91.3% in 2011. In 2011 4.28% of pixels, amounting to an area of 107.19 km, previously designated as primary forest had an MTCI of < 2 which is clearly within the range of soil pixels as established in Chapter 3 (see Figure 3.7). Comparison between the years in Figure 6.3 highlights that there has been significant change in pixel MTCI values for evergreen forest in Edo between 2005 and 2011. There are similarities in the distributions such as the mode which is 2.88 and 2.81 in 2005 and 2011 respectively and the distinct lack of pixels with an MTCI value higher than 3.8. This suggests consistency between the two images and gives an upper limit of primary evergreen forest MTCI values. However it can be seen that there are also large changes between the distributions, namely the group of pixels where MTCI values are < 2 in 2011 which could be argued to have degraded from prior values of 3.25 in 2005 suggesting a change in MTCI of > 1 to represent deforestation. To further test the compatibility of MERIS imagery from 2005 and 2011 and establish the consistency of the change the difference in MTCI pixel values was calculated and the resulting distribution is presented in Figure 6.4.

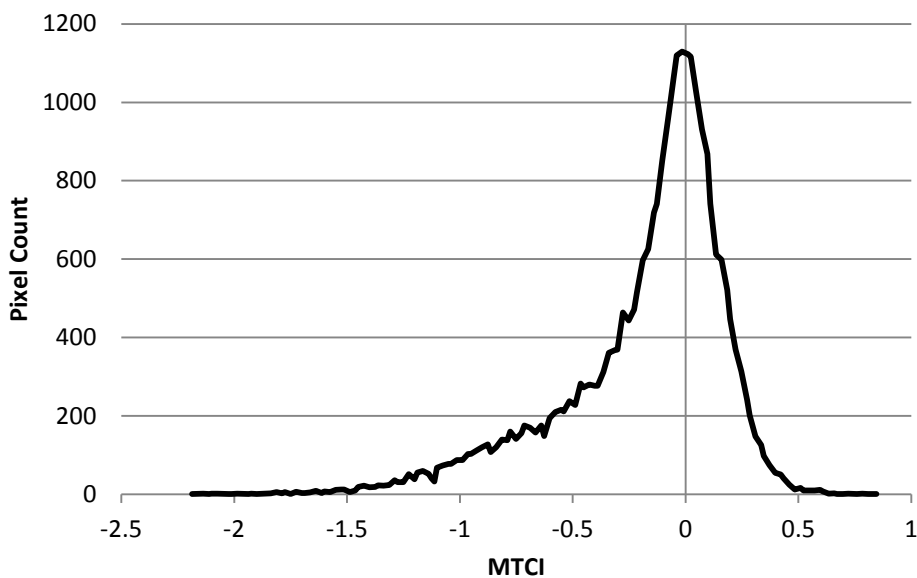


Figure 6.4: MTCI difference for evergreen forest pixels between 2005 and 2011, Edo state, Nigeria.

As expected it can be seen that the majority of evergreen forest pixels had little to no change in MTCI between 2005 and 2011 with a consistent symmetrical curve between ± 0.25 where the mode is 0.02. Positive MTCI pixel values indicate recovery or growth over the time period. 99% of the pixels where MTCI increased did so by less than 0.5 and 95% by less than 0.33. On the other hand of the pixels that decreased over the time period 37.6% were by more than 0.33 and 25.1% by more than 0.5. Not one of the 18,360 evergreen forest pixels increased in MTCI by over 0.85 yet 1101 decreased by more than 1. As the mode is close to 0 at the centre of a skewed

William James Frampton

distribution it suggests the MERIS imagery and application of the MTCI is stable between the years for these single images. With the caveat in mind that this is a comparison between two single images the skewed data suggests that there has been strong deforestation in the Edo state. Calculating the area of deforestation inside Edo using MTCI requires a threshold to be configured for which a given pixel is considered to have been deforested. Considering 99% of pixels that increased with regards to MTCI between 2005 and 2011 did so by less than 0.5 pixel decreases by more than 0.5 could be argued to be an acceptable threshold to indicate deforestation, or at least substantial degradation in the forest condition, while a decrease in MTCI of more than 1 suggests total deforestation. These thresholds will consequently be used to geographically and temporally present the extent of degradation and deforestation for the region. Nevertheless it should be noted that change in photosynthetic capability can be represented by absolute change in MTCI irrelevant of using a threshold for which results are exhibited later on in this chapter in section 6.6.

Table 6.2: Deforestation in the Edo State between 2005-2011 *based from 2000 GLC estimates of evergreen forest

Threshold	Pixels Flagged	Area	Percentage of Total Forest*
0.5 MTCI	4619	415.71 km ²	16.4%
1 MTCI	1101	99.09 km ²	4.0%

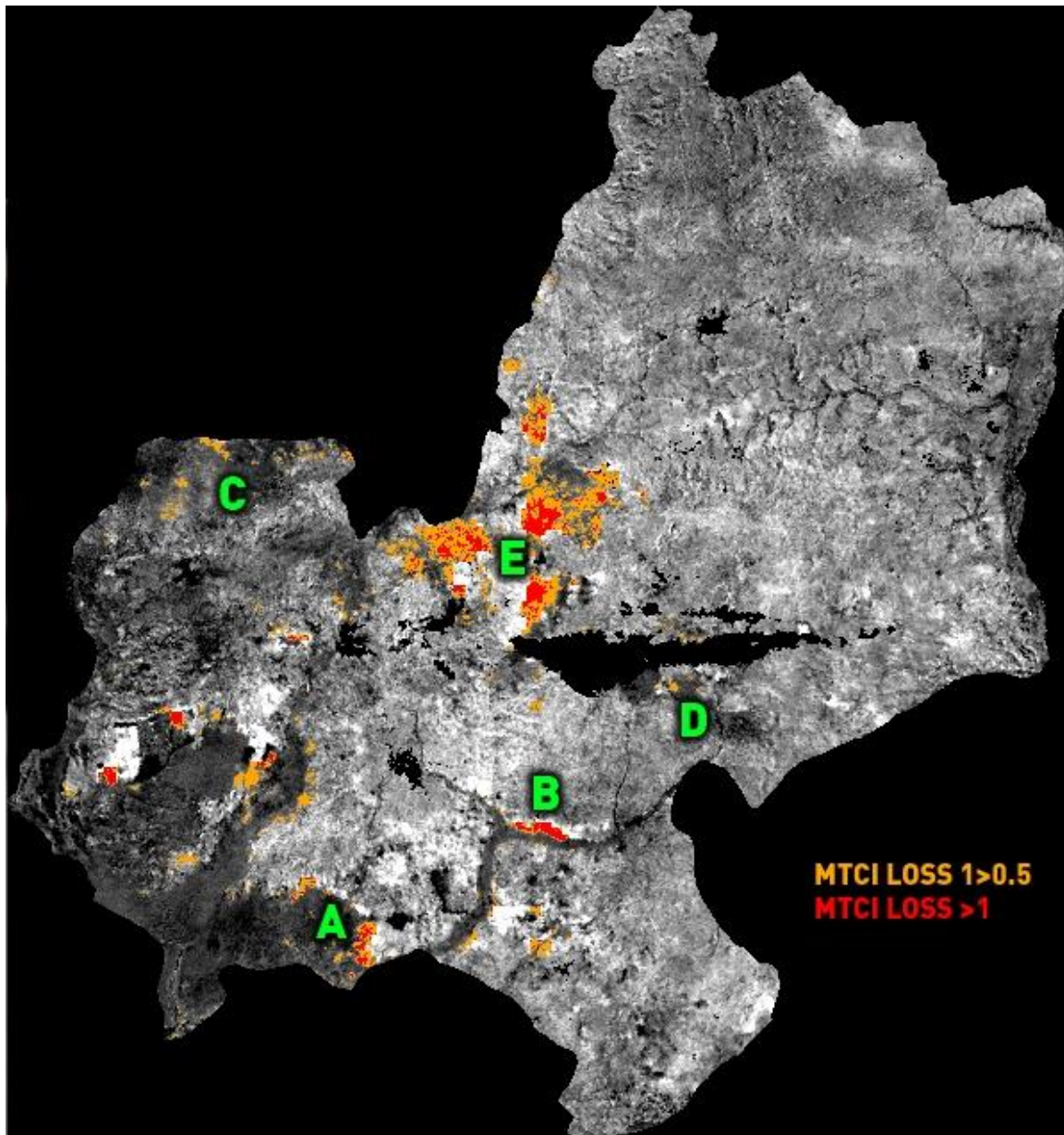


Figure 6.5: MTCI loss in evergreen forest for the Edo state between 2005-2011. Locations of test sites are provided for further discussion.

Figure 6.5 shows the extent of deforestation with respect to evergreen forests between 2005 and 2011. It can be seen that the forests in the south west were not significantly affected albeit there has been 17.1 km² of flagged deforestation at location A. There has been a similar situation in the narrow band of forest that follows the Ossiomo River at location B where 14.31 km² of intensive deforestation has occurred in the northern parts of the forest. Interestingly no deforestation was found to the south of the river which itself is likely an inconvenience to access from Benin City. Forests near the north-western borders of Edo at location C are relatively untouched. The same can also be said about the eastern forests at location D where only minor degradation has occurred. The most extensive and complete deforestation was found in areas north north east of

Benin City at location E where 259.29 km² has been flagged as deforested. These findings correlate with those by Hansen (et al. 2013).

6.4. Deriving Deforestation by Year

Until the launch of Sentinel 2, which will retrieve multiple spectral measurements directly on the RE at 20 m spatial resolution, the MTCI is limited to acquisitions of 300 m using the MERIS dataset that will be continued with the launch of Sentinel 3. Consequently by using the MTCI to assess deforestation means the method is unable to compete with very high spatial resolution maps that have been produced with sensors such as Landsat at 30 m (Hansen et al. 2013). However MERIS data has the advantage of excellent temporal resolution which can allow deforestation to be monitored more frequently or have an increased probability of a clear sky acquisition within a set time period. The aforementioned Nigerian tropical climate limits the scale of this method to an annual assessment but it could be used at a higher temporal resolution in other parts of the world.

The difference in pixel based MTCI measurements was calculated for each of the years between 2005 and 2011 for the entire Edo state. Preliminary histogram analysis of the resulting product indicated that there were differences between the years. This can be attributed to issues with atmospheric correction and view geometry in the calculation of BOAVI (MTCI). Examples of this are shown in Figure 6.6.

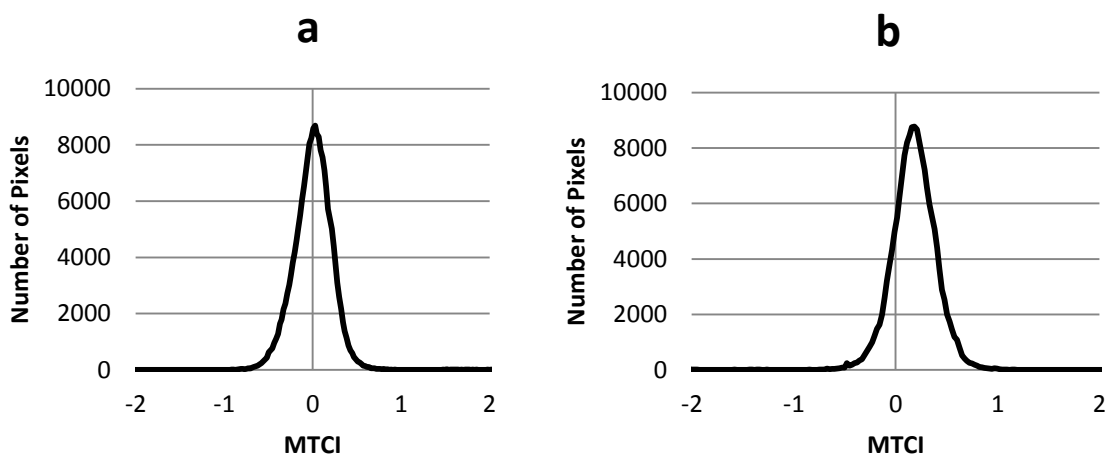


Figure 6.6: MTCI pixel differences in the Edo state for a) 2005-2006 and b) 2006-2007.

It can be seen that there is minimal difference between average MTCI for 2005 and 2006 (Figure 6.6(a)) while there is significant difference for 2006 and 2007 (Figure 6.6(b)). The centre of the distribution for 2006-2007 is 0.19 which would give the false indication of decreased MTCI across

the majority of the image in locations where no actual change occurred. Consequently the differences in distributions were noted so that they could be later applied during threshold analysis which would enhance continuity throughout the timespan of the dataset. The differences in MTCI are displayed in Table 6.3. It should be noted that, while there are some variations, the MTCI for the Edo state is consistently decreasing with time from 2005-2011. This was to be expected from a region with some of the highest rates of deforestation in Nigeria and will be further investigated later.

Table 6.3 Differences in average MTCI between 2005 and 2011.

Year	2005-2006	2006-2007	2007-2008	2008-2009	2009-2010	2010-2011	Average
Normalised Difference	0.02	0.19	0.06	0.04	-0.02	0.06	0.06
Area Flagged	337 km ²	163 km ²	380 km ²	334 km ²	562 km ²	278 km ²	342 km ²

To visualise deforestation in the Edo state by the year that it happened a fixed threshold of 0.5 MTCI which then was adjusted by the difference between the years outside of the 0.06 average. As an example for a pixel to be flagged between 2006-2007 there had to be a change of 0.63 MTCI whereas for 2009-2010 a smaller change of 0.42 resulted in the pixel being flagged for deforestation that year. The results are presented in Figure 6.7.

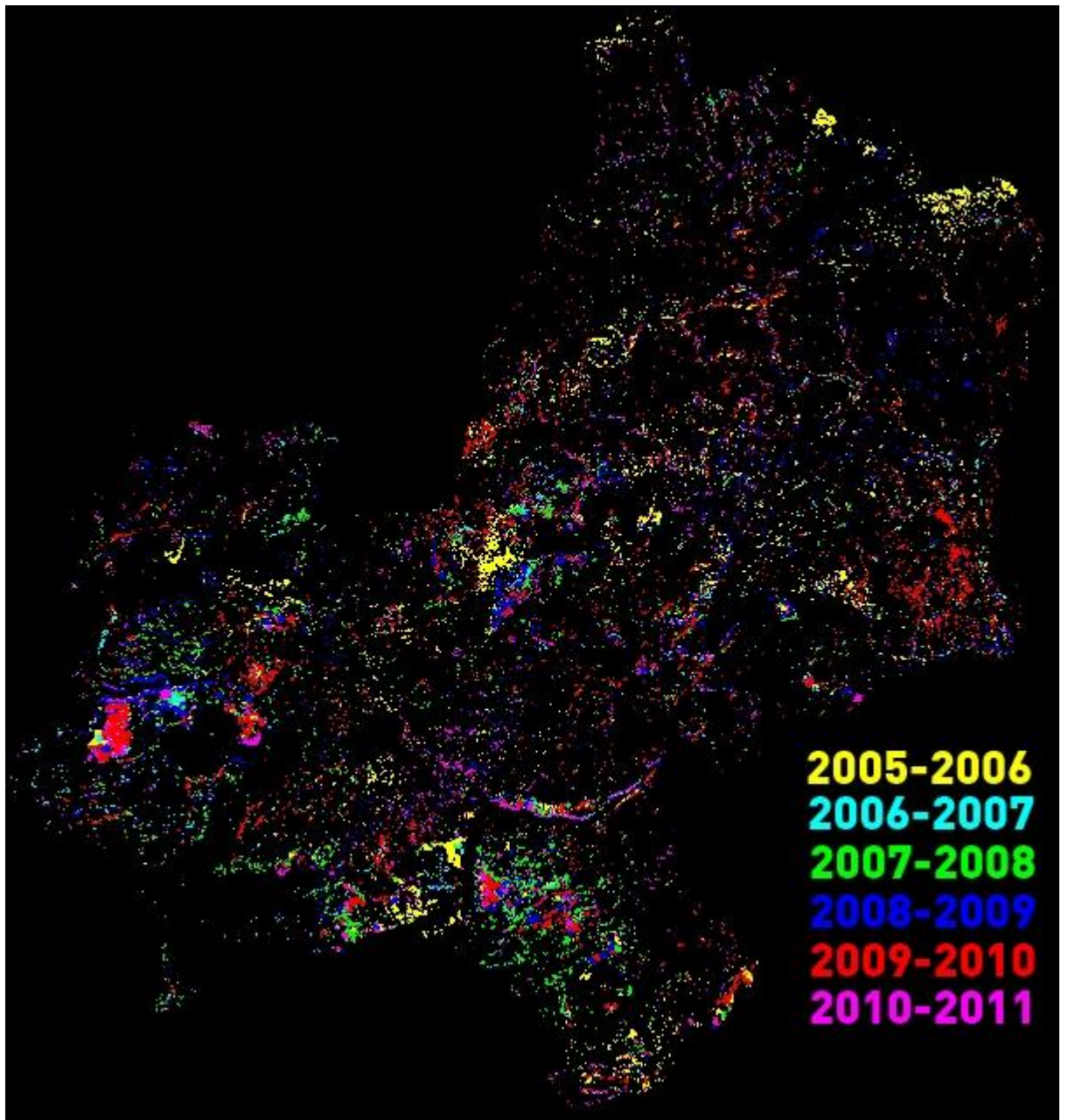


Figure 6.7: Deforestation by year for the Edo State, Nigeria.

As the MTCI is a statistical measure of chlorophyll content the method is unable to distinguish between loss of photosynthetic capability of primary and secondary forest as well as woodland or agricultural land. To investigate the performance of the method sites of extensive deforestation in primary forests that had been established previously in Figure 6.5 were selected to further investigate at an annual scale.

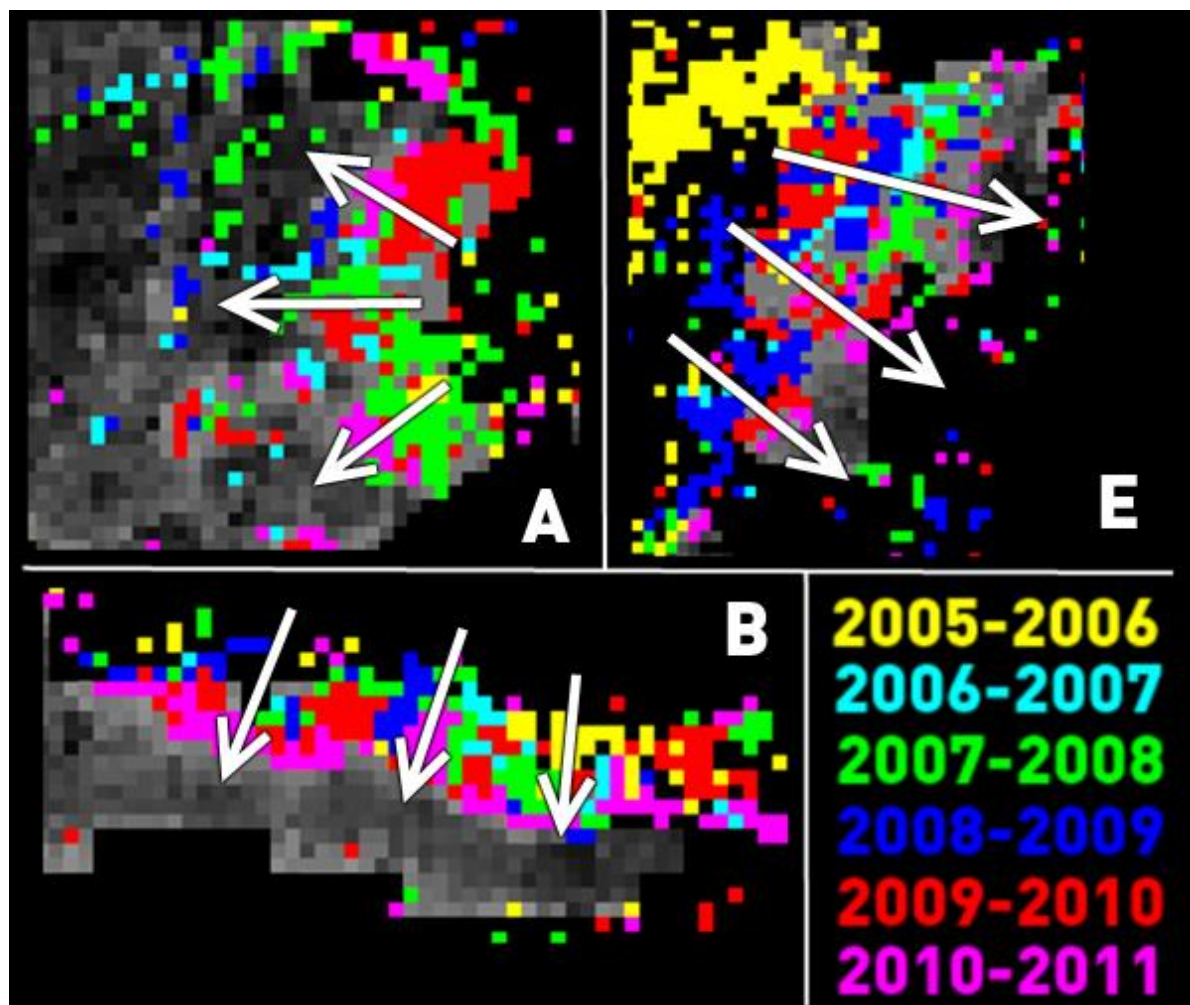


Figure 6.8: Annual deforestation at sites a, b and e.

Theoretically deforestation should be seen to progress inwards over the temporal period which has been indicated by the arrows on Figure 6.8. At site A it should be noted that deforestation was focused at three points from where it spread into the forest (Figure 6.9).



Figure 6.9: MERIS (300 m) imagery highlighting three point deforestation during 2005-2011 for site A.

William James Frampton

Data indicates there was a large deforestation event during 2007 in middle and south of the test site. Sequentially in 2009 the central deforestation was expanded and a large new event occurred towards the north which continued deeper into the forest in 2011. Overall the direction of the deforestation appears to expand chronologically into the forest. However there are some smaller discrete areas that were flagged during 2007 and 2008 which are situated deeper than the 2011 deforestation events. These locations are likely to be localised events separate to the continuous expansions from the east and were not flagged in the 2005-2011 data suggesting partial recovery. Site B shows strong continuity of the deforestation from the extents of the forest inwards.

Deforestation events that occurred in 2011 are adjacent to events in the previous year and so on. At site E there is a general trend of deforestation inwards with the 2011 events deepest in the forest and those that occurred in 2005 furthest out towards the northwest. However between these two dates the other years of deforestation are not chronological as might be expected. The data suggests that deforestation has occurred from towards the centre of the site outwards. With regards to assessing the performance of the annual deforestation data a key assumption has to be made; that the deforestation begins at the borders of the forest and develops inwards. Without ground data it is difficult to hypothesise otherwise.

6.5. Establishing Recovery of the Forest.

To be able to investigate how a deforested location recovers an event must be documented early within the timespan of the dataset. This can be established by subtracting the MTCI of Edo in 2006 from that in 2005. MTCI data for each year was firstly cleaned for erroneous pixels and subsetted via the evergreen forest GlobCover to ensure only primary forests were assessed. Using this dataset test sites were established which exhibited the largest levels of deforestation in 2005 which could then be monitored for recovery throughout the remaining time period. Sites are shown in Figure 6.10 and their areas are documented in Table 6.4. It can be seen that there are areas of pixels that are within the Edo boundaries but omitted from the analysis as they were flagged during the BOAVI processing chain.

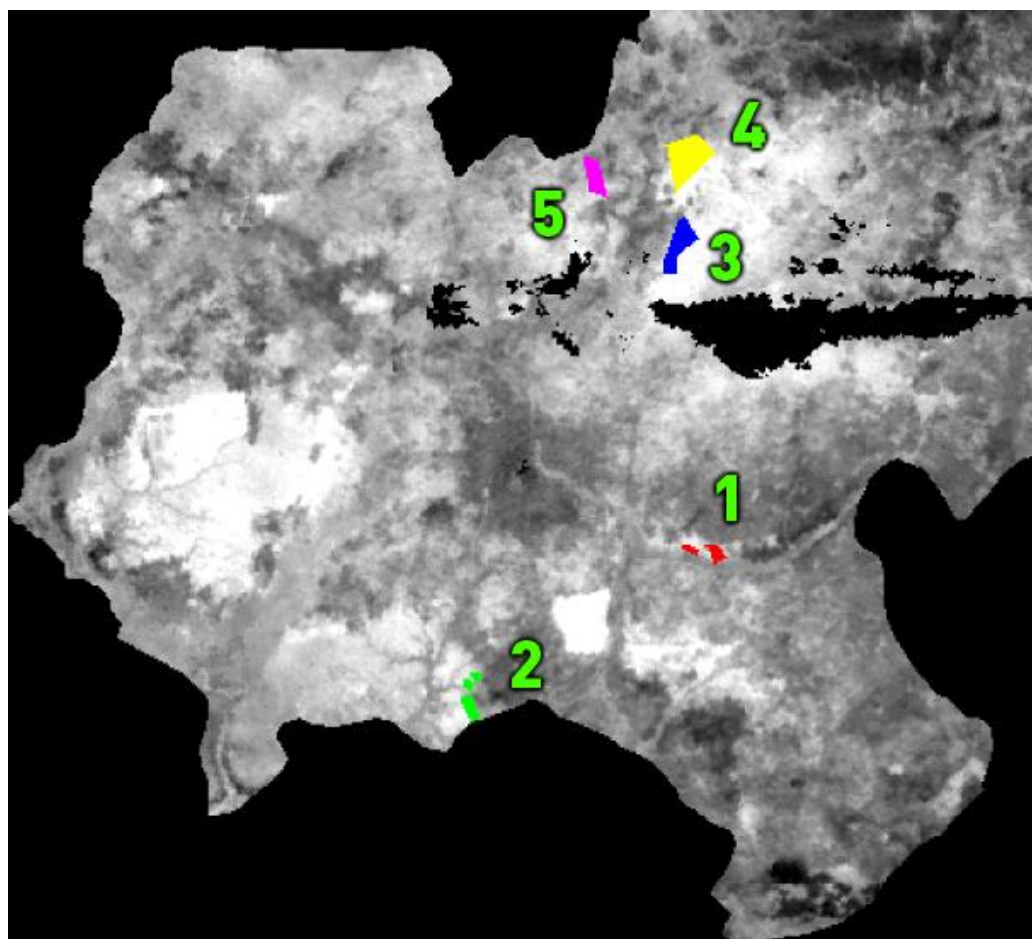


Figure 6.10: 2005-2006 deforestation test site locations.

Table 6.4: Size of primary forest deforestation test sites in the Edo state.

Test Site	1	2	3	4	5
Area	5.04 km ²	5.22 km ²	15.57 km ²	26.37 km ²	9.9 km ²

Test sites were assigned as irregular polygons as each localised case of deforestation was equally irregular. At sites 1 and 2 two polygons were selected to increase the overall size of the test site as the heaviest deforestation was separated by several kilometres. Average MTCl of the test sites was extracted for each year to assess the deforestation event and if it subsequently recovers. To investigate the continuity of the data set the average MTCl values of several large areas, totalling 65.34 km², deep inside south-western and northern evergreen forests were extracted and compared throughout the time span (Figure 6.11). With the assumption that the MTCl of these central locations should be stable differences could consequently be attributed to solar and view geometry variations and then used to normalise the 2005 recovery test site data.

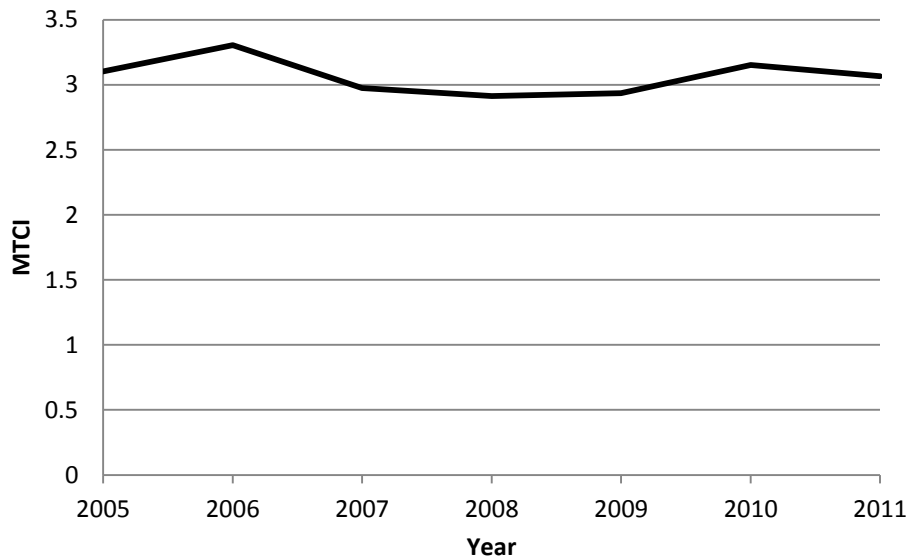


Figure 6.11: Average MTCI of forest calibration test site.

It can be seen that for the stable forest area the MTCI varied between 2.91 and 3.30. The percentage difference between the areas MTCI value and the average over the time period was in turn used to normalise the test sites MTCI data which is presented in Figure 6.12.

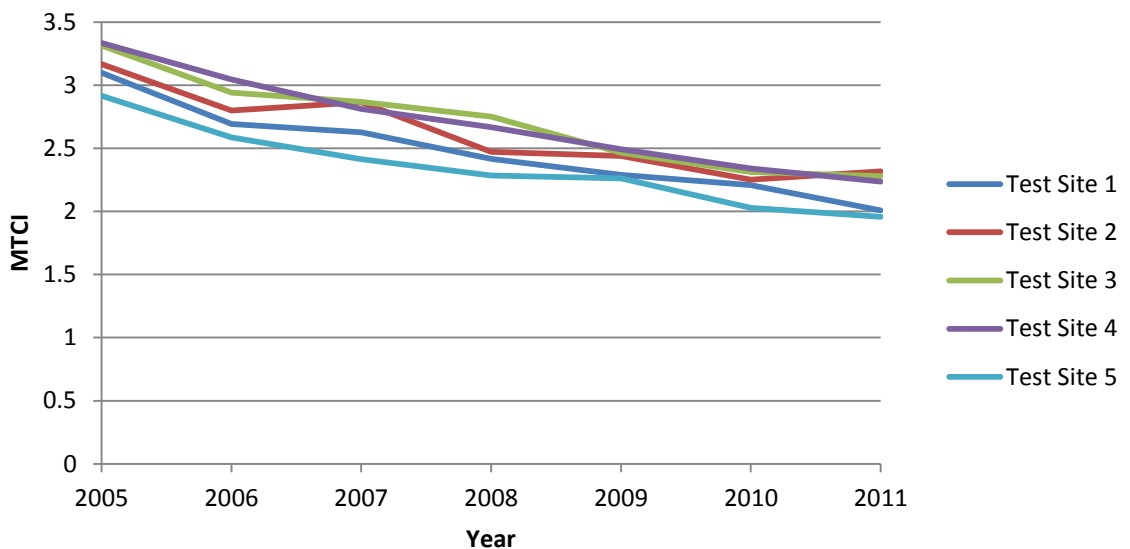


Figure 6.12: Monitoring the MTCI of test sites after a deforestation event.

Results suggest no recovery occurred at any of the sites, in fact MTCI continued to decrease consistently at every site throughout the time period. This suggests that not the entire canopy was removed entirely with further degradation in the sequential years. It was considered that this could be a problem of scale and so 300 m² pixel values were tracked individually in an attempt to find discrete locations within the test sites that recovered, however results were no different. In turn locations were investigated that were deforested for the first time during 2007. These

locations showed the same post event degradation as test sites that were first deforested in 2005. To monitor the recovery of the photosynthetic capabilities of forest it would ideally require complete removal of the entire canopy in the space of a year or so. Locations such as this could not be found at 300 m spatial resolution. These findings suggest that while forest loss year is a useful indication of when and where deforestation begins, which can be used when establishing policies and focusing resources for sustainable management, degradation of the photosynthetic capabilities of the forest occurs over a longer timespan than year of initial detection.

6.6. Predicting the loss of potential carbon sequestration.

Without availability of ground data there is limited possibility to equate localised above-ground biomass (AGB) values for the evergreen forests in the state of Edo and then quantify the changes in AGB. There are default values as suggested by the IPCC (2006) under Tier 1 guidance which states for primary tropical forests the AGB is 30,000 t/km² with a sequestration rate of 700 t/km²/yr. This can be combined with the levels of deforestation that have been previously presented in Table 6.2 to provide an overall figure in changes in AGB.

Table 6.5: Total loss of AGB and potential sequestration for the Edo region between 2005 and 2011 due to deforestation of primary forests.

Deforestation Threshold	Pixels Flagged	Area (km ²)	AGB (t)	AGB Growth (t/yr)
> 0.5 MTCI	4619	415.71	12,471,000	290,997
> 1 MTCI	1101	99.09	2,972,700	69,363

The estimates of how much carbon and potential sequestration that has been lost largely differ depending on the threshold of MTCI that is considered to have been deforested. Realistically sequestration rates of locations that changed by 0.5 MTCI between 2005 and 2011 will not have fallen completely to 0 but have certainly degraded below their original values. To gain an estimate of this the average MTCI value of the entire area of evergreen forest cover (based on 2000 GLC) was calculated for each year and normalised based on forest locations which remained unchanged through the time period.

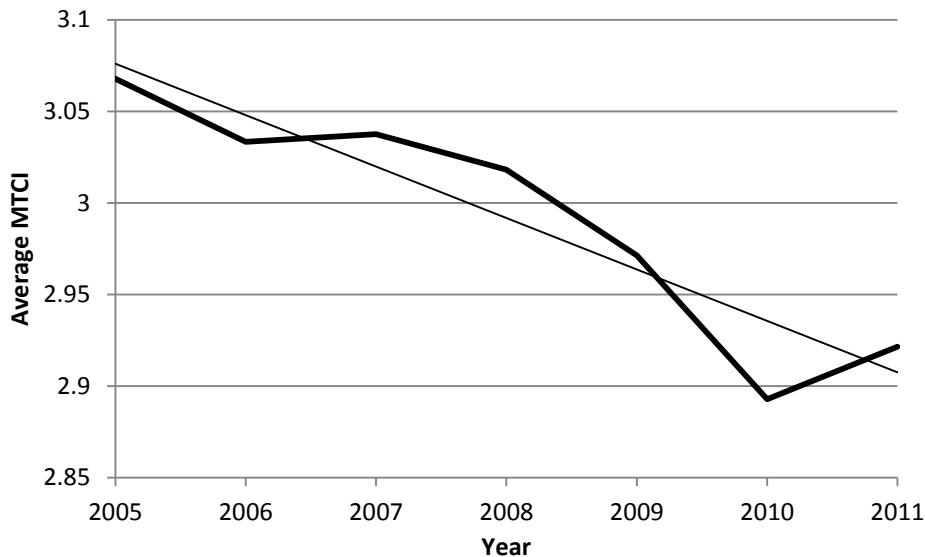


Figure 6.13: Average MTCI of evergreen forest for the Edo state between 2005 and 2011 based on land category from GLC2000 data.

Results indicate that the average MTCI of evergreen forest in Edo has decreased by 0.025 every year between 2005 and 2011 with a coefficient of determination of 0.87. It should be considered that the MTCI does not scale linearly from 0 and that locations without any photosynthetic capabilities can have values of 1 to as high as 1.8. What this means is that the total reduction of 0.15 MTCI is likely to be a 7.5% drop in photosynthetic capability of the total area. Considering that the estimated area of evergreen forest was 2497.05 km² in 2005 which should be able to sequester 700 t/km²/yr the likely loss in carbon sequestration per year due to deforestation in Edo is 131,095 t/yr.

6.7. Conclusions

Results have shown that the MTCI is capable of annually investigating deforestation at a Tier 1 level. Estimates suggest 4% of the total evergreen forest present in Edo has been completely deforested between 2005 and 2011 and 16.4% has been significantly degraded. Analysis into the average cloud cover of the rainforests of Nigeria suggest that there is a 2-3 month time window of opportunity each year between November and January in which clear sky acquisitions are likely. Although one of the key strengths of MERIS is frequent temporal coverage the abundant cloud cover significantly limits analysis throughout the year. Consequently the use of Landsat or SPOT focused between November and January would provide enhanced spatial resolution irrelevant of poor temporal coverage throughout the rest of year compared to MERIS. Using the changes in MTCI values between years, it was demonstrated that it may be possible to distinguish between deforestation and degradation. However, the unavailability of any field data and the coarse

William James Frampton

spatial resolution limits this analysis to provide broad assessment of a region rather than providing location specific information on change in forest cover/condition. It should also be considered that the use of optical remote sensing might not be optimal for rainforest locations and the use SAR would allow coverage at a monthly scale rather than annual. ESA plan to launch Biomass (ESA 2012d), such a device, in 2020. Although this chapter has focused on 300 m resolution MERIS data which will be continued by OLCI aboard S-3, the methodology described will easily be reproducible using S-2's MSI which will operate at 20 m resolution.

Chapter 7: Conclusions and Future Work

7.1. Summary

For over 40 years since the launch of Landsat in 1972 the difference between the maximum absorption of red light due to chlorophyll and the high reflectivity of the cell structure in the adjacent NIR has been used to estimate the biophysical variables of vegetation at a global scale. The NDVI, first reported by Rouse et al. (1973) and popularised by Tucker (1979), is still today the most commonly used method for calculating many aspects of vegetation dynamics. During the 20 years after its introduction many investigations sought to enhance calculation of the NDVI (Clevers 1988; Huete 1988; Kaufman and Tanré 1992; Qi et al. 1994; Rondeaux et al. 1996; Gilabert et al. 2002) with adjustments that often required additional information to mitigate uncertainties. The main problem with such adjustments is that incorporation of additional scene specific information affects the universal applicability, operational use and dynamic response of the algorithm. During this time many papers were published that looked towards the REP as a viable calculation of chlorophyll content, a key driver in photosynthesis (Gates et al. 1965; Collins 1978 Horler et al. 1983; Curran 1989; Dawson and Curran 1998), yet no satellite sensors were capable of its retrieval operationally. These approaches were novel as the majority of studies that had used the NDVI focused purely on its relationship with LAI. In 2002 the launch of Envisat MERIS enabled the operational measurement of reflectance directly on the RE at a medium spatial resolution. While planned as a research and development sensor the success of MERIS led to Copernicus (previously GMES) operational services. One such product was the MTCI a surrogate REP index that was implemented as a standard level 2 global product (Dash and Curran 2004) due to its correlation with chlorophyll.

Advances in the radiometric, temporal, spectral and spatial attributes of satellite sensors drive innovation of entirely new algorithms as well as enabling the refinement and validation of current methods. Out of the five Sentinel missions two will retrieve reflectances in the optical region as well as measurements directly on the RE which enables estimation of REP. S-3 will continue the long running MERIS dataset and with three sensors planned for launch the resulting tandem operation will mean the entire terrestrial environment is monitored every two days at the equator improving with increasing latitude (ESA 2011b). Long running datasets such as these are paramount in providing perspective for investigations into surface and climate change and the impacts they bring for ecological viability and phenological transitions in vegetation (Zhu et al. 2013). On the other hand with two spectral bands measuring reflectance directly on the RE the radiometric capabilities of S-2 will be unparalleled for an operational satellite sensor for use with

vegetative studies. Furthermore the sensor will have a fine spatial resolution of 20 m which should enhance the accuracy of the retrieval of the biophysical parameters of vegetation.

The MTCI-EVAL project was conducted to evaluate and validate the MTCI algorithm. Several key factors were established that influenced its performance; the soil background, view geometry and aerosol optical thickness. It was found that as the MTCI puts large weight on the reflectance of the RE band in relation to the position of the red and NIR the effect of the soil background reflectance at low canopy covers can cause significant uncertainty. Consequently there is much scope for research to devise a method to account for or mitigate this uncertainty. Current methods of accounting for the influence of soil have been argued to have significant issues as without extensive ground data they result in loss of dynamic vegetation response. To further investigate this issue on the MTCI MERIS training data were investigated to explore the green up period for vegetation and subsequently used to establish an algorithm to enhance the capabilities of the MTCI at low canopy covers which typically have values of below two. Test sites were selected in Iowa to characterise the phenological development of corn and soybean over an entire growing season in 2005. Various stages of canopy development were documented for both crops and subsequently each had their spectral reflectances contrasted with background soil measurements using MERIS data. The largest differences were found using MERIS bands 5, 8 and 10 which were combined to form the Soil Discrimination Index (SDI). Initial investigations showed that the SDI was more sensitive to low density vegetative changes than the NDVI or the MTCI. Consequently a suggested threshold was calibrated for the SDI by applying it to 40 separate soils from the ASTER spectral soil library which found most common soil types varied between 0.6 and 0.9. Sequentially this was applied to a separate data set from Dalhart Texas which found only 0.04% of pixels with an MTCI above 2.1 were flagged with an SDI of 0.9. Application of the SDI as a soil flag will notify the user that a given MTCI result is likely due to a soil background with a naturally high VI output thereby increasing the robustness of the MTCI at values below 2. The flag will be most useful when using the MTCI across large scenes with many varying canopy covers and soil background types and conditions. Of specific note is that the flag should increase the accuracy of the MTCI when used to estimate photosynthetic capabilities of an area. As a by-product of the research it was also found that corn and soybean can be differentiated between using the MTCI over the growing season. Subsequently the SDI was applied to two study sites in Spain as an initial validation of the flag. While it performed well analysis highlighted two issues that are worth investigating in future study. Firstly, that inclusion of green reflectance into the formula results in less robust flagging of senescent vegetation and secondly, that the flag performs better in a forest environment than an agricultural setting. While work has applied the SDI to three separate

William James Frampton

environments in different parts of the world utilising multiple datasets further application is recommended to validate its performance as a soil discriminator.

During the investigation to mitigate the influence of soil while working with multiple VIs, datasets and test sites it became apparent that ground data would greatly enhance confidence in the derivation of methods to retrieve the biophysical parameters of vegetation. As S-2 will be the first sensor to have multiple spectral bands directly on the RE at a high spatial resolution operating at a global scale it holds much promise for vegetative monitoring. Two field campaigns, SicilyS2EVAL and SEN3Exp, were used to create a 60 ESU dataset of LAI and LCC measurements to compare with synthetic S-2 data generated from contemporaneous hyperspectral acquisitions using CASI-1500 and Specim EAGLE sensors. Investigations into the correlation between LAI, LCC and canopy chlorophyll content also incorporated data from PROSAIL models (Jacquemoud and Baret 1990; Verhoef 1984, 1985). It was found that the PROSAIL models compared well with the field data in the NIR and green bands but failed to agree in the red part of the spectrum. The parts of the spectrum that were most strongly correlated with chlorophyll were between 660-690 nm and 750+ nm. Of note is that S-2 band 3 (542.5-577.2 nm), according to the data presented, will not be retrieving the optimal wavelengths that were found between 525-555 nm. S-2 band 6, which is a new RE/NIR band with respect to previous satellite sensors such as RapidEye and MERIS, was found to, as a replacement for MERIS band 10 (753.75 nm +/- 3.75 nm), receive increased mixed signal from the RE as it is situated at the peak of the RE rather than slightly beyond it. This meant that S-2 band 7, which is similar to MERIS band 12 (775 nm +/- 7.5 nm), was found to be the optimal band for capturing the vegetative signal in the NIR based on the SicilyS2EVAL and SEN3Exp data sets. Two new methods were proposed to estimate the biophysical variables of vegetation using S-2 MSI data, IRECI and S2REP. IRECI incorporates four bands on, and either side of, the RE while S2REP is a version of REP estimation for S-2 using linear interpolation as used on previous sensors by Guyot and Baret (1988) and Clevers et al. (2000). Each method utilises direct estimation of the slope of the RE the main capability of S-2 MSI which differentiates it from other globally operational sensors. IRECI was found to have the highest correlation with canopy chlorophyll content followed by NDI45 (Delegido et al. 2011b) and the NDVI. A similar conclusion was drawn for LAI with IRECI and NDI45 the best performers. However for LCC S2REP and the MTCI, the only two indices that solely characterise the RE, were the methods with the best correlations. Unlike many previous studies this work incorporates multiple field campaigns with many sampling points and a wide range of vegetation types.

Following the assessment of the new avenues for investigation that S-2 will bring work proceeded to evaluate the application of MTCI using S-2 and S-3. With regards to S-3 OLCI it was important to assess the continuity the platform would have with Envisat MERIS. The only significant difference

that could be established was that of the view angles as S-3 will be tilted 12.58° away from the sun to minimise glint. This leads to a maximum observed view angle of 55.6° , 15.6° higher than that of MERIS. This difference found to cause a mean relative difference of 2.3% to the MTCI by using an annual data set from Spain with canopy variables forward modelled using the PROSAIL model (Baret et al. 1992, Jacquemoud et al. 2009). Application of the MTCI using S-2 is much more complicated than S-3 due to the large spectral differences the sensor has with Envisat MERIS. The combined effect means that S2TCI will be between 44.28% and 68.8% higher than the MTCI and an initial formula has been provided to convert between the indices. Also of note is that findings suggest that using MSI band 7 will be more favourable than band 6 in the S2TCI formula. It should be noted that this investigation used field campaign data to evaluate the impact of spectral changes on the MTCI algorithm. This study highlighted the spectral similarities between the sensors and since both will be in orbit at the same time there is much interest in downscaling between S-3 and S-2 as it could increase the temporal coverage of S-2 dramatically; especially so until a pair of S-2 satellites are working in tandem. By using methods which were originally developed by Gao et al. (2006) for Landsat and MODIS work has synergised MERIS and CHRIS data to investigate the opportunities for the future Sentinel satellites. Synthetic S-2 imagery was successfully generated from MERIS images at times of the year where it was not available. Nevertheless the optimal pairing during July could only achieve a relative accuracy of 20-50% throughout the year which suggests the use of a single paired image, while useful for certain applications, is insufficient. Findings strongly indicate that the time of the year that S-2 and S-3 imagery is linked will be of critical importance and the best results were achieved when the canopy was at maximum density. It should be noted that the point spread function was not considered which is a possible limitation and should be investigated in future work (Amorós-López et al. 2013). Nevertheless this study is unique in the sense that it covered the complete growing season to provide a detailed understanding of the fusion models performance throughout the year.

A final investigation was devised to showcase a potential application of Sentinel data within a REDD+ framework. The evergreen forests of Edo, a state in Nigeria, were assessed for degradation using MERIS data as a surrogate for S-3. The aim of the work was to assess the change in photosynthetic capabilities of the land cover under the REDD+ framework. It was immediately found that extensive cloud cover in the area prevented measurements using optical sensors outside of an annual resolution. A dataset was created using MOD06 to further investigate the cloud coverage over Nigeria which indicated that there is a window of opportunity, between November to January, during which clear sky acquisitions are obtainable. By using the MTCI to estimate changes in forest cover it was found that between 2005 and 2011 99.09 km^2 of

William James Frampton

evergreen forest had been completely deforested while 415.71 km² had been significantly degraded or deforested. These figures are between 4% and 16.4% of the total area of evergreen forest that had covered the Edo state in 2005. The investigation showed that will be possible to indicate deforestation by year using S-3 data with a method easily quantifiable using threshold analysis and while it has been demonstrated at a regional scale it could easily be applied nationally or even globally. In addition several sites were investigated for post degradation/deforestation recovery, however over the studies six year time scale none experienced overall site regrowth. In fact it was found that the photosynthetic capabilities of the sites continued to decrease past the initial event. This suggests that deforestation in Edo, at least at a 300 m scale, is progressive rather than absolute and without ground data a sensor with high spatial resolution would be required for further investigation. By using the default Tier 1 guidance values of AGB from the IPCC (2006) the MTCI was used to predict the total loss of potential carbon sequestration. It was estimated that the primary forests of the Edo state sequestered 131,095 t less of carbon in 2011 than in 2005. Nevertheless it should be considered that the use of optical remote sensing might not be optimal for rainforest locations and the use synthetic-aperture radar (SAR) would allow coverage at a monthly scale rather than annual. While currently technology such as this does not exist ESA plan to launch Biomass (ESA 2012d), such a device, in 2020. Although this chapter focused on 300 m resolution MERIS data which will be continued by OLCI aboard S-3, the methodology described will easily be reproducible using S-2 MSI which will operate at 20 m resolution substantially enhancing confidence in results.

7.2. Key Outcomes

- Many investigations have sought to enhance calculation of VIs through adjustments that often require additional information to mitigate uncertainties. The main problem with such adjustments is that incorporation of additional scene specific information affects the universal applicability, accessibility for the user, operational use and dynamic response of VIs and so should be avoided.
- Application of the SDI using a threshold of 0.9 has been shown to increase the robustness of the MTCI at low canopy covers and has been initially validated in three separate parts of the world.
- The MTCI has been shown to be a robust measure of LCC and will be applicable to S-2 and S-3. This study has also suggested which bands to use in the algorithms; S2TCI and OTCI.
- With two spectral bands measuring reflectance directly on the RE the radiometric capabilities of S-2 will be unparalleled for an operational satellite sensor for use with vegetative studies allowing accurate characterisation of the RE region and enhanced estimation of the REP.

- Multiple field campaigns have been used to develop and validate algorithms to optimally retrieve the biophysical variables of vegetation using S-2. The following were found as optimal methods.
 - To measure LAI research suggests using the IRECI or the NDVI.
 - To measure LCC research suggests using S2REP or the MTCI.
 - To measure canopy chlorophyll content research suggests using the IRECI or the NDVI.
- Preliminary comparison between the S-2 and S-3 sensors using S2TCI and OTCI has been conducted and an equation: $S2TCI = 1.6866 * MTCI - 0.3406$ (Eq. (7.1)) has been suggested to directly contrast results between sensors.
- The possibilities of a S-2/S-3 fusion model have been demonstrated through integration of the STARFM algorithm. Synthetic S-2 data was successfully generated from MERIS imagery at times of the year where high resolution acquisitions were unavailable.
- The MTCI was used to showcase an application of S-3 within the REDD+ framework.
 - Deforestation and degradation was presented geographically, a method that is easily reproducible.
 - It was found that 415.71 km² of rainforest was deforested between 2005 and 2011 within the state of Edo, Nigeria; 16.4% of the total primary forest that Edo had in 2005.

7.3. Limitations

- Inclusion of the green band makes the SDI more sensitive at low canopy covers when vegetation is growing and healthy yet, according to preliminary validation, depreciates the correlation during senescence.
- Accurately reproducing S-2 data requires hyperspectral acquisitions which consequently limits the scope of available field campaigns for validating algorithms pre-launch. While multiple campaigns have been used to derive the IRECI and S2REP further validation is required to see if the algorithms produce similar results for other campaigns.
- An algorithm has been provided to directly compare between the MTCI and S2TCI, however, further investigation is required to validate this equation for other datasets in different parts of the world.
- While STARFM was used to synergise S-2 and S-3 there was an average pixel error of 20-50% for the optimal base pair. A suggestion to enhance this error is provided in 7.4.2..
- Using optical sensors such as S-2 and S-3 to monitor rain forest is problematic due to cloud cover during the majority of the year. Consequently it may indeed be more suitable to use SAR data in future REDD+ applications. Nevertheless Biomass, which will be the first operational SAR sensor, is not planned for launch until 2020.

7.4. Future Work

During the course of research a series of lessons have become apparent from which a number of recommendations can be proposed for future work to follow.

7.4.1. Enhanced Field Campaign Procedure

Through participation in multiple field campaigns, and processing of many conducted by 3rd parties, during the research of this thesis it has been found that methodologies within vegetative remote sensing vary considerably. Datasets differ with respect to: sensor, location, operating team, time of year, view geometry and field campaign procedures. As the discovery of new methods of retrieving vegetative biophysical parameters, as well as refining current ones, depends on the quality data sets the aforementioned differences can not only add considerable uncertainty but affect the compatibility of research. This can consequently result in the fragmentation of methods and lack of further validation following a successful finding. Involvement in the validation of the MTCI has emphasised the benefits of extensive research using a specific vegetation index as the robustness of the product increases with each step taken. If there was an opportunity to conduct a follow up field campaign, ignorant of project constraints, this work proposes that several key points are considered.

- LCC and LAI must be treated individually and given equal importance.
- Measurements of LCC should have destructive calibration that follows well documented procedure (Moran and Porath 1980, Moran 1982)
- ESU size should be well documented and linked as closely as possible to the sensor being investigated.
- Radiometric and atmospheric adjustments should be as contemporaneous as possible with the sensor flight.
- While having multiple measurements in the same field will strengthen the characterisation of an individual ESU they should be combined and are not a substitute for variety with respect to crop and spatial distribution.
- Although multiple hyperspectral acquisitions are likely to be costly ideally a field campaign should be conducted over the length of a growing season thus allowing methods to account for phenological changes in the study site.

Of significant concern is that methods are only strongly correlated to the field campaign in which they occurred or even the 'snapshot' of the phenological state of the vegetation. Two novel indices that were presented in Chapter 4, S2REP and IRECI, require extensive cross validation in

the future to avoid this pitfall. However validating indices of the future Sentinel sensors is problematic as it requires hyperspectral data before their launch.

7.4.2. Downscaling Method with Multiple Pairings

Chapter 5 highlighted that fusion models used in downscaling perform best when the high and low spatial pairing is made during the maximum canopy extent. However while such a pairing was accurate in predicting dense vegetation it overestimated vegetative cover during sparse canopy conditions. By adding in multiple pairs of data that document the canopy at the maximum and minimum vegetative states the model could effectively be assigned the correct range of values between which the predictions can operate. Consequently the use of low spatial resolution data to track changes during the phenological transitions of the target vegetation should have significantly increased accuracy. Furthermore as most downscaling methods consider linear mixture models which may not hold true in a dynamic environment of crops there is opportunity to perform class based modelling through the analysis of spectral information. Combining modelling of each class separately and maximum and minimum canopy measurements should increase robustness of the model and hold many prospects for a S-2 S-3 fusion model.

7.4.3. Retrieval of Biophysical Variables

During the early stages of vegetative remote sensing research focused on correlation with canopy density. Many studies and field campaigns did not give adequate consideration to LCC and canopy chlorophyll content which resulted in indices that focused on the SR and sequential enhancing of the NDVI. Later on the chemistry and biology of vegetation became a significant interest within remote sensing and focus shifted to the behaviour of the RE to deepen understanding of vegetation dynamics. LAI, LCC and their combination canopy chlorophyll content all have distinct uses and equally separate methods of optimal calculation. It is highly recommended that all those who undertake future research connected to the remote sensing of vegetation realise this. There is great scope for research in upscaling leaf scale chemistry and the effects of phenological transitions to help further understand canopy dynamics.

7.4.4. Further Comparison of OTCI and S2TCI

Although this analysis has given an initial insight into how the MTCI will change with application using future Sentinel sensors using field campaign data further validation with other datasets at different locations would be required to validate and improve the presented algorithm to directly compare between data of the two sensors. To achieve this before launch hyperspectral data

William James Frampton

would be required such as CHRIS or airborne acquisitions contemporaneously with a field campaign that considers discussion in 7.4.1..

7.5. Concluding Remarks

Review of literature suggests LAI, LCC and chlorophyll content are frequently not, as they should be, treated separately at each stage of vegetative investigation. The findings of this thesis suggest that LAI is best measured using the SR/NDVI while an estimate of REP is a more robust measure of LCC. The combination of these two variables, canopy chlorophyll content, is therefore best derived through characterising each of the spectral regions sensitive to vegetation; the red, RE and NIR with an index such as IRECI. Findings emphasise that the L2 MERIS product the MTCI, which has been explored in detail, is a robust measure of LCC and also canopy chlorophyll content. Finally, it is recommended that emphasis is placed on deriving and validating retrieval methods using S-2 MSI as the two bands directly on the RE mean it is not only spatially, but radiometrically superior to S-3 and will consequently allow better characterisation of the RE. This, and future sensor improvements, will help overcome the problem of saturation and enable the remote acquisition of the biophysical parameters of vegetation in unprecedented detail.

References

- ASRAR, G., FUCHS, M., KANEMASU, E. T., and HATFIELD, J. L., 1984. Estimating absorbed photosynthetic radiation and leaf-area index from spectral reflectance in wheat. *Agronomy Journal*, **76**, 300–306.
- ANDRIEU, B., BARET, F., JACQUEMOUD, S., MALTHUS, T. and STEVEN, M., 1997. Evaluation of an improved version of SAIL model for simulating bidirectional reflectance of sugar beet canopies. *Remote Sensing of Environment*, **60**, 247-257.
- ASRAR, G., Ed. 1989. Theory and applications of optical remote sensing. New York, Wiley.
- AMORÓS-LÓPEZ, J., GÓMEZ-CHOVA, L., ALONSO, L., GUANTER, L., ZURITA-MILLA, R., MORENO, J., CAMPS-VALLS, G., 2013. Multitemporal fusion of Landsat/TM and Envisat/MERIS for crop monitoring. *International Journal of Applied Earth Observation and Geoinformation*, **23**, 132-141.
- AZIMUTH SYSTEMS UK, 2005. Airborne Remote Sensing Hyperspectral Direct Georeferencing Package AZGCORR User's Manual Version 5.0.0, Azimuth Systems UK.
- BADHWAR, G. D., MacDONALD, R. B., and MEHTA, N. C., 1986. Satellite-derived leaf-area-index and vegetation maps as input to global carbon cycle models – a hierarchical approach. *International Journal of Remote Sensing*, **7**, 265-281.
- BALDRIDGE, A. M., HOOK, S. J., GROVE, C. I., and RIVERA, G., 2009. The ASTER spectral library version 2.0. *Remote Sensing of Environment*, **113**, 711-715.
- BANNINGER, C. 1991. Phenological changes in the red edge shift of Norway spruce needles and their relationship to needle chlorophyll content. Physical Measurements and Signatures in Remote Sensing, European Space Agency, Noordwijk, 155-158.
- BARET, F., GUYOT, G., and MAJOR, D. J., 1989. TSAVI: A vegetation index which minimizes soil brightness effects on LAI and APAR estimation. Geoscience and Remote Sensing Symposium, IGARSS'89. 12th Canadian Symposium on Remote Sensing.
- BARET, F., and GUYOT, G., 1991. Potentials and limits of vegetation indices for LAI and APAR assessment. *Remote Sensing of Environment*, **35**, 161-173.

William James Frampton

- BARET, F., JACQUEMOUD, S., GUYOT, G., and LEPRIEUR, C., 1992. Modelled analysis of the biophysical nature of spectral shifts and comparison with information content of broad bands. *Remote Sensing of Environment*, **41**, 133–142.
- BARET, F., JACQUEMOUD, S., and HANOCQ, J. F., 1993. The soil line concept in remote sensing. *Remote Sensing Reviews*, **7**, 65–82.
- BERK, A., ANDERSON, G. P., ACHARYA, P. K., HOKE, A. M., CHETWYND, J. H., BERNSTEIN, L. S., SHETTLE, E. P., MATTHEW, M. W., and ADLER-GOLDEN, S. M., 2003. MODTRAN4 Version 3 Revision 1 User's Manual. Technical report, Air Force Research Laboratory, Hanscom Air Force Base, MA, USA.
- BLACKBRIDGE, 2014. RapidEye – High Resolution Satellite Imagery. <http://www.blackbridge.com/rapideye/products/index.html> (accessed 18.02.2014)
- BONAN, G. B., 1995. Land – atmosphere interactions for climate system models: coupling biophysical, biogeochemical, and ecosystem dynamical processes. *Remote Sensing of Environment*, **51**, 57– 73.
- BOOCHS, F., KUPFER, G., DOCKTER, K., and KUHBAUCH, W., 1990. Shape of the Red Edge as vitality indicator for plants. *International Journal of Remote Sensing*, **11**, 1741–1753.
- BOYD, D. S., and FOODY, G. M., 2010. An overview of recent remote sensing and GIS based research in ecological informatics. *Ecological Informatics*, **6**, 25-36.
- BOYD, D. S., ALMOND, S., DASH, J., CURRAN, P. J., and HILL, R. A., 2011. Phenology of vegetation in Southern England from Envisat MERIS terrestrial chlorophyll index (MTCI) data. *International Journal of Remote Sensing*, **32**, 8421-8447.
- BOYD, D. S., ALMOND, S., DASH, J., CURRAN, P. J., HILL, R. A., and FOODY, G. M., 2012. Evaluation of Envisat MERIS terrestrial chlorophyll index-based models for the estimation of terrestrial gross primary productivity. *Geoscience and Remote Sensing Letters*, **9**, 457–461.
- BOYER, M., MILLER, J., BELANGER, M., and HARE, E., 1988. Senescence and Spectral Reflectance in Leaves of Northern Pin Oak (*Quercus palustris* Muenchh.). *Remote Sensing of Environment*, **25**, 71-87.
- BROGE, N. H., and LEBLANC, E., 2000. Comparing prediction power and stability of broadband and hyperspectral vegetation indices for estimation of green leaf area index and canopy chlorophyll density. *Remote Sensing of Environment*, **76**, 156–172.

William James Frampton

- BROGE, N. H., and MORTENSEN, J. V., 2002. Deriving green crop area index and canopy chlorophyll density of winter wheat from spectral reflectance data. *Remote Sensing of Environment*, **81**, 45–57.
- BUSCHMANN, C., and NAGEL, E., 1993. In vivo spectroscopy and internal optics of leaves as basis for remote sensing of vegetation. *International Journal of Remote Sensing*, **14**, 711 – 722.
- CAMPBELL, G. S., and NORMAN, J. M., 1990. The description and measurements of plant canopy structure. In, *Plant Canopies: Their Growth, Form and Function*, Russell, G., Marshall, B., and Jarvis, P. G., Eds. Cambridge, U.K. Cambridge University Press, 1–19.
- CAMPBELL, G. S., and NORMAN, J. M., 1998. *An introduction to Environmental Biophysics*. Springer, New York.
- CAMPBELL, N.A., REECE., J., 2005. *Biology*. 7th edition, Pearson/Benjamin Cummings.
- CAMPBELL, N. A., WILLIAMSON, B., HEYDEN, R.J., 2006. *Biology: Exploring Life*. Boston, Massachusetts: Pearson Prentice Hall.
- CARTER, G., DELL, T., and CIBULA, W., 1996. Spectral reflectance characteristics and digital imagery of a pine needle blight in the south eastern United States. *Canadian Journal of Forest Research*, **26**, 402-407.
- CECCATO, P., FLASSE, S., TARANTOLA, S., JACQUEMOUD, S., and GRÉGOIRE, J., 2001. Detecting vegetation leaf water content using reflectance in the optical domain. *Remote Sensing of Environment*, **77**, 22-33.
- CHEN, J.M., and BLACK, T.A., 1992. Defining leaf area index for non-flat leaves. *Agricultural and Forest Meteorology*, **57**, 1–12.
- CHEN, J. M., 1996. Optically based methods for measuring seasonal variation in leaf area index of boreal conifer forests. *Agricultural and Forest Meteorology*, **80**, 135–163.
- CHUVIECO, E., DESHAYES, M., STACH, N., COCERO, D., & RIAÑO, D., 1999. Short-term fire risk: foliage moisture content estimation from satellite data. *Remote sensing of large wildfires in the European Mediterranean Basin*, 17-38.
- CIAIS, P., DENNING, A. S., TANS, P. P., BERRY, J. A., RANDALL, D. A., COLLATZ, G. J., SELLERS, P. J., WHITE, J. W. C. TROILIER, M., MEIJER, H. A. J., FRANCEY, R. J., MONFRAY, P., and HEIMANN, M., 1997. A three-dimensional synthesis study of $\delta^{18}\text{O}$ in atmospheric CO_2 . 1. Surface fluxes. *Journal of Geophysical Research*, **102**, 5857-5872.

William James Frampton

- CLEVERS, J. G. P. W., 1988. The derivation of a simplified reflectance model for estimation of leaf area index. *Remote sensing of environment*, **25**, 53-69.
- CLEVERS, J. G. P. W., 1994, Imaging spectrometry in agriculture - plant vitality and yield. In, Hill, J., and Mégier, J., 1994, Indicators Imaging Spectrometry — a Tool for Environmental Observations. *Eurocourses: Remote Sensing*, **4**, 193-219, Kluwer Academic Publishers, Dordrecht.
- CLEVERS, J. G. P. W., and BÜKER, C., 1991. Feasibility of the red edge index for the detection of nitrogen deficiency. In Proceedings 5th International Coll. 'Physical Measurements and Signatures in Remote Sensing', Courchevel, France, ESA SP-319, 165–168.
- CLEVERS, J. G. P. W., DE JONG, S.M., EPEMA, G.F., and ADDINK, E.A., 2000. MERIS and the Red Edge index. Second EARSeL Workshop on Imaging Spectroscopy, Enschede, 2000.
- CLEVERS, J. G. P.W., DE JONG, S. M., EPEMA, G. F., VAN DER MEER, F., BAKKER, W. H., SKIDMORE, A. K., 2002. Derivation of the red edge index using MERIS standard band setting. *International Journal of Remote Sensing*, **23**, 3169–3184.
- COLLINS, W., 1978. Remote sensing of crop type and maturity. *Photogrammetric Engineering and Remote Sensing*, **44**, 43–55.
- CONDIT, H. R., 1970. The spectral reflectance of American Soils. *Photogrammetric Engineering and Remote Sensing of Environment*, **36**, 955-966.
- CURRAN, P. J., 1980. Multispectral remote sensing of vegetation amount. *Progress in Physical Geography*, **4**, 315-341.
- CURRAN, P. J., 1989. Remote sensing of foliar chemistry. *Remote Sensing of Environment*, **30**, 271-278.
- CURRAN, P. J., DUNGAN, J. L., MACLER, B. A., PLUMMER, S.E., and Peterson, D.L., 1992. Reflectance Spectroscopy of Fresh Whole Leaves for the Estimation of Chemical Concentration. *Remote Sensing of Environment*, **39**, 153-166.
- CURRAN, P. J., JUPIEC, J. A., and SMITH, G. M., 1997. Remote sensing the biochemical composition of a slash pine canopy. *IEEE Transactions on Geoscience and Remote Sensing*, **35**, 415-520.
- DAINTITH, J, 2008. A Dictionary of Chemistry. 6th edition, Oxford University Press.
- DASH, J., and CURRAN, P. J., 2004. The MERIS terrestrial chlorophyll index. *International Journal of Remote Sensing*, **25**, 5403-5413.

William James Frampton

- DASH, J., and CURRAN, P. J., 2006. Relationship between herbicide concentration during the 1960s and 1970s and the contemporary MERIS Terrestrial Chlorophyll Index for southern Vietnam. *International Journal of Geographical Information Science* **20**, 929–939.
- DASH, J., CURRAN, P. J., TALLIS, M. J., LLEWELLYN, G. M., TAYLOR, G., and SNOEIJ, P., 2010a. Validating the MERIS Terrestrial Chlorophyll Index (MTCI) with ground chlorophyll content data at MERIS spatial resolution. *International Journal of Remote Sensing*, **31**, 5513-5532.
- DASH, J., JEGANATHAN, C., ATKINSON, P. M., 2010. The use of MERIS Terrestrial Chlorophyll Index to study spatio-temporal variation in vegetation phenology over India. *Remote Sensing of Environment*, **114**, 1388-1402.
- DAUGHTRY, C. S. T., WALTHALL, C. L., KIM, M. S., BROWN de COLSTOUN, E., and McMURTEY III, J. E., 2000, Estimating corn leaf chlorophyll concentration from leaf and canopy reflectance, *Remote Sensing Environment*, **74**, 229-239.
- DAWSON, T. P., CURRAN, P. J., 1998. A new technique for interpolating the reflectance red edge position. *International Journal of Remote Sensing*, **19**, 2133-2139.
- DELEGIDO, J., VERGARA, C., VERREIST, J., GANDIA, S., MORENO, J., 2011. Remote Estimation of Crop Chlorophyll Content by Means of High-Spectral-Resolution Reflectance Techniques. *Agronomy Journal*, **103**, 1834–1842.
- EIDENSHINK, J. C., BURGAN, R. E., and HAAS, R. H., 1990. Monitoring fire fuels condition by using time series composites of Advanced Very High Resolution Radiometer (AVHRR) Data. *Proceedings of Resource Technology*, **90**, 68-82.
- EMELYANOVA, I. V., McVICAR, T. R., VAN NIEL, T. G., LI, L., T., and VAN DIJK, A., I., J., M., 2013. Assessing the accuracy of blending Landsat-MODIS surface reflectances in two landscapes with contrasting spatial and temporal dynamics: A framework for algorithm selection. *Remote Sensing of Environment*, **133**, 193-209.
- ESA, 2010. GMES Sentinel-2 Mission Requirements Document. esamultimedia.esa.int/docs/S2-Data_Sheet.pdf (accessed 12.12.2011).
- ESA, 2010b. https://earth.esa.int/web/guest/missions/esa-operational-eo-missions/envisat/content?p_r_p_564233524_assetIdentifier=implementation-of-envisat-extension-orbit-in-october-2010-6999 (accessed 10.12.2011)
- ESA, 2011. ESA future missions – overview. <https://earth.esa.int/web/guest/missions/esa-future-missions>. (accessed 11.03.2011).

William James Frampton

ESA, 2011b. Sentinel-3 Mission Requirements Traceability Document (MRTD)

ESA, 2011c. GMES overview. http://www.esa.int/esaLP/SEMRR10DU8E_LPgmes_0.html (accessed 12.12.2011).

ESA, 2012a. <https://earth.esa.int/web/guest/missions/esa-operational-eo-missions/envisat/history> (accessed 30.01.2012).

ESA, 2012b. <http://earth.esa.int/ers/eeo4.10075/ERS1.5.html> (accessed 31.01.2012).

ESA, 2012c. http://www.esa.int/esaLP/SEM097EH1TF_LPgmes_0.html (accessed 31.01.2012).

ESA, 2012d. Biomass report for mission selection, available at:

http://esamultimedia.esa.int/docs/EarthObservation/SP1324-1_BIOMASSr.pdf (accessed 04.04.2014).

ESA, 2014. Sentinel-2 MSI product types. <https://sentinel.esa.int/web/sentinel/user-guides/sentinel-2-msi/product-types> (accessed 14.05.2014).

ESA, 2014b. Proba-1 mission homepage. <https://earth.esa.int/web/guest/missions/esa-operational-eo-missions/proba> (accessed 17.05.2014).

ESA, 2014c. Biomass mission homepage.

http://www.esa.int/Our_Activities/Observing_the_Earth/The_Living_Planet_Programme/Earth_Explorers/Future_missions/About_future_missions (accessed 28/11/2014)

FARMSTAR, 2011. FARMSTAR – Sustainable farming with satellites.

<http://www.spotimage.co.jp/web/en/896-farmstar-sustainable-farming-with-satellites.php> (accessed 12.12.2011).

FEDERER, C. A., and TANNER, C.B., 1966. Spectral distribution of light in the forest. *Ecology*, **47**, 555-560.

FERRIER, G., 1995. Evaluation of apparent surface reflectance estimation methodologies.

International Journal of Remote Sensing, **16**, 2291-2297.

FOODY, G. M., and ATKINSON, P. M., 2002. Uncertainty in remote sensing and GIS: Fundamentals.

Chichester: Wiley & Sons.

FRA 2010. Global Forest Resources Assessment 2010: Main Report, Food and Agriculture

Organization of the United Nations

William James Frampton

- FRAMPTON, W. J., VUOLO, F., DASH, J. D., MILTON, E. J., 2010. Quantifying the effect of soil on retrieval of chlorophyll content from remotely sensed data. In: Proceedings of the 2010 RSPSoc and Irish Earth Observation Symposium 'Visualising the World: From the Sea-bed to the Cloud-tops', 1st-3rd September, Cork, Ireland.
- FRAMPTON, W. J., DASH, J., WATMOUGH, G. R., and MILTON, E. J., 2011. Estimating vegetation chlorophyll content from ESA's Sentinel-2 Multi-Spectral Instrument. In, Annual Conference of the Remote Sensing and Photogrammetry Society: Earth Observation in a Changing World (RSPSoc 2011), Bournemouth, GB, 13 - 15 Sep 2011.
- FRAMPTON, W. J., DASH, J., WATMOUGH, G. R., and MILTON, E. J., 2013. Evaluating the capabilities of Sentinel-2 for quantitative estimation of biophysical variables in vegetation. *Journal of Photogrammetry and Remote Sensing*, **82**, 83-92.
- FUNG, I., 2002. Carbon Cycle. Encyclopedia of Physical Science and Technology. 417-429. Academic Press.
- GADM, 2014. GADM database of Global Administrative Areas, <http://www.gadm.org/> (accessed 05.02.2014).
- GAO, F., MASEK, J., SCHWALLER, M., and HALL, F., 2006. On the blending of the Landsat and MODIS surface reflectance: predicting daily Landsat surface reflectance. *Transactions on Geoscience and Remote Sensing*, **44**, 2207-2218
- GATES, D.M., KEEGAN, H.J., SCHLETER, J.C. and WEIDNER, V.R. 1965. Spectral properties of plants. *Applied Optics*, **4**, 11-20.
- GAUSMAN, H.W., 1974. Leaf reflectance of near-infrared. *Photogrammetric Engineering & Remote Sensing*, **40**, 183-192.
- GCOS, 2010. Ensuring the availability of global observations for climate. <http://www.wmo.int/pages/prog/gcos/index.php?name=Publications> (accessed 14.12.2011).
- GILABERT, M. A., GONZÁLEZ-PIQUERAS, J., GARCÍA-HARO, F. J., and MELIÁ, J., 2002. A generalized soil-adjusted vegetation index. *Remote Sensing of Environment*, **82**, 303-310.
- GITELSON, A. A. 2004. Wide dynamic range vegetation index for remote quantification of biophysical characteristics of vegetation. *Journal of Plant Physiology*, **161**, 165–173.

William James Frampton

- GITELSON, A.A., KAUFMAN, Y.J., and MERZLYAK, M.N., 1996. Use of a green channel in remote sensing of global vegetation from EOS-MODIS. *Remote Sensing of Environment*, **58**, 289-298.
- GITELSON, A. A., VINA, A., CIGANDA, V., RUNDQUIST, D. C., and ARKEBAUER, T. J., 2005. Remote estimation of canopy chlorophyll content in crops. *Geophysical Research Letters*, **32**, 1-4.
- GLENN, E. P., HUETE, A. R., NAHLER, P. L., NELSON, S. G., 2008. Relationship between remotely-sensed vegetation indices, canopy attributed and plant physiological processes: what vegetation indices can and cannot tell us about the landscape. *Sensors*, **8**, 2136-2160.
- GMES, 2012. <http://www.gmes.info/> (accessed 31.01.2012).
- GÓMEZ-CHOVA, L., ALONSO, L., GUANTER, L., CAMPS-VALLS, G., CALPE, J., and MORENO J., 2008. Correction of systematic spatial noise in push-broom hyperspectral sensors: application to CHRIS/PROBA images. *Applied Optics*, **47**, 46-60.
- GRAETZ, R. D., 1990. Remote sensing of terrestrial ecosystem structure: an ecologist's pragmatic view. *Remote sensing of biosphere functioning*, New York: Springer-Verlag, 5-30.
- GREEN B.R., DURNFORD D.G., 1996. The chlorophyll-carotenoid proteins of oxygenic photosynthesis. *Annual Review of Plant Physiology Plant Molecular Biology*, **47**, 685-714.
- GROSS, J., 1991. *Pigments in vegetables: chlorophylls and carotenoids*. Van Nostrand Reinhold, New York, 225-237.
- GUANTER, L., ALONSO, L., and MORENO, J., 2005a. A method for the surface reflectance retrieval from PROBA/CHRIS data over land: application to ESA SPARC campaigns. *Transactions on Geoscience and Remote Sensing*, **43**, 2908-2917.
- GUANTER, L., ALONSO, L., and MORENO, J., 2005b. First results from the PROBA/CHRIS hyperspectral/multiangular satellite system over land and water. *Geoscience and Remote Sensing Letters*, **2**, 250-254.
- GUYOT, G. and BARET, F., 1988. Utilisation de la haute resolution spectrale pour suivre l'état des couverts vegetaux. Proceedings, 4th International Colloquium 'Spectral Signatures of Objects in Remote Sensing', Aussois, 18 - 22 January 1988, Paris: ESA, ESA Publication SP-287, 279-286.

William James Frampton

- GUYOT, G., BARET, F., and MAJOR, D. J., 1988. High spectral resolution: determination of spectral shifts between the red and the near infrared. *International Archives of Photogrammetry and Remote Sensing*, **11**, 740–760.
- HABOUDANE, D., MILLER, J. R., PATTEY, E., ZARCO-TEJADA, P. J., STRACHAN, P. J., and STRACHAN, I., 2004. Hyperspectral vegetation indices and novel algorithms for predicting green LAI of crop canopies: Modeling and validation in the context of precision agriculture. *Remote Sensing of Environment*, **90**, 337–352.
- HANKAMER, B., BARBER, J., BOEKEMA, E. J., 1997. Structure and membrane organization of photosystem II in green plants. *Annual Review of Plant Physiology Plant Molecular Biology*, **48**, 641-671.
- HARRIS, A., DASH, J., 2010. The potential of the MERIS Terrestrial Chlorophyll Index for carbon flux estimation. *Remote Sensing of Environment*, **114**, 1856-1862.
- HAY, S. I., 2000. An Overview of Remote Sensing and Geodesy for Epidemiology and Public Health Application. In, HAY, S. I., RANDOLPH, S. E., and ROGERS, D. J., 2000, *Remote Sensing and Geographical Information Systems in Epidemiology*. Bodmin, Cornwall: Elsevier Science.
- HECHT, S., and COCKBURN, A., 1989. *The Fate of the Forest* (London: Verso).
- HILKER, T., WULDER, M. A., COOPS, N. C., SEITZ, N., WHITE, J. C., GAO, F., JEFFERY, G., MASEK, G., and STENHOUSE, G., 2009. Generation of dense time series synthetic Landsat data through data blending with MODIS using a spatial and temporal adaptive reflectance fusion model. *Remote Sensing of Environment*, **113**, 1988-1999.
- HORLER, D. N. H., BARBER, J., and BARRINGER, A. R., 1980. Effects of heavy metals on the absorbance and reflectance spectra of plants. *International Journal of Remote Sensing*, **1**, 121.
- HORLER, D. N. H., DOCKRAY, M., and BARBER, J., 1983. The red edge of plant leaf reflectance. *International Journal of Remote Sensing*, **4**, 273–288.
- HUETE, A.R., 1988. A Soil-adjusted vegetation index. *Remote Sensing of the Environment*, **25**, 295-309.
- HUETE, A.R., DIDAN, K., MIURA, T., RODRIGUEZ, E.P., GAO, X., and FERRERIA, L.G., 2002. Overview of the radiometric and biophysical performance of the MODIS vegetation indices. *Remote Sensing of Environment*, **83**, 195-213.

William James Frampton

- HUETE, A. R., POST, D. F., and JACKSON, R. D., 1984. Soil spectral effects on 4-space vegetation discrimination. *Remote Sensing of Environment*, **15**, 155-165.
- ICPB, 2008. <http://www.iowacorn.org/cms/en/corneducation/faq/faq.aspx> (accessed 12.01.2012).
- IPCC 2006. Agriculture, forestry and other land use. In: EGGLESTON, H.S., BUENDIA, L., MIWA, K., NGARA, T., TANABE, K. (Eds.), IPCC Guidelines for National Greenhouse Gas Inventories, Prepared by the National Greenhouse Gas Inventories Programme. IGES, Japan.
- IPCC, 2007. Climate Change 2007: The Physical Science Basis. Contribution of Working Group I to the Forth Assessment: Report of the Intergovernmental Panel on Climate Change. Cambridge, United Kingdom and New York, NY, USA, Cambridge University Press.
- JACQUEMOUD, S., BARET, F., ANDRIEU, B., DANSON, F. M. and JAGGARD, K., 1995. Extraction of Vegetation Biophysical Parameters by Inversion of the PROSPECT + SAIL Models on Sugar Beet Canopy Reflectance Data. Application to TM and AVIRIS Sensors. *Remote Sensing of Environment*, **52**, 163-172.
- JACQUEMOUD, S., VERHOEF, W., BARET, F., BACOUR, C., ZARCO-TEJADA P.J., ASNER, G.P., FRANÇOIS, C., USTIN, S.L., 2009. PROSPECT + SAIL Models: a review of use for vegetation characterization, *Remote Sensing of Environment*, **113**, S56-S66.
- JEFFREY, A., 1985. Mathematics for Engineers and Scientists (Wokingham, UK: Van Nostrand Reinhold), 708–709.
- JEGENATHAN, C., DASH, J., and ATKINSON, P. M., 2010. Mapping the phenology of natural vegetation in India using a remote sensing-derived chlorophyll index. *International Journal of Remote Sensing*, **31**, 5777-5796.
- JORDAN, C. F. 1969. Derivation of Leaf-Area Index from quality of light on the forest floor. *Ecology*, **50**, 663-666.
- KANEMASU, E. T. 1974. Seasonal canopy reflectance patterns of wheat, sorghum, and soybean, *Remote Sensing of Environment*, **3**, 43–47.
- Kaufman, Y. J., 1989. The atmospheric effect on remote sensing and its corrections. Theory and Applications of Optical Remote Sensing, J. Wiley, New York, 336-428.
- KAUFMAN, Y.J., and TANRÉ, D. 1992. Atmospherically resistant vegetation index for EOS-MODIS. *IEEE transactions on geosciences and remote sensing*, **30**, 261-270.

William James Frampton

- KAUTH, R. J., and THOMAS, G. S., 1976. The tasselled cap--A graphic description of the spectral-temporal development of agricultural crops as seen by Landsat. Proceedings of the Symposium on Machine Processing of Remotely Sensed Data, LARS, Purdue University, West Lafayette, Indiana, 41-51.
- KEALY, P., and DELWART, S., 1999. The MERIS ground segment. *International Journal of Remote Sensing*, **20**, 1747-1756.
- KEELING, C. D., PIPER, S. C., and HEIMANN, M., 1996. Global and hemispheric CO₂ sinks deduced from changes in atmospheric O₂ concentration. *Nature*, **375**, 218-221.
- KERR, J., OSTROVSKY, M., 2003. From space to species: ecological applications for remote sensing. *Trends in Ecology and Evolution*, **18**, 299-305.
- KIM, M. S., 1994. The Use of Narrow Spectral Bands for Improving Remote Sensing Estimation of Fractionally Absorbed Photosynthetically Active Radiation (fAPAR). *Masters Thesis. Department of Geography, University of Maryland, College Park, MD.*
- KIMES, D. S., 1982. Dynamics of directional reflectance factor distributions for vegetation canopies. *Applied Optics*, **22**, 1364-1372.
- KNIPLING, E. B., 1970. Physical and physiological basis for the reflectance of visible and near-infrared radiation from vegetation. *Remote Sensing of Environment*, **1**, 155-159.
- KOLLENKARK, J. C., VANDERBILT, V. C., DAUGHTRY, C. S. T., BAUER, M. E., 1982. Influence of solar illumination angle on soybean canopy reflectance. *Applied Optics*, **21**, 1179-1184.
- KREIGLER, F. J., MALILA, W. A., NALEPKA, R. F., and RICHARDSON, W., 1969. Preprocessing transformations and their effects on multispectral recognition. Proceedings of the Sixth International Symposium on Remote Sensing of Environment, 97-131.
- KUUSK, A., 1991. The hot-spot effect in plant canopy reflectance. Photon – vegetation interactions. Applications in Optical Remote Sensing and Plant Ecology. R.B. Myneni and J. Ross (Ed.), Springer-Verlag, New York, 139– 159.
- LAMB, D. W., STEYN-ROSS, M., SCHAARE, P., HANNA, M. M., SILVESTER, W., and STEYN-ROSS, A., 2002. Estimating leaf nitrogen concentration in ryegrass (*Lolium* spp.) pasture using the chlorophyll Red Edge: Theoretical modelling and experimental observations. *International Journal of Remote Sensing*, **23**, 3619–3648.

William James Frampton

- LEBLANC, S. G., 2002. Correction to the plant canopy gap size analysis theory used by the tracing radiation and architecture of canopies (TRAC) instrument. *Applied Optics*, **31**, 7667–7670.
- LeFEBURE, 2012. <http://lefebure.com/farming/2005/october/> (accessed 12.01.2012).
- LICHTENTHALER, H. K., 1987. Chlorophylls and carotenoids: pigments of photosynthetic biomembranes. *Methods in Enzymology*, **148**, 350-382.
- Li-COR INC., 1992. LAI-2000 plant canopy analyzer instruction manual.
- MAJOR, D. J., SCHAALJE, G. B., WIEGAND, C., and BLAD, B. L., 1992. Accuracy and sensitivity analyses of sail model-predicted reflectance of maize. *Remote Sensing of Environment*, **41**, 61–70.
- McGREGOR, J., and GORMAN, A. J., 1994. Some considerations for using AVHRR data in climatological studies: I. Orbital characteristics of NOAA satellites. *International Journal of Remote Sensing*, **15**, 537-548.
- METTERNICHT, G., 2003. Vegetation indices derived from high-resolution airborne videography for precision crop management. *International Journal of Remote Sensing*, **24**, 2855-2877.
- MILLER, G. P., FUCHS, M., HALL, M. J., ASRAR, G., KANEMASU, E. T., JOHNSON, D. E., 1984. Analysis of seasonal multispectral reflectances of small grains. *Remote Sensing of Environment*, **14**, 153-167.
- MILTON, E.J., BLACKBURN, G.A., ROLLIN, E.M., DANSON, F.M., 1994. Measurement of the spectral directional reflectance of forest canopies: a review of methods and a practical application. *Remote Sensing Reviews*, **10**, 285–308.
- MORAN, R., 1982. Formulae for determination of chlorophyllous pigments extracted with N,N-dimethylformamide, *Plant Physiology*, **69**, 1376-1381.
- MORAN, R., and PORATH, D., 1980. Chlorophyll determination in intact tissues using N,N-dimethylformamide, *Plant Physiology*, **65**, 478-479.
- MORISSETTE, J. T., BARET, F., PRIVETTE, J. L., MYNENI, R. B., NICKESON, J. E., GARRIGUES, S., SHABANOV, N. V., WEISS, M., FERNANDES, R. A., LeBLANC, S. G., KALACSKA, M., SANCHEZ-AZOFEIFA, G. A., CHUBEY, M., RIVARD, B., STENBERG, P., RAUTIAINEN, M., VOIPIO, P., MANNINEN, T., PILANT, A. N., LEWIS, T. E., LIAMES, J. S., COLOMBO, R., MERONI, M., Busetto, L., COHEN, W. B., TURNER, D. P., WARNER, E. D., PETERSEN, G. W., SEUFERT, G., and COOK, R., 2006. Validation of global moderate-resolution LAI products: a framework proposed within the CEOS Land Product Validation subgroup. *IEEE Transactions in Geosciences and Remote Sensing*, **44**, 1804-1817.

William James Frampton

MYNENI, R. B., HALL, F. G., SELLERS, P. J., MARSHAK, A. L., 1995. The interpretation of spectral vegetation indexes. *IEEE transactions on geosciences and remote sensing*, **33**, 481-486

MYNENI, R.B., MAGGION, S., LAQUINTA, J., PRIVETTE, J. L., GOBRON, N., PINTY, B., KIMES, D. S., VERTRAETE, M. M., WILLIAMS, D. L., 1995. Optical Remote Sensing of Vegetation: Modelling, Caveats, and Algorithms. *Remote Sensing of Environment*, **51**, 169-188.

NASA, 2014. Earth Observing 1, Sensors – Hyperion. <http://eo1.usgs.gov/sensors/hyperion> (accessed 12.03.2014).

NCAVEO, 2005. Network for Calibration and Validation of Earth Observation data, School of Geography, University of Southampton, www.ncaveo.ac.uk/special_topics/atmospheric_correction/ (accessed 16.12.2009).

NOAA, 2011. <http://www.noaa.gov/satellites.html> (accessed 25.02.2012).

NOAA, 2012. Monthly Station Normals of Temperature, Precipitation, and Heating and Cooling Degree Days cdo.ncdc.noaa.gov/climatenormals/clim81/TXnorm.pdf (accessed 12.02.2012).

NÚÑEZ, J., OTAZU, X., FORS, O., PRADES, A., PALA, V., and ARBIOL, R., 1999. Multiresolution-based image fusion with additive wavelet decomposition. *Geoscience and Remote Sensing*, **37**, 1204-1211.

PALTRIDGE, G. W., and MITCHELL, R. M., 1990. Atmospheric and viewing angle correction of vegetation indices and grassland fuel moisture content derived from NOAA/AVHRR. *Remote Sensing of Environment*, **31**, 121 – 135.

PARUELO, J. M., GARBULSKY, M.F., GUERSCMAN, J.P., JOBBAGY, E.G., 2004. Two decades of Normalized Difference Vegetation Index changes in South America: identifying the imprint of global change. *International Journal of Remote Sensing*, **25**, 2793-2806.

PEARSON, R. L., and MILLER, L. D., 1972. Remote mapping of standing crop biomass for estimation of the productivity of the shortgrass prairie. *Proceedings of the Eighth International Symposium on Remote Sensing of Environment*, Environmental Research Institute of Michigan, 1357-1381.

PETTORELLI, N., VIK, J., MYSTERUD, A., GAILLARD, J., TUCKER, C., and STENSETH, N., 2005. Using the satellite derived NDVI to assess ecological responses to environmental change. *Trends in Ecology and Evolution*, **20**, 503-510.

William James Frampton

- POSTEL, 2012. <http://postel.mediasfrance.org/en/BIOGEOPHYSICAL-PRODUCTS/Land-Surface-Reflectance/GLOBCOVER-Project/> (accessed 25.01.2012).
- QI, J., CHEBOUNI, A., HUETE, A. R., KERR, Y. H., and SOROOSHIAN, S., 1994. A Modified Soil Adjusted Vegetation Index. *Remote Sensing of Environment*, **48**, 119-126.
- RAST, M., BÉZY, J.L., BRUZZI, S., 1999. The ESA Medium Resolution Imaging Spectrometer MERIS – a review of the instrument and its mission. *International Journal of Remote Sensing*, **20**, 1681-1702.
- RICHARDSON, A. J., and WIEGAND C. L., 1977. Distinguishing vegetation from soil background information. *Photogrammetric Engineering and Remote Sensing*, **43**, 1541-1552.
- RICHTER, R., 2008. Atmospheric/Topographic Correction for Airborne Imagery: ATCOR-4 User Guide, version 4.3 January 2008. DLR – German Aerospace Centre, Wessling, Germany.
- RONDEAUX, G., STEVEN, M., and BARET, F., 1996. Optimization of soil-adjusted vegetation indices. *Remote Sensing of Environment*, **55**, 95-107.
- ROUJEAN, J. L., and BREON, F. M., 1995. Estimating PAR absorbed by vegetation from bidirectional reflectance measurements. *Remote Sensing of Environment*, **51**, 375–384.
- ROUSE, J. W., R. H. HAAS, J. A. SCHELL, and DEERING, W. D., 1973. Monitoring vegetation systems in the Great Plains with ERTS. Third ERTS Symposium, NASA SP-351, 309-317.
- RUNNING, S. W., and COUGHLAN, J. C., 1988. A general model of forest ecosystem processes for regional applications, I. Hydrologic balance, canopy gas exchange and primary production processes. *Ecological Modelling*, **42**, 125-154.
- SANGER, J. E., 1971. Quantitative investigation of leaf pigments from their inception in buds through autumn coloration to decomposition in falling leaves. *Ecology*, **52**, 1075-1089.
- SELLERS, P. J., 1987. Canopy reflectance, photosynthesis and transpiration. *International Journal of Remote Sensing*, **8**, 1335-1372.
- SEN3Exp, 2011. Sentinel-3 Experimental Campaign Final Report, ESA. <http://earth.esa.int/campaigns/DOC/> (accessed 24.07.2011).
- SITCH, S., SMITH, B., PRENTICE, I. C., ARNETH, A., BONDEAU, A., CRAMER, W., KAPLAN, J., LEVIS, S., LUCHT, W., SYKES, M., THONICKE, K., and VENEVSKI, S., 2003. Evaluation of ecosystem dynamics, plant geography and terrestrial carbon cycling in the LPJ Dynamic Vegetation Model. *Global Change Biology*, **9**, 161-185.

William James Frampton

- SMITH, G. M., MILTON, E. J., 1999. The use of the empirical line method to calibrate remotely sensed data to reflectance. *International Journal of Remote Sensing*, **20**, 2653-2662.
- STONER, E. R., and BAUMGARDNER, M. F., 1981. Characteristic variations in reflectance of surface soils. *Soil Science Society of America Journal of Remote Sensing*, **20**, 2423-2441.
- TANAKA, R., and TANAKA, A. 2000. Chlorophyll b is not just an accessory pigment but a regulator of the photosynthetic antenna. *Porphyrins*, **9**, 240-245
- THOME, K. J., 2004. In-flight intersensor radiometric calibration using vicarious approaches. Post-launch calibration of satellite sensors, MORAIN, S. A., and BUDGE, A. M., London, Taylor and Francis, 95-102.
- THOME, K. J., SCHILLER, S., CONEL, J. E., ARAI, K., and TSUCHIDA, S., 1998. Results of the 1996 Earth Observing System vicarious calibration joint campaign at Lunar Lake Playa, Nevada (USA). *Metrologia*, **35**, 631-638.
- TUCKER, C.J., 1977. Asymptotic nature of grass canopy spectral reflectance. *Applied Optics*, **16**, 1151-1156.
- TUCKER, C. J., 1979. Red and photographic infrared linear combinations for monitoring vegetation. *Remote Sensing of Environment*, **8**, 127-150.
- TUCKER, C. J., 1980a. Remote sensing of leaf water content in the near infrared. *Remote Sensing of Environment*, **10**, 23-32.
- TUCKER, C. J., 1980b. Radiometric resolution for monitoring vegetation: How many bits are needed? *International Journal of Remote Sensing*, **1**, 241-254.
- UNESCO, 2007. Biosphere Reserve Information: Sierras de Cazorla, Segura y Las Villas. <http://www.unesco.org/mabdb/br/brdir/directory/biores.asp?mode=all&code=SPA+06> (accessed 28.12.2009).
- UNITED NATIONS CONFERENCE ON DESERTIFICATION, 1977. Desertification: Its Causes and Consequences (Oxford: Pergamon).
- USDA NASS, 1997. Usual planting and harvesting dates 1997, Washington, D.C. : U.S. Dept. of Agriculture, Agricultural Statistics Board, NASS.
- USDA NASS, 2010. Usual planting and harvesting dates 2010, Washington, D.C.: U.S. Dept. of Agriculture, Agricultural Statistics Board, NASS.

William James Frampton

- VERDEBOUT, J., JACQUEMOUD, S., and SCHMUCK, G., 1994. Optical properties of leaves: modelling and experimental studies. In, HILL, J., and MÉGIER, J., 1994. Indicators Imaging Spectrometry — a Tool for Environmental Observations. Eurocourses: Remote Sensing, **4**, 193-219, Kluwer Academic Publishers, Dordrecht.
- VERHOEF, W., 1984. Light scattering by leaf layers with application to canopy reflectance modelling: the SAIL model. *Remote Sensing of Environment*, **16**, 125–141.
- VERHOEF, W., 1985. Earth observation modelling based on layer scattering matrices. *Remote Sensing of Environment*, **17**, 165–178.
- VERHOEF, W., and BACH, H., 2003. Simulation of hyperspectral and directional radiance images using coupled biophysical and atmospheric radiative transfer models. *Remote Sensing of Environment*, **87**, 23–41.
- VERNON, L. P., 1960. Spectrophotometric Determination of Chlorophylls and Pheophytins in Plant Extracts. *Analytical Chemistry*, **32**, 1144-1150.
- VERSTRAETE, M. M., PINTY, B., and CURRAN, P. J., 1999. MERIS potential for land applications. *International Journal of Remote Sensing*, **20**, 1747-1756.
- WALKER, J. J., DE BEURS, H. M., WYNNE, R. H., and GAO, F., 2012. Evaluation of Landsat and MODIS data fusion products for analysis of dryland forest phenology. *Remote Sensing of Environment*, **117**, 381,393.
- WANG, D., MORTON, D., MASEK, J., WU, A., NAGOL, J., XIONG, X., LEVY, R., VERMOTE, E., and WOLFE, R., 2012. Impact of sensor degradation on the MODIS NDVI time series. *Remote Sensing of Environment*, **119**, 55-61.
- WATMOUGH, G. R., DASH, J., FRAMPTON, W. J., and VUOLO, F., 2011. MTCI-EVAL: MERIS extended validation and exploratory approach for high resolution optical sensor Technical Note 2. European Space Agency, April 2011.
- WEINREB, M. P., FLEMING, H. E., McMILLIN, L. M., and NEUENDORFFER, A. C., 1981. Transmittances for the TIROS Operational Vertical Sounder. Washington D. C.: National Oceanic and Atmospheric Administration.
- WELLBURN, A. R., 1994. The spectral determination of chlorophylls a and b, as well as total carotenoids, using various solvents with spectrophotometers of different resolution. *Journal of Plant Physiology*, **144**, 307-313.

William James Frampton

WIDLÓWSKI, J.-L., PINTY, B., GOBRON, N., VERSTRAETE, M. M., DINER, D. J., 2004. Canopy structure parameters derived from multi-angular remote sensing data for terrestrial carbon studies. *Climatic Change*, **67**, 403-415.

WIFFEN, D. H., 1972. Spectroscopy. Longman, London.

WILHELM, W. W., RUWE, K., SCHLEMMER, M.R., 2000. Comparisons of three Leaf Area Index Meters in a Corn Canopy. *Crop Science*, **40**, 1179-1183.

WOODCOCK, C.E., STRAHLER, A.H., 1987. The factor of scale in remote sensing. *Remote Sensing of Environment*, **21**, 311–332.

ZHU, Z., BI, J., PAN, Y., GANGULY, S., ANAV, A., XU, L., SAMANTA, A., PIAO, S., NEMANI, R.R., MYNENI, R.B., 2013. Global Data Sets of Vegetation Leaf Area Index (LAI)3g and Fraction of Photosynthetically Active Radiation (FPAR)3g Derived from Global Inventory Modelling and Mapping Studies (GIMMS) Normalized Difference Vegetation Index (NDVI3g) for the Period 1981 to 2011. *Remote Sensing*, **5**, 927-948.

ZURITA-MILLA, R., KAISER, G., CLEVERS, J. G. P. W., SCHNEIDER, W., and SCHAEPMAN, M. E., 2009. Downscaling time series of MERIS full resolution data to monitor vegetation seasonal dynamics. *Remote Sensing of Environment*, **113**, 1874-1885.